NASA CR

DOT/FAA/DS-89/14

202600-19-T

Technical Report

SYNTHETIC APERTURE RADAR IMAGERY OF AIRPORTS AND SURROUNDING AREAS

Archived SAR Data

AD-A216 876

R.G. ONSTOTT
D.J. GINERIS

NASA Langley Research Center
Hampton, VA 23665-5225
Contract No. NAS1-18465

DTIC
S ELECTE D
JAN 19 1990
B

ERIM P.O. Box 8618
Ann Arbor, MI 48107-8618

90 01 17 067

FOREWORD

This is the final report for Phase I for Contract NAS1-18465 Processed Synthetic Aperture Radar (SAR) Data, sponsored by National Aeronautics and Space Administration (NASA) Langley Research Center (LaRC). This report is the first of a series of three reports. The overall effort has as its thrust the statistical description of the ground clutter at an airport and in the surrounding area. In Phase I of this activity, SAR data of airports which existed in the Environmental Research Institute of Michigan (ERIM) SAR data archive were examined for utility to this program. Eight digital backscatter coefficient images at high resolution and coarse resolution were created. The coarse resolution images were provided to NASA LaRC for use in their Microburst/Clutter/Radar simulation program, whereas the high resolution images underwent a statistical clutter analysis at ERIM. During Phase II of this program, SAR data were collected on an opportunity basis at Philadelphia International Airport using a set of radar parameters which more closely matched those which are anticipated to be encountered by an aircraft on its approach to an airport. A second report will be prepared to describe these data and the clutter study results. During Phase III, a dedicated SAR mission was flown of the Denver Stapleton International Airport and surrounding area. A wide variety of geometries and scene contents were acquired. These data and study results are presented in the third report.

The work reported here was performed by members of the Radar Science Laboratory, Advanced Concepts Division, Environmental Research Institute, under the direction of Dr. S.R. Robinson. The principal investigator for this project was Dr. R.G. Onstott. The contract was monitored by E.M. Bracalente, NASA Langley Research Center, Hampton, Virginia.

The authors gratefully acknowledge the support of the Radar Science Laboratory Staff during the project, in particular, Mr. Christopher C. Wackerman, Mr. David Kletzli, Mr. Steven Lerman, Mr. Charles Harkness, Ms. Rita Woods, Ms. Janice Anquetil, and Ms. Marsha Allen.

i

TABLE OF CONTENTS

TABLE OF CONTENTS (cont.)

LIST OF TABLES

LIST OF FIGURES

LIST OF FIGURES (cont.)

LIST OF FIGURES (cont.)

viii

LIST OF FIGURES (cont.)

I. INTRODUCTION

Low altitude microburst windshear represents a significant hazard to
aircraft, particularly during take-off and landing; the intense down
drafts and the resultant divergent outflow, can have a significant
effect on the lift characteristics of the endangered aircraft. When
encountered at low altitude, the pilot has little time to react
correctly to maintain safe flight. The Federal Aviation Administration
(FAA), jointly with the National Aeronautics and Space Administration
(NASA), has sponsored an investigation into the development of airborne
sensors to detect microburst windshear. One sensor of interest is a
microwave Doppler radar operating at X-band or higher frequencies.
Critical to the analysis of the capability of such a sensor to perform
this detection is the microwave backscatter description of both the
microburst event and the clutter background, especially during the
approach and departure from an airport. The Environmental Research
Institute of Michigan (ERIM) has provided NASA Langley Research Center
(LaRC) with eight high-resolution calibrated synthetic aperture radar
(SAR) images of selected airport scenes from the ERIM SAR data archive
for use in their Microburst/Clutter/Radar simulation program and to
statistically characterize the ground clutter surrounding these
airports. In addition, statistical analyses of these airport
environments have been performed by ERIM to describe the range of
scattering conditions encountered.

NASA LaRC has developed a Microburst/Clutter/Radar simulation
program to assess the performance of Doppler radars for this application
and to test potential signal processing techniques. The simulation
program models the output of an airborne Doppler radar as it views a
low-level microburst along the approach to an airport. Inputs to this
simulation includes the airport ground clutter data base, a simulated
microburst data base, the operating parameters of the proposed weather
radar, and candidate signal processing software for use in detection.
In the operation of the simulation program the received signal amplitude
level for each range bin is calculated. Each range bin includes

1

contributions from both the microburst and the ground clutter.

Many questions arose during this study. What is the general description of the airport clutter environment? How does this environment change from airport to airport? How complex does an airport scene have to become before it degrades detection? In general, the limits of detectability of microburst events must be established for an airborne Doppler radar to be an effective tool in the prevention of aircraft windshear catastrophes. ERIM has performed a clutter analysis of each of the eight images. Although the data in these images were obtained at high incidence angles, the results of the analysis still provide significant information for establishing limits of detectability. Clutter types, mean backscatter intensities, probability distributions, and areal extent of the clutter types in each image have been determined. With the analysis of the statistical characteristics of clutter in each scene, the effects of scene composition were studied. These results may then be extrapolated to describe the clutter at candidate airports.

II. IMAGE SELECTION

The inventory of archived SAR data at ERIM was examined and potential scenes were selected to provide clutter estimates of the environment at and around airports. The SAR data are in strip map format with signal amplitude proportional to the reflectivity of the imaged area.

The inventory was first examined to determine the number of potential airport scenes. A second sort was implemented to select only the digitally recorded data. It was determined that the costs associated with tne processed SAR data effort would be reduced by using digital data only. The processing and calibration of optical/digital (hybrid) data products is more difficult and more costly. The archive was further examined to gather additional information regarding the area imaged, the data collection modes, the radar parameters used, and the ability to calibrate the images. From this refined list of scenes, eight images were selected as potential candidates for use in the NASA LaRC simulation model.

Scenes included the Willow Run, the Ottawa (Canada), the Victoria (British Columbia), Comox (BC), and the Peconic River (Long Island, New York) airports (see Table 1). Two flight track orientations are provided for the Willow Run Airport and may be utilized in the study of the importance of aspect angle on the backscatter response. Overall, depression angles (boresight) range from 18° to 78°. In many cases, there were multiple passes from which to choose. This allowed for some selectivity as to where the airport is positioned in the SAR scene and to the composition of the scene. Of the sites selected, two were observed during the spring, four during the summer, one during the fall, and one during winter (there was no snow cover present).

The principle criteria for image selection was image geometry, scene content, and small depression angle. The ideal image geometry is illustrated in Figure 1. Image dimensions of 11.8 km in azimuth and 13.8 km in range were desired to provide a full clutter background for use in the LaRC simulation program. The airport in the scene was to be

3

centered in the far 4.8 km of the image with the runway of interest oriented perpendicular to the flight line of the radar. The combination of proper airport orientation and incidence angle are to be employed by NASA to simulate the backscatter signals which an airborne radar would received from on a 3° glide slope. All images selected were acquired at 9.375 GHz. There is some polarization diversity among the images selected. An additional requirement was that the data collected contain the information necessary which would allow the airport image to be radiometrically calibrated. High urban, industrial, and residential content in the images was desired since these areas produce characteristically high radar clutter backscatter coefficients and represent the most problematic scene to an incoming airborne radar.

A description of these eight airport clutter scenes is presented in Table 1. Images 1, 2, and 5 are of the Willow Run Airport located near Ypsilanti, Michigan. These images are composed of urban, industrial, and rural regions and are temporally and polarization diverse. Four images were acquired during missions flown in Canada. The images are of the Ottawa International Airport, the Comox CFB, and the Victoria International Airport. These data were collected during the summer months, when backscatter intensities from natural targets such as trees and farmland would be at their greatest. Each of these images contain a combination of water, forest, urban, and agricultural areas. The two images of the Victoria International Airport were acquired at VV and HH polarizations. Image 7 contains the Peconic River Airport which is located on Long Island, New York. It has some urban content and a large variety of agricultural clutter, of which some has been ground truthed.

The eight images used in this analysis have the following ground coverage:

Image	Azimuth Coverage (m)	Ground Range Coverage (m)
1	5907 m	6155 m
2	10322 m	7770 m
3	7686 m	7016 m
4	8548 m	9786 m
5	9475 m	7770 m
6	7903 m	8652 m
7	5907 m	9366 m
8	8770 m	9366 m

These images have less coverage than that which would be produced by the ideal image geometry. The reasons for this reduced coverage are varied. The CV580 SAR system used to record this data had a limited resolution (1.5 m) and swath width which limited the ground coverage in range which it could obtain. In addition, since this archival data was originally recorded for purposes other than the windshear project, the flight and image geometrics used were not optimized for maximum range coverage and small depression angles. Azimuth coverage was limited by the availability of data, resolution size, and computing power.

The images which will be produced from the dedicated flights and which are described in the third report of this series will match the required image geometry. The P3 SAR has the ability to collect image data at coarser resolutions and larger swath widths. Both of these features serve to increase range coverage. In addition, the SAR processor will be modified to increase the number of azimuth records which can be processed at one time. This will serve to increase the azimuth coverage of the images. Finally, the flight and image geometries will be optimized for the windshear project during the dedicated flights so that the ideal image geometry can be obtained.

III. PROCESSING OF SAR DATA

Once the archival images were selected, unprocessed data were
retrieved from high density digital tapes and converted to phase
histories, formed into digital images, and then radiometrically
calibrated. The many step image processing sequence used to produce the
final ground clutter images is given in Figure 2.

Each phase history tape represents a 4096 element x 4096 element
image. With a pixel spacing of 1.44 m in azimuth and 1.5 m in range,
each processed image is a reflectivity map of a 5898 m by 6144 m area.
To achieve an azimuthal image width approaching 14 km, it was necessary
to process two 4096 element by 4096 element images (represented in
Figure 2 by Images "B" and "E") and digitally mosaic them together prior
to image compression.

The phase histories are focused in azimuth and range. This is
achieved by convolving these data with a match filter of the transmitted
radar chirp in azimuth and range. The data were then radiometrically
corrected in range to compensate for the effects of range fall off (R^4)
and antenna gain pattern variations. The images were then compressed to
the 21 m resolution required by the NASA LaRC simulation program. This
compression was performed by associating 14 pixel x 14 pixel areas,
integrating the power contained in these areas, and outputting the
resultant amplitude to a pixel in the "compressed image." A resolution
of 20.16 m in azimuth and a 21 m in range resulted. The compressed
image was then converted from the slant range plane to the ground range
plane using a technique employing upsampling. In upsampling, the image
data were Fourier transformed to the frequency domain, zero padded to
obtain the bandwidth needed for the desired resolution, and then
transformed back into the spatial domain. This conversion may cause a
ringing effect for bright targets which was removed by Fourier
transforming the data to the frequency domain, weighting the data with a
cosine or gaussian function, and converting back to the spatial domain
before the slant to ground range conversion was applied.

Absolute calibration of these data was performed on the

7

radiometrically corrected 4096 element x 4096 element images.
Generally, the backscattering radar cross-section of a point target, σ, is given by:

$$\sigma = \frac{P_I - P_N}{K} \tag{1}$$

where P_I = measured image intensity of the target,

     P_N = receive noise power, and

     K = system gain function of the radar.

If $P_I \gg P_N$, then $P_I - P_N \simeq P_I$. Using this approximation

$$\sigma = \frac{P_I}{K} \tag{2}$$

Converting equation 2 to decibels (i.e., σ dB = 10 log σ) we have

$$\sigma = P_I - K \quad dB. \tag{3}$$

When operating the SAR in its linear range a linear relationship exists between the 10 log of the measured intensity of the point target and the true backscattering radar cross-section (in dB) of the calibration references. The slope of the function is unity and the y-intercept of the function is a measure of the system gain function. To illustrate the determination of K, a calibration diagram for Image 1 is provided in Figure 3. In this Figure, the measured image intensifies of known reflectors are plotted against the expected theoretical backscattering radar cross-section of the reflectors. In an ideal system, these two values will equal each other. In a real system, system effects cause the measured image intensities to be offset from their expected values by a constant which is K, the system gain function. Since the radar is a linear system, the measured image intensity of a reflector increases as the reflectors expected value increases. The function which describes this trend is a linear function with a slope of unity. When a

8

line with a slope of unity is fit to the points in the plot in Figure 3,
the Y-intercept of the line is K, the system gain function, and provides
us with an estimate of the system offset. Once the system gain function
is known, the image may then be calibrated absolutely and converted to
backscatter coefficients. The backscatter coefficients in the slant
range image are given by:

$$\sigma^o = \frac{P_I - P_N}{K} \cdot \frac{\sin \theta}{r_a r_r} \tag{4}$$

Where σ^o = backscatter coefficient or Normalized Radar Cross Section
(NRCS)

P_I = measured intensity of the image,

P_N = receive noise intensity of the image,

K = system gain function of the radar,

θ = incidence angle,

r_a = resolution in azimuth, and

r_r = resolution in range.

Next, the minimum image mean intensity value (i.e., from no return areas
from within the image) is determined. The minimum mean intensity and
receiver noise are then equated. Given K and P_N the slant range image
was converted to scattering coefficients by applying equation 4. The
results were then validated by comparing the backscatter coefficients of
key distributed targets with published values. After the calibration
was validated, the backscatter coefficient conversion was applied to the
ground range image using the equation:

$$\sigma^o = \frac{P_I - P_N}{K} \cdot \frac{1}{r_a r_r} \tag{5}$$

The 'B' and 'E' subimages were then merged, the mosaic oriented to
the desired configuration, written to tape with a vector file containing

9

incidence angle information, and then sent to NASA for use in the simulation program.

IV. CLUTTER ANALYSIS PROCEDURES

Establishing the criteria for which microburst events may be detected, requires a careful characterization of airport clutter. The questions that arise immediately are: what are the types of clutter which commonly occur at an airport, how does the clutter environment change with incidence angle and polarization, and what is the density and location of strong returns at an airport? Clutter analyses were performed on each of the eight images in order to address these questions. The ERIM analyses were performed on 4096 element x 4096 element, slant range NRCS images with the finest resolution possibilities allow precise sampling of both distributed and point targets. These have one independent sample per resolution cell.

Two methods of clutter analysis were performed. In the first method, the entire image was examined. A statistical analysis of the image was performed providing information about the mean and standard deviation, and a histogram was also produced. In addition, many thresholds were used to determine the density and location of strong scattering sources. A series of images was generated where pixels with backscatter coefficients less than the threshold value were set equal to -40 dB and the intensities of the pixels which had backscattering values equal to or greater than the threshold were unchanged. The second series of analyses were performed using selected areas in the airport scene. Critical clutter types were located and extracted for a detailed statistical analysis. This included the determination of mean, variance, standard deviation, and the estimation of a probability density function which fit the data. These detailed clutter statistics are provided in Appendix A. Areas of similar clutter type were merged and composite histograms generated. The goal of this method of analysis was to characterize each of the different kinds of clutter in the airport scene. The results of the clutter analysis are given in the following section.

11

Image 1

The SAR data shown in Figure 4 were collected of the Willow Run Airport during December of 1984 using a vertical transmit polarization and a vertical receive polarization (i.e., VV polarization) and at incidence angles which range from 45° to 73°. This particular radar pass imaged much of the urban and industrial area to the west of the airport. During this period the ground was not snow covered, the deciduous trees were leafless and the agricultural areas harvested.

Table 2 and Figure 5 summarize the results of a clutter analysis of 10% of the image. The areas selected for analysis are indicated on Image 1 found in Appendix A. In general, cross sections from all terrian types were low. This is expected for backscatter at large incidence angles. Seasonal effects (i.e., during dormant conditions) have also contributed to the low backscatter coefficients. A histogram produced of the entire image is given in Figure 6. The mean backscatter coefficient value for the image is about -7 dB and approximately 65% of the data lies within 5 dB of this mean. Average returns from the distributed targets are typically less than -6 dB where as returns from selected cultural targets are -8 dB and greater. Thresholding was used to determine the location of areas of clutter within the image and the percentages of the image which are made up of specific clutter groups. Table 3 summarizes the thresholding results for each of the eight images. For Image 1, the frequency of occurrence in each of the given bins are as follows:

Bin	% of Image
below -10 dB	52.76%
-10 dB to -5 dB	32.98%
-5 dB to 0 dB	13.00%
0 dB to 5 dB	1.13%
5 dB to 10 dB	0.12%
above 10 dB	0.004%

Images which were thresholded are displayed in Figures 7 through 11. With a threshold of 10 dB (Figure 11), virtually all of the image is undetected. Only four areas in the image produce returns above 10 dB. The brightest returns come from industrial areas in the near range of the image west of the airport and from buildings at the airport which are just east of the runways. In the 5 dB to 10 dB range more of the industrial and urban clutter west of the airport is detected. In addition, hangars and other buildings east and south of the airport begin to appear. The inclusion of those pixels with NRCS values of 0 dB to 5 dB adds more urban man-made clutter to the scene, and radar facing shoreline areas in near range are distinguishable. From -5 dB to 0 dB, there is an increase in the amount of shoreline scatter and in the amount of scatter from forested areas in near range. All urban and industrial areas, as well as scattered buildings and billboards at the airport and around the airport, are visible. With the addition of the -10 dB to -5 dB NRCS values forested areas throughout the scene become distinguishable. The remaining backscatter coefficients have a value less than -10 dB and come from grassy fields, water, road, and runway areas of the image. The largest area of very low return in the image is produced by the airport grounds.

In general, about 14% of the image contain backscatter coefficients greater than -5 dB and only a small fraction of these are located on the airport grounds. Most of the strong returns (backscatter coefficients above +5 dB) are created in the urban and industrial areas to the west of the airport. The dihedrals, corners, and facets characteristics of cultural objects may produce strong backscatter. With an incidence angle in this part of the scene of approximately 45° (see Table 1), the returns from these targets are near their maximum (see Appendix B).

In Figure 12, the reflectivity map of Image 1 has been simulated for the depression angle of 3°. The procedure used to do this simulation is provided in Appendix C. From the reflectivity map that is created we see that the number of high returns has decreased. The returns from distributed scenes have fallen off dramatically and provide very weak backscatter. The absolute levels of the returns from cultural

targets were preserved, but are also expected to experience some reduction at this angle. The high returns in the image are associated with the industrial areas surrounding the airport. Returns from hangers, planes, trucks, and other airport equipment are low. Experimental data is provided for comparison in Appendix D.

Image 2

The SAR data shown in Figure 13 were collected of Willow Run
Airport during April of 1984 using HH-polarization and at incidence
angles which range from 36° to 64°. Willow Run is surrounded by a
variety of cultural targets and some forest and agricultural land. As
these data were acquired in early spring, we anticipate the effects of
leafless, budding trees and wet soil upon the NRCS values. Most crops
are not yet planted, leaving much of the agricultural fields reasonably
barren.

Table 4 and Figure 14 summarize the results of a clutter analysis
of 8.6% of the image. The areas selected are indicated on the Figure of
Image 2 found in Appendix A. Backscatter coefficients from the runways
and water areas are the lowest (less than -20 dB). Farmland, fields,
and forest areas produce backscatter which ranged between -20 dB to -10
dB, and, in general, established the background intensity for much of
the airport clutter scene. From the image histogram (Figure 15) we can
see that the mean NRCS for the image is approximately -10 dB and
approximately 64.5% of the data lies within 5 dB of this mean. Average
backscatter coefficients from most distributed targets have values less
than -10 dB and backscatter coefficients from cultural targets are -4 dB
and greater. The shoreline clutter has backscatter coefficients of -6
to -8 dB. By thresholding we determined the location of areas of
similar backscatter intensity within the image and also the percentages
of the image which are made up of specific clutter groups (Figures 16-20
and Table 4). For Image 2, 69.25% of the image has a NRCS below -10 dB.
This indicates that approximately 70% of the scene consists of returns
characteristic of water, runways, forest, fields, or grass. The other
31.5% of the image has values of -10 dB or greater and are categorized
as follows:

15

Bin	% of Image
Below -10 dB	69.25%
-10 dB to -5 dB	24.58%
-5 to 0	4.72%
0 dB to 5 dB	1.21%
5 dB to 10 dB	0.23%
above 10 dB	0.02%

Approximately 30% of the image consists of urban or industrial clutter, such as factories, houses, or parked vehicles. The strongest backscatter coefficients (10 dB and up) come from factories and urban areas just to the west of the airport in the near range of the image. In the 5 dB to 10 dB range we see an increase in the number of backscatter coefficients from the area west of the airport. In addition, man-made targets near the airport and in far range (east of the airport) begin to appear. These backscatter coefficients arise from the airport hangers and residential areas. From 0 dB to 5 dB we see an increase in the number of backscatter coefficients throughout the image. Many more backscatter coefficients can be distinguished in the urban and industrial areas of the image. In the -5 dB to 0 dB range hangars and planes at the airport become visible. The industrial plants surrounding the airport are clearly identifiable and urban point targets such as mobile homes, billboards, and bridges can be discerned. With the addition of the -10 dB to -5 dB bin all the man-made targets in the scene are visible, and we begin to also see backscatter coefficients from distributed targets at small incidence angles.

Image 3

The SAR data shown in Figure 21 were collected of the Ottawa International Airport, Ottawa, Canada during August 1984 using HH-polarization and at incidence angles which range from 39° to 64°. Ottawa Airport is surrounded by substantial fields and areas of forests. In August, we expect radar scattering from distributed targets to be enhanced since most crops and forests in this region are at their maximum growth stage at this time. Scattering from man-made or cultural targets would be expected to be the same.

Clutter analyses were performed on 7.1% of this image and the results are summarized in Table 5 and Figure 22. The areas selected for analysis are indicated on the Figure 3A of Appendix A. Backscatter coefficients from runway and water areas are quite low, while the coefficients from fields and forests are considerably higher than those backscatter coefficients from similar targets in Image 2. This is attributed to the increased leaf area present in the agricultural areas of Image 3 as well as the slight difference in incidence angle between the two images. From the image histogram (Figure 23) we can see that roughly 95% of the image backscatter coefficients occur between -20 dB and 0 dB. Very few backscatter coefficients exist above 0 dB or below -20 dB. This fits the agricultural nature of the scene. The specular surfaces have NRCS's of -20 dB or below, distributed targets have NRCS's of around -15 dB to 0 dB, and the cultural targets such as buildings and parked planes have values greater than 0 dB. Urban areas and shorelines have values similar to those of Image 2. For urban areas, NRCS is generally -3 dB and for shorelines it is -7 dB.

Approximately 40% of the image have backscatter coefficients below -10 dB. The 60% of the backscatter coefficients which measure -10 dB or above can be divided into the following 6 dB bins:

17

Bin	% of Image
below - 10 dB	40.69%
-10 dB - -5 dB	24.8%
-5 dB - 0 dB	32.4%
0 dB - 5 dB	1.8%
5 dB - 10 dB	0.29%
above 10 dB & up	0.03%

Figures 24 through 28 are of images which have been thresholded. In the 10 dB and above range there are few values. The backscatter which are received at this level come primarily from man-made clutter located northeast of the airport. In addition, some of the backscatter arise from within the airport grounds. These backscatter come from a building located at the end of the northeast runway and from fences located just to the east of the northwest/southeast runway. When backscatter coefficient of 5 dB or greater are included in the analysis much more of the cultural areas surrounding the airport come into view. Residential areas and large buildings can be detected. The number of returns from the area directly surrounding the image have also increased, but the total number of returns coming from airport clutter is still small compared to those coming from residential areas near the airport. With the addition of those backscatter coefficients of 0 dB and above all cultural areas clearly come into view. Buildings and targets around the airport are also well defined. The inclusion of the -5 dB to 0 dB range the forested areas of the image become discernable. With an exception of a small strip of forest located southwest of the airport, the forested areas of the scene can be delineated from fields, roads, and other smooth surfaces in the scene using these backscatter levels. With the inclusion of those backscatter levels between -10 dB and -5 dB, the strips of forest and shorelines southwest of the image become visible. All fields and roads in near range are also defined. As seen in the statistical summary and threshold images. Backscatter from the specular surfaces such as runways and grassy areas surrounding the runways have values of less than -10 dB.

18

Image 4

The SAR data shown in Figure 29 were collected of the Comox
Canadian Forces Base during August of 1983 using VV-polarization and at
incidence angles which ranged from 13° to 58°. The air force base is
located in British Columbia. Like Image 3, the data were collected
during the summer when forests, fields, and agricultural areas are at
the height of their growing season in this region. Roughly one third of
the image content is water, some wave motion is visible. An extensive
and prominent shoreline meanders throughout the entire image. The land
area is covered with forests. Most of the grass and agricultural fields
in the image lie in the vicinity of the air force base.

Nineteen percent of the image was sampled for the clutter analysis.
The areas which were selected are indicated on Image 4, found in
Appendix A. A general brightening of the image in near range can be
observed. This is attributed to specular backscattering effects of the
ocean at small incidence angles (Daley 1973, Masako et al 1986, Wright
1968) but may also be caused by a residue antenna effect. From the
statistical summary provided in Table 6 and Figure 30, the mean
backscatter coefficient from the ocean surfaces was -16 dB across the
whole image. The forest has a mean backscatter coefficient of -10 dB,
the runways of the airport have a mean backscatter coefficient of -20
dB, and the grassy areas and agricultural areas a backscatter
coefficient of about -13 dB. From the histogram (Figure 31) of the
entire image we can see that the mean backscatter coefficient is about
-8 dB and that approximately 67.5% of the image lies within 8 dB of the
mean. The high mean backscatter coefficient of Image 4 is due, in part,
to the returns from the land area and the specular backscatter
coefficient of the ocean in near range. As a result, the histogram does
not reflect the image composition as well as those of Images 1, 2, and 3.

The use of thresholding enabled us to analyze the sources of high
backscattering coefficients. In Image 4, 44.8% of the backscatter
coefficients are less than -10 dB. Those backscatter coefficients of
-10 dB and above can be broken down into the following bins:

19

Bin	% of Image
below -10 dB	44.8%
-10 dB - -5 dB	37.73%
-5 dB - 0 dB	12%
0 dB - 5 dB	5.3%
5 dB - 10 dB	.23%
above 10 dB	0.002%

Visual examination of the thresholded images (Figures 32 through 36)
shows us that about two-thirds of the data in the image have backscatter
coefficients of -10 dB and above, which comes from the specular effects
in near range. The remainder of the backscatter coefficients come from
the land mass area. There are very few man-made targets producing
backscatter coefficients above 10 dB. In the 5 dB to 10 dB bin there
are a few backscatter coefficients from the shoreline and a man-made
targets (including reflectors) around the airport. Backscatter
coefficients observed in the very near range (incidence angle of 12°)
are due to the specular nature of the ocean surface. A large number of
sea states will produce backscatter coefficients of this magnitude at
this incidence angle (Masako et al 1986, Wright 1968). When backscatter
coefficients in the range from 0 dB to 5 dB are added, more of the
shoreline and buildings around the airport can be seen. Four corner
reflectors are also detected. Planes are still not visible at this
stage but structures on the airfield are defined. With the addition of
-5 dB to 0 dB backscatter coefficients the shoreline which faces the
radar is fully delineated. Parts of the shoreline parallel to the look
direction of the radar are also defined. Buildings at the airport are
now clearly visible, and certain forested areas are also discernable.
At this stage, the distinction between forested and grassy areas are
apparent. When -10 dB to -5 dB backscatter coefficients are added
almost all important image content is present except for clutter in the
far range and the returns from short grass, fields, and runways. All
major man-made targets at the airport are detectable; for example, the
planes on the tarmac. In addition, the shoreline is well defined.

Specular returns from the ocean are very bright. When the image is transformed to an incidence angle of 87° the specular returns from the ocean vanish. Parts of the shoreline still yield bright returns and hard targets at the airport are still visible. Planes on the tarmac are difficult to distinguish at this angle. Their returns are low.

Image 5

The SAR data shown in Figure 37 were collected of the Willow Run Airport during April 1984 using VV-polarization and at incidence angles which ranged from 36° to 64°. As in Image 2, we expect to see the effects of springtime conditions. Unlike Image 2, however, Image 5 was recorded in VV-polarization so a comparison of the two images provides us with some insight into the differences in scattering which are caused by differences in polarization.

Table 7 and Figure 38 present the results of a clutter analysis of 10.1% of the image. The areas which were used for analysis are illustrated in Image 5 provided in Appendix A. Backscatter coefficients from this image are in most cases higher than backscatter coefficients from Image 2. This is summarized in Table 8. For distributed scenes, as the incidence angles increase from nadir the backscatter coefficients at HH-polarization decrease more rapidly than at VV-polarization. In this instance, the backscatter coefficients are about 5 dB lower for HH-polarization. In the case of the man-made targets and the urban areas, they also tended to show a decrease of about 3 dB. Backscatter coefficients from the near range of the image are generally high, they may be due to incidence angle effects. The image may also be somewhat saturated, as evidenced by the dark halos around the high reflectance areas. The backscatter coefficients from the water and runway areas are the lowest in the scene and all distributed natural targets have NRCS values less than -8 dB. Backscatter coefficients from man-made targets and shorelines are the strongest. A histogram of the entire image (Figure 39), shows that its mean is approximately -5 dB and most of the backscatter coefficients are within 5 dB of this mean.

Thresholding the image into 5 dB bins gives the following NRCS breakdown.

Bin	% of Image
below -10 dB	7.7%
-10 to -5 dB	41.75%
- 5 to 0 dB	29.41%
0 to 5 dB	13.26%
5 to 10 dB	6.49%
above 10 dB	1.38%

Thresholded images are provided in Figures 40-44. Unlike Images 1 through 4, Image 5 has only a small percentage of NRCS values below -10 dB and the majority of NRCS values in this image are in the -10 to -5 dB range. By analyzing where specific backscatter coefficients are in the image, the cause for the general increase in backscatter coefficient level may be determined. Backscatter coefficients with values above 10 dB are located in the very near range, with a few outlayers located in the urban and industrial areas west of the airport. In the range from 5 dB to 10 dB, we see an increase in the number of values from all land targets in the very near range. Some of the urban areas also become distinguishable and backscatter coefficients from buildings in the range can be seen. With the addition of backscatter coefficients of value 0 dB to 5 dB, most hard targets in the image are detected and buildings at the airport are defined. There is an increasing number of backscatter coefficients coming from near range. In the -5 db to 0 dB range, forested areas throughout the image are detected. The shorelines are distinguishable and buildings throughout the image are well defined. Farmland, water areas, runways and grassy fields are still undetectable. When backscatter coefficients from -10 dB to -5 dB are included, most of the image is defined. The overall image brightness is due to an enhancement in scattering due to polarization effects and possibly some saturation.

Image 6

The SAR data shown in Figure 45 were collected of the Victoria International Airport in British Columbia during July using 1983 VV-polarization and an incidence angle range from 25° to 60°. As these data were obtained in the summer we expect to see the effects of summertime conditions on the radar scatter of the image.

Table 9 and Figure 46 present the results of a clutter analysis of 2.5% of the image. Although this percentage is small, much of the image consists of water and small blocks of forests which could be characterized without as many clutter samples as were used for the other images. The areas used for analysis are illustrated in Appendix A. As in the earlier images, the clutter backscatter coefficients seem to separate themselves into two value groups. In this case, all the distributed targets have NRCS values less than -8 dB and all the point target-like features have σ values greater than -2 dB. The image shows some brightening in near range which is probably due to the specular nature of the ocean at this angle as in Image 4. The image histogram is given in Figure 47. The majority of the returns in the image lie between 0 dB and -10 dB. This is due in part to the backscatter coefficients from the farmlands, fields, and forest, and in part to the higher backscatter coefficients in near range.

The results of thresholding Image 6 are given in Table 3. They are:

Bin	% of Image
below -10 dB	32.15%
-10 to -5 dB	56.28%
- 5 to 0 dB	10.06%
0 to 5 dB	1.49%
5 to 10 dB	0.01%
above 10 dB	0.00%

The locations of the thresholded values are illustrated in Figures 48 through 52. No returns surpass the 10 dB threshold. In the 5 dB to

10 dB range a few values begin to show up in the vicinity of the airport. In the 0 dB to 5 dB range, there is an appearance of the specular backscatter coefficients from the ocean in near range. A number of backscatter coefficients appear along the shorelines in both near and far range, and a few values can be seen in the land area. In the -5 dB to 0 dB range, there is an increase in the number of NRCS values from the shoreline as well as an increase in specular values from the water. Most of the coast is defined and some backscatter coefficients appear in the forested area in the far range of the image. Throughout the land mass, the forests appear to be interspersed with roads and fields, so these NRCS values may be coming from the edges of clumps of trees. In this range, a few peculiarities in the image also show up. Vertical banding of the backscatter coefficients in far range may be due to turbulence during the collection flight. A horizontal band of NRCS values which can be detected not far from the near edge of the image may be a residual antenna effect. In the -10 dB to -5 dB range, all backscatter coefficients from the land are visible except those NRCS values from a few roads and the runways. Most of the water is still undetected. A horizontal band at the far edge of the image may also be a residual antenna effect.

Image 7

The SAR data shown in Figure 53 were collected of the Peconic River Airport in Long Island, New York during early September using VV-polarization and covers incidence angles from 43° to 72°. At this point in time, vegetation has probably ended its growth stage and may be in the process of drying. This image is unusual because there is a large variety of crop clutter.

Table 10 and Figure 54 present the results of a clutter analysis of 0.53% of the data. The areas which were used are illustrated in Appendix A. Once again the distributed targets are low, approximately -7 dB, while the point targets are higher. Two exceptions to this are the shoreline areas and parked autos. Shorelines may have lower returns since, being the edges of pond instead of oceans or rivers, they may not have the steep banks which produce the high returns. Parked autos may produce low returns since they are composed of curved surfaces which do not reflect all energy back to the radar. The image histogram in Figure 55 shows that the NRCS values are evenly distributed over the 0 dB to -25 dB range. Thresholding provides the following NRCS value distribution:

Bin	% of Image
below -10 dB	69.25%
-10 to -5 dB	18.66%
- 5 to 0 dB	11.99%
0 to 5 dB	0.29%
5 to 10 dB	0.01%
above 10 dB	0.00%

Approximately 90% of the image has backscatter coefficients of -5 dB or below. This fits with the agricultural nature of the image. We would not expect that the mean NRCS value from the image would be high because of the large number of crop fields in the image. The thresholding results are presented in Figures 56 through 60. There are no returns

26

above 10 dB and very few in the 5 dB to 10 dB bin. The NRCS values that do exist come from features along the runway, possibly runway lights, and from a few buildings in the airport area. In the 0 dB to 5 dB range, there is an appearance of an increased number of backscatter coefficients from the buildings at the airport. More runway lights can be seen and the calibration array is evident. Radar facing shorelines are existent and the edges of some brighter fields in near range can be seen. With the addition of backscatter coefficients from -5 dB to 0 dB, buildings at the airport are defined. Some of the fields located in near range are also visible. This may be an incidence angle effect. The incidence angles which are subtended by the image are from 43° to 72°. Around 60° to 65° the backscatter response of most crops and grasses tend to fall off quickly as compared to backscatter coefficients in the 25° to 60° range (Ulaby, 1986). With the addition of scatter in the -10 dB to -5 dB range, almost all of the fields in the nearest 1/3 of the image become visible, while runways, water, and fields in the far range are still undefined. The exception is an area in near range to the west of the airport. This area has a shape and structure similar to that of fields surrounding it but has extremely low returns. This area may be a flooded field.

Image 8

The SAR data shown in Figure 61 were collected of the Victoria
International Airport in British Columbia during July 1983 using HH-
polarization at an angle range of 16° to 60°.

Table 11 and Figure 62 present the results of a clutter analysis of
2% of the data. The areas which were used are illustrated in Appendix
A. The results of the analysis of Image 8 and Image 6 are very similar
to each other. There are a few exceptions. The NRCS values for the
water and runway areas of Image 8 are about 3 dB higher in Image 8 than
in Image 6 and the returns for the farmlands, wharf and shoreline are
about 4 dB lower in Image 8 than in Image 6. The differences in the
forest and farmland backscatter coefficients may be due to polarization
differences (Ulaby, 1986). A higher water NRCS value combined with
lower NRCS value from the wharf and the shoreline may indicate that the
ocean was rougher on the day the Image 8 was collected. A rougher sea
state would cause higher ocean backscatter coefficients and would also
decrease the dihedral reflection off of objects which lie at the water's
edge. A histogram of the image is presented in Figure 63. Most values
lie between 0 dB and -15 dB but a significant number of NRCS values
(15%) lie above 0 dB. The thresholded images, Figures 64 through 68,
illustrate the location of the backscatter coefficients. For Image 8 we
have

Bin	% of Image
below -10 dB	51.04
-10 to -5 dB	21.37%
- 5 to 0 dB	12.18%
0 to 5 dB	14.03%
5 to 10 dB	1.37%
above 10 dB	0.00%

In the 5 dB to 10 dB bin there are a few NRCS values from the near range
shoreline with the majority of the backscatter coefficients coming from

28

the near edge water areas. This effect echoes the specular water backscatter coefficients seen in Image 4 and is expected since the incidence angle to the near edge is 16°. In the 0 dB to 5 dB range the number of specular NRCS values from the near edge of the image are increased and more backscatter coefficients from radar facing shorelines are visible. A boat and a few buildings around the airport are also evident. In the -5 dB to 0 dB range, more of the far range shoreline and bright backscatter coefficients throughout the land area are evident. Except for a small bay to the north of the airport, all of the near range of the image is visible. In the -10 db to -5 dB range, most of the near range land area and both the and far range shoreline are defined. All buildings around the airport can be detected although the runways themselves still have few NRCS values. All the boats in the harbor are visible. A band of pixels at far range may be a residual antenna effect and a darkening of the areas around some of the buildings at the airport may indicate some small signal suppression.

In Images 4, 7, and 8 a general brightening of the images can be observed in near range. Some of the brightening effect in Images 4 and 8 is due in part to the specular effects of the ocean surface at low incidence angles (i.e., 12° for Image 4 and 16° for Image 8). But for Image 7 there is no ocean surface to provide a specular effect. Image 7 was then analyzed to find the cause of the bright returns in near range. Table 12 was created which shows the antenna depression angle used for each image, the range of incidence angles subtended by each image, and the degrees off of bore sight subtended by each image. The SAR antenna pattern is believed to be accurate within 15° of boresight (see Figure 69). Beyond this point, the shape of the antenna pattern was estimated based on the expected antenna pattern shape (i.e., antenna range measurements). In our processing sequence, the accuracy of the estimate is continually checked when data is calibrated. Radiometrically corrected data were compared to data measured using scatterometers to verify the correction. Image 7, as well as Images 4 and 8 are more than 30° off of boresight in their near range. The estimate of the antenna pattern function beyond 30° is probably lower than the actual antenna

29

pattern and hence when the images were radiometrically corrected, they were over-corrected in near range. This would cause the brightening in near range which is seen in Image 7 and somewhat in Images 4 and 8 where it is combined with specular effects.

For cross references purposes, Table 13 presents each image number and the figures and tables which correspond to it.

V. CLUTTER RESULTS BY CLUTTER TYPE

As discussed previously in Section IV, the second method of clutter analysis which was performed involved examining the characteristics of each clutter category within an image and then combining the clutter groups for images. This procedure allows the characterization of clutter for a generic airport scene. The method of analysis proceeded as follows. Clutter types in each image were determined, located, and then extracted. A statistical analysis was performed which included calculation of the mean, variance, standard deviation, and the fit of a probability density function. Areas of similar clutter type were merged and a histogram for each clutter type was generated. The mean and variance of each merged group was also calculated. The results of these analyses are described in the following sections.

a) Forest, Fields, Cropland, and Water

Presented in Figures 70-73 are the histograms of the merged subimages for forest, field, cropland, and water clutter. The histograms from each image are overlain with similar histograms from other images so that they may be compared.

The first observation which can be made is that the histograms from the similar clutter groups and from different images cluster together. Water returns cluster in a range from -35 dB to -10 dB with the exception of the water clutter of Image 5 which appears bimodal. This is probably due to the fact that the subimages which were extracted for analysis contained shoreline data as well. The field and farmland backscatter coefficients cluster between -30 dB and 0 dB. The exception here being Image 7 which has a much more uniform distribution of NRCS values. A visual examination of the image, as well as ground truth data, (Larson et al, 1985) attest to the variety of clutter in the scene, and this large variety of fields may contribute to Image 7's more uniform distribution. Forest backscatter coefficients cluster between approximately -25 dB and 5 dB.

In these four cases, the histograms within the clutter group have

31

the same basic shape. The means of the histograms are different because of the difference in incidence angle ranges used in the various images. Generally, clutter areas imaged at smaller incidence angles will have brighter returns. Polarization differences may also cause differences in the mean NRCS values among the images. The probability distribution functions for the water clutter group should be distinguishable from the distribution functions for the other clutter groups.

b) Roads and Runways

Histograms for clutter from the highway sub-images and the runway sub-images are presented in Figures 74 and 75. In general, the backscatter coefficients from both the roads and runways are low. The main group of runway clutter histograms lies in a range from -40 dB to -10 dB while a second group lies between -30 dB and 0 dB. The road clutter for Image 7 exhibits low backscatter coefficients which are characteristic for the larger incidence angles. The shapes of the histograms for the runway clutter areas are similar to those of farmlands and fields, but the means of the runway clutter sub-images are much lower in value. Differences in the mean NRCS values among the images are due to incidence angle and polarization effects.

c) Urban and Industrial Areas

Histogram for man-made distributed clutter scenes are given in Figures 76 through 78. The means of all groups are somewhat higher than that of natural distributed targets and the probability density functions for the man-made scenes are more Gaussian in nature than that of the natural scenes. The histograms for urban and plant areas are virtually identical, while the histograms for building clutter are more broad. Like the previous clutter groups, the differences in the mean NRCS values are due to differences in the incidence angle and polarization among the images.

There is a great deal of similarity between the histograms of the urban areas and those of the forest areas. This trend is illustrated in Figures 79 through 81. Each of these plots represents a comparison of

32

the histograms created by combining all sampled urban and forest areas within an image. The Willow Run images are used since they have large well documented areas of both urban and residential areas and forest. The similarity among the histograms is interesting and is attributed to the presence of trees in the residential and urban areas. Tree canopies often provide a strong backscatter return and absorb the radar energy preventing a contribution from potential dihedrals which form at the junctions of the walls of buildings and the ground. In the case of Image 2, (Figure 80), the means of the forrest and urban clutter are also very similar. For Images 1 and 5, (Figures 79 and 81), the mean values differ significantly. Since Images 1 and 5 were recorded with VV-polarization and Image 2 was recorded with HH-polarization, the differences between the mean values of the forest and urban areas for the images may be due to polarization effects.

d) Point Targets

In this section we have examined the histograms of man-made clutter in the images. It is the man-made objects which generally have the highest backscatter coefficients in the airport scenes and which will provide the largest sources of false alarms in a weather radar designed for wind burst detection. The histograms of several clutter scenes for man-made objects are illustrated in Figures 82 through 88. Most point target sub-images consist of a small cluster of pixels which surrounds a bright object. Windows sampling the man-made clutter sample low return background pixels as well. The histograms reflect the large variance of the data. The smallest bright targets, automobiles and point targets do not have well defined distribution functions (See Figures 82 and 83) because of the small number of points which could be sampled. Larger bright objects such as planes, piers, boats, bridges and docks (Figures 84 to 89) have distributions which are reasonably well defined. They do, however, exhibit some contamination from the surrounding clutter. This contamination is especially prominent in the pier clutter histogram for Image 8 and in the bridge clutter histograms for Images 2 and 5. The airplane clutter histograms appear to be bimodal in nature. A

33

main lobe at low dB values may be due to background pixels in the sub-images, whereas a smaller side lobe at larger dB values may actually represent those pixels which can be attributed to NRCS values from the planes. This is most evident in the histograms for Images 1, 2, and 5. Differences in mean NRCS for the hard targets are probably due to incidence angle effects in the images since polarization is generally unaffected by the types of man-made targets present in the data.

VI.   THE EFFECTS OF RADAR POLARIZATION ON CLUTTER

Optically processed synthetic aperture radar (SAR) images of Image 2 have been assembled to examine qualitatively the polarization properties of the clutter scene at and surrounding the airport. These images are illustrated in Figures 89, 90, and 91. In general, the contrast between the microwave signatures at X-band of the various natural clutter at each of the four linear polarizations is very similar. In addition, the backscatter levels between the like polarizations are very similar; the cross-polarized returns are typically 8 to 15 dB lower. The most dramatic demonstration of polarization effects was seen for the man-made objects. As in the case for natural clutter, there were only subtle differences between the like polarized signatures. At cross-polarization, however, nearly all the returns from the man-made objects were significantly suppressed; so much so that they were reduced to levels at or below the surrounding natural clutter.

Optical images were produced at three linear polarizations: VV (vertical-transmit and vertical receive), HH (horizontal-transmit and horizontal-receive) and VH (vertical-transmit and horizontal-receive). In the case of this analysis the various clutter scenes may be broken into the following categories:

(1) Runways and roads;
(2) Grass and croplands;
(3) Forest;
(4) Point sources, vehicles, and parked aircraft; and
(5) Buildings and plants.

Runways and roads produce very low backscatter and are of no concern. A significant portion of the airport grounds is in grass. In this analysis we will use grass as our grey scale baseline and reference the returns from the other clutter regions to this intensity. From these optically produced non-calibrated images, the calibrated digital images, and from literature, only minor differences exist in the cross-

sections of grass and cropland. Returns are relatively low compared to the more troublesome scatterers in the airport clutter scene. The like-polarized returns at VV and HH show that they produce similar backscatter contrasts, i.e., between the various fields and the forest. Forest and tree lines typically produce the strongest natural target returns. In general, for the natural clutter scenes operating at VV, HH, and VH, and HV polarizations produce similar types of backscatter responses. The greatest difference is that the cross-polarized returns are 8 to 15 dB lower than at like polarization.

In the case of the airport clutter scene, polarization effects are dramatic for man-made objects. Qualitatively one would indicate that the responses of these objects are similar for VV and HH polarizations. There are noticeable differences. Returns at HH-polarization appear to be greater, but this may be due to effects such as how the photographic image was processed. The image formed at cross-polarization illustrates the polarization properties of man-made clutter. Overall, the strong point scatterers which dominate the clutter scenes at like polarization are almost totally absent in the cross-polarized image. As an example, in the like polarized images Plant A shows thirteen rows of strong point-like scatterers. In the cross-polarized image the roof of the plant shows a uniform texture and no dominant scatterers. Furthermore, in the cross-pol image the returns from mobile homes at a mobile home park (these show up as well-organized, high-return, rectangular features) are only slightly different from the surrounding natural clutter. Scatter from billboards is absent and returns from the parked aircraft appear to be greatly reduced.

Note that system performance has a role. Cross-polarized returns from targets with strong like polarized backscatter coefficients may occur because the cross-polarization isolation of the transmit-receive antennas may not be high enough to prevent contamination from like-polarized returns.

VII. RESULTS AND CONCLUSION

The analysis of the eight images from ERIM's archives has provided us with some important information concerning clutter returns from airport scenes. Clutter backscatter responses for the same clutter type were very similar. Differences in their means were attributable to differences in incidence angle. Probability density functions which describe the scattering of a particular clutter type were nearly identical from image to image. This is an important result because it indicates a high degree of stability in the returns which would be expected from clutter around an airport. A Doppler radar set to detect microburst wind shear at one particular airport may not have to compensate radically for different clutter scene as the plane travels from airport to airport.

In all images the distributed targets such as forest, fields, runways, and residential areas rarely have a mean NRCS greater than -5 dB. Since most airports are placed on the outskirts of the cities they service, they would most likely be surrounded by these types of clutter.

Forest and urban residential areas are statistically similar, but have slightly different means (about 2 dB apart). This similarity is probably due to the presence of trees in the residential areas. Airports located in this type of area would not present a problem to a wind shear radar since the background clutter surrounding the airport would be of relatively low value. The effect of leaves in motion should, however, be considered.

Although only 2% to 3% of the data in each image is above 0 dB, most of this high return data is located in the immediate vicinity of the airport. These high returns would have the potential to interfere with windshear detection.

Through the analysis of these eight images we have gained information about the types and characteristics of radar clutter surrounding airports. There is much more to be done however. Further analysis of high clutter objects must be performed. The data analyzed here has shown that although only a fraction of the clutter surrounding

37

the airport is of an intensity to be of concern, almost all of it is located at the airport. A detailed analysis of the clutter from specific types of building, planes, and other airport vehicles should be performed. The motion of vehicles and planes should also be examined.

As anticipated, the data in the SAR archive did not have the breadth to fully describe the range of airport clutter scenes possible. This is, of course, the impetus behind Option 1 which is to collect additional clutter data using the NADC/ERIM P-3 SAR on a not-to-interfere basis during the calibration flights of the sensor, and Option 3 in which dedicated SAR data collections will be conducted. The archive has allowed us to begin to survey the clutter environment at a few selected airports. This information will be enriched by gathering data at smaller depression angles. Potentially, only three of the eight images selected will have depression angles as low as 10°. Digital data in the archive was collected at either VV or HH polarizations. Few simultaneous data sets were made with both polarizations. However, several data collections were made where optically processed data were collected at like and cross polarizations. Future collections will extend this to include VV, VH, HV, and HH, potentially. This is important in determining how the polarization properties of the clutter scene can be exploited beneficially to suppress the return from potentially troublesome scattering scenes. It has been determined by NASA LaRC personnel that an airport scene of 13 km x 13 km is optimum. Since the airports were used as a reference target or for calibration, a map composed of only one strip over the airport is typical. At present, it is possible to produce a 6 km x 13 km image using existing strip map data. The remainder of the scene may be filled in by a variety of techniques employed by NASA LaRC personnel. These may include folding the scenes about the airport or by filling in with an average background backscatter coefficient. Future data collections have been designed so that multiple passes are made and a full 13 km x 13 km scene is imaged. In addition, airports can be specifically selected for the type of clutter environment that they may present to a doppler radar. For example, the range of scenes may include an airport surrounded by

38

agricultural and urban areas (i.e., Willow Run), water (i.e., Logan), tall buildings due to immediate location to a city (i.e., JFK, San Francisco, and Logan), and mountains (i.e., Denver).

Every additional airport or urban image collected can provide us with more information about the radar clutter expected at an airport. The more information that we have about airport clutter the better we will be able to distinguish it from potentially fatal windshear clutter. This analysis has been but one step down this path. Hopefully many more steps will follow.

REFERENCES

Ament, W.S., MacDonald F.C., and Shewbridge R.D., Radar Terrain
Reflections for Several Polarizations and Frequencies, NOTS TP 2339,
Trans. 1959 Symposium on Radar Return, Part 2, University of New Mexico,
Albuquerque, 11-12 May 1969.

Bracalente, E.M., Britt C.L., and Jones W.R., Airborne Doppler Radar
Detection of Low Altitude Windshear, paper presented at The AIAA
Conference on Sensor and Measurement Techniques for Aeronautical
Application, Sept 7-9, 1988/Atlanta, GA. AIAA-88-4657.

Bush, T.F., Ulaby, F.T., and Metzler, T., (1975). Radar Backscatter
Properties of Milo and Soybeans, University of Kansas, RSL Technical
Report, 177-59.

Cosgriff, R.L., Peake, W.H. and Taylor, R.C., (1960). Terrain
Scattering Properties for Sensor System Design Engineering Experiment
Station Bulletin, Ohio State University, Vol. XXIX, No. 3.

Daley, J.C. (1973). Wind Dependence of Radar Sea Return, JGR Vol. 78,
No. 33, pgs. 7823-7833.

Guinard, N.W., and Daley, J.C., (1970). An Experimental Study of a Sea
Clutter Model, Proc. IEEE, vol. 58, pgs. 543-550.

Lyzenga, D.R., Maffett, A.L., and Shuchman, R.A., (1983). The
Contribution of Wedge Scattering to the Radar Cross Section of the Ocean
Surface, IEEE Transactions on Geoscience and Remote Sensing, Vol. GE-21,
No. 4, pgs. 502-505.

Masuko, H., Okamoto, K., Shinmada, M., and Niwa, S., (1986).
Measurements of Microwave Backscattering Signatures of the Ocean Surface
Using X Band and Ka Band Airborne Scatterometers, JGR Vol. 91, No. C11,
pgs. 13065-13083.

Ruck, G.T., Barrick, D.E., Stuart, W.D., and Krichbaun, C.K., (1970).
Radar Cross Section Handbook Plenum Press.

Sloknik, M.I., (1970). Radar Handbook, McGraw Hill Book Co.

Stiles, W.H., Ulaby, F.T., and Wilson, E., (1979). Backscatter of Roads
and Roadside Surfaces, RSL Technical Report 377-1, University of Kansas.

Ulaby, F.T., Moore, R.K., Fung, A.K., (1986). Microwave Remote Sensing,
Vol. III, From Theory to Applications, Artzch House.

Valenzuela, G.R., Laing, M.B., and Daley, C., (1971). Ocean Spectra for
the High-Frequency Waves from Airborne Radar Measurements, J. Marine
Res. 29, pgs. 69-84.

TABLE 1
AIRPORT CLUTTER SCENES ACQUIRED FROM ERIM SAR DATA ARCHIVE

NASA LaRC Image #	Date	Pass	Scene	Polarization	Depression Angle (°)	Incidence Angle Range (°)	Aircraft Flight Direction	Radar Look Direction
1	17 December 1984	4	Willow Run Airport Ypsilanti, Michigan	VV	22	45 to 73	South-bound	Left (East)
2	7 April 1984	4	Willow Run Airport Ypsilanti, Michigan	HH	28	36 to 64	North-bound	Right (East)
3	2 August 1984	4	Ottawa International Airport Ottawa, Canada	HH	24	39 to 64	South Southeast	Right (WSW)
4	3 August 1983	7	Comox CFB British Columbia, Canada	VV	42	12 to 58	Northeast	Left (NW)
5	7 April 1984	3	Willow Run Airport Ypsilanti, Michigan	VV	28	33 to 63	North-bound	Right (East)
6	25 July 1983	1	Victoria International Airport British Columbia, Canada	VV	40	25 to 60	North-bound	Left (West)
7	7 September 1984	1	Peconic River Airport Long Island, N.Y.	HH	15	43 to 72	Northwest	Right (NE)
8	26 July 1983	2	Victoria International Airport British Columbia, Canada	HH	40	16 to 60	South-bound	Right (West)

TABLE 2
STATISTICAL SUMMARY
IMAGE 1 - X1395

Category	Mean (dB)	STD/Mean (dB)	Min. (dB)	Max. (dB)	Number of Points
Urban	-8.26	4.85	-45.00	19.07	76,245
Interchange	-11.30	1.28	-45.00	5.90	68,753
Automobile	4.65	2.24	-15.33	8.56	396
Hanger	-5.86	2.73	-15.37	18.11	11,205
Tarmac	-8.58	4.35	-15.33	16.12	5,529
Runway	-17.92	0.98	-45.00	-5.96	3,477
Water	-18.57	1.20	-45.00	-6.40	88,917
Shoreline	-3.87	4.04	-45.00	18.17	2,121
Forest	-8.76	0.74	-45.00	3.74	14,661
Plant	-5.34	6.39	-45.00	22.76	180,330
Field	-14.30	0.61	-45.00	-2.19	257,166
Farm	-12.56	2.61	-45.00	-1.11	134,199

TABLE 3

PERCENTAGE OF OCCURRENCE OF RADAR BACKSCATTER COEFFICIENTS WHICH FALL WITHIN 5 dB INTERVALS FOR EACH AIRPORT SCENE

Image #	Date	below -10 dB	-10 to -5 dB	-5 to 0 dB	0 to 5 dB	5 to 10 dB	above 10 dB
1	17 December 1984	52.76%	32.98%	13.00%	1.13%	0.12%	0.004%
2	7 April 1984	69.25%	24.58%	4.72%	1.21%	0.23%	0.02%
3	2 August 1984	40.69%	24.80%	32.42%	1.78%	0.29%	0.03%
4	3 August 1983	44.80%	37.73%	12.00%	5.27%	0.23%	0.002%
5	7 April 1984	7.70%	41.75%	29.41%	13.26%	6.49%	1.38%
6	25 July 1983	32.15%	56.28%	10.06%	1.49%	0.01%	0.00%
7	7 September 1984	69.05%	18.66%	11.99%	0.29%	0.01%	0.00%
8	26 July 1983	51.04%	21.37%	12.18%	14.03%	1.37%	0.00%

TABLE 4

STATISTICAL SUMMARY
IMAGE 2 - X944

Category	Mean (dB)	STD/Mean (dB)	Min. (dB)	Max. (dB)	Number of Points
Bridge	4.10	5.43	-40.42	21.82	1,800
Building	-2.50	7.55	-40.35	20.83	16,200
Farmland	-14.07	2.27	-39.75	9.70	391,000
Field	-14.38	-0.19	-39.89	-3.44	134,000
Forest	-12.46	0.72	-39.70	1.17	341,300
Plant	-2.19	10.19	-40.62	30.15	262,500
Prkd Plns	-3.07	4.95	-40.13	12.01	1,000
Pt. Target	3.96	0.85	-13.96	10.77	125
Runway	-21.66	0.69	-39.95	-12.79	4,500
Shoreline	-6.59	0.95	-40.04	3.36	1,800
Urban	-3.64	7.77	-40.92	24.40	67,500
Water	-26.50	2.72	-39.77	-11.54	215,000

TABLE 5
STATISTICAL SUMMARY
IMAGE 3 - X1084

Category	Mean (dB)	STD/Mean (dB)	Min. (dB)	Max. (dB)	Number of Points
Building	0.12	2.25	-39.78	11.16	4,025
Field	-11.52	2.87	-39.79	9.99	601,600
Forest	-4.33	1.03	-40.30	9.82	386,400
Plant	-0.07	7.09	-40.27	23.48	37,800
Prkd Plns	3.46	7.68	-39.62	23.00	1,380
Runway	-20.57	2.13	-39.78	-9.87	7,000
Shoreline	-7.57	2.31	-39.57	4.65	2,400
Urban	-5.58	9.53	-39.83	22.66	106,000
Water	-20.86	2.19	-39.63	-8.94	39,550

TABLE 6
STATISTICAL SUMMARY
IMAGE 4 - X952

Category	Mean (dB)	STD/Mean (dB)	Min. (dB)	Max. (dB)	Number of Points
Building	1.13	3.12	-38.85	14.66	20,310
Field	-12.52	0.56	-38.72	0.41	88,000
Forest	-10.57	1.26	-38.55	5.15	265,000
Runway	-19.68	1.80	-39.01	-5.93	19,350
Shoreline	-6.48	0.10	-35.69	2.01	7,100
Water	-16.10	0.72	-39.94	-3.45	1,910,000

TABLE 7

STATISTICAL SUMMARY
IMAGE 5 - X1404

Category	Mean (dB)	STD/Mean (dB)	Min. (dB)	Max. (dB)	Number of Points
Bridge	5.91	5.00	-40.17	22.78	1,800
Building	1.10	4.10	-40.11	18.23	6,800
Farmland	-9.22	1.30	-39.66	6.68	367,500
Field	-9.56	0.45	-39.74	2.91	259,000
Forest	-8.06	0.97	-39.61	8.01	342,000
Plant	-3.27	8.71	-40.24	26.82	180,500
Prkd Plns	-0.62	6.93	-39.96	18.71	1,125
Pt. Target	11.36	-3.96	6.60	13.85	54
Runway	-13.18	1.05	-39.76	-3.45	3,600
Shoreline	-2.12	1.88	-39.84	9.54	1,800
Urban	-0.04	7.23	-40.56	27.22	67,500
Water	-9.65	1.80	-40.20	3.61	454,000

53

TABLE 8
STATISTICAL SUMMARY
IMAGE 2 & IMAGE 5

Category	(HH - Pol) Image 2 Mean (dB)	(VV - Pol) Image 5 Mean (dB)	VV - HH (dB)
Bridge	4.10	5.91	1.8
Building	-2.50	1.10	3.6
Farmland	-14.07	-9.22	4.9
Field	-14.38	-9.56	4.8
Forest	-12.46	-8.06	4.4
Plant	- 2.19	-3.27	-1.1
Prkd Plns	-3.07	-0.62	2.5
Pt. Target	3.96	11.36	7.4
Runway	-21.66	-13.18	8.48
Shoreline	-6.59	-2.12	4.47
Urban	-3.64	-0.04	3.6
Water	-26.50	-9.65	16.85

TABLE 9
STATISTICAL SUMMARY
IMAGE 6 - X931

Category	Mean (dB)	STD/Mean (dB)	Min. (dB)	Max. (dB)	Number of Points
Building	-1.29	4.31	-26.22	13.21	4,800
Docks	-1.67	3.95	-40.27	11.13	200
Farmland	-8.51	0.25	-39.91	2.10	2,000
Field	-9.82	0.55	-40.15	0.52	60,000
Forest	-8.42	1.49	-40.30	5.96	295,925
Pier/Wharf	-1.90	6.17	-39.94	17.69	2,280
Pt. Target	13.40	1.01	-6.80	20.21	125
Runway	-15.06	0.91	-40.19	-6.06	5,900
Shoreline	0.79	0.31	-34.00	9.21	1,175
Water	-17.46	1.76	-39.62	-6.54	35,000

TABLE 10
STATISTICAL SUMMARY
IMAGE 7 - X1137

Category	Mean (dB)	STD/Mean (dB)	Min. (dB)	Max. (dB)	Number of Points
Building	-0.64	4.72	-31.90	15.45	840
Farmland	-7.87	0.39	-37.32	1.96	9,800
Field	-15.15	0.55	-37.10	-5.04	33,500
Forest	-15.77	1.04	-37.37	-5.26	18,400
Highway	-29.63	0.45	-37.02	-23.07	100
Prkd Autos	-6.79	1.83	-26.87	0.65	50
Pt. Target	16.96	2.28	-15.64	25.31	100
Runway Light	1.21	-0.76	-8.47	5.49	18
Road Sign	-1.64	-0.82	-19.25	3.49	16
Runway	-21.82	0.61	-37.17	-12.13	3,875
Shoreline	-8.17	0.42	-22.78	-2.41	180
Water	-25.79	1.45	-37.06	-15.05	21,300

TABLE 11
STATISTICAL SUMMARY
IMAGE 8 - X946

Category	Mean (dB)	STD/Mean (dB)	Min. (dB)	Max. (dB)	Number of Points
Boat	5.47	0.76	-11.42	15.36	450
Building	-1.78	3.75	-32.63	12.86	4,675
Farmland	-12.38	0.43	-41.29	-1.72	20,000
Field	-9.64	0.52	-41.72	1.69	45,000
Forest	-8.76	1.57	-41.94	8.75	278,125
Pier/Wharf	-6.06	5.99	-41.10	11.34	600
Pt. Target	12.51	1.30	-9.57	19.64	125
Runway	-12.47	0.65	-41.78	-1.96	13,500
Shoreline	-3.49	0.34	-32.71	4.02	1,050
Urban	-3.85	3.29	-42.54	12.61	7,500
Wake	-9.02	0.37	-40.53	-1.49	650
Water	-14.44	-0.30	-40.91	-7.73	25,000

TABLE 12

ANTENNA DEPRESSION ANGLE
AND IMAGE INCIDENCE ANGLE
INFORMATION

Image	Antenna Depression Angle (Deg)	Incidence Angle (Deg)	Angle off of Boresight (Deg)
1	22	45 - 73	-23° - 5°
2	28	36 - 64	-26° - 2°
3	24	39 - 64	-27° - 2°
4	42	12 - 58	-36° - +10°
5	28	33 - 63	-29° - +1°
6	40	25 - 60	-25° - +10°
7	15	43 - 72	-32° - -3°
8	40	16 - 60	-34° - +10°

TABLE 13

CROSS REFERENCE TABLE IMAGES 1 THROUGH 8

Image #	SAR Image Figure #	Statistical Table #	Bar Chart Figure #	Histogram Figure #	σ^0 Step Figure #	PDF Figure #	Appendix Figure #	Appendix Table #
1	X1395	#2	#5	#6	7-11	70, 71, 72 73, 74, 76 77, 78	A-1, C-6	A-1
2	X944	#4	#14	#15	16-20	70, 71, 72 73, 74, 76 77, 78	A-2, C-7	A-2
3	X1084	#5	#22	#23	24-28	70, 71, 73 74, 76, 77 78	A-3, C-8	A-3
4	X952	#6	#30	#31	32-36	70, 71, 73 74, 78	A-4, C-9	A-4
5	X1404	#7	#38	#39	40-44	70, 71, 72 73, 74, 76 77, 78	A-5, C-10	A-5
6	X931	#9	#46	#47	48-52	70, 71, 72 73, 74, 78	A-6, C-11	A-6
7	X1137	#10	#54	#55	56-60	70, 71, 72 73, 74, 75 78	A-7, C-12	A-7
8	x946	#11	#62	#63	64-68	70, 71, 72 73, 74, 76 78	A-8, C-13	A-8

15765 m

2488 m

5935 m

Target Area

6000 m

1880 m

31°

10°

11.8 km

4.8 km

9 km

NEAR RANGE-

13.8 km

Vertical View

0.524 m

3°

10 km

Side View
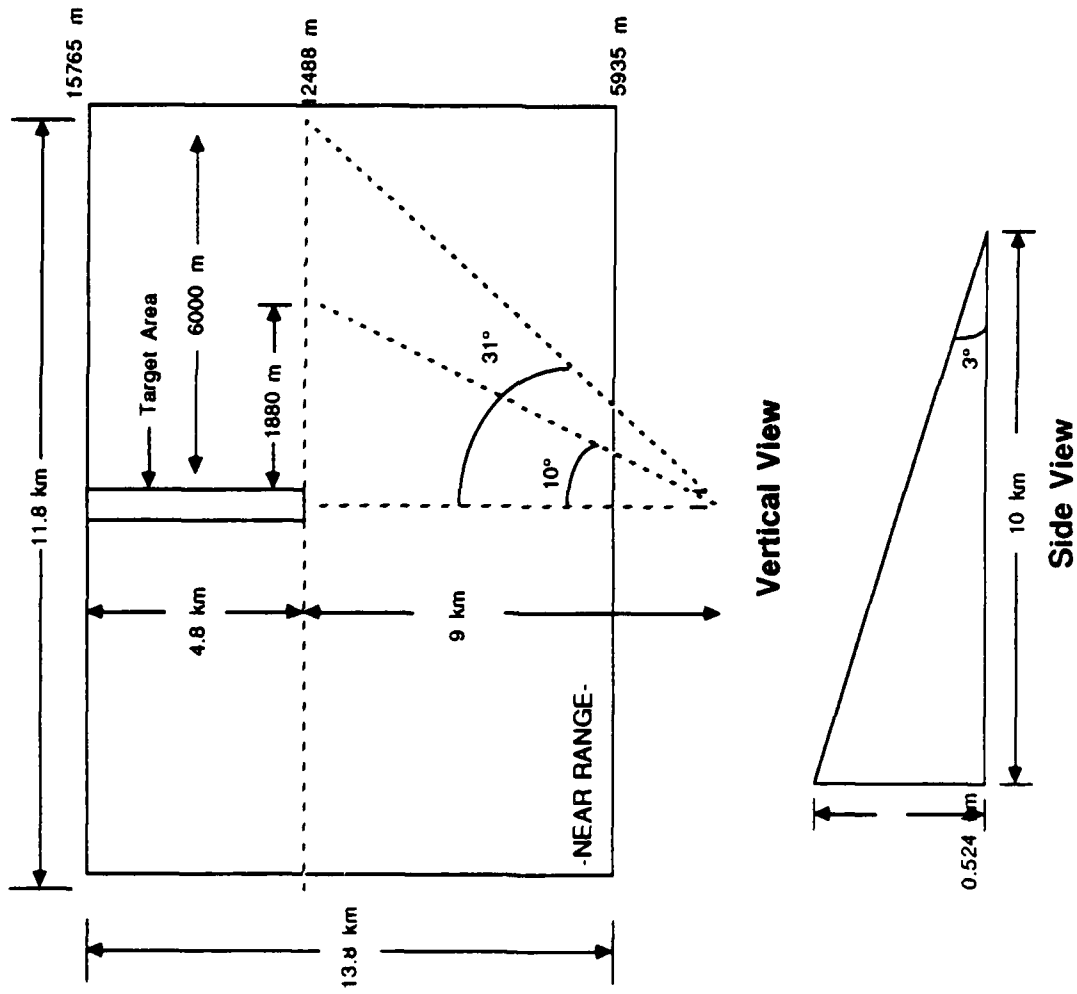
Desired Resolution: 21 m x 21 m

Figure 1.   Image Geometry
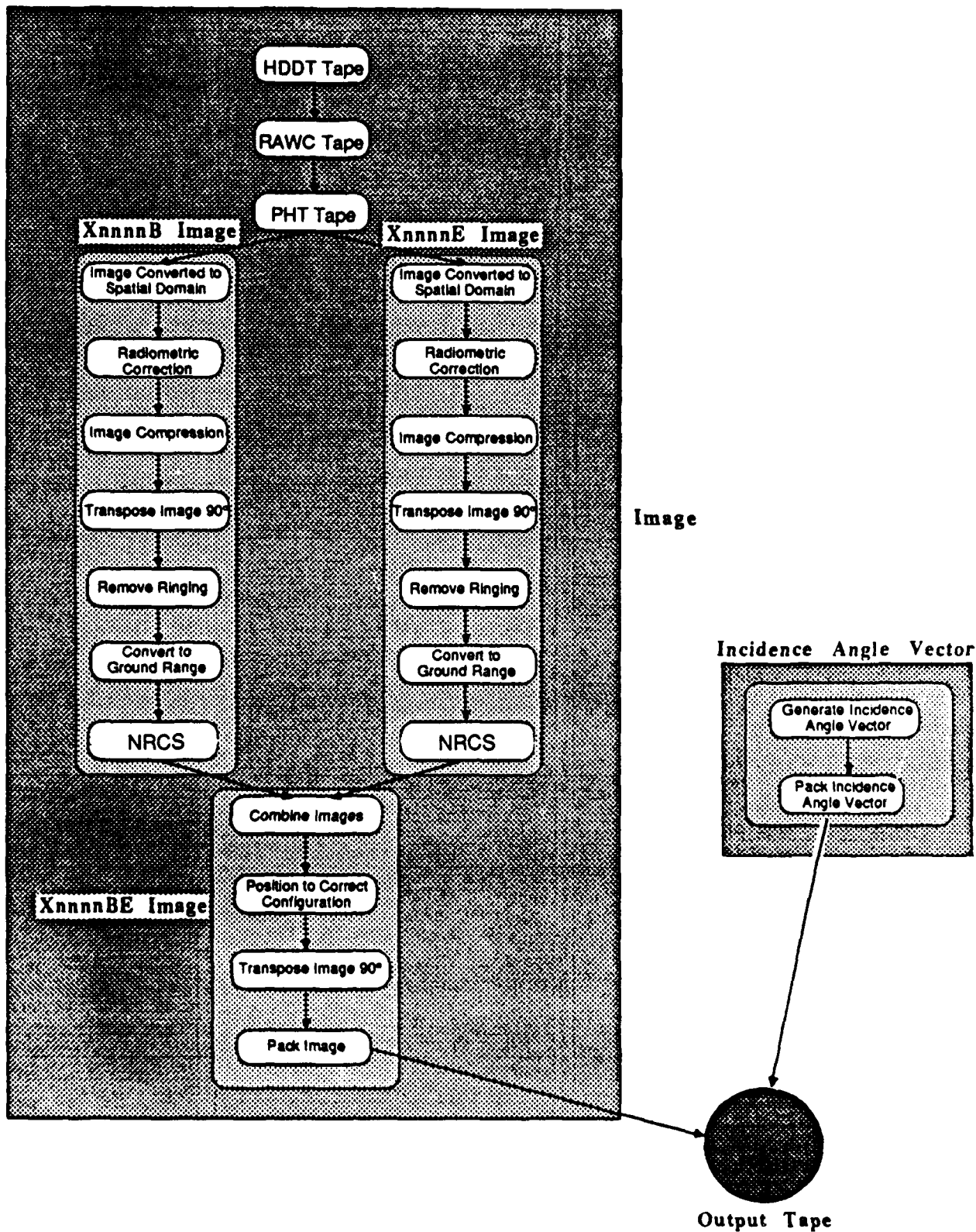
Figure 2.   Flowchart Showing Image Processing Sequences

P$_1$ (dB)

Slope = 1

K = System Gain Function of the Radar

Theoretical Radar Cross Section (dB)
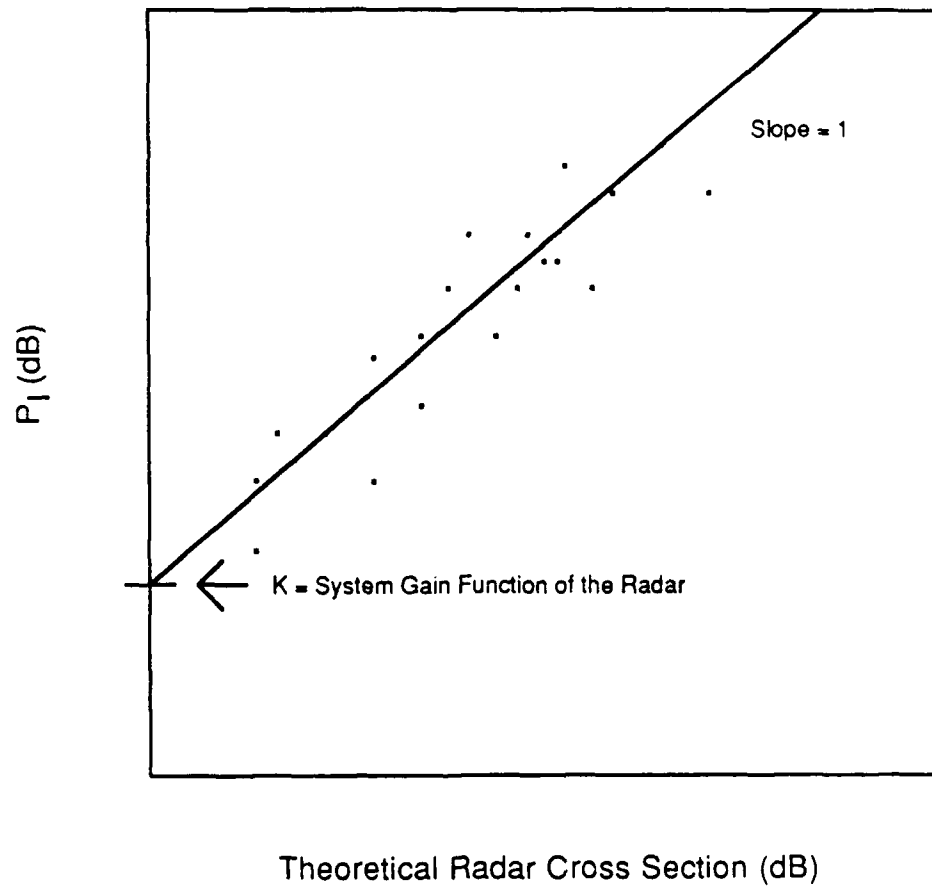
Figure 3. Determination of System Gain Function
from Reference Targets

71

N →
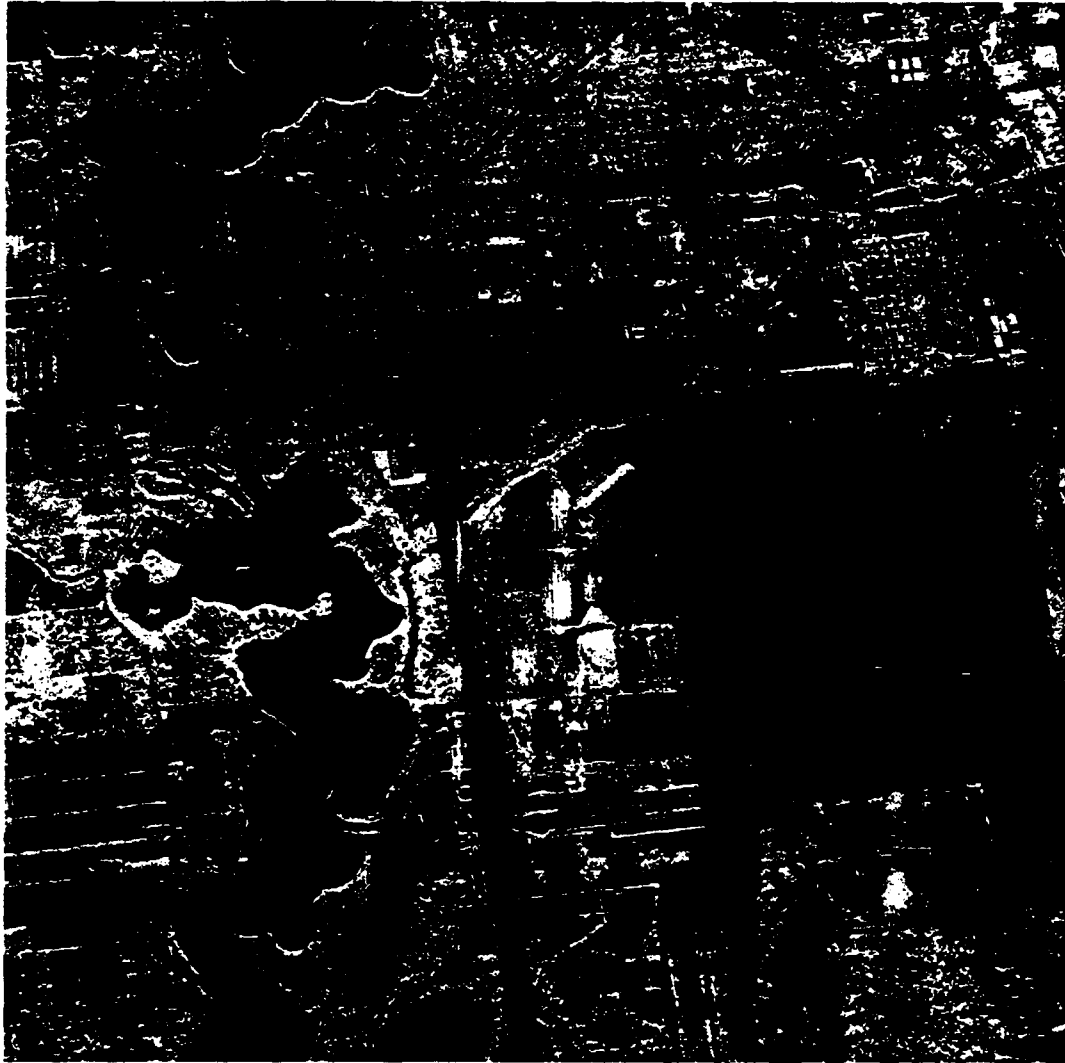
89-11292

1117 m
0

0   1072 m

Figure 4.   Willow Run Airport Observed December 1984
             Using VV Polarization - Image 1
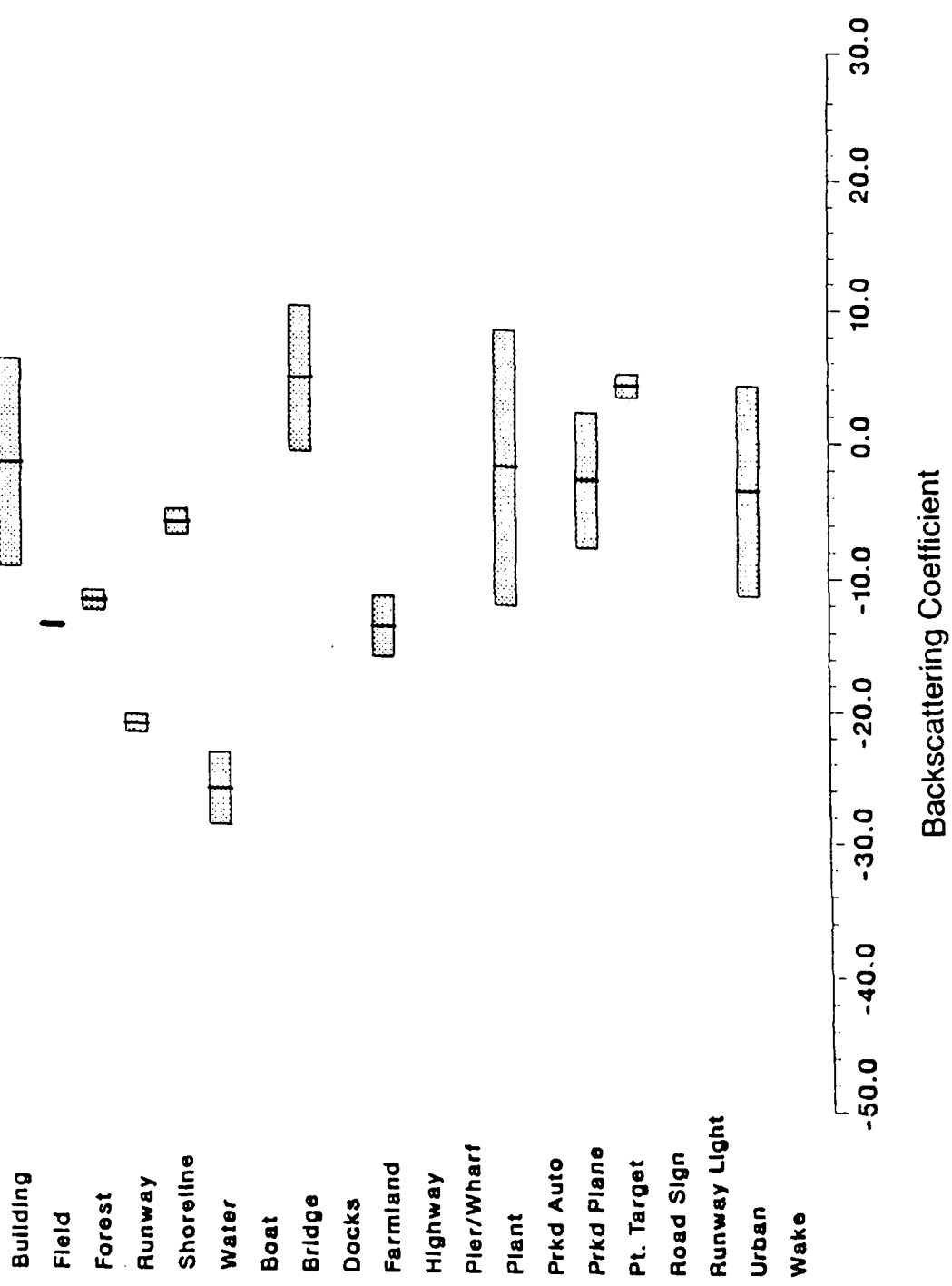
Figure 5. Image 1 Bar Chart Presentation of Means and Standard
Deviation for a Variety of Airport Clutter Scenes

75
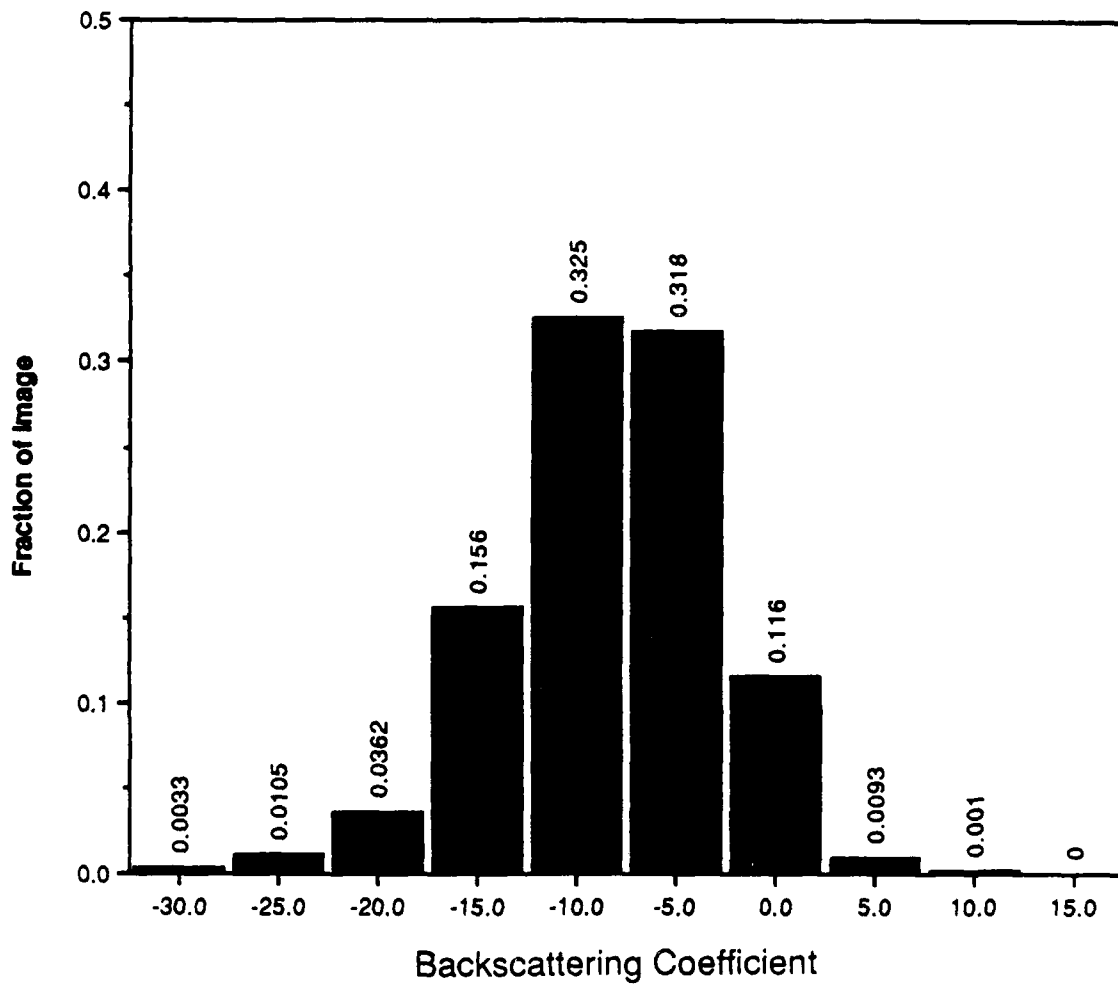
**Figure 6.   Histogram of Radar Scattering Cross-Sections for Image 1**

89-11872

89-11254-19

Figure 7. Image 1: -10 dB Threshold

79

89-11873

Figure 8.   Image 1: -5 dB Threshold

88-1125-4-24

81
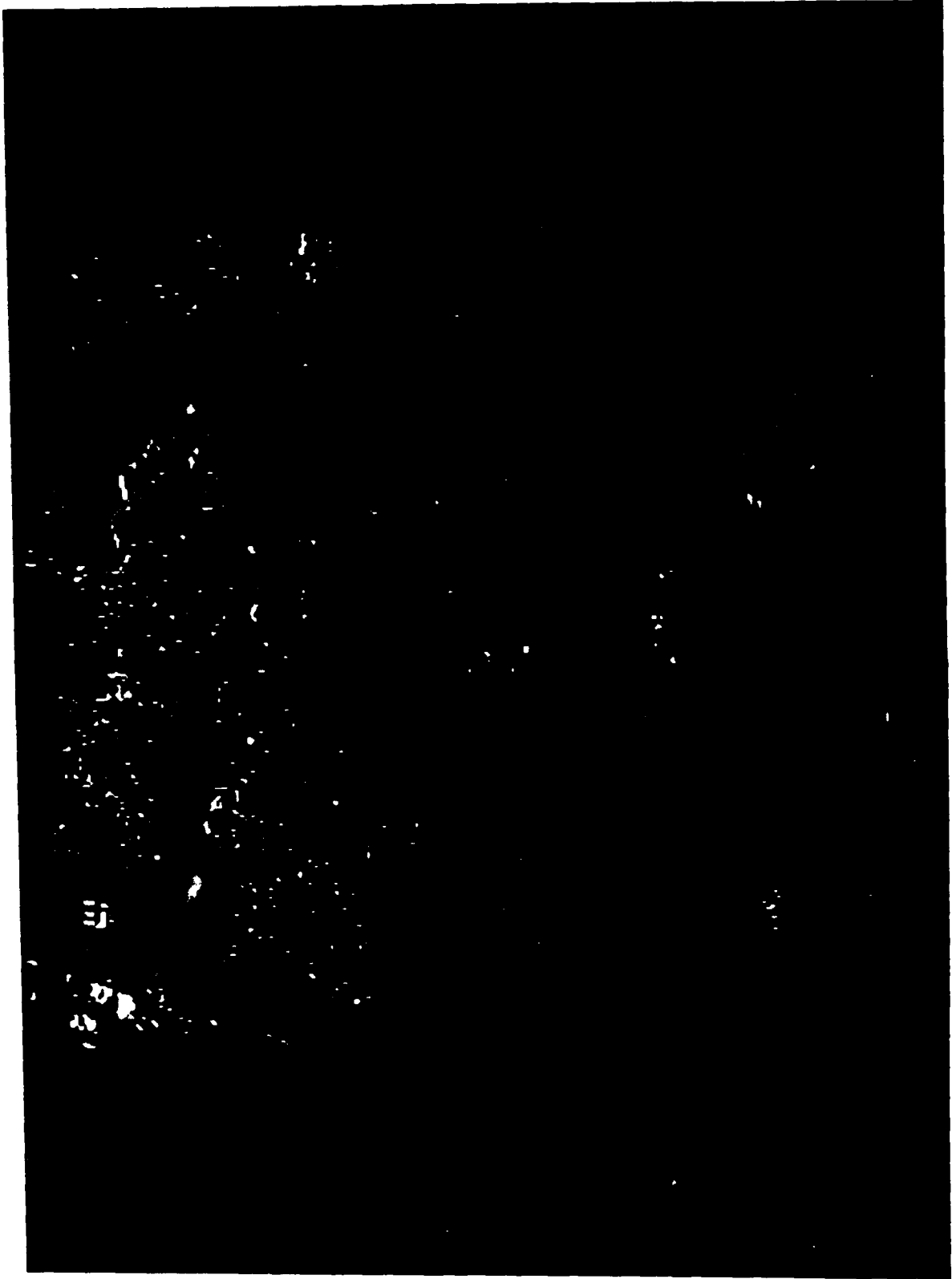
89-11874

88-1125-4-27

Figure 9.   Image 1: 0 dB Threshold
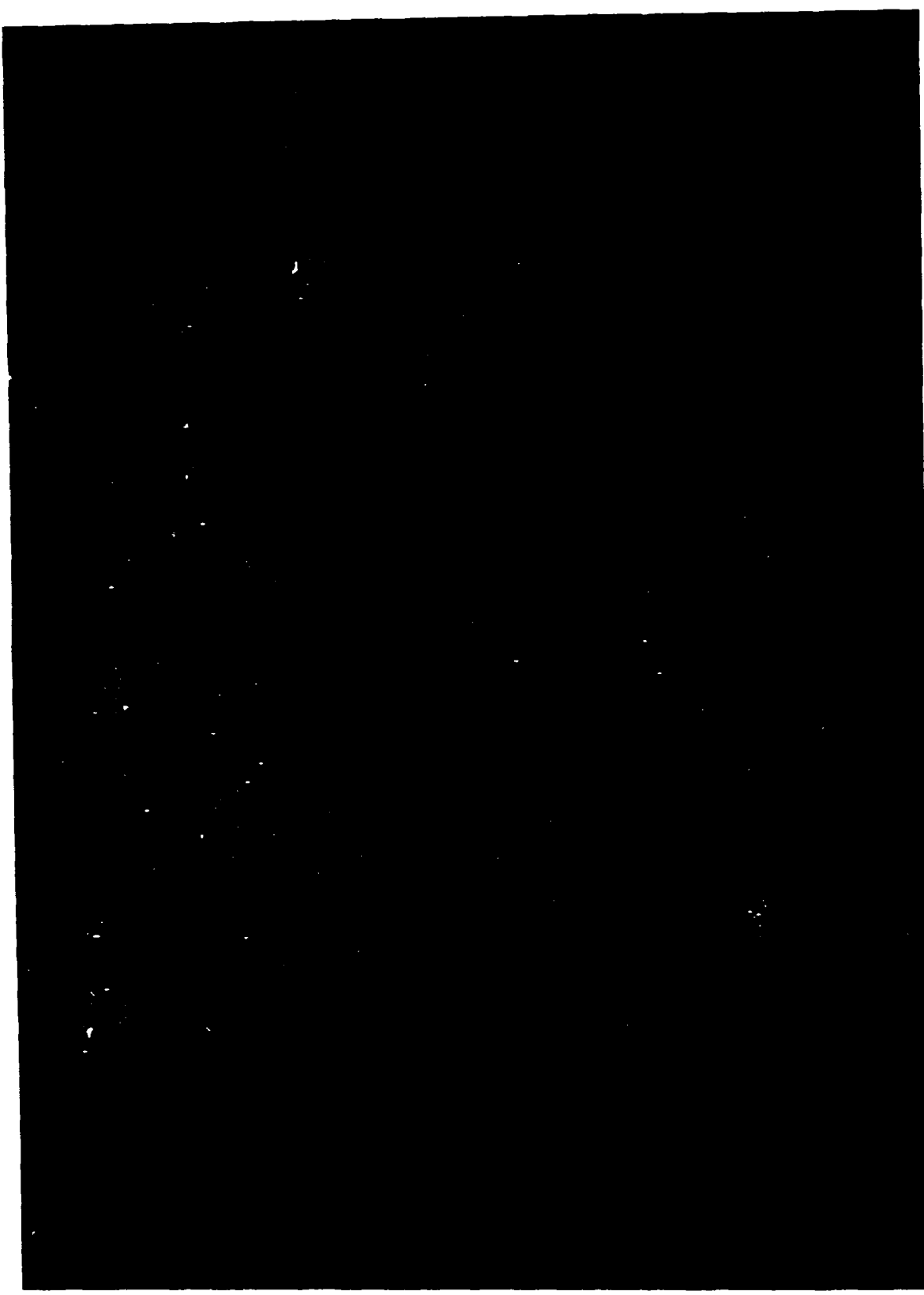
Figure 10. Image 1: 5 dB Threshold

89-11876
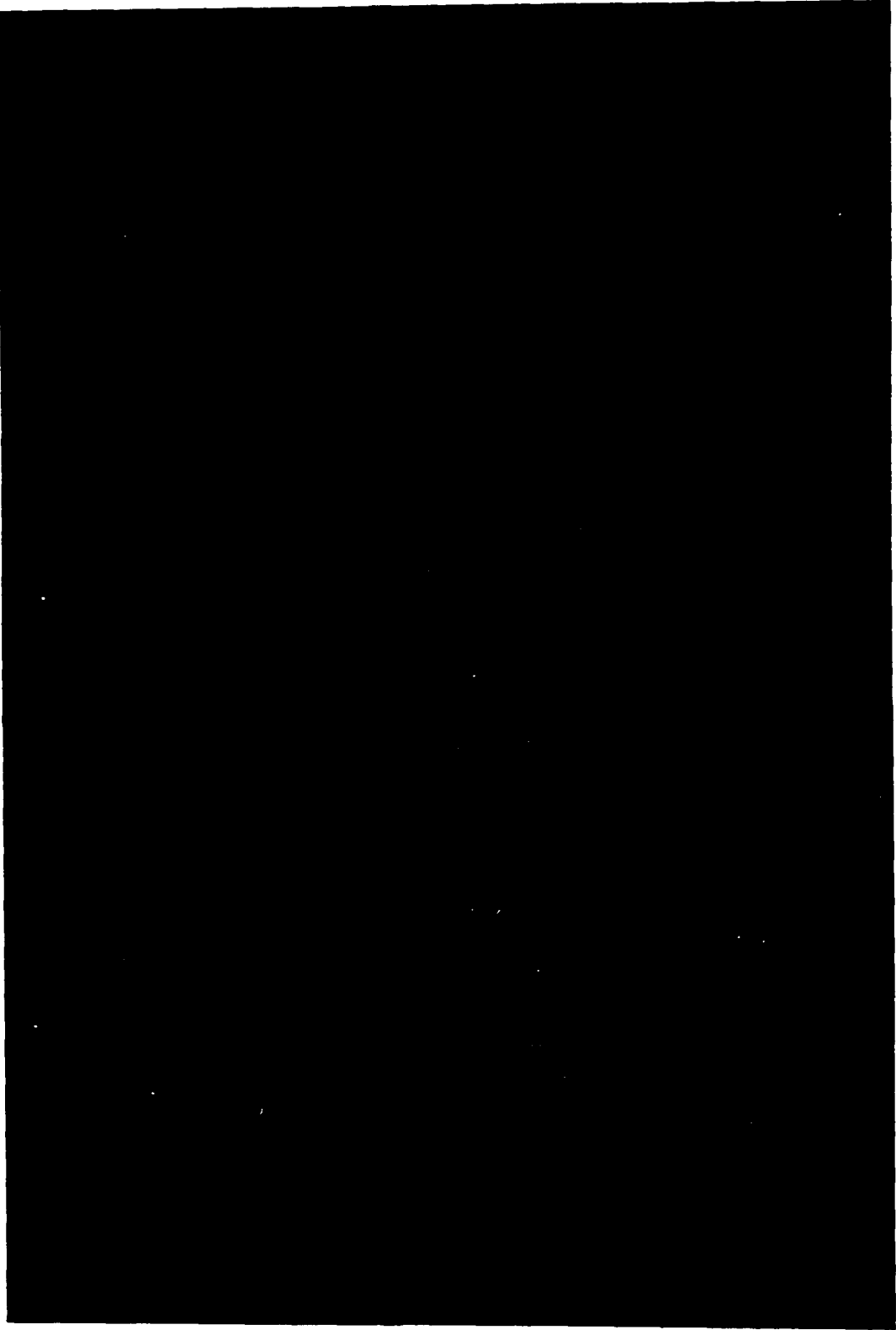
88 11254 33

Figure 11. Image 1: 10 dB Threshold

(a) Image 1

(b) Image 1 - Simulated at 87°

Figure 12. Backscatter Coefficients in Image 1 were Scaled to Produce a Simulated Radar Reflectivity Map at an 87° Incidence Angle

→ N

89-11848

1117 m

0   1072 m

Figure 13.   Willow Run Airport Observed April 1984 Using
HH Polarization - Image 2

Building
Field
Forest
Runway
Shoreline
Water
Boat
Bridge
Docks
Farmland
Highway
Pier/Wharf
Plant
Prkd Auto
Prkd Plane
Pt. Target
Road Sign
Runway Light
Urban
Wake

-50.0 -40.0 -30.0 -20.0 -10.0 0.0 10.0 20.0 30.0

Backscattering Coefficient
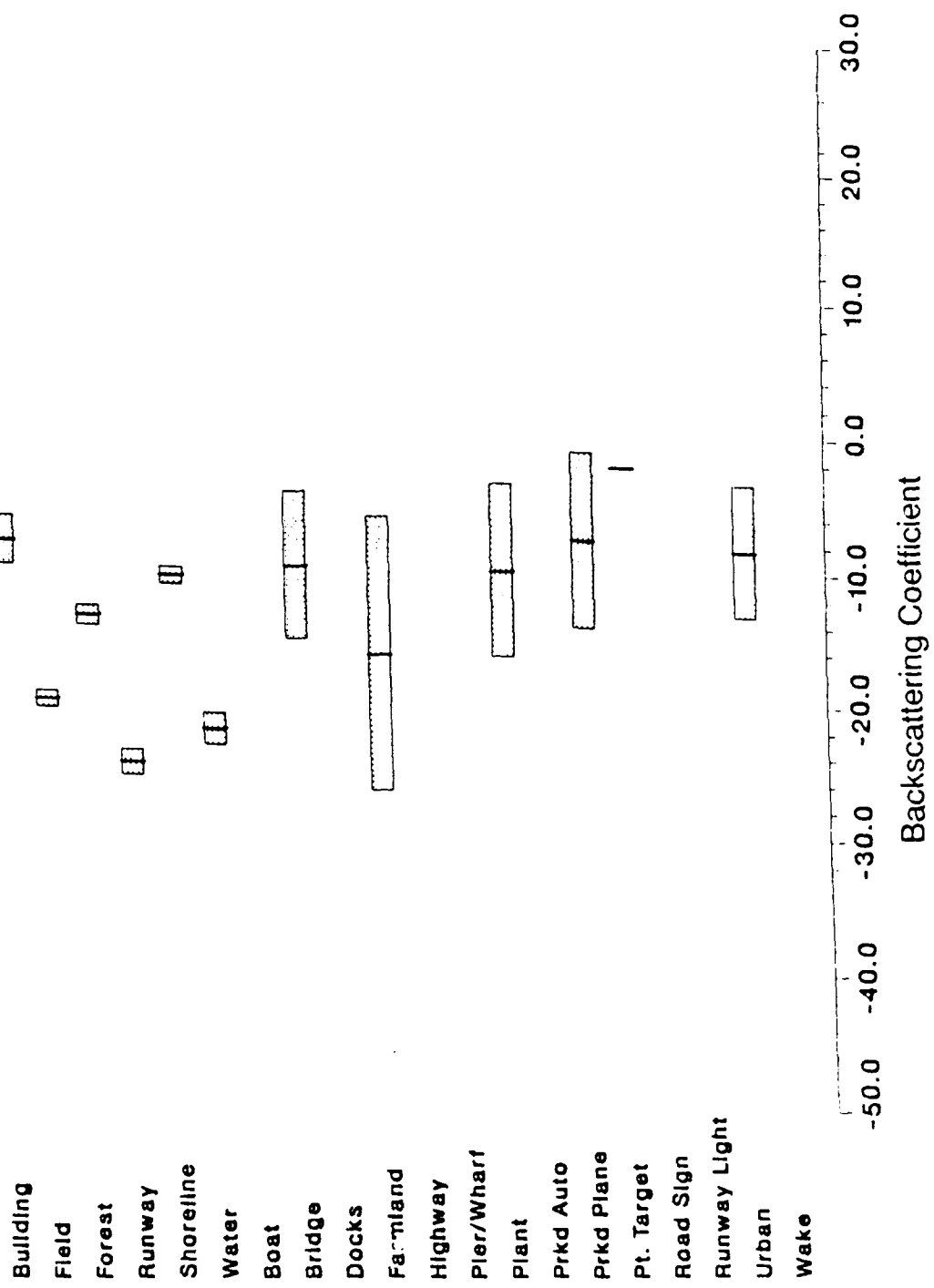
Figure 14.   Image 2 Bar Chart Presentation of Means and Standard
Deviation for a Variety of Airport Clutter Scenes

93
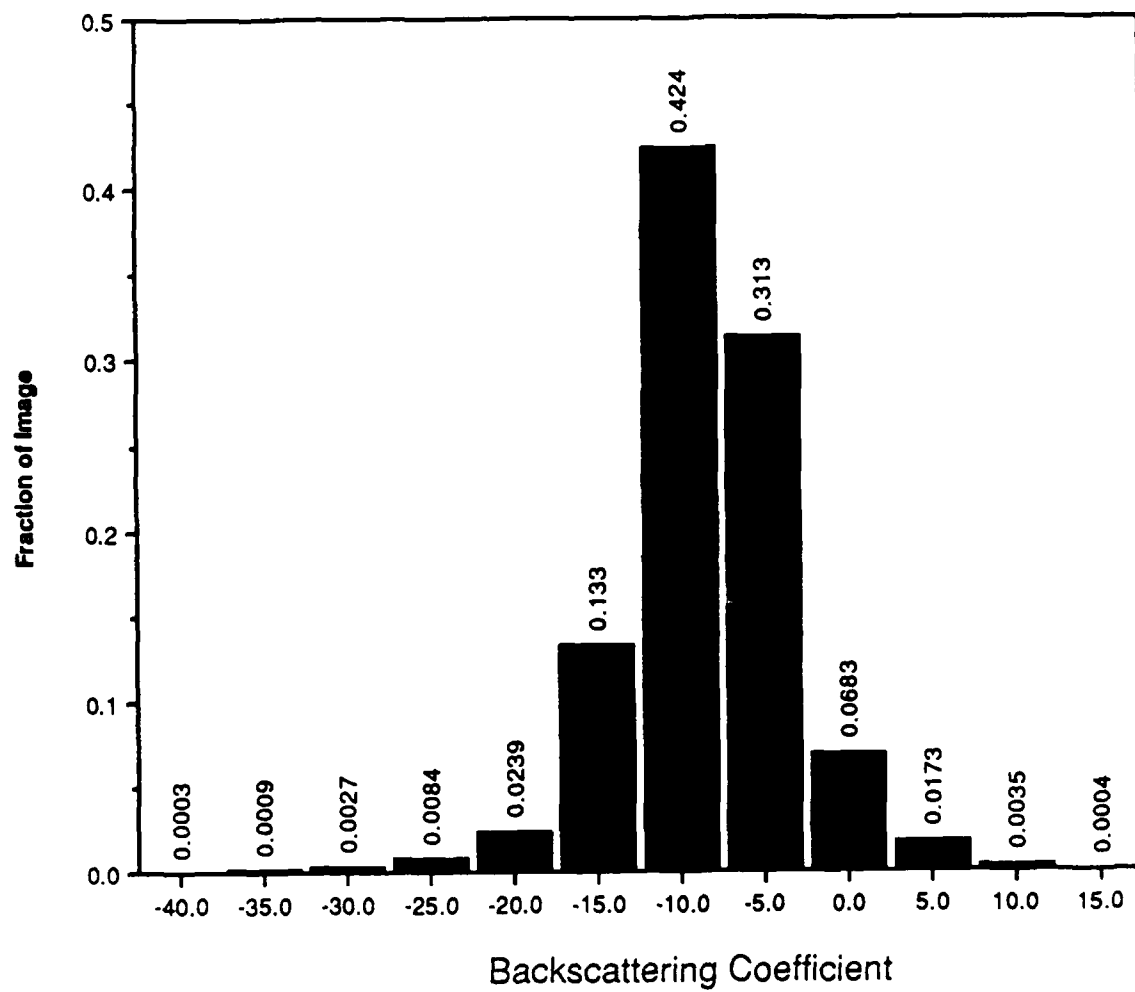
Figure 15.   Histogram of Radar Backscatter Coefficents for Image 2

Figure 16. Image 2: -10 dB Threshold

89-11878

89-11254-34

Figure 17. Image 2: -5 dB Threshold

89-11879

88-11254-36A
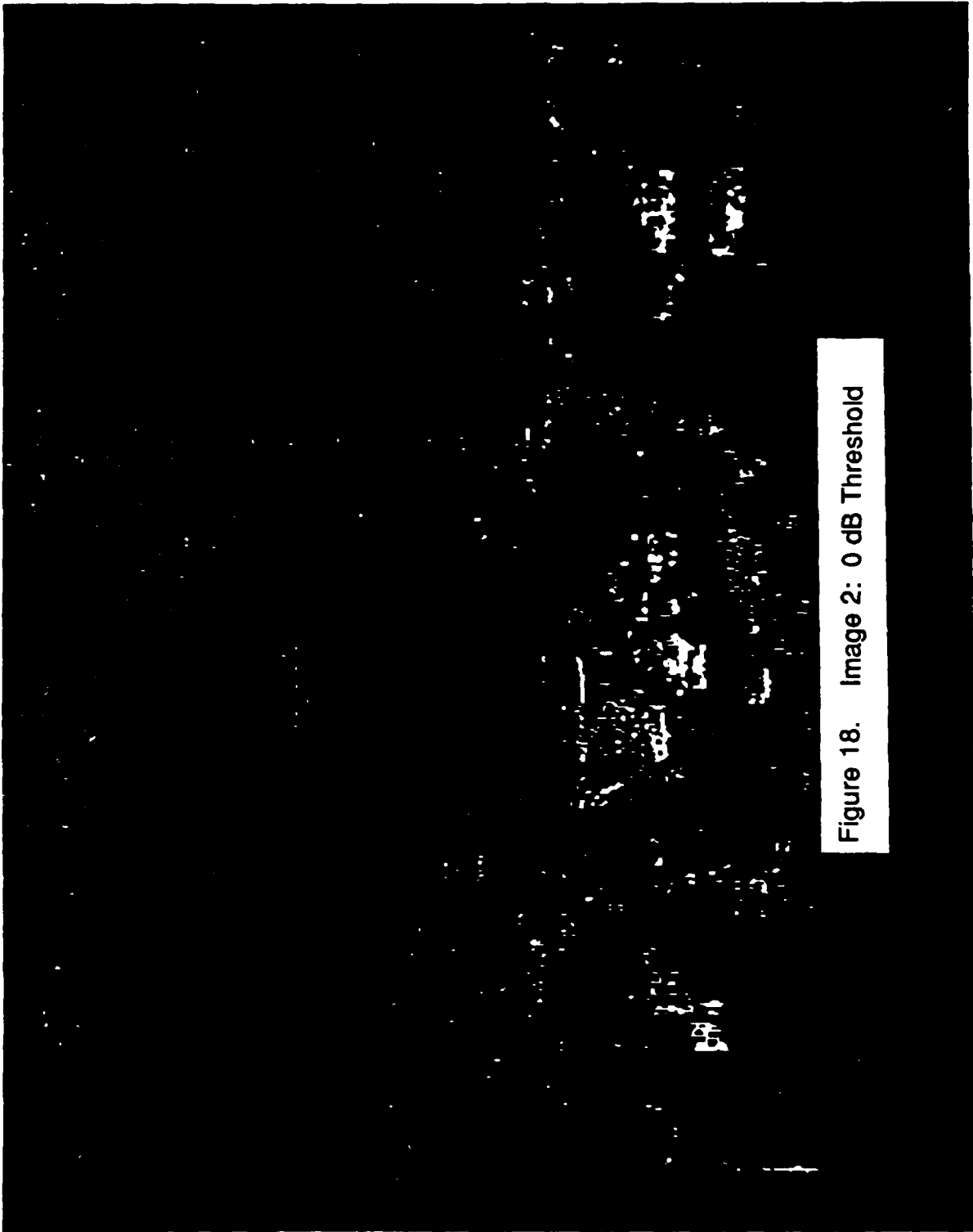
Figure 18.   Image 2: 0 dB Threshold

89-11934
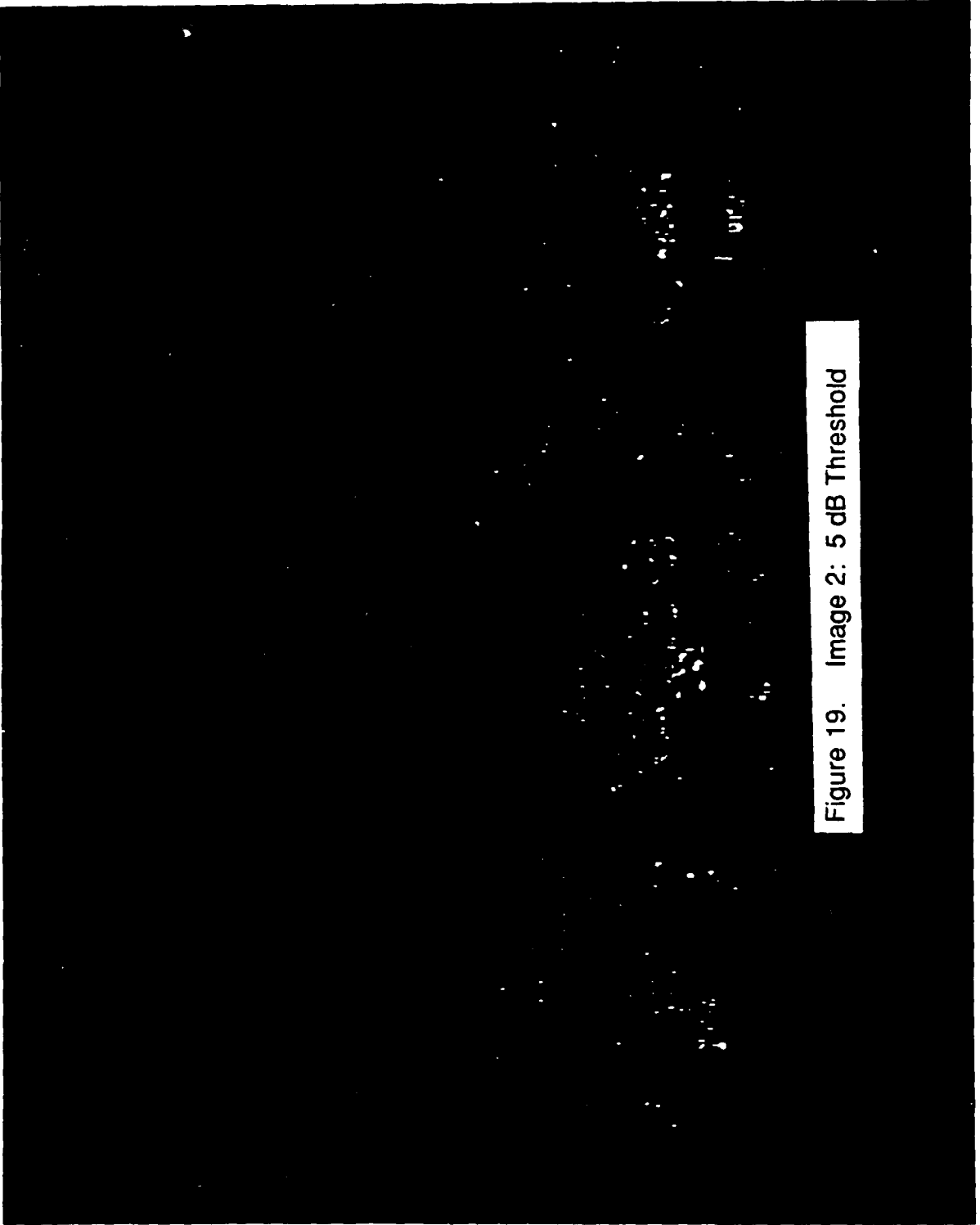
Figure 19.   Image 2: 5 dB Threshold

88-11278-9
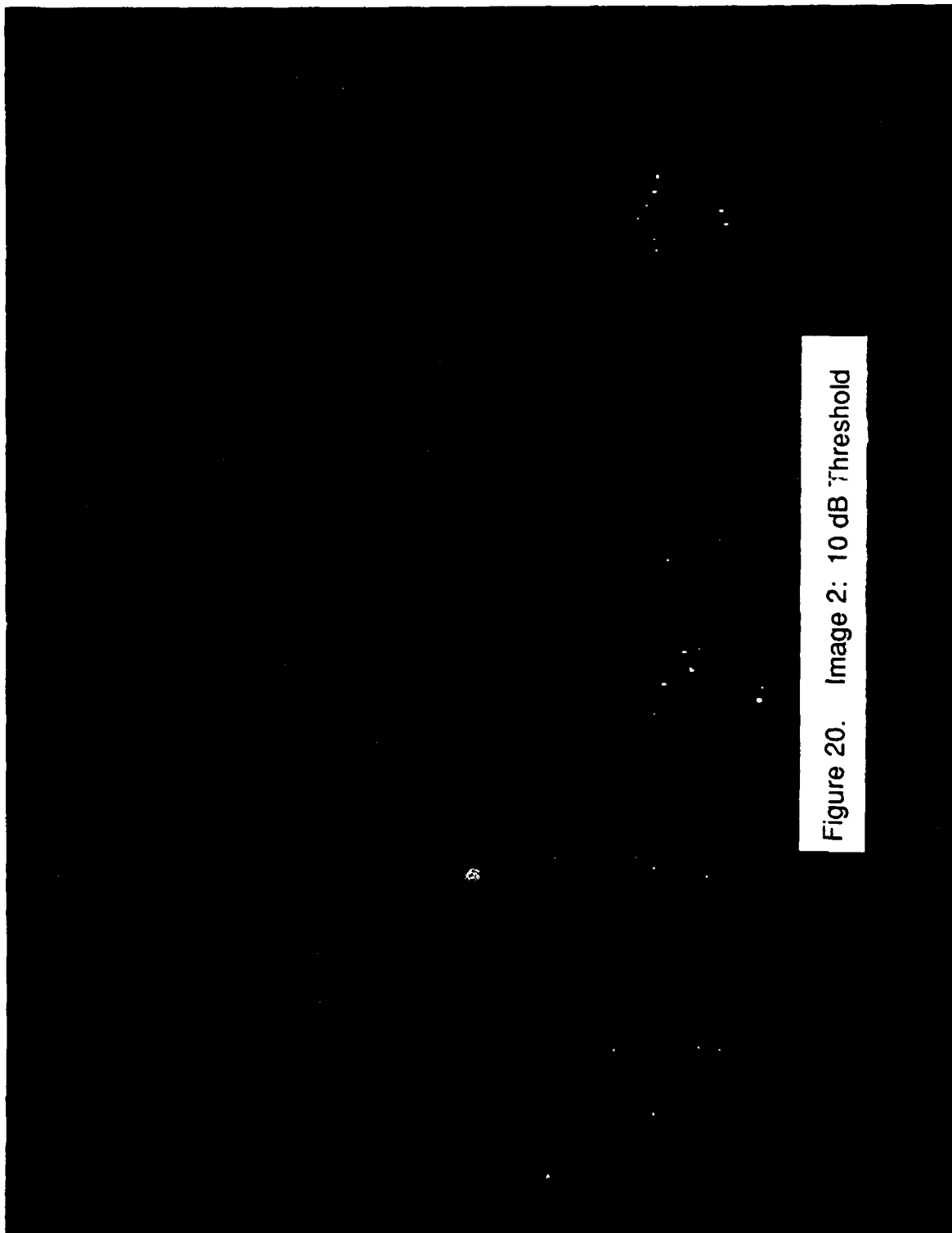
Figure 20.   Image 2: 10 dB Threshold

88 112/B 10

105

N

88-11448

1117 m

0

0   1072 m

Figure 21.   Ottawa International Airport Observed August 1984
              Using HH Polarization - Image 3
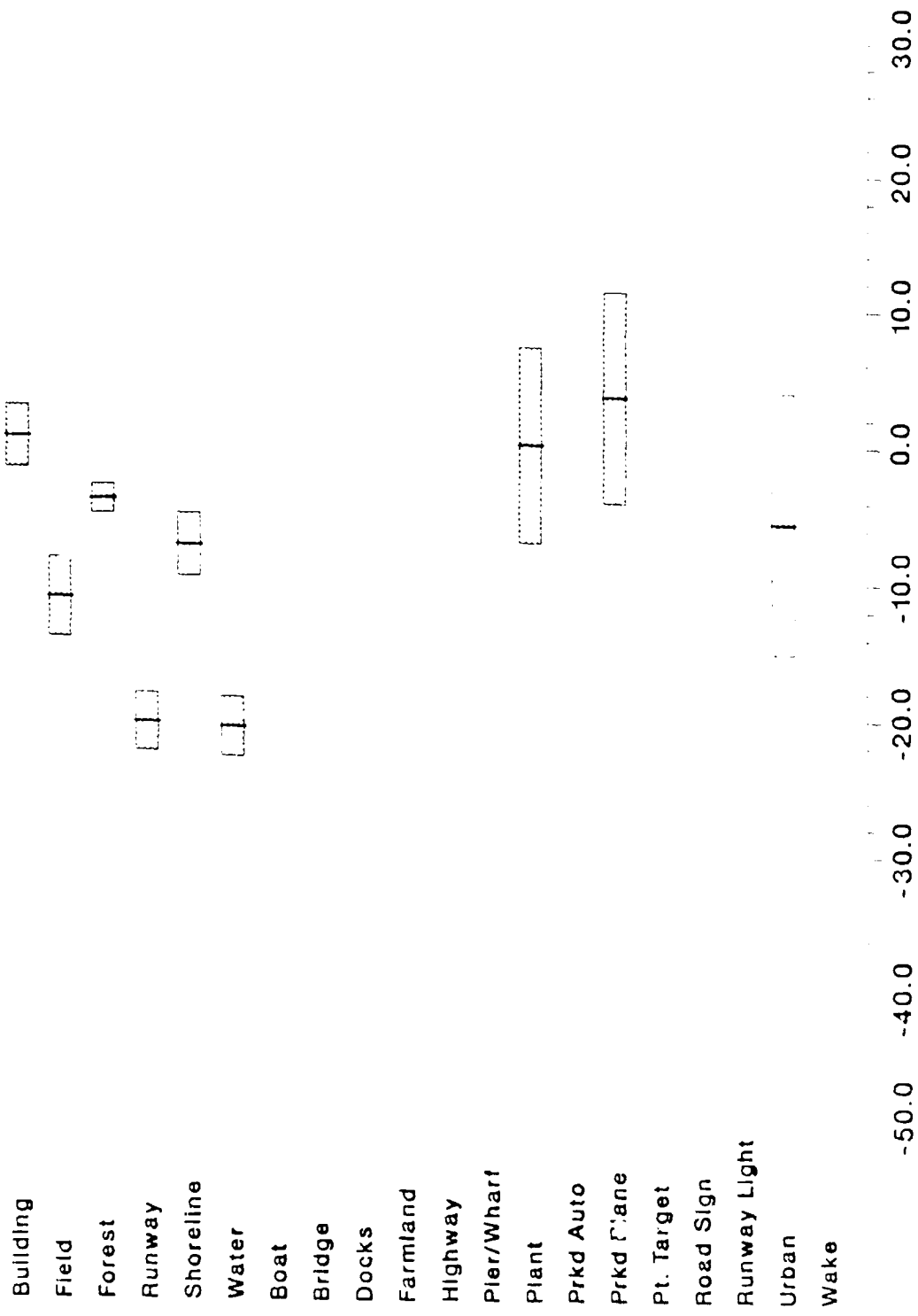
Figure 22. Image 3 Bar Chart Presentation of Means and Standard Deviation for a Variety of Airport Clutter Scenes
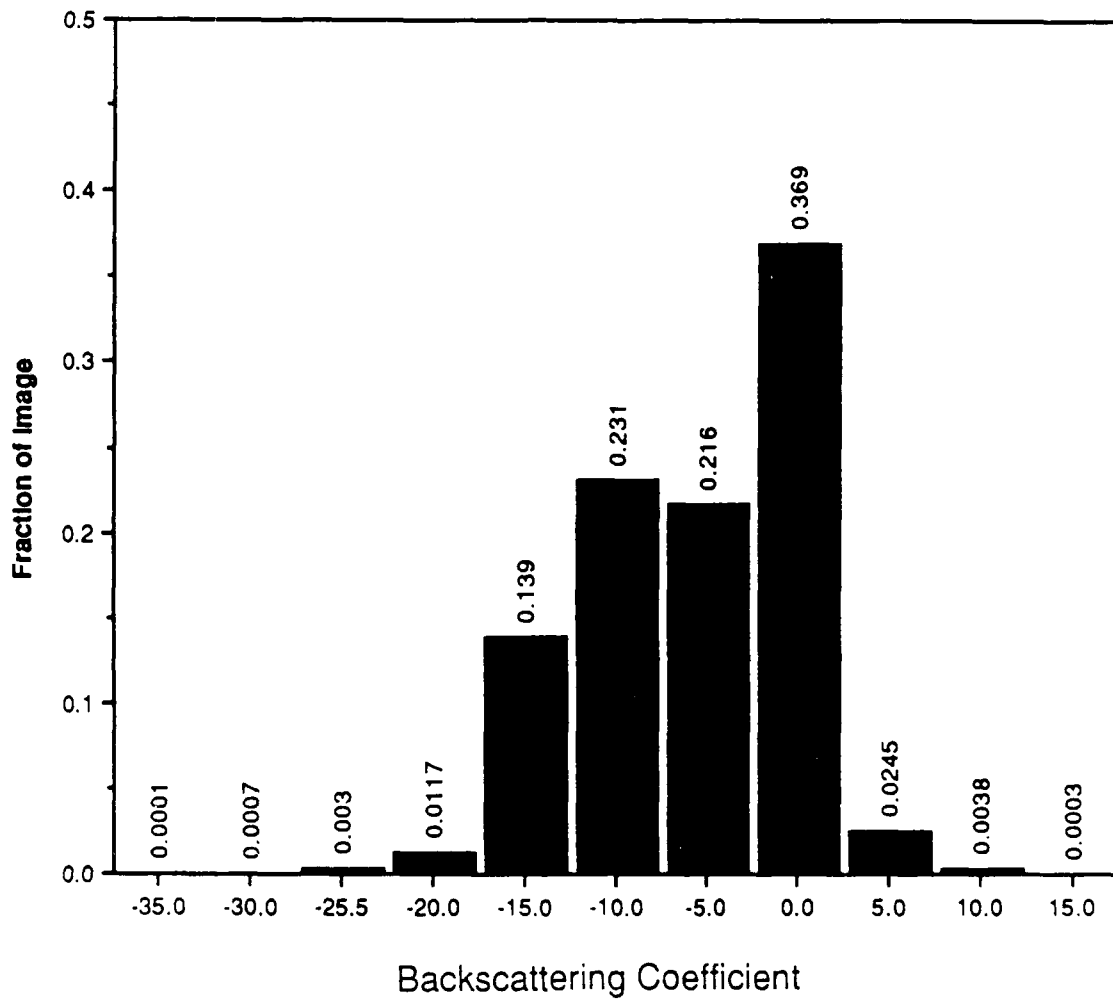
Figure 23. Histogram of Radar Backscattering Coefficients for Image 3

89-11883
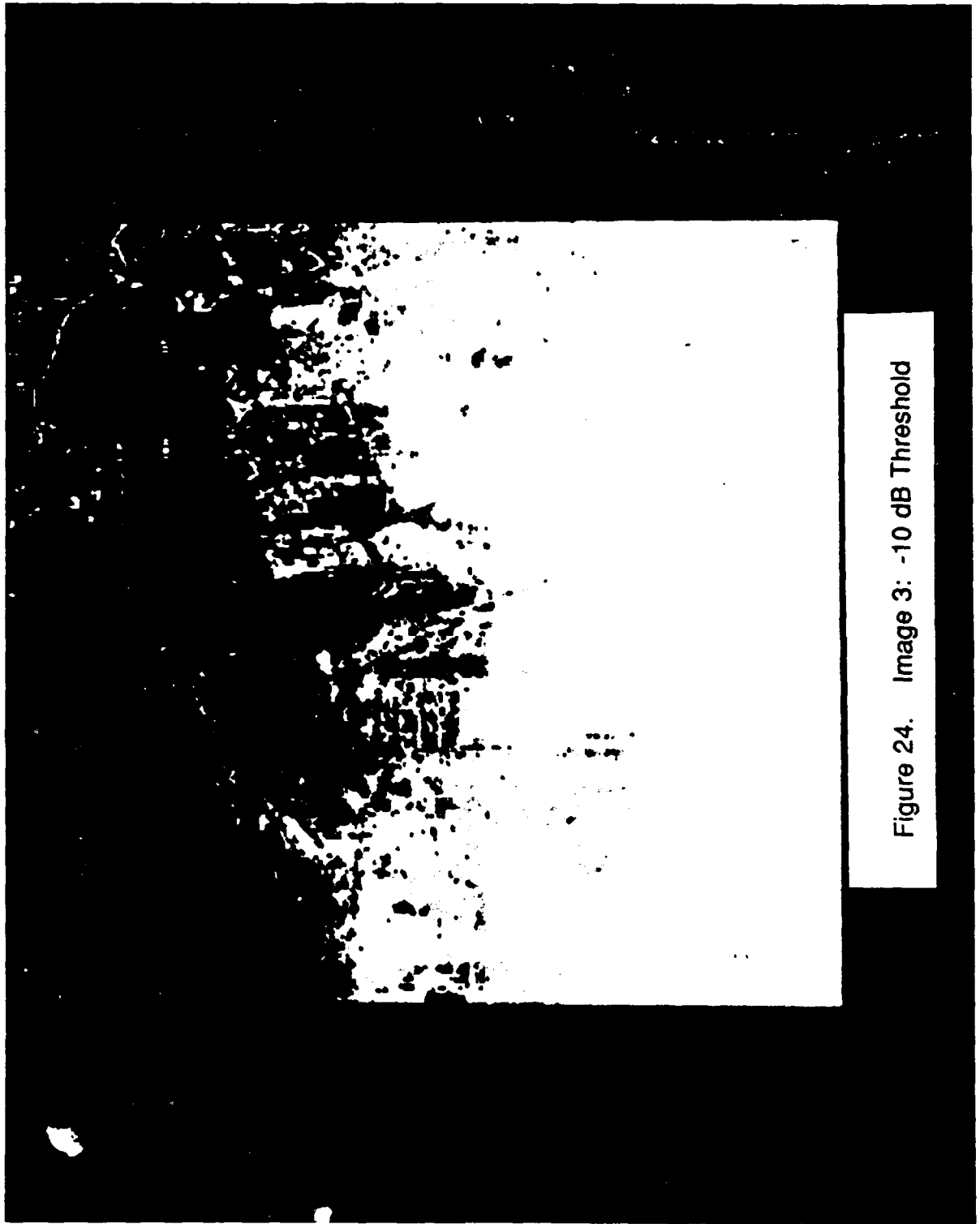
88-11278-15

Figure 24.   Image 3: -10 dB Threshold
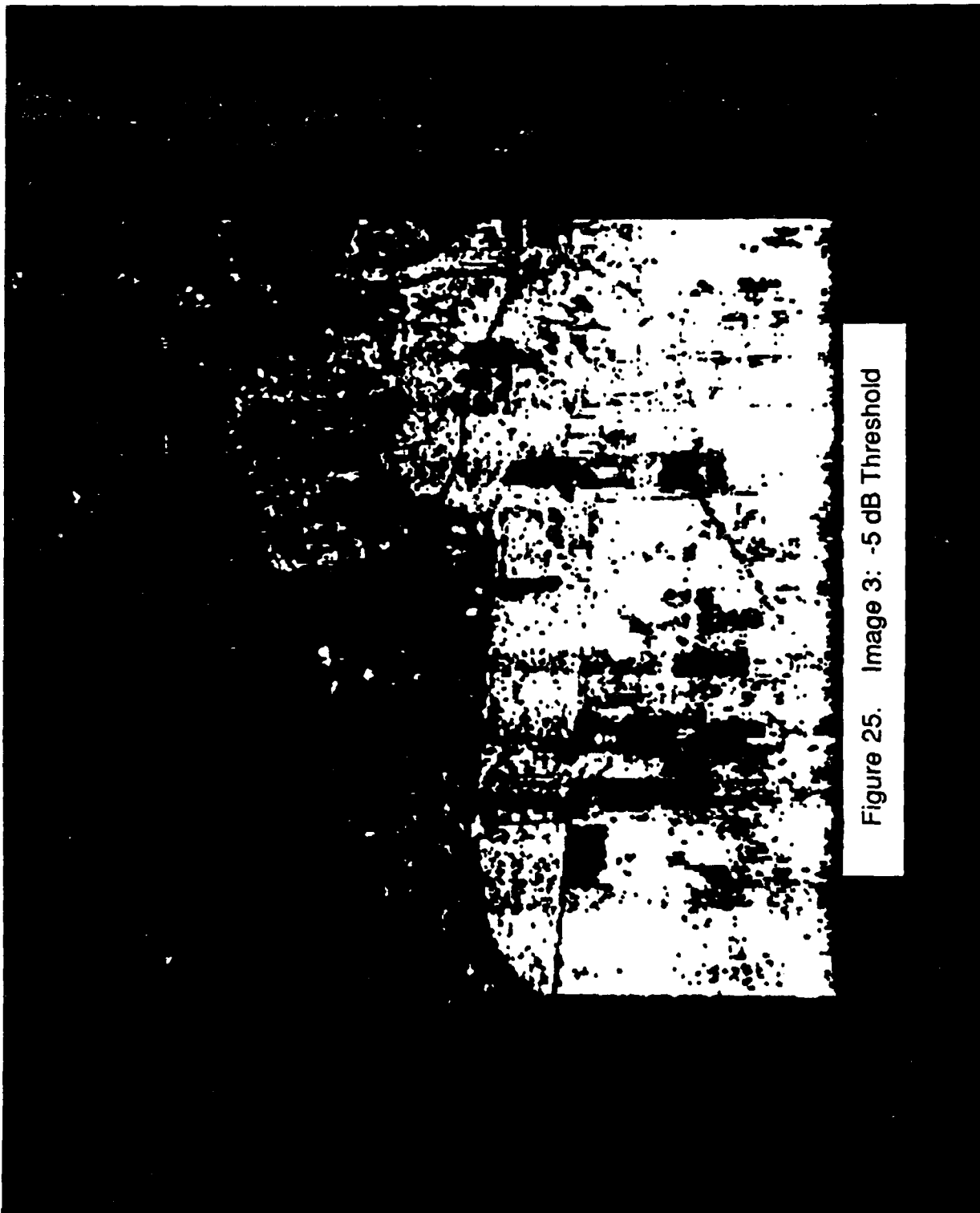
Figure 25. Image 3: -5 dB Threshold

115

Figure 26. Image 3: 0 dB Threshold

89-11884

86-11278 21

117
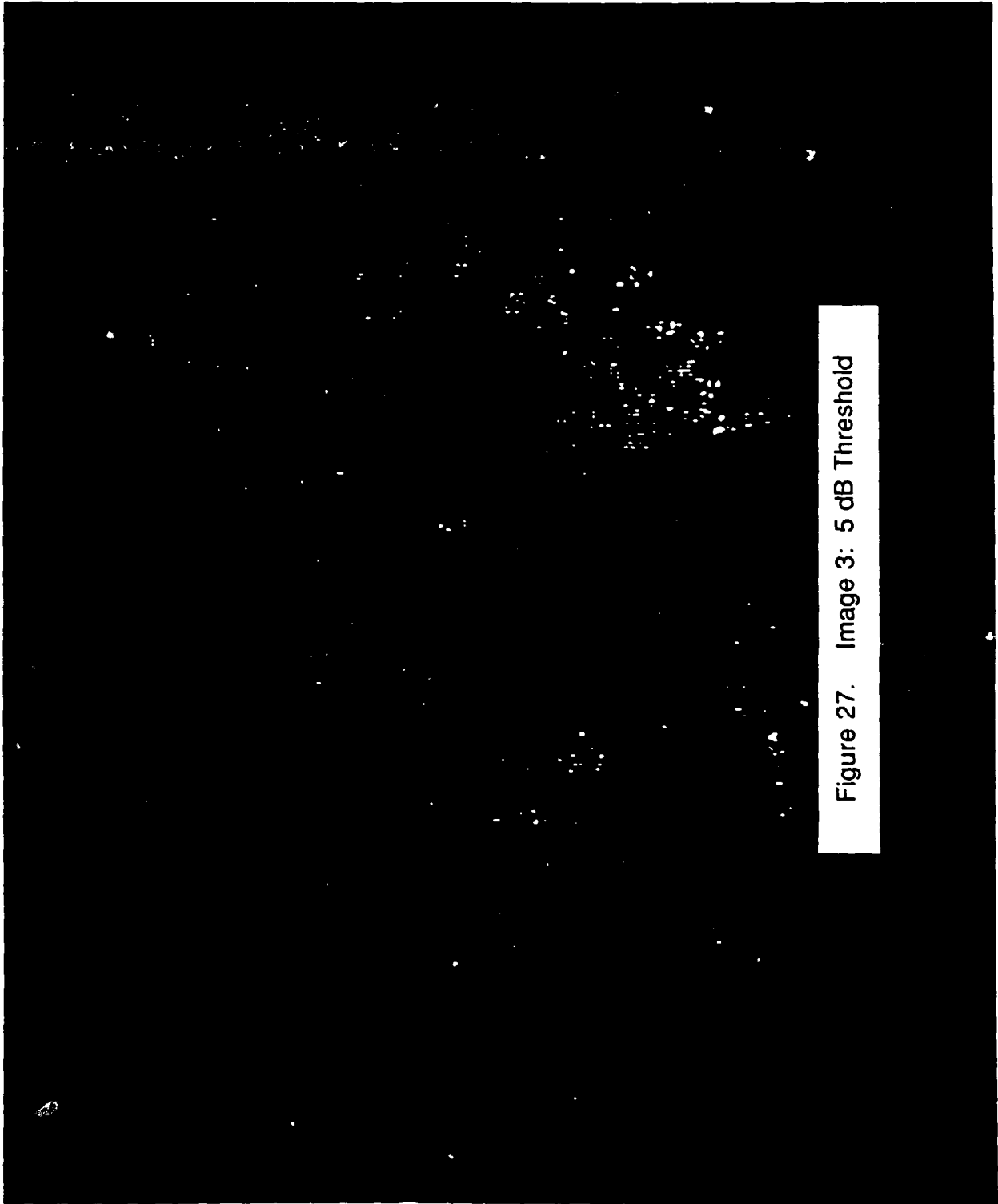
Figure 27.   Image 3: 5 dB Threshold
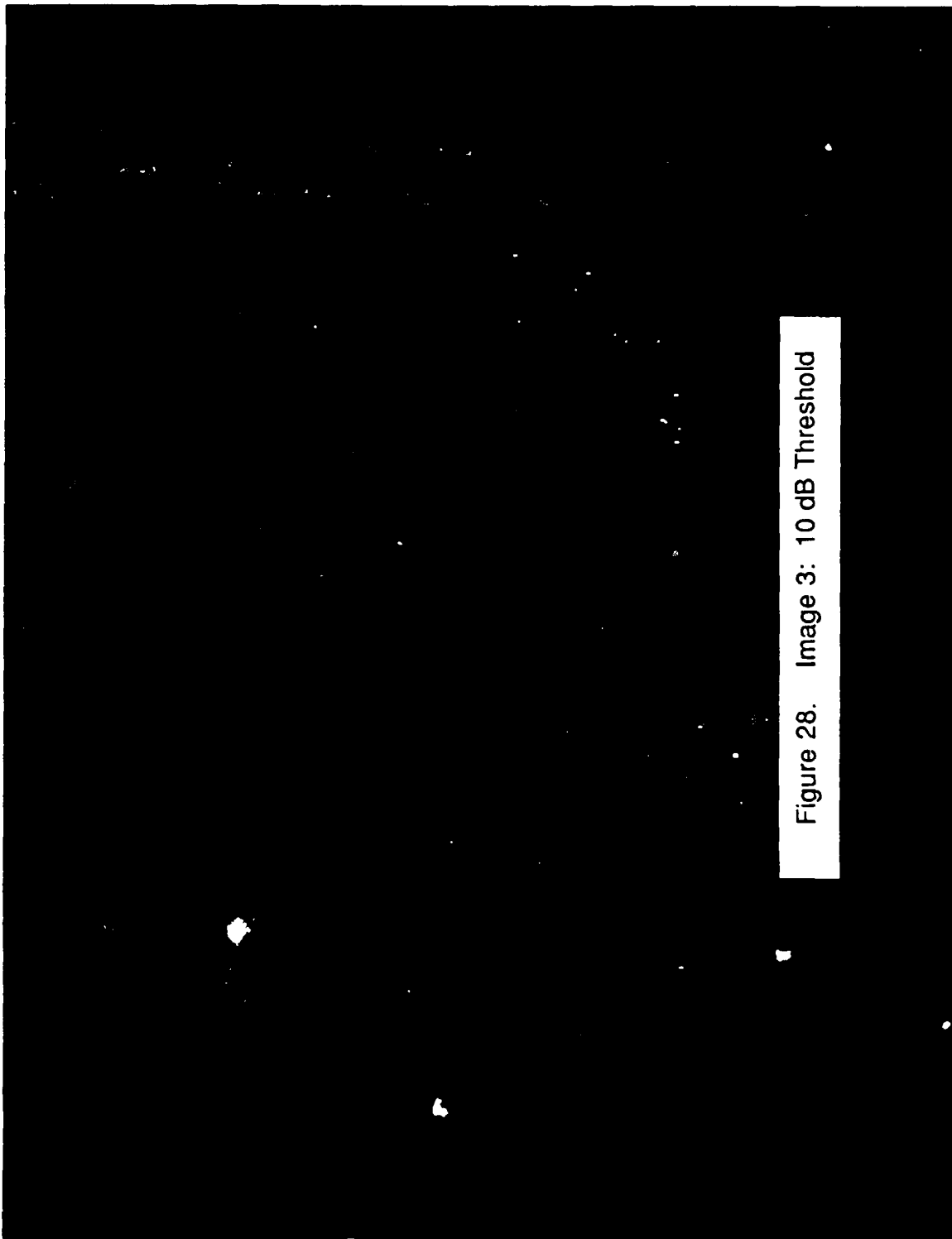
89-11887

Figure 28. Image 3: 10 dB Threshold

121
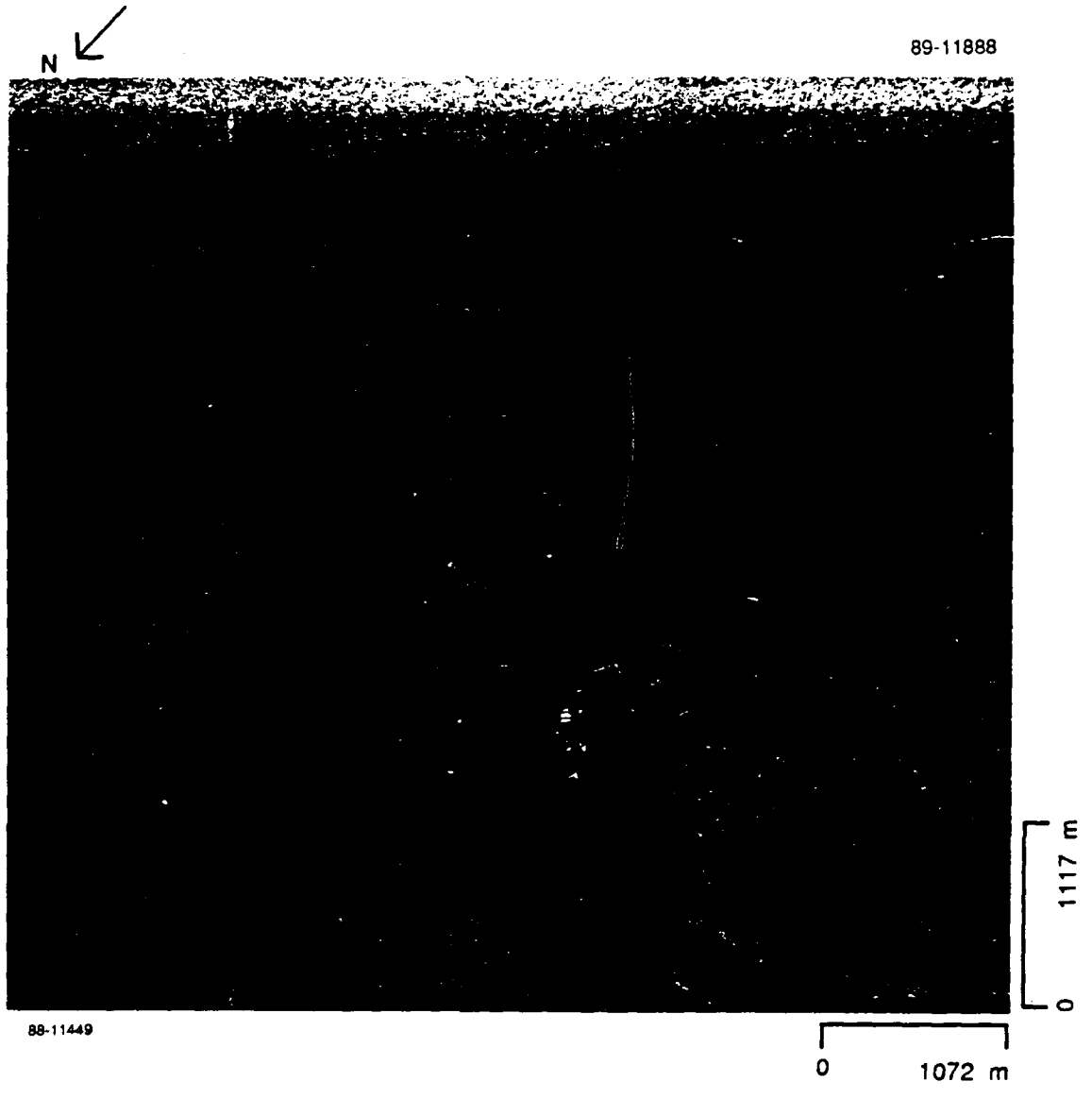
Figure 29.   Comox CFB Observed August 1983 Using VV Polarization -
Image 4
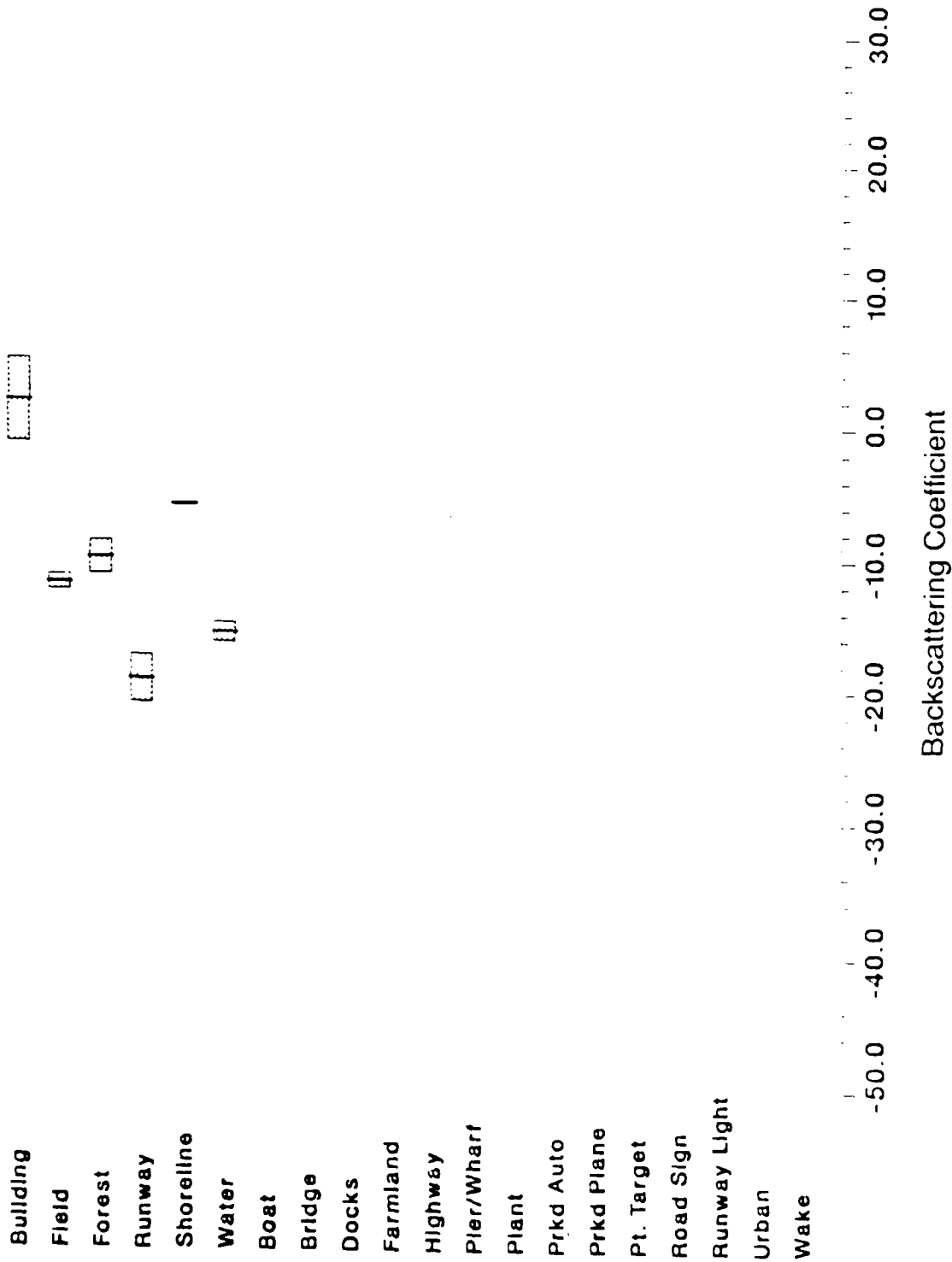
Figure 30. Image 4 Bar Chart Presentation of Means and Standard Deviation for a Variety of Airport Clutter Scenes

125
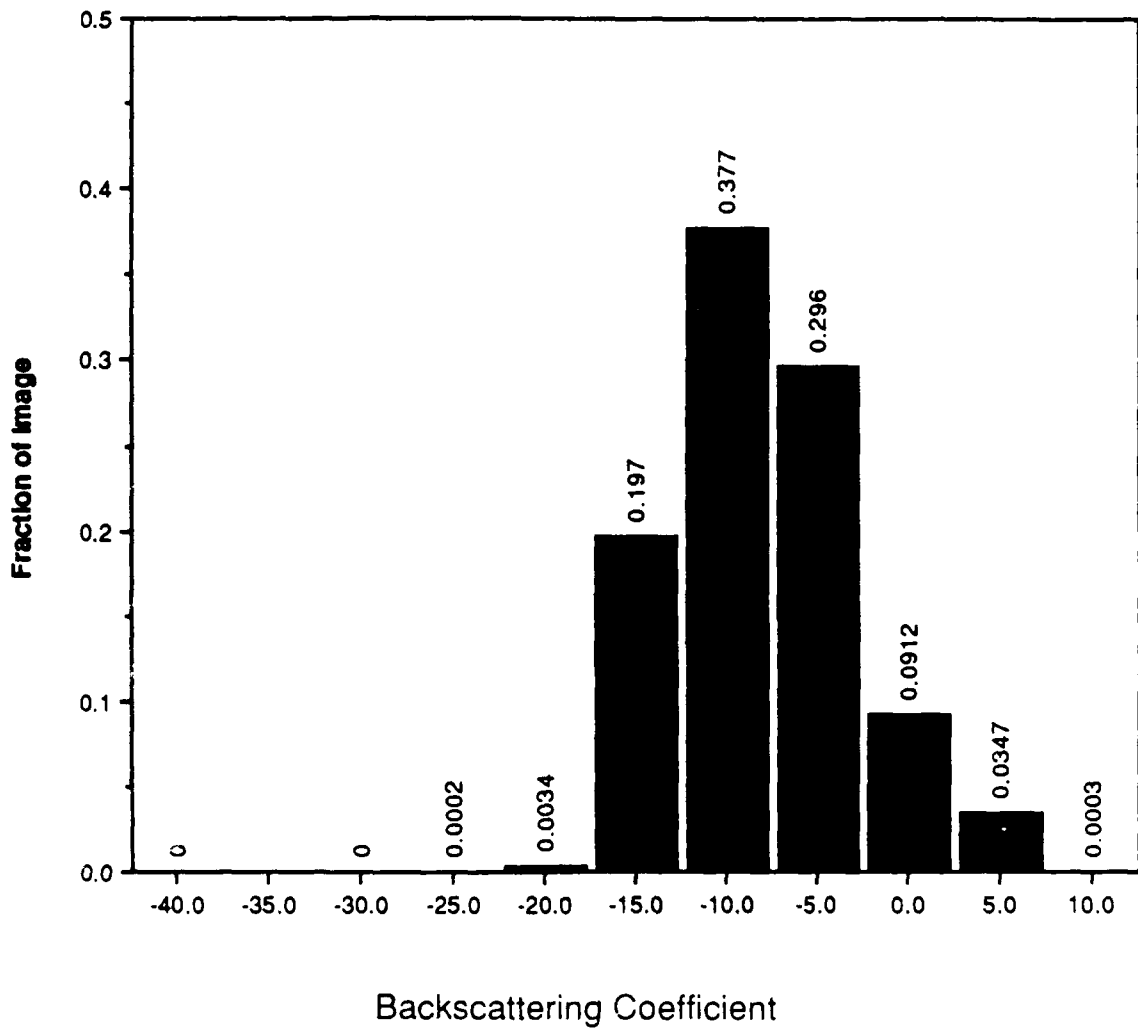
Figure 31.   Histogram of Radar Backscatter Coefficients for Image 4

127

89-11889

Figure 32. Image 4: -10 dB Threshold

88-11278 28

129

Figure 33.   Image 4: -5 dB Threshold

89-11890

88-11278-33

131

Figure 34. Image 4: 0 dB Threshold

89-11892
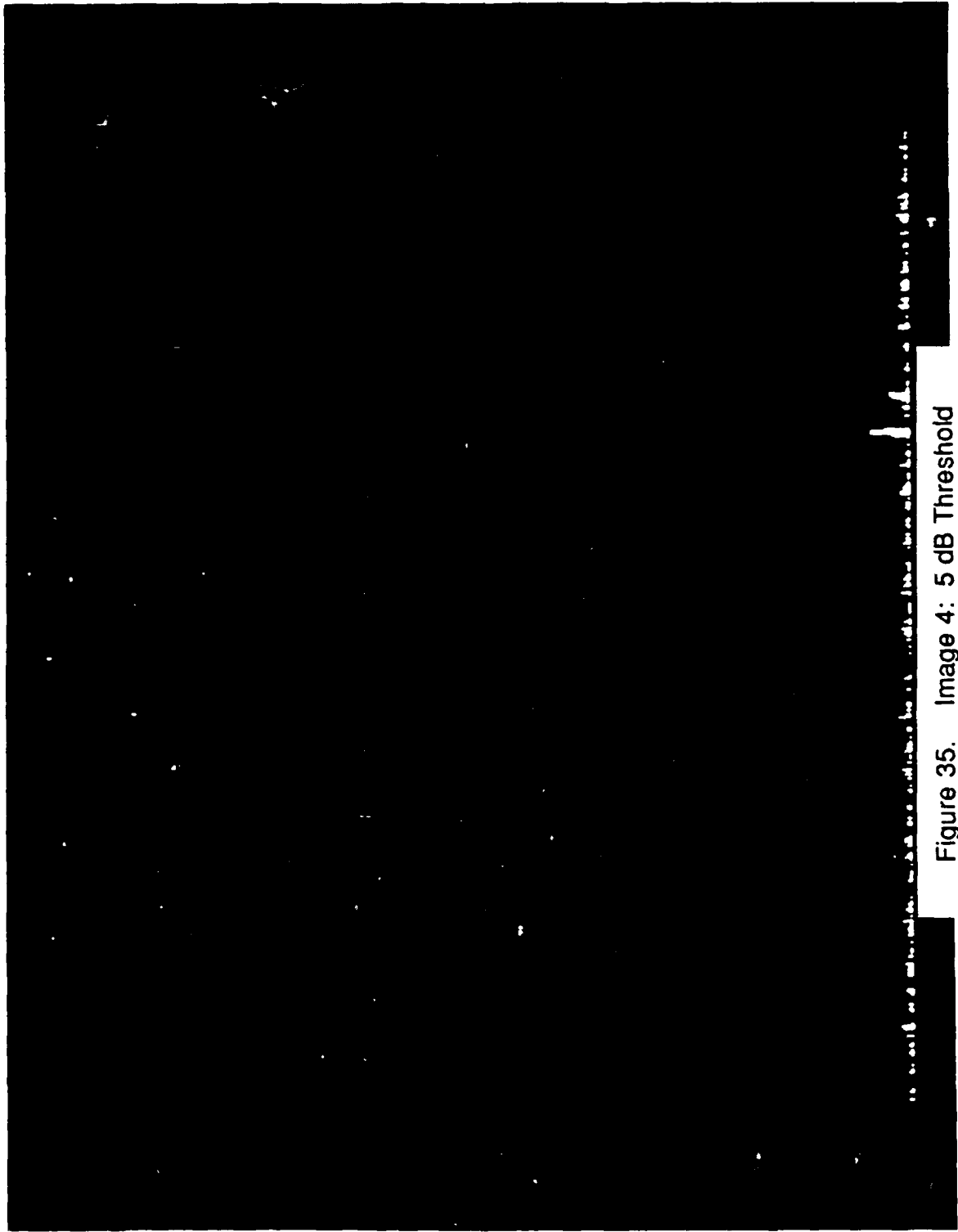
Figure 35.   Image 4: 5 dB Threshold

88-11278-37

89-11893
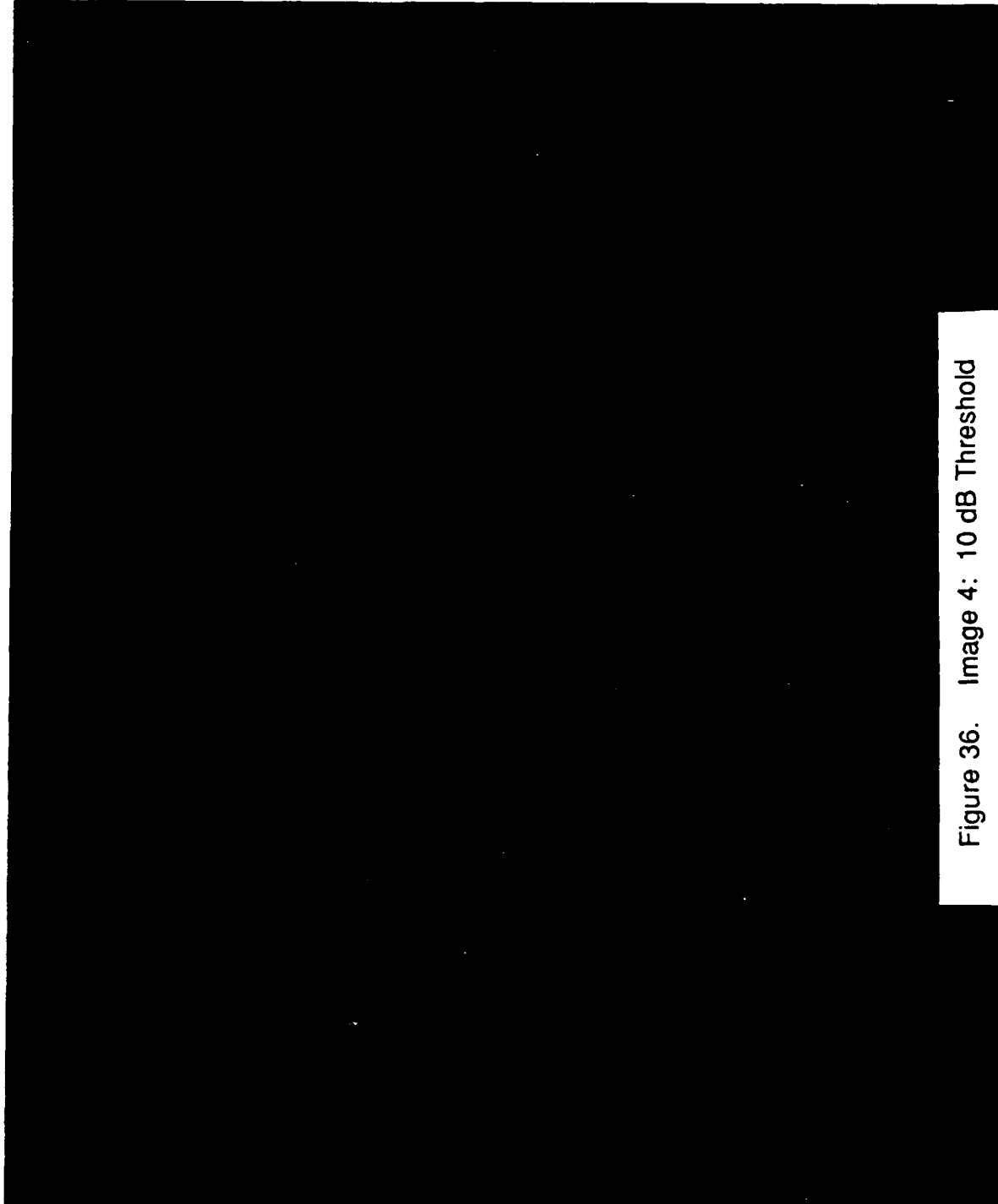
Figure 36. Image 4: 10 dB Threshold

88-11279 5
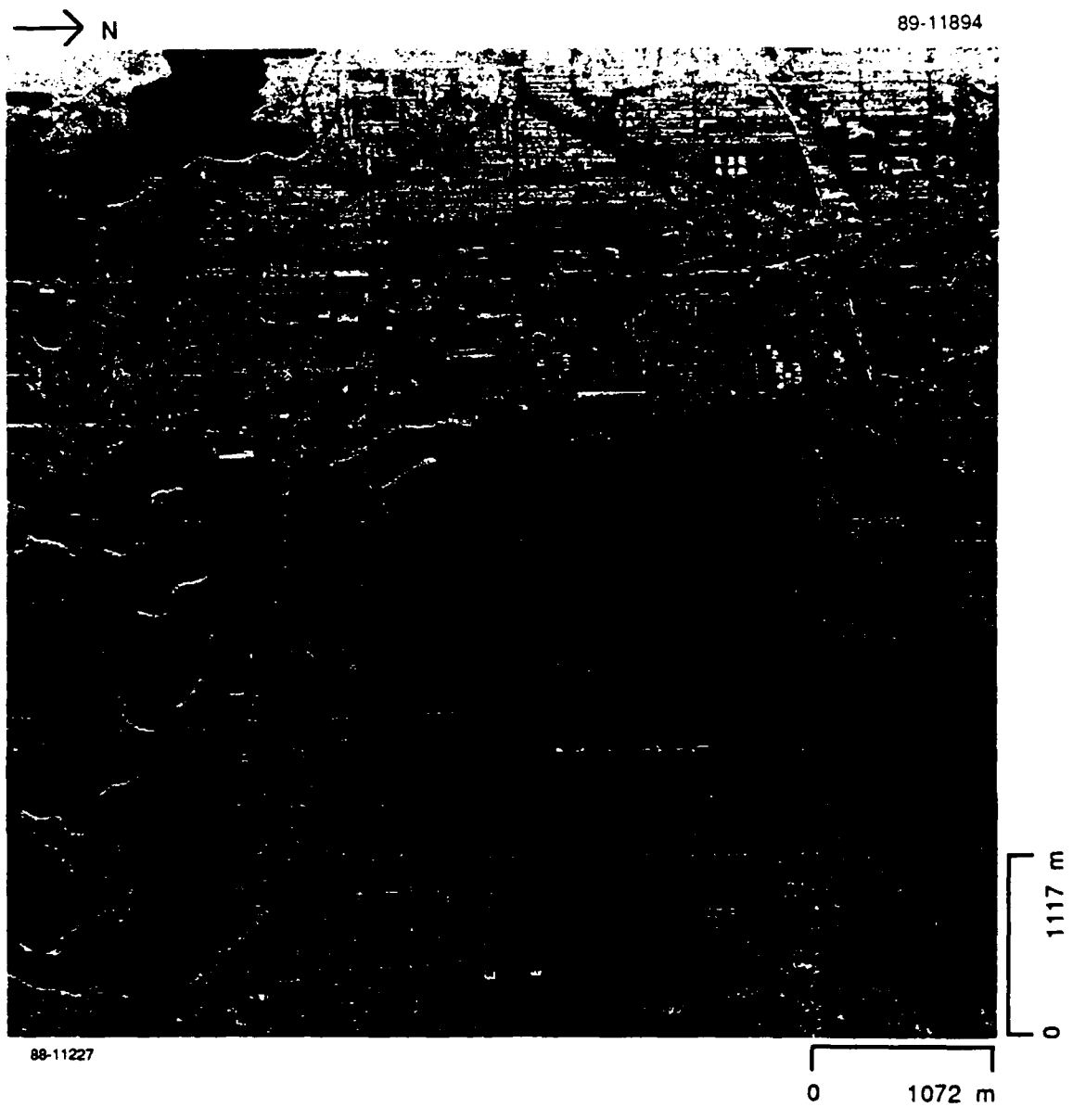
Figure 37. Willow Run Airport Observed April 1984 Using VV Polarization - Image 5
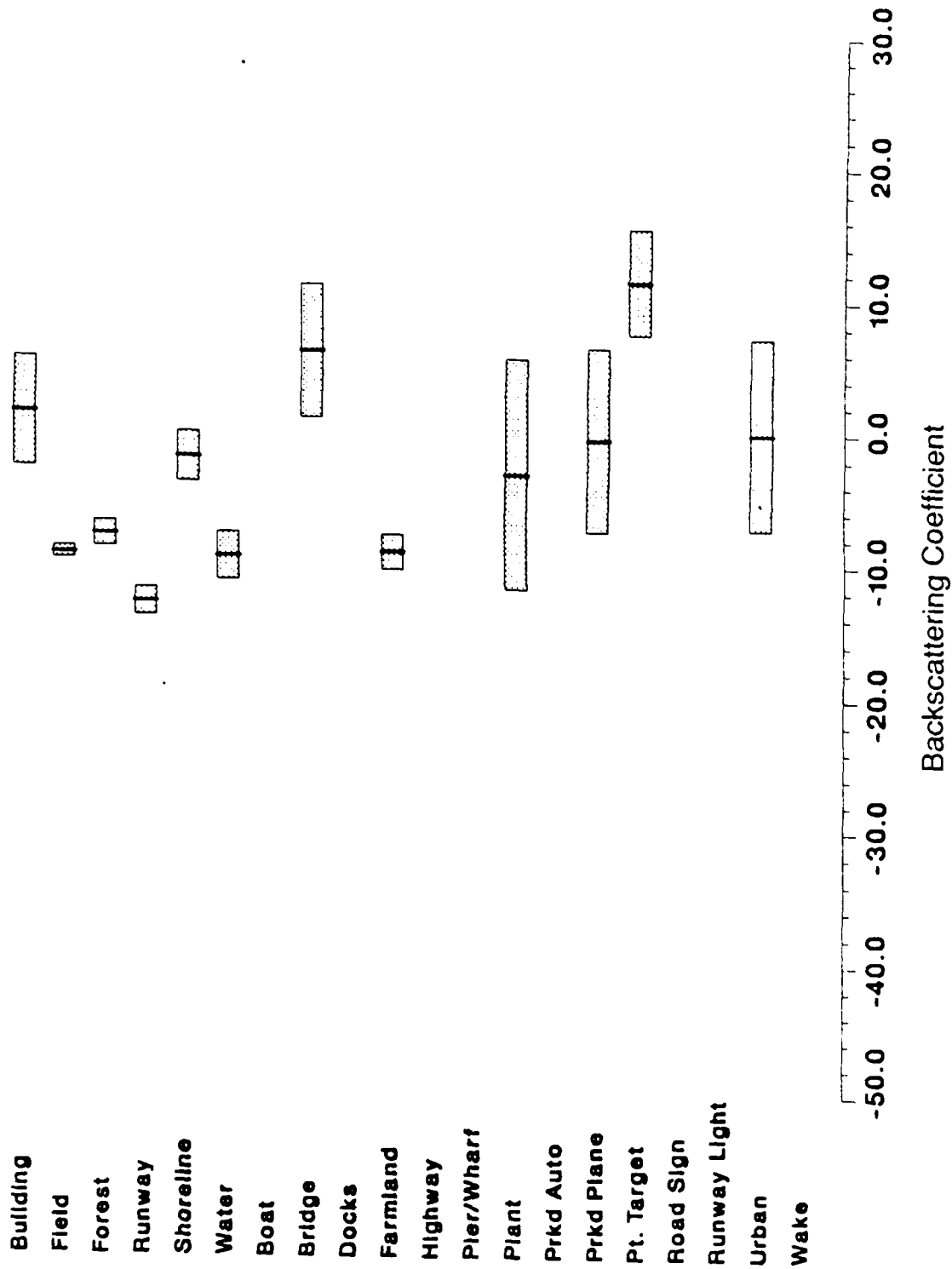
Figure 38.   Image 5 Bar Chart Presentation of Means and Standard
   Deviation for a Variety of Airport Clutter Scenes
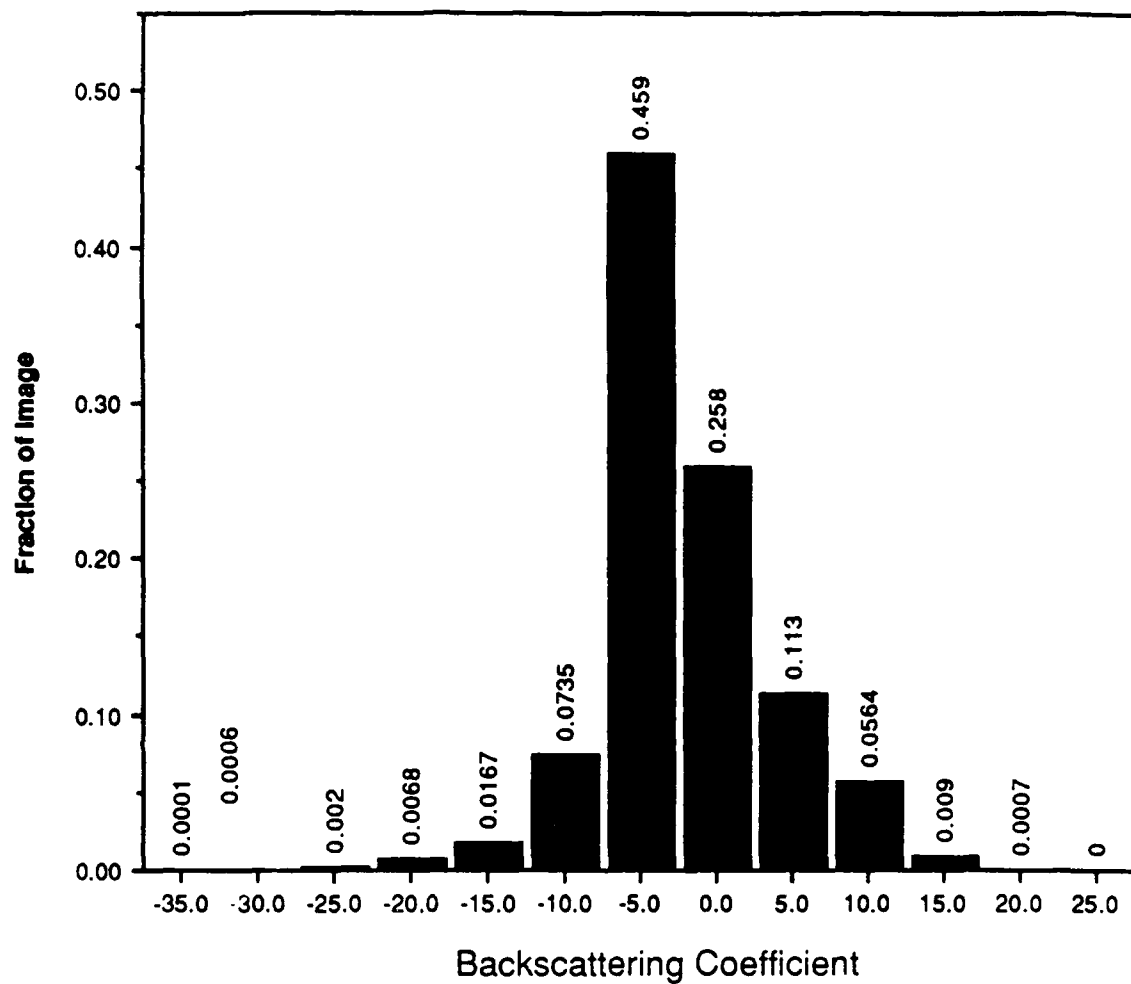
Figure 39.   Histogram of Radar Backscatter Coefficients for Image 5
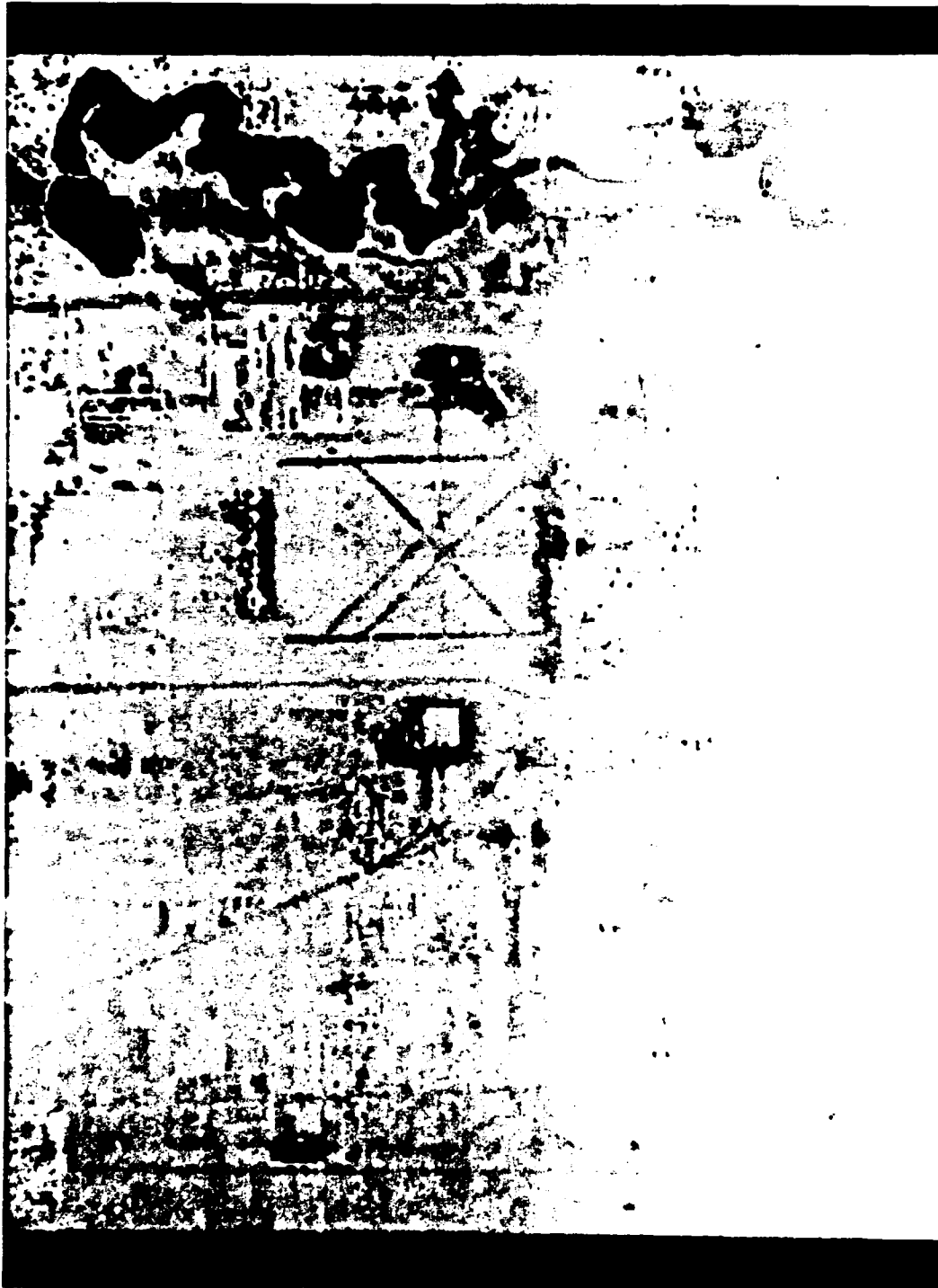
Figure 40. Image 5: -10 dB Threshold

Figure 41. Image 5: -5 dB Threshold

147

89-11897

Figure 42. Image 5: 0 dB Threshold

88-11279-14

149
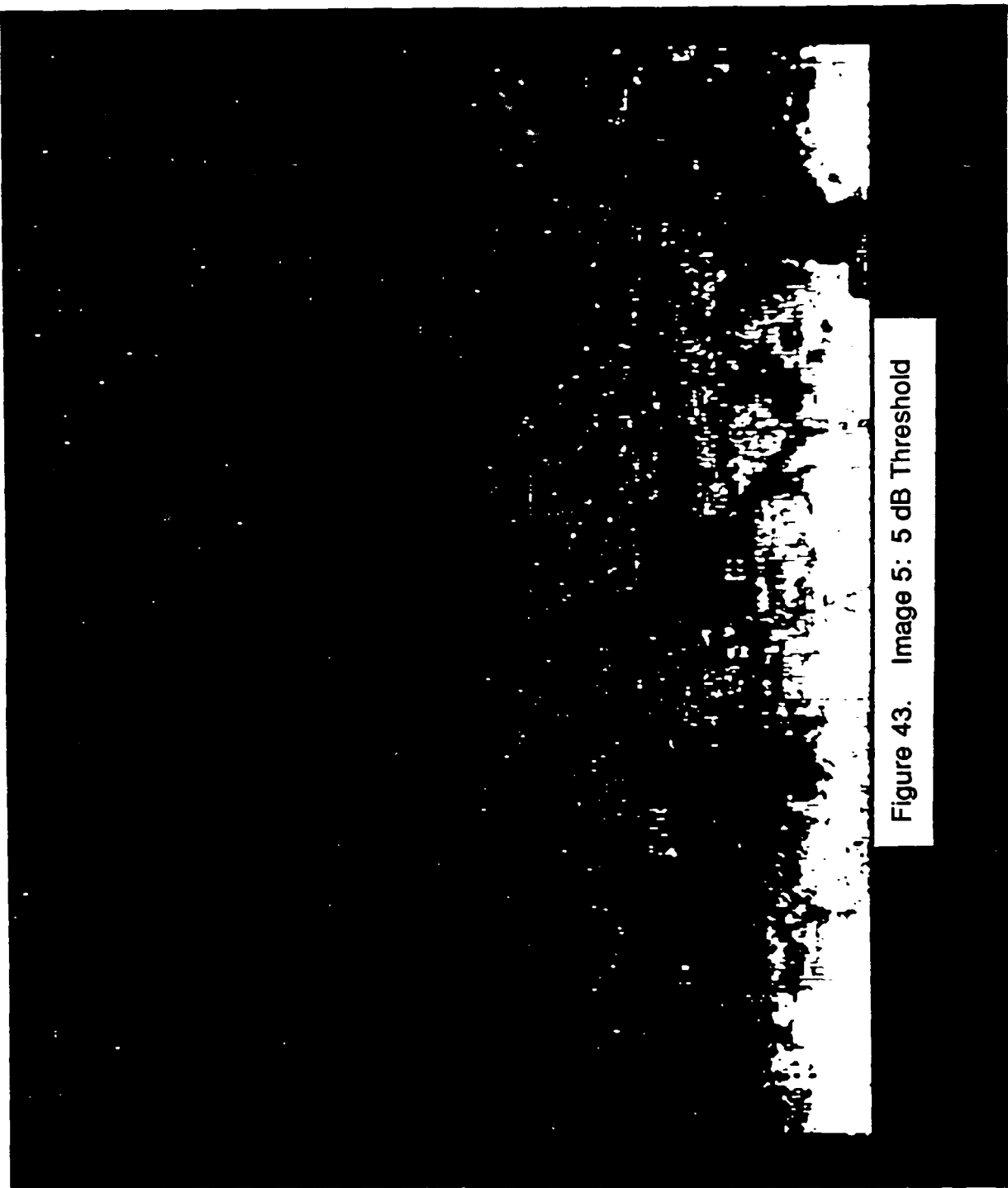
Figure 43. Image 5: 5 dB Threshold
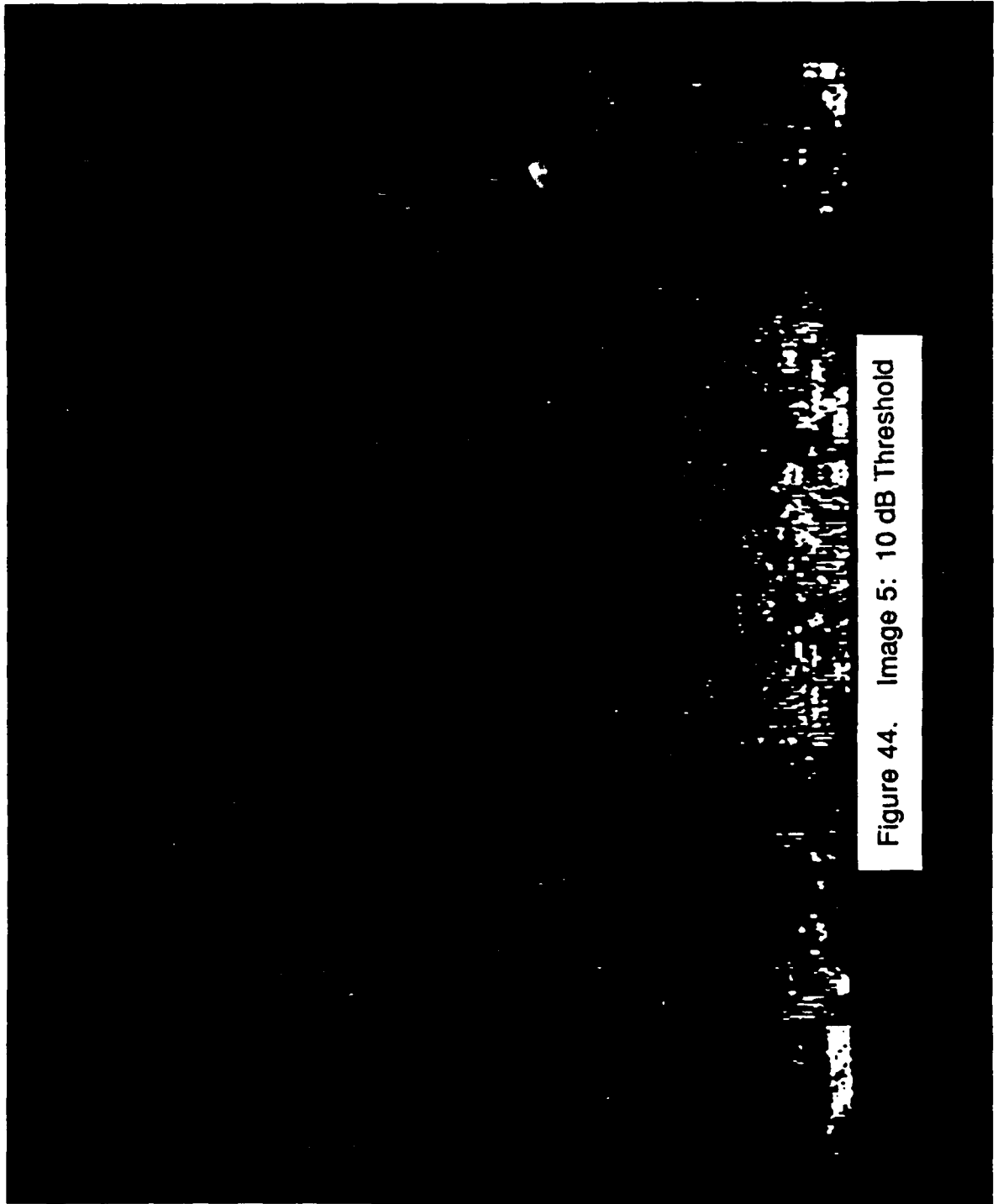
Figure 44. Image 5: 10 dB Threshold
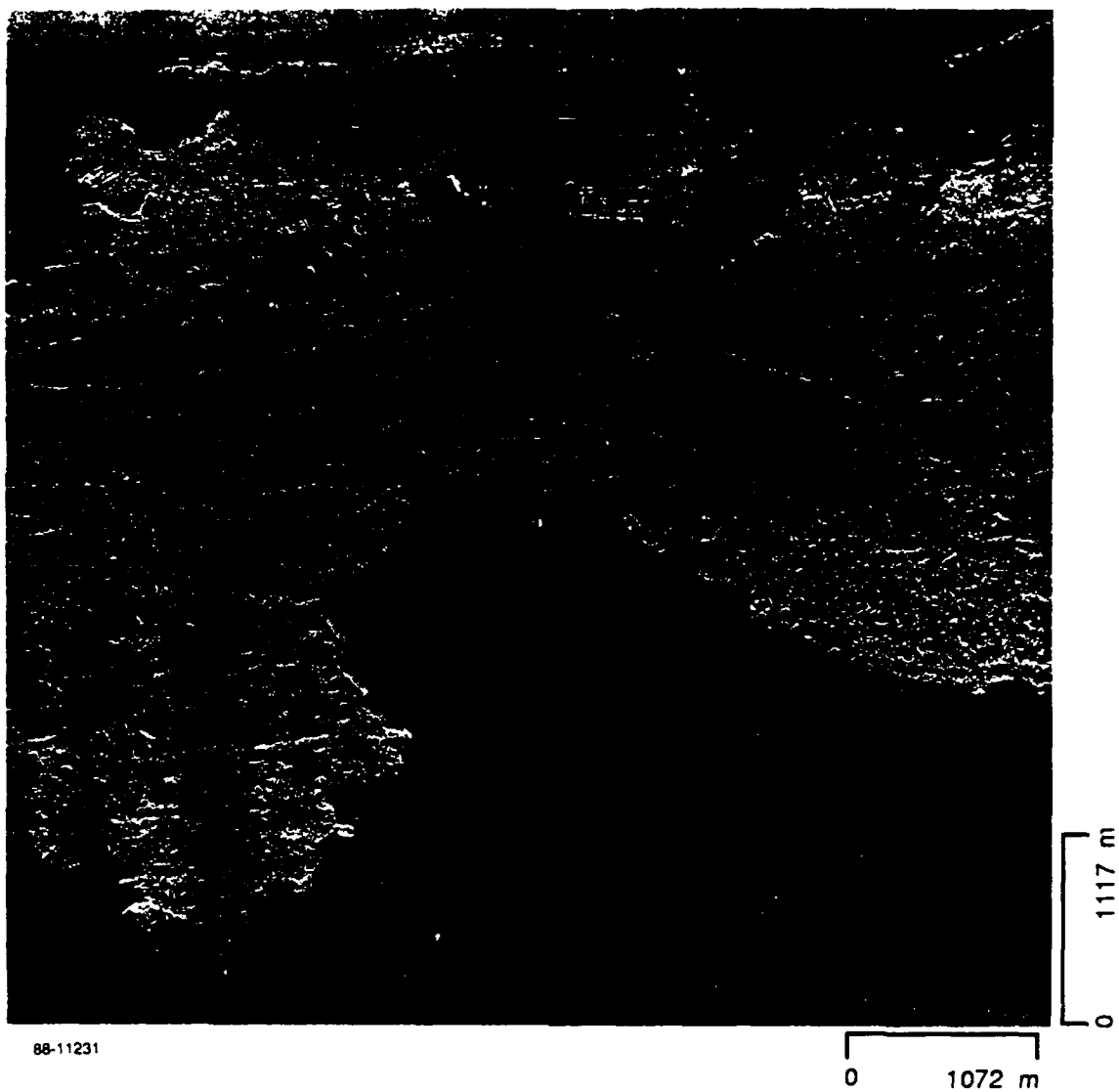
Figure 45.   Victoria International Airport Observed July 1983
Using VV Polarization - Image 6
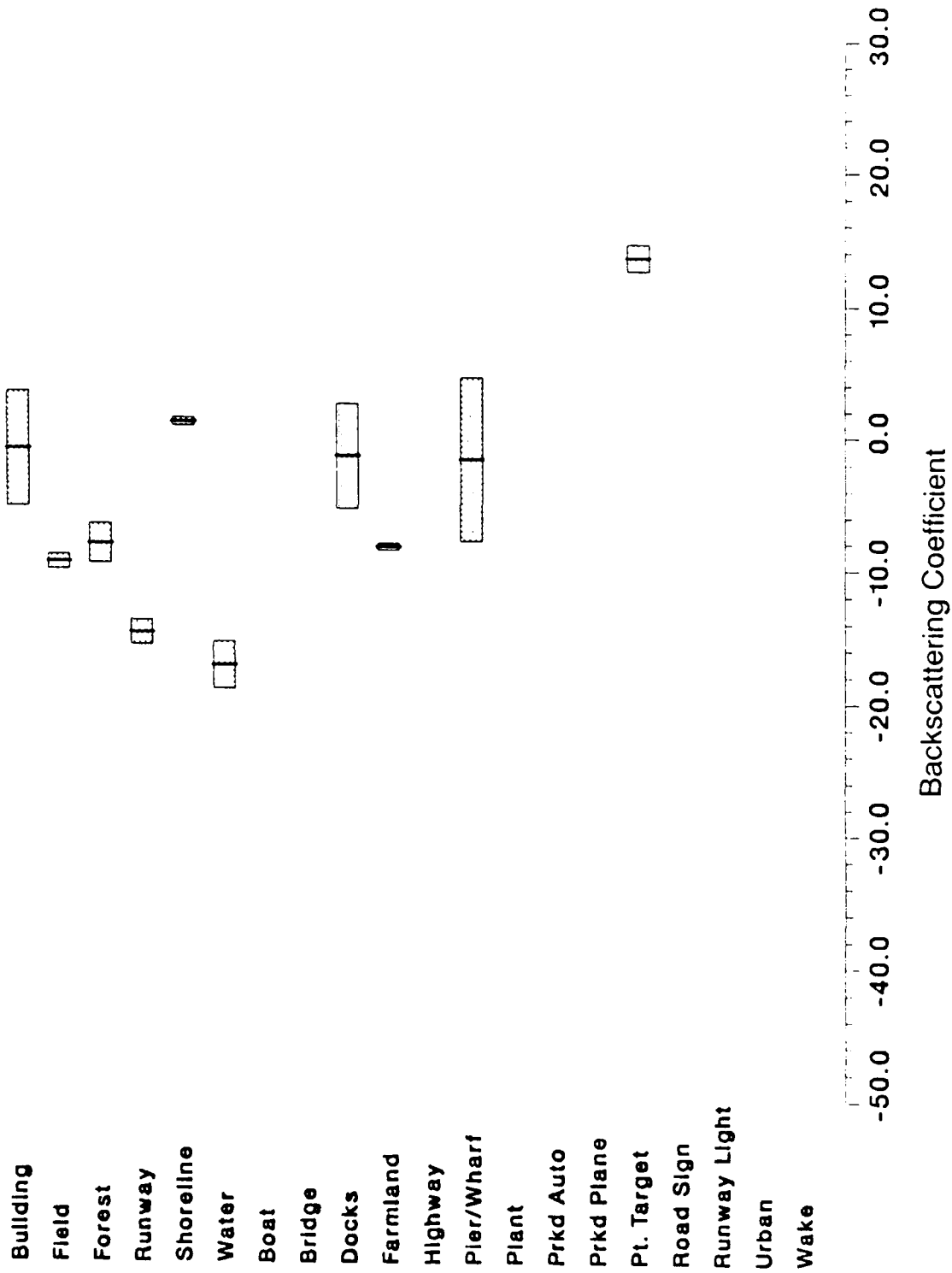
Figure 46.   Image 6 Bar Chart Presentation of Means and Standard
Deviation for a Variety of Airport Clutter Scenes

Fraction of Image

0.50

0.40

0.30

0.20

0.10

0.00

0.0003 0.001 0.0061 0.0307 0.0975 0.348 0.452 0.0573 0.0071

-35.0 -30.0 -25.0 -20.0 -15.0 -10.0 -5.0 0.0 5.0

Backscattering Coefficient
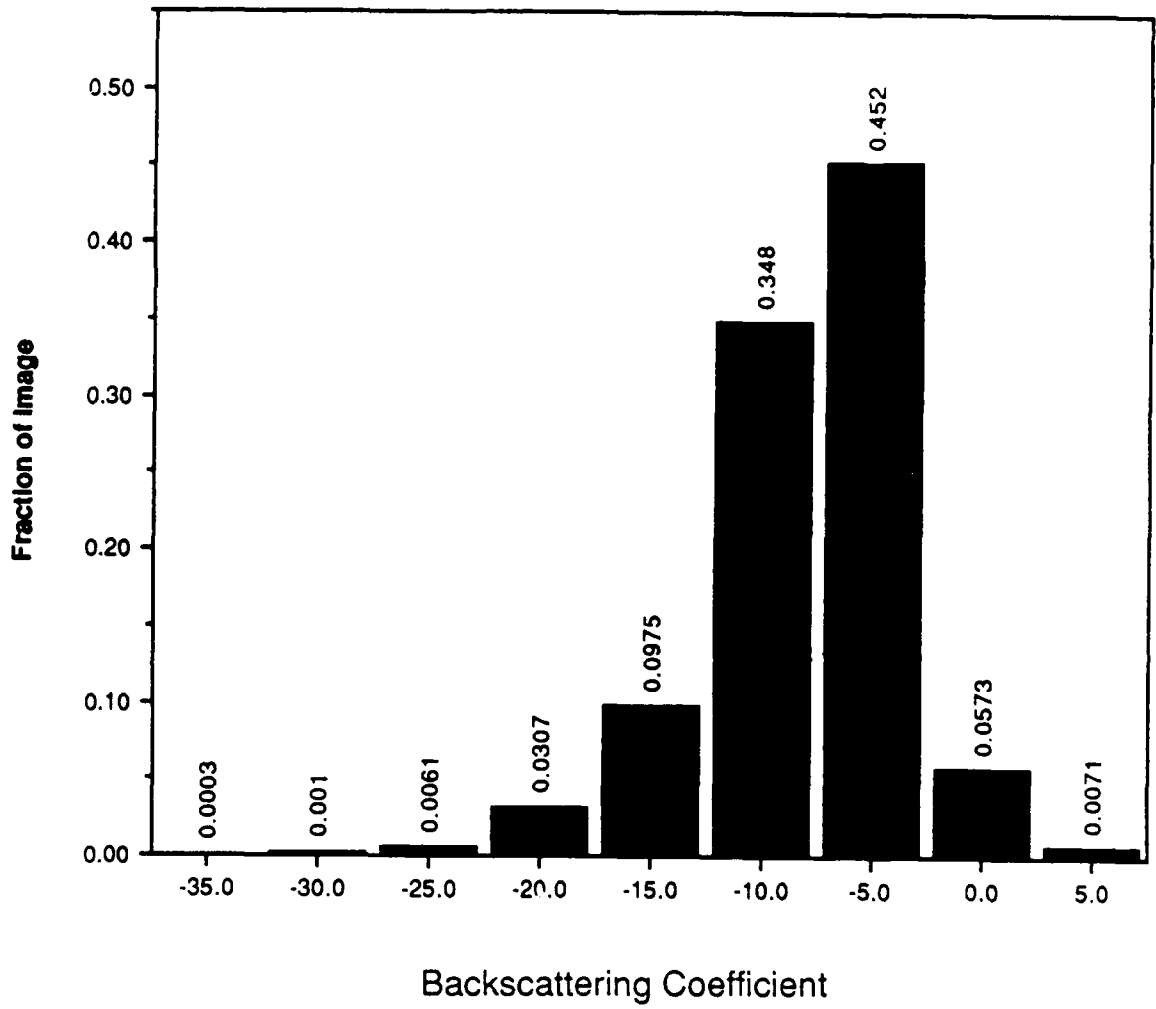
Figure 47.   Histogram of Radar Backscatter Coefficients for Image 6

159

Figure 48.   Image 6: -10 dB Threshold

89-11901

88-11279-23

161
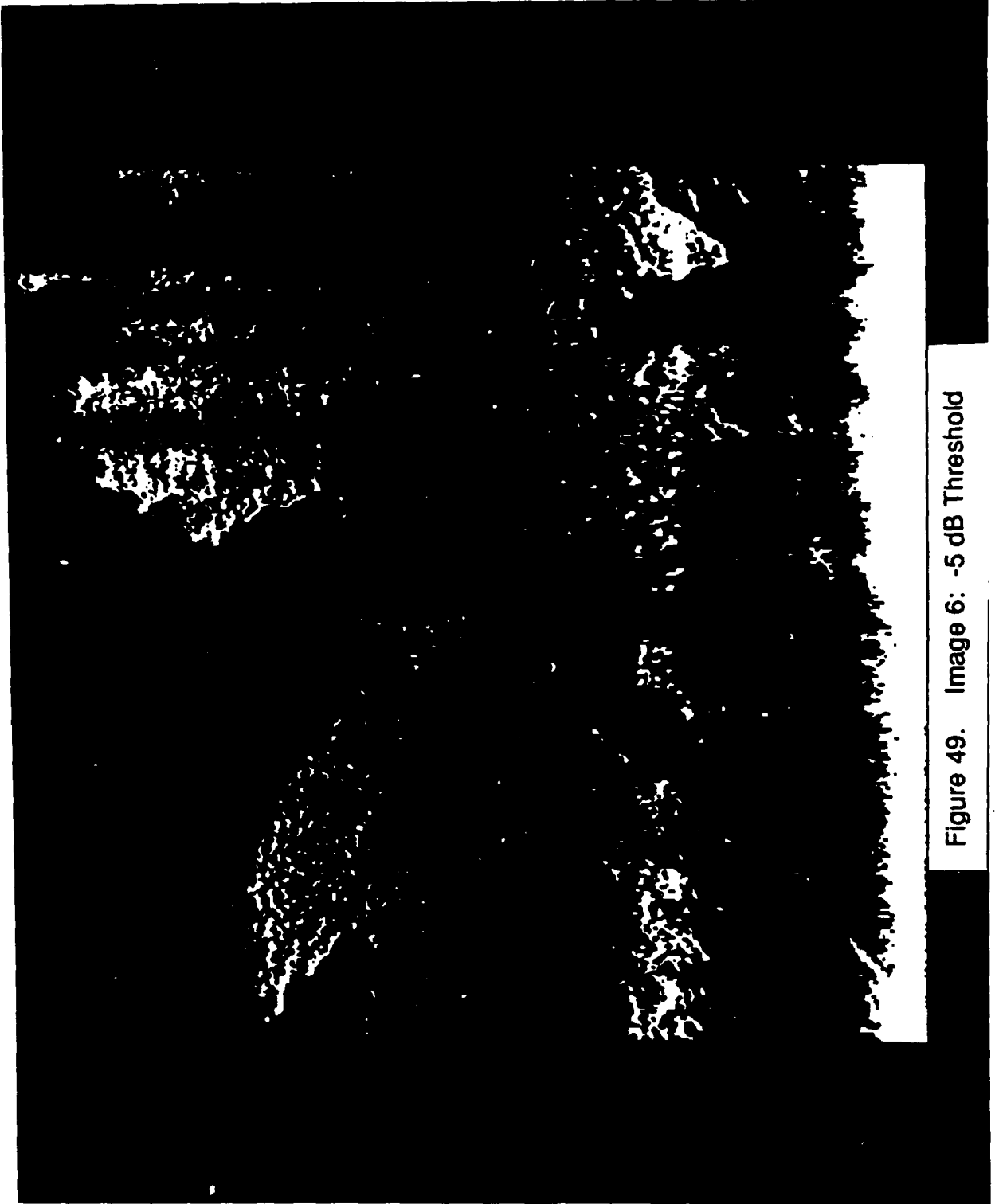
Figure 49. Image 6: -5 dB Threshold
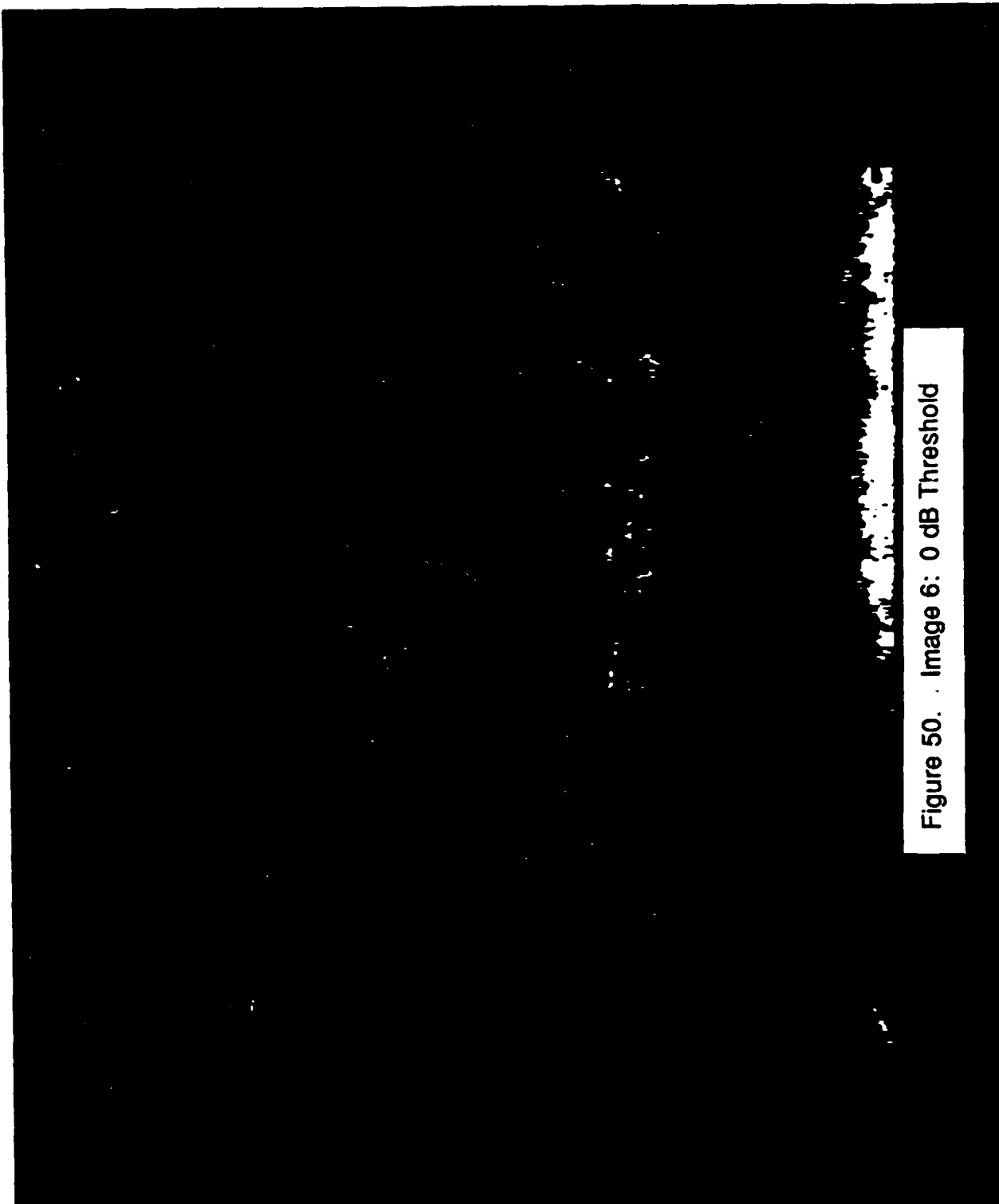
89-11902

88-11279-27

Figure 50. . Image 6: 0 dB Threshold

89-11903
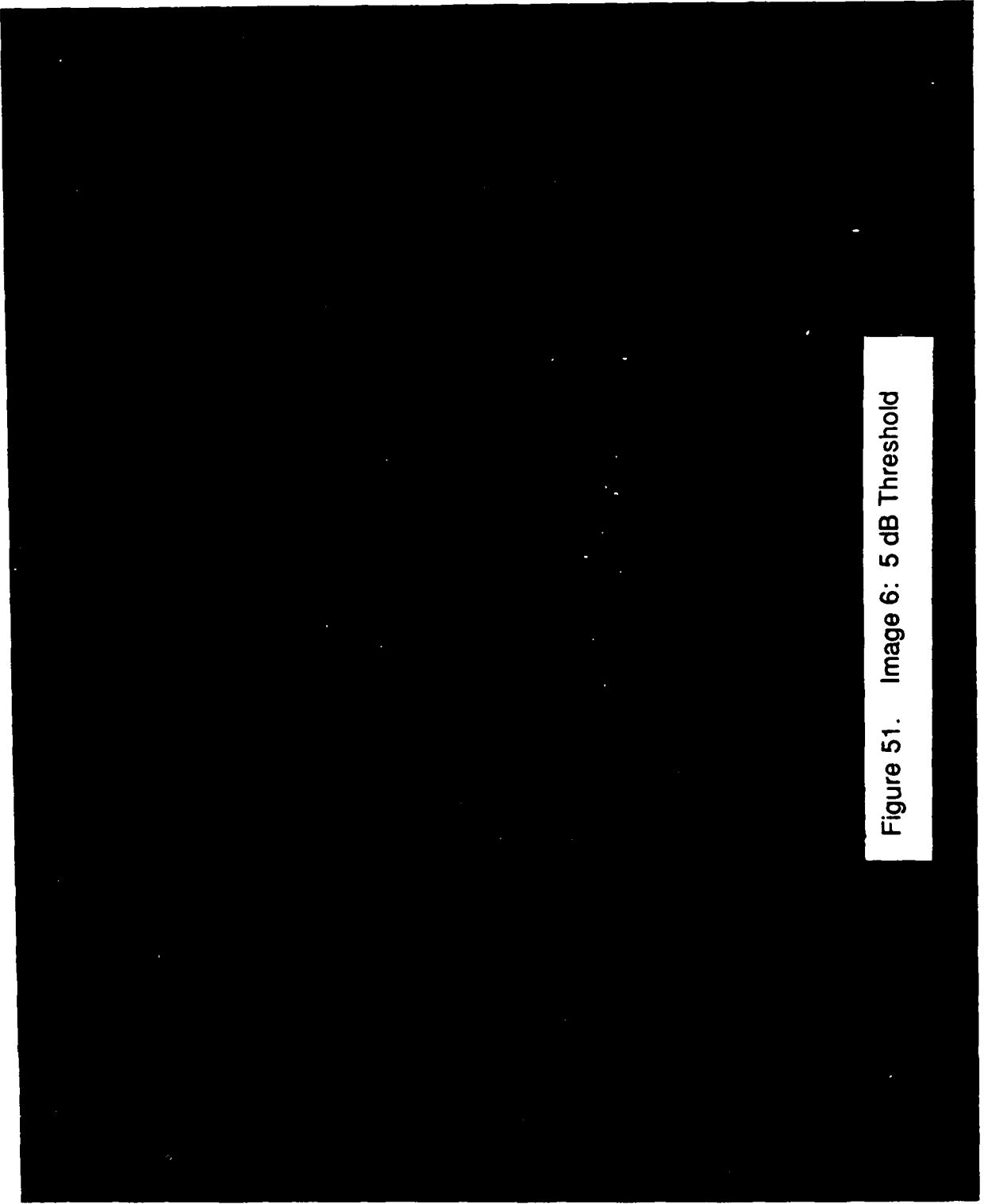
88-11279-28

Figure 51.   Image 6: 5 dB Threshold

89-11905
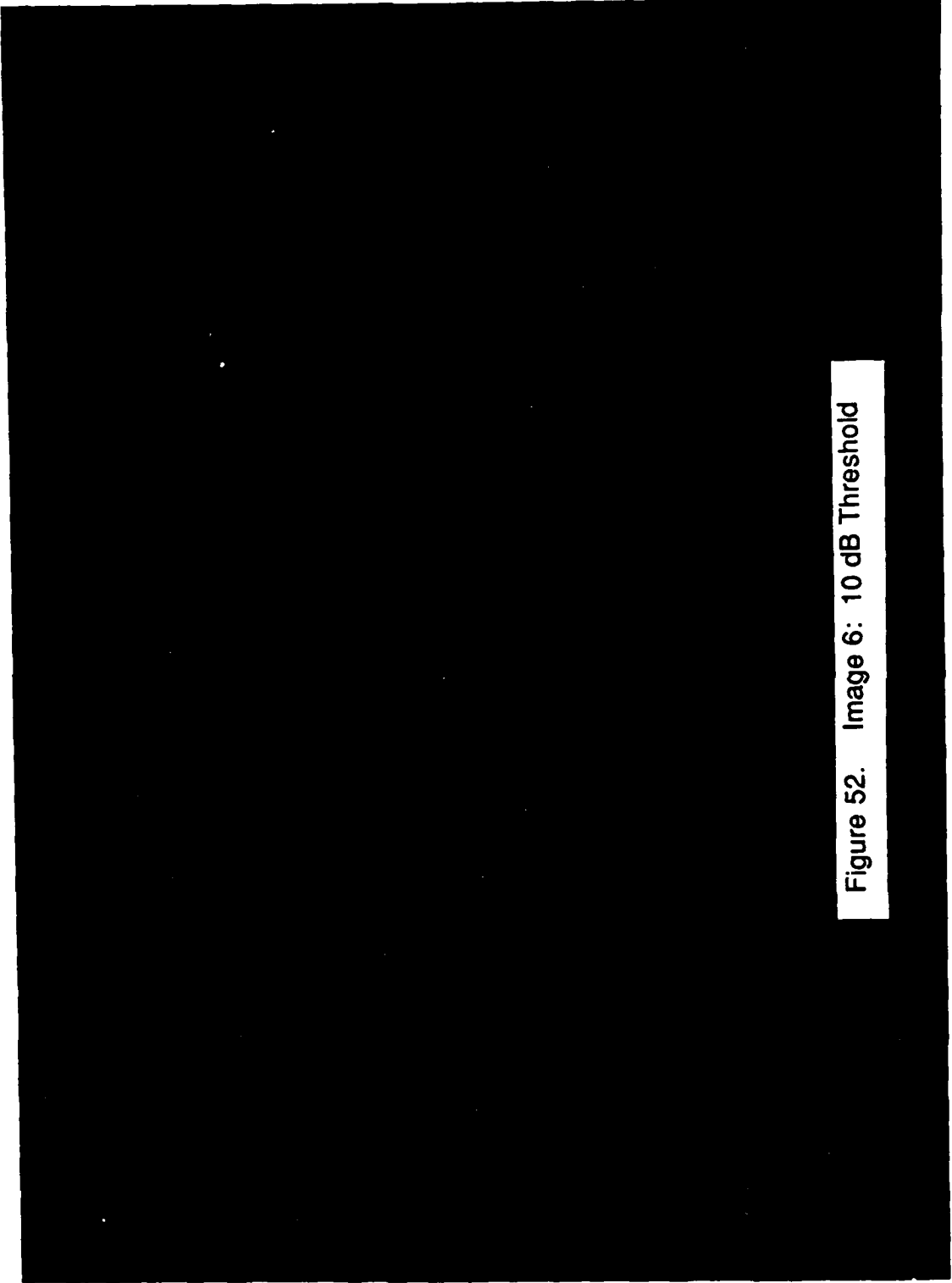
Figure 52.   Image 6:   10 dB Threshold

88-11279-34

169
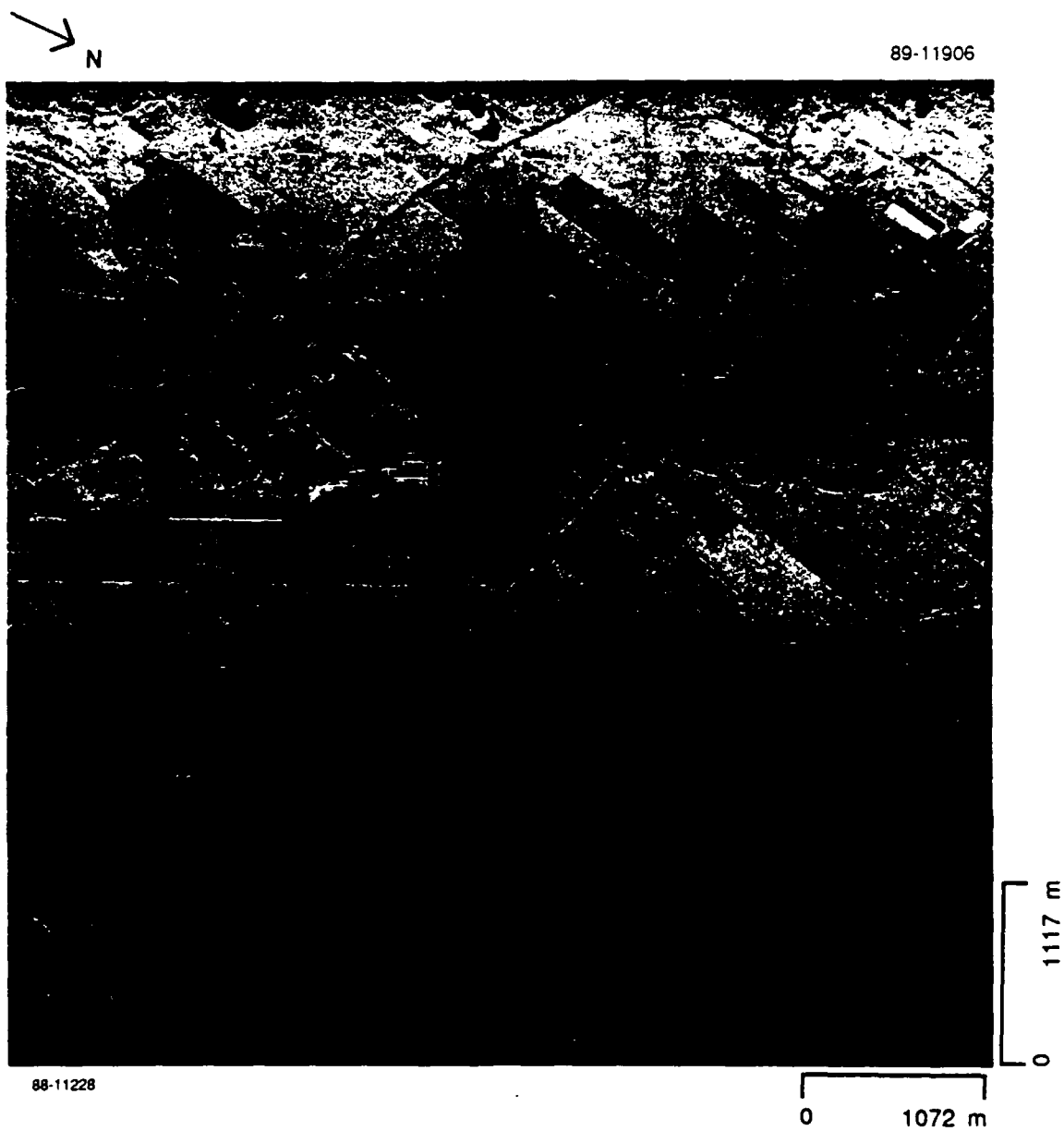
Figure 53. Peconic River Airport Observed September 1984
Using HH Polarization - Image 7
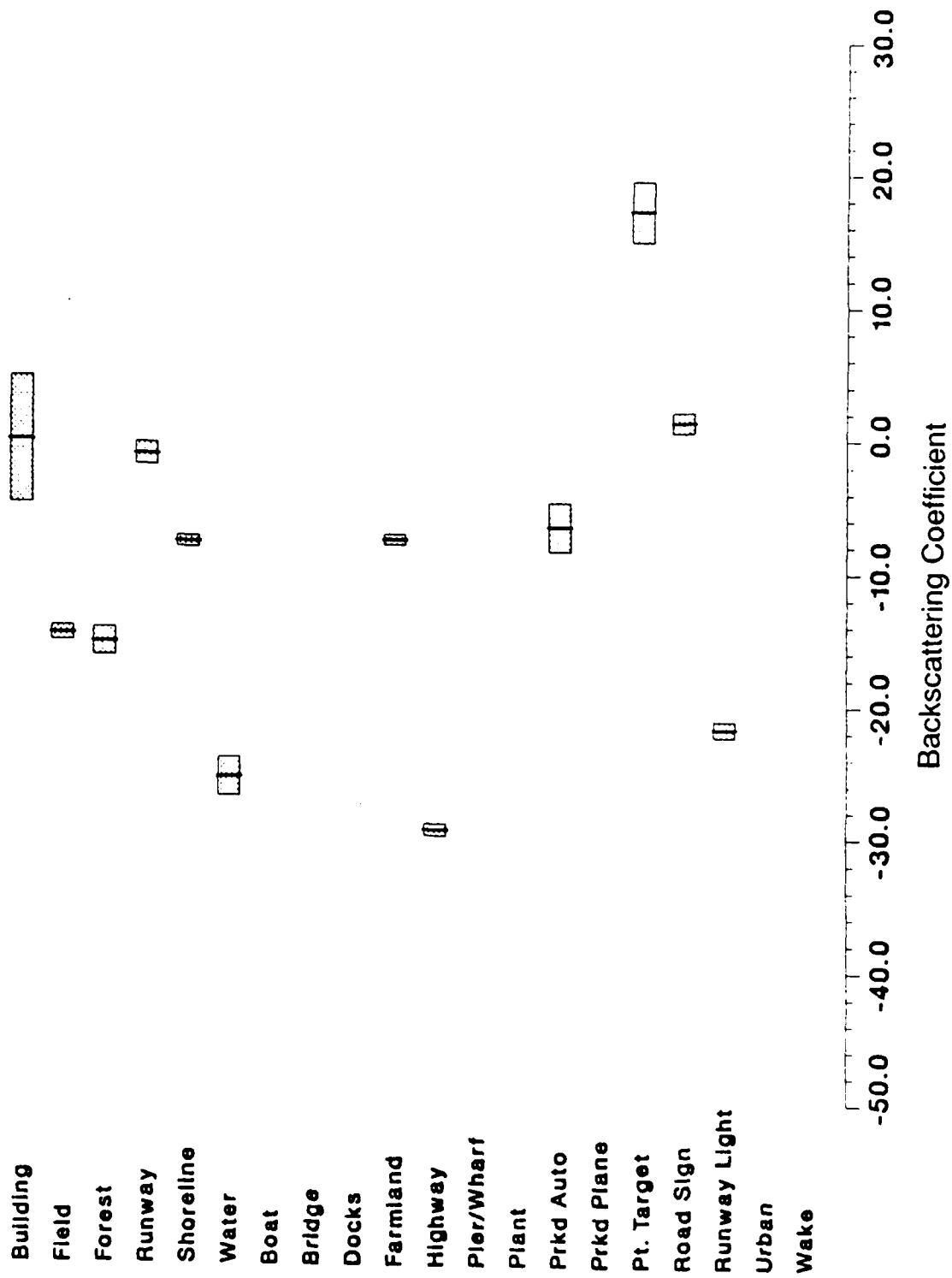
Figure 54. Image 7 Bar Chart Presentation of Means and Standard Deviation for a Variety of Airport Clutter Scenes
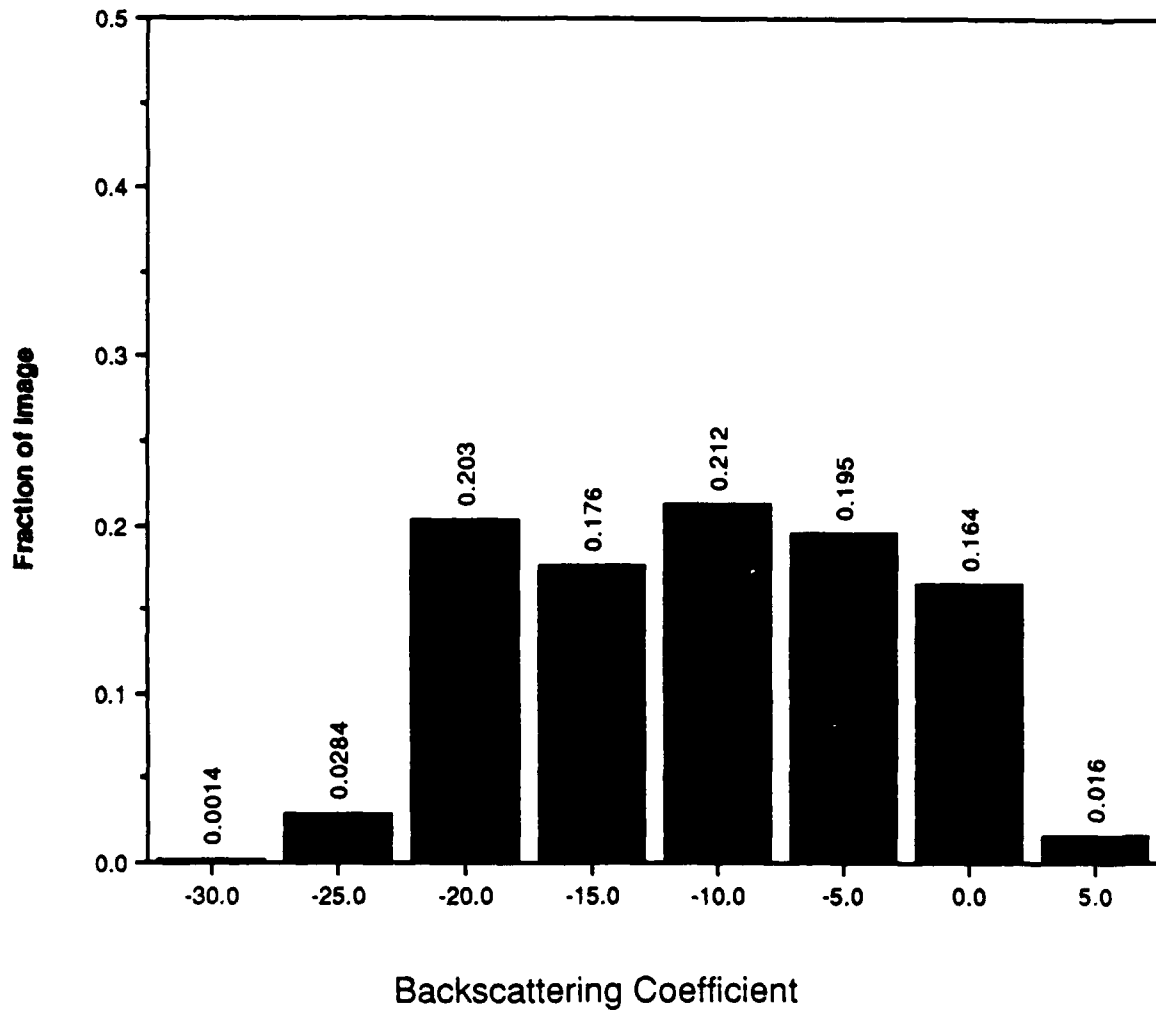
Figure 55.   Histogram of Radar Backscatter Coefficients for Image 7

89-11907
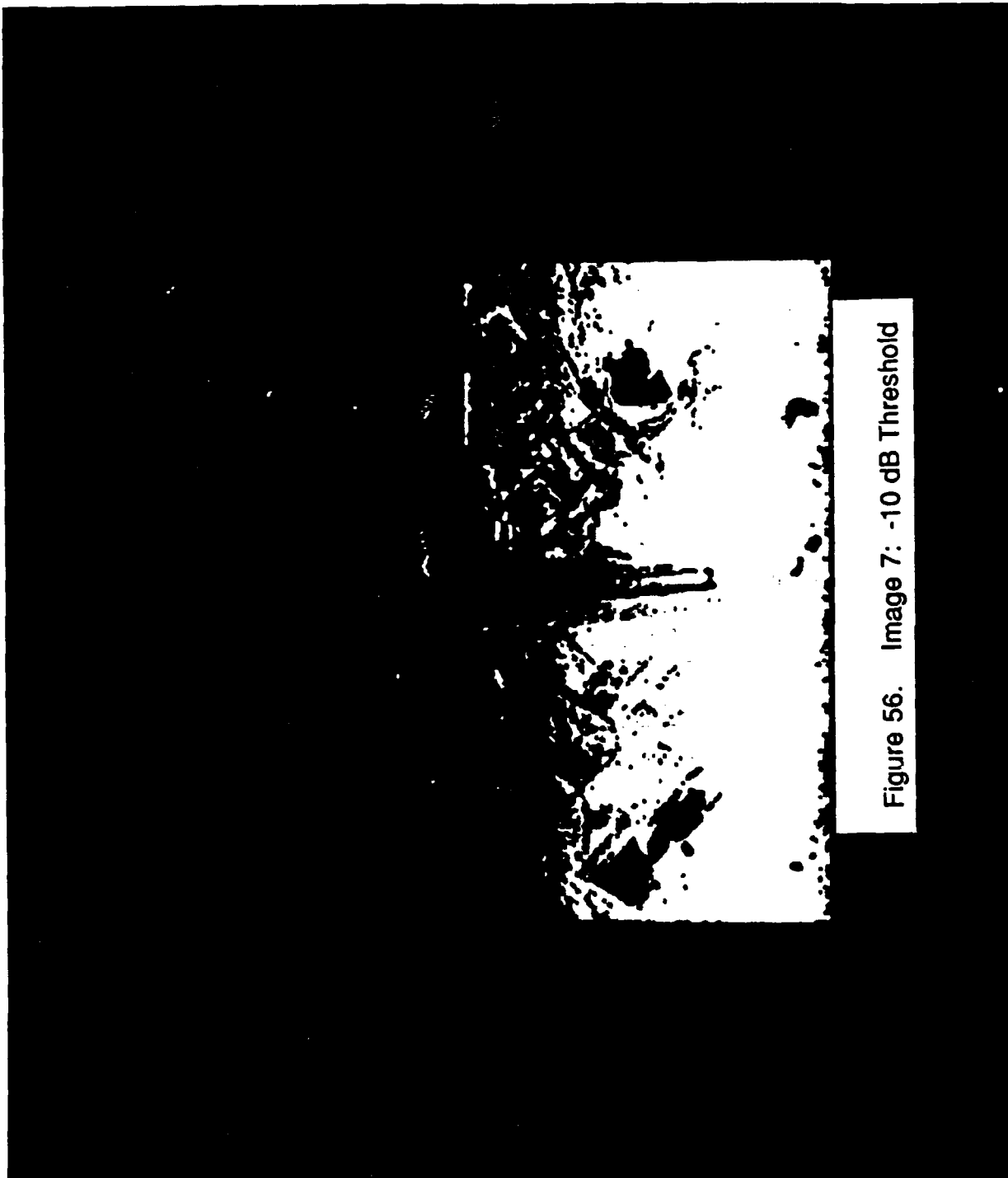
Figure 56. Image 7: -10 dB Threshold

88-11280-2A

177
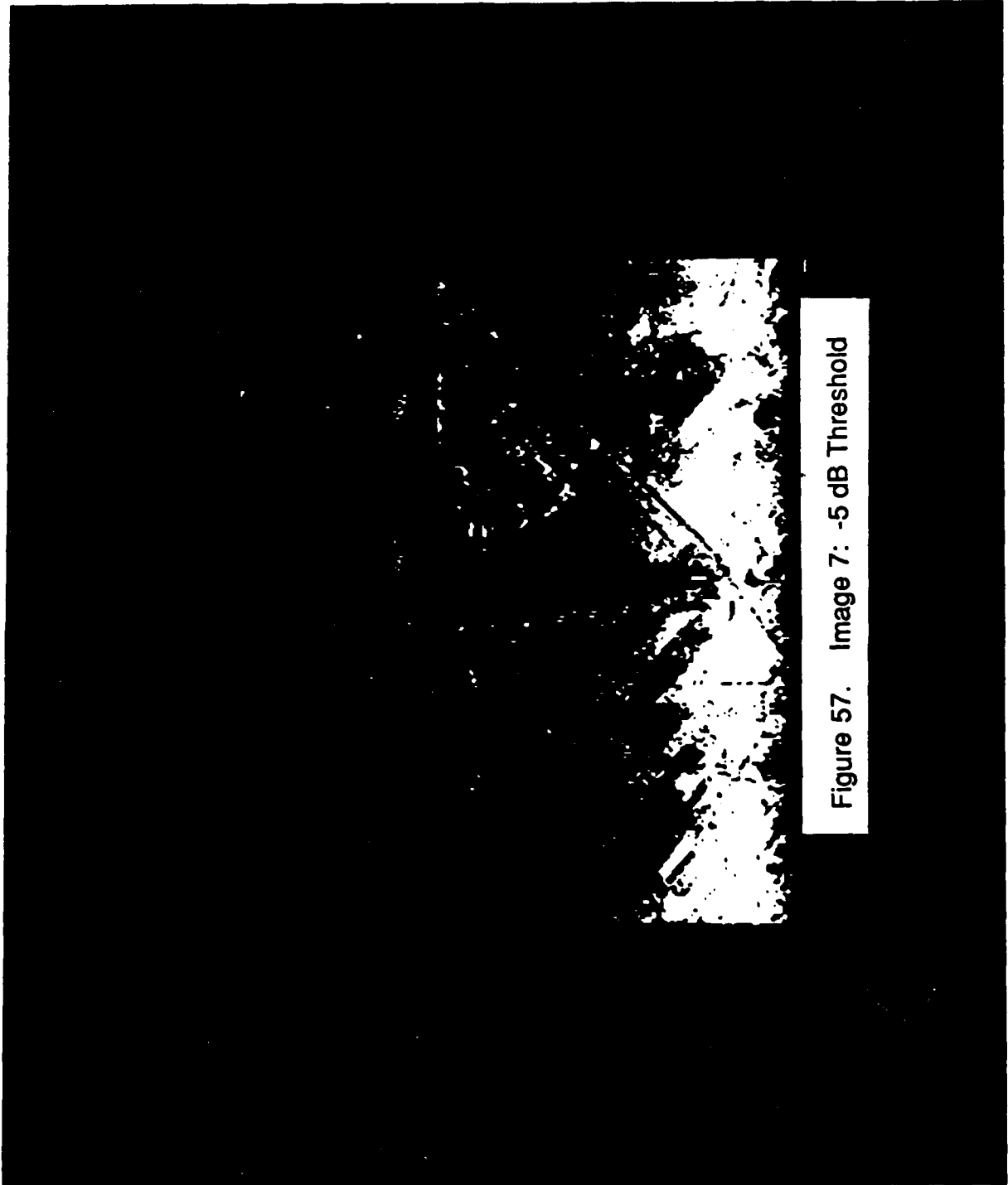
Figure 57.   Image 7: -5 dB Threshold

89-11908

88-11280-4A

179

Figure 58.   Image 7: 0 dB Threshold

89-11909

88-11280-7A

181
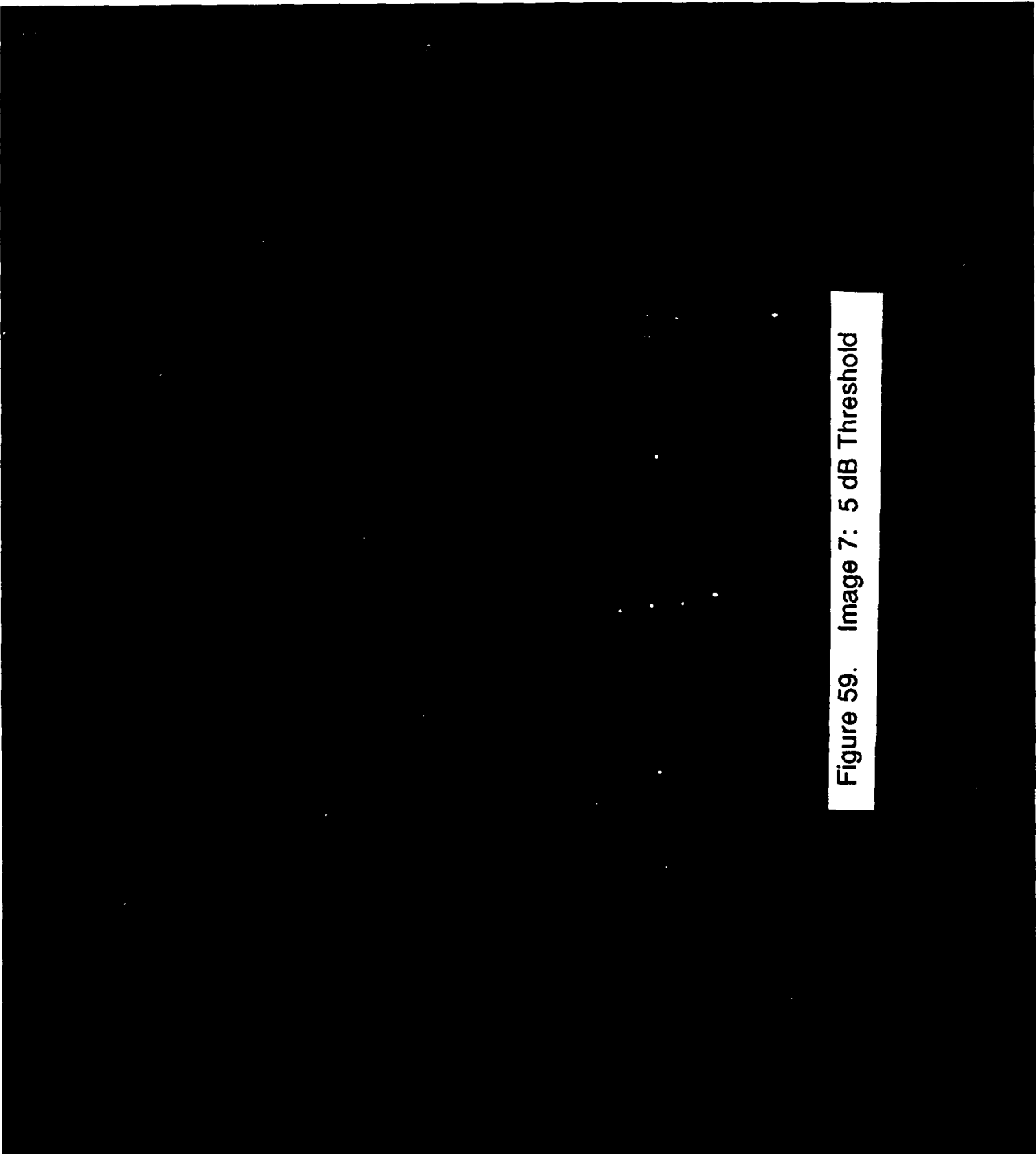
Figure 59.   Image 7: 5 dB Threshold

89-11910
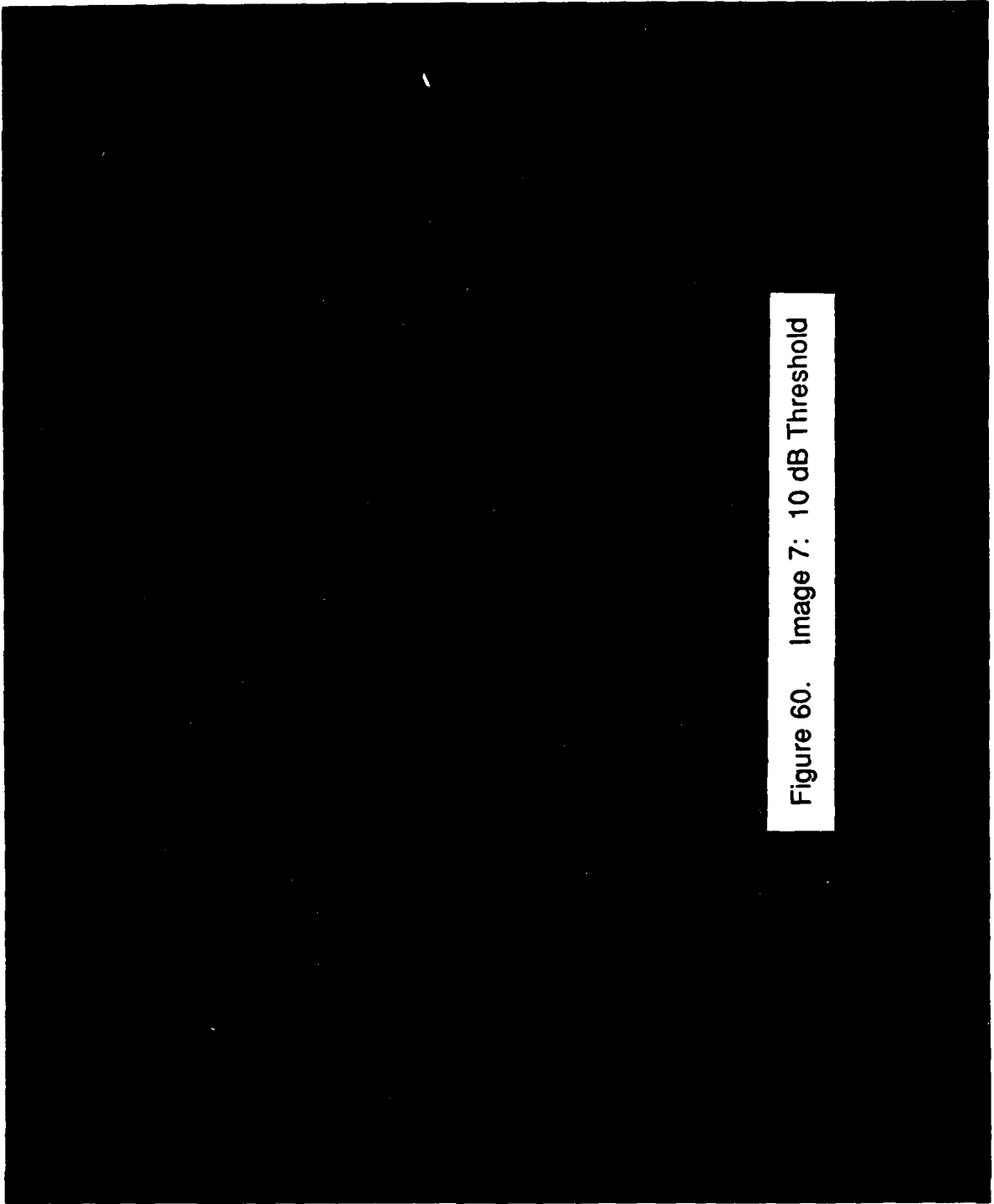
88-11280-11A

Figure 60.   Image 7: 10 dB Threshold
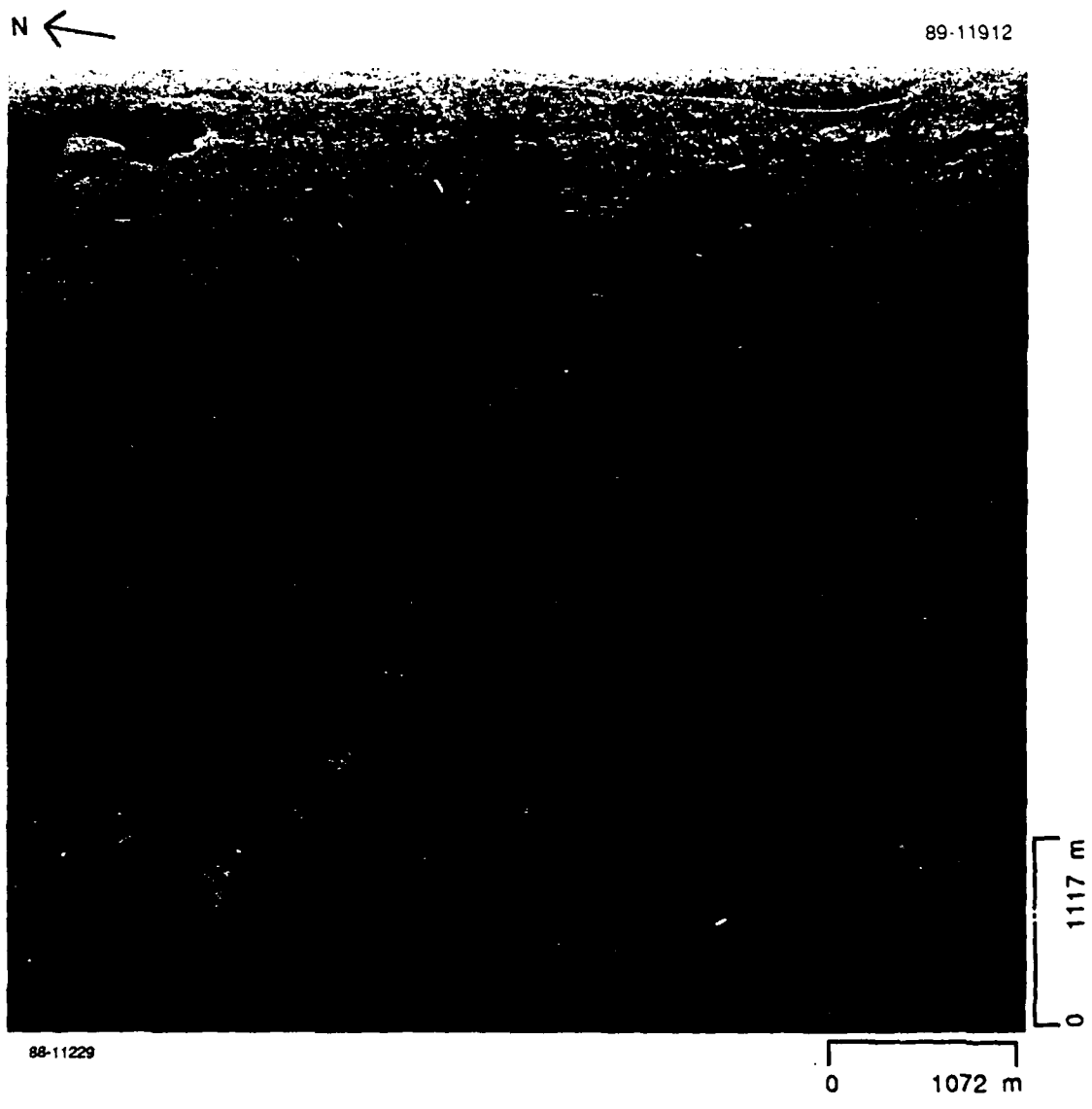
Figure 61.   Victoria International Airport Observed July 1983
              Using HH Polarization - Image 8
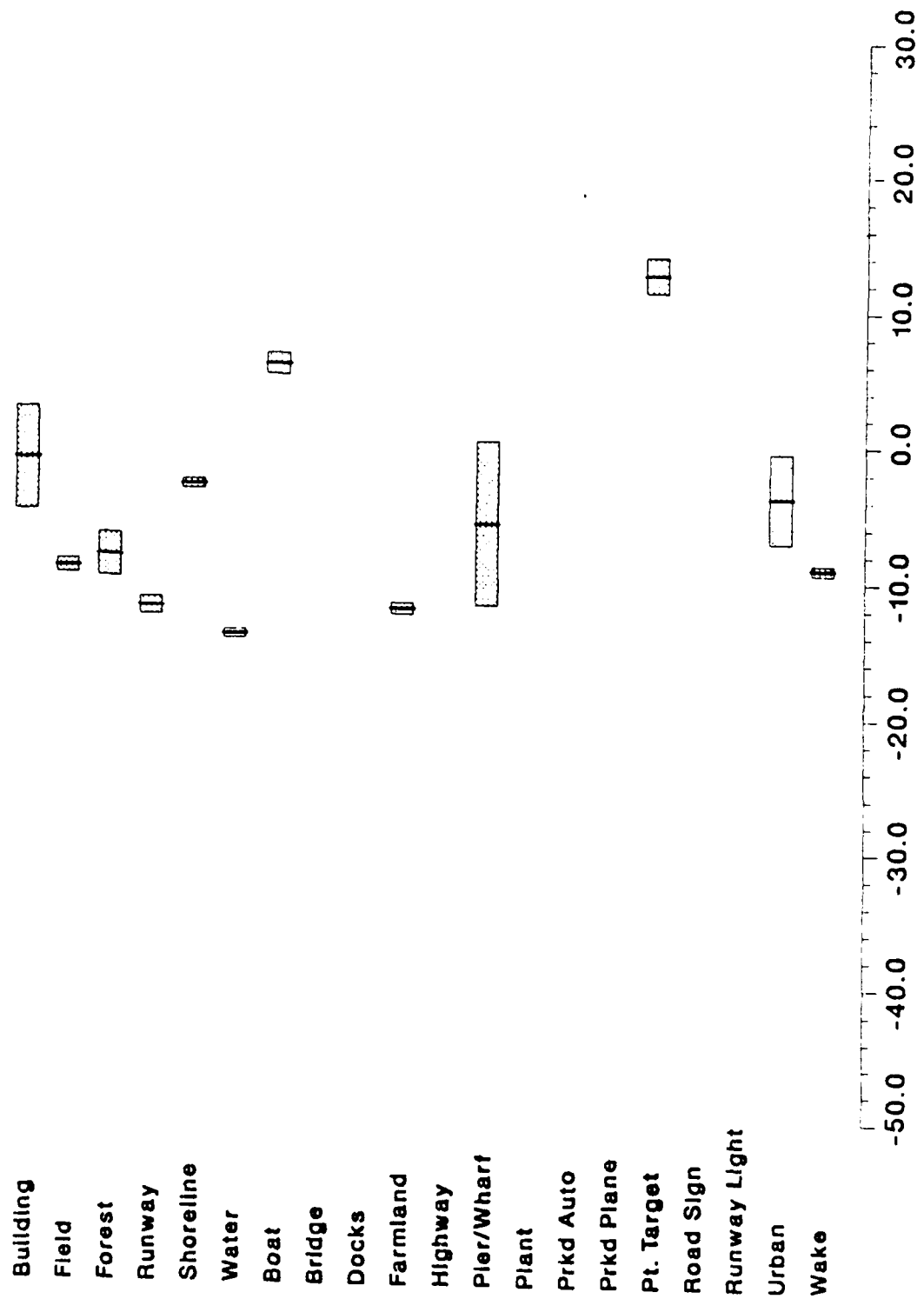
Figure 62.   Image 8 Bar Chart Presentation of Means and Standard
Deviation for a Variety of Airport Clutter Scenes
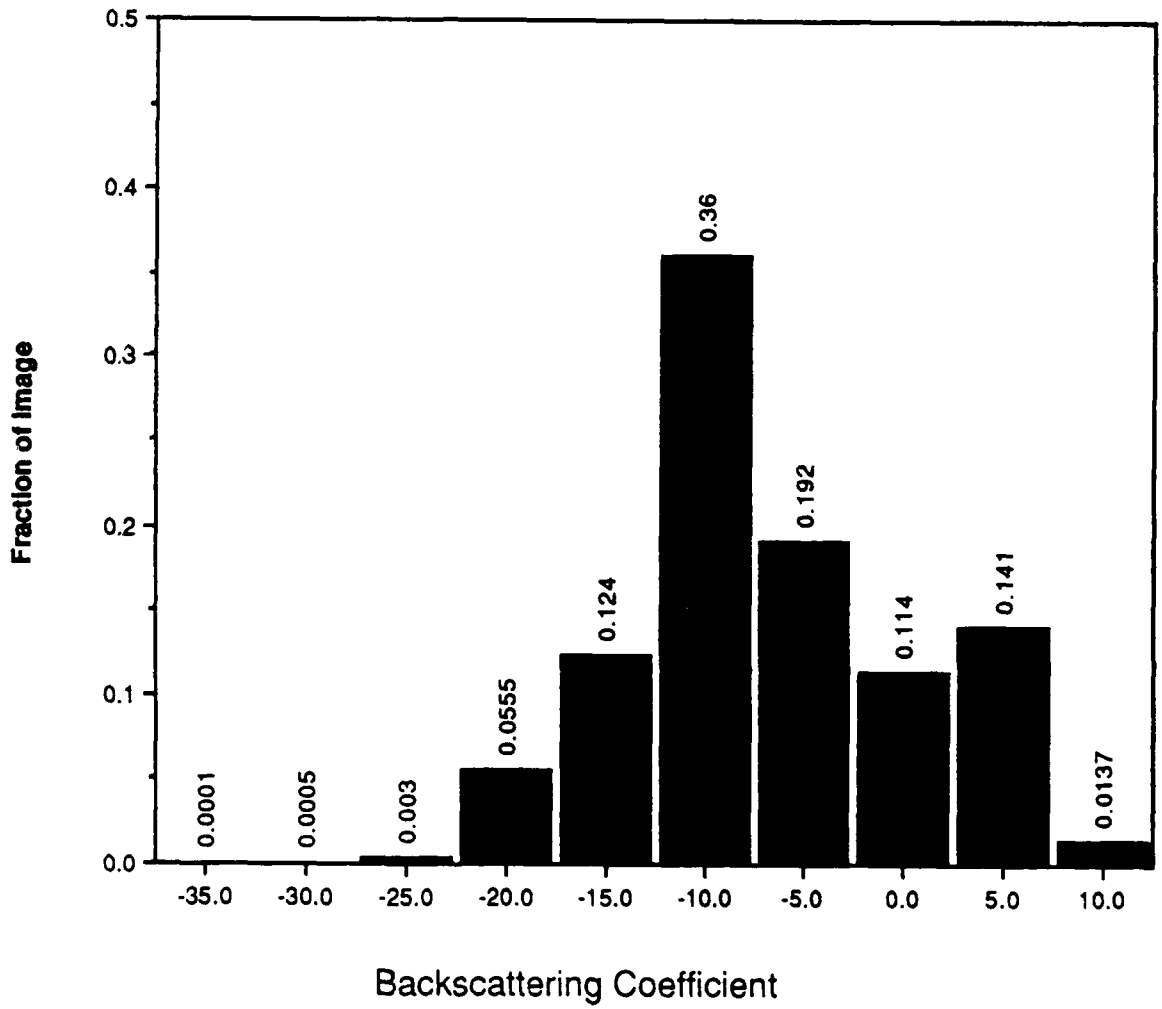
Figure 63.   Histogram of Radar Backscatter Coefficients for Image 8

89-11913
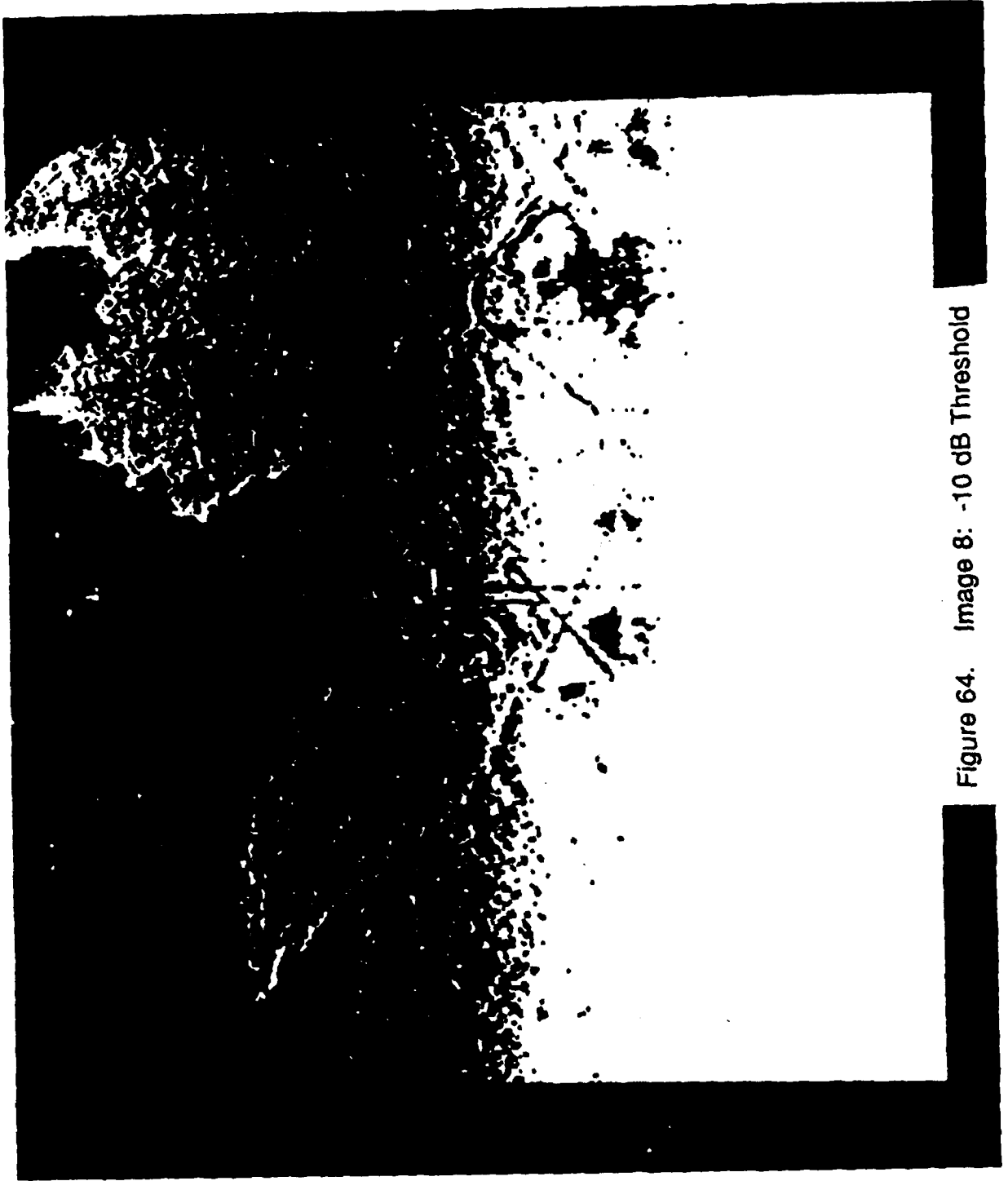
Figure 64.   Image 8: -10 dB Threshold

88-11280-16A

193
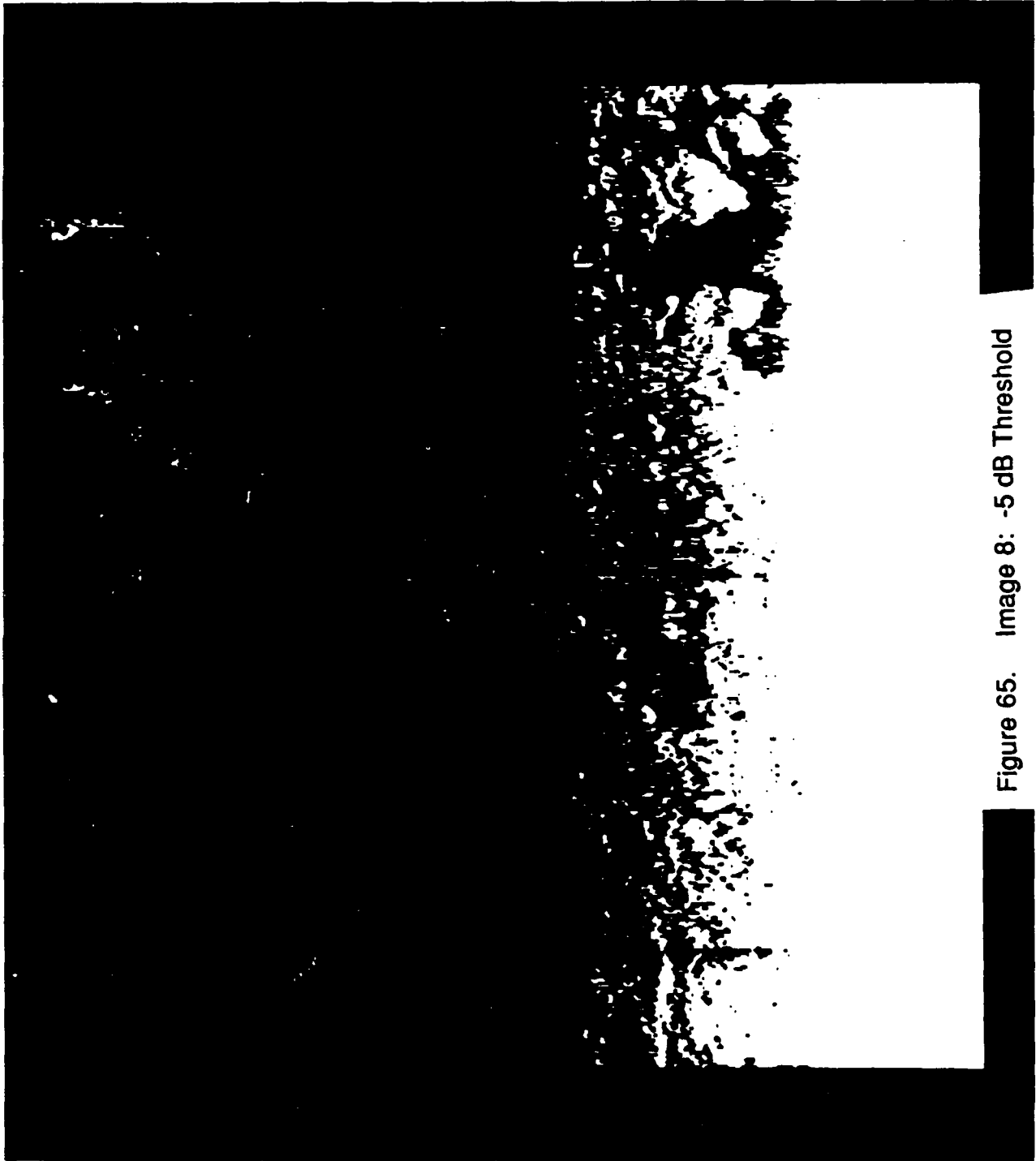
Figure 65.   Image 8: -5 dB Threshold

89-11914

88-11280-19A
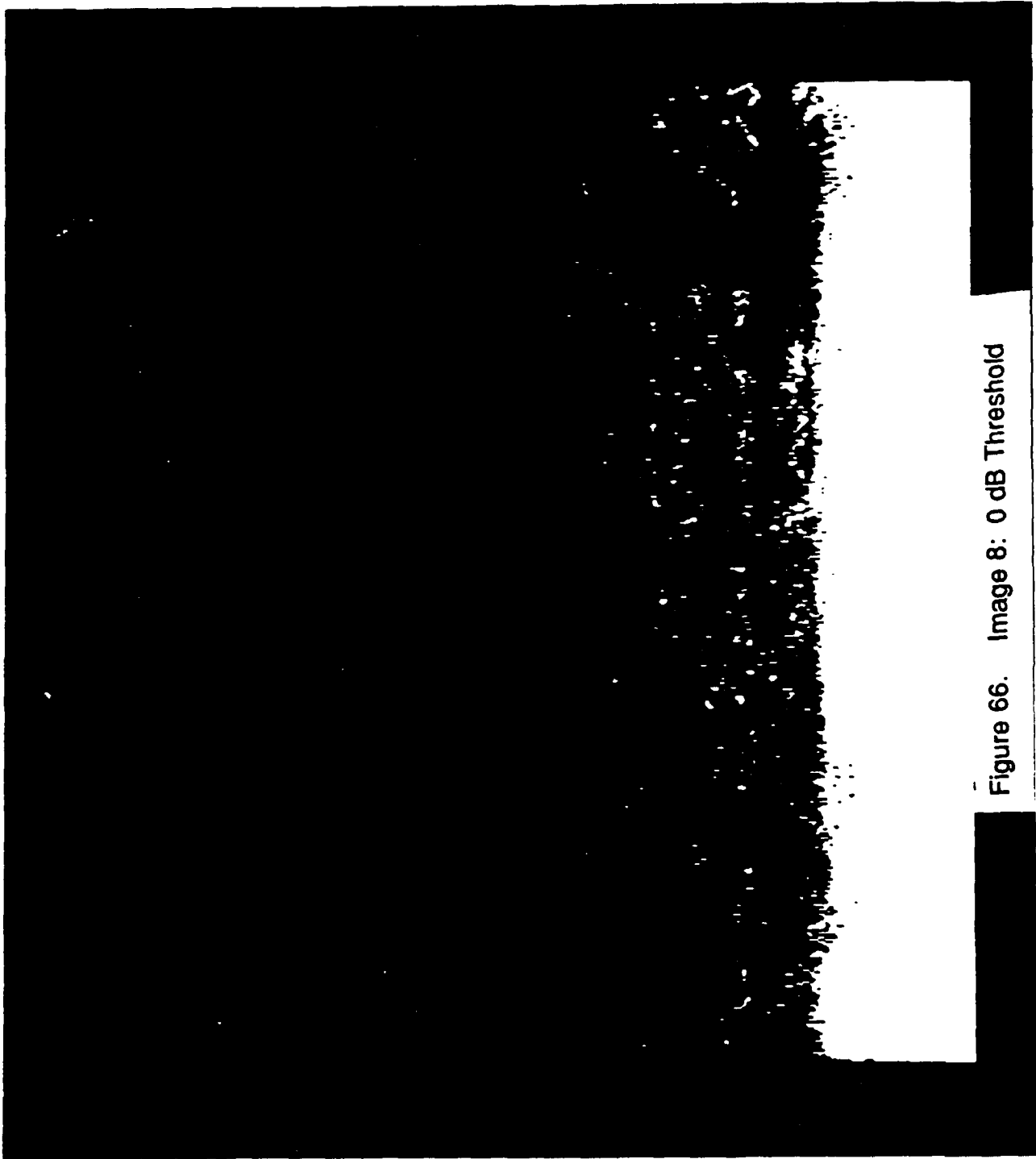
Figure 66. Image 8: 0 dB Threshold
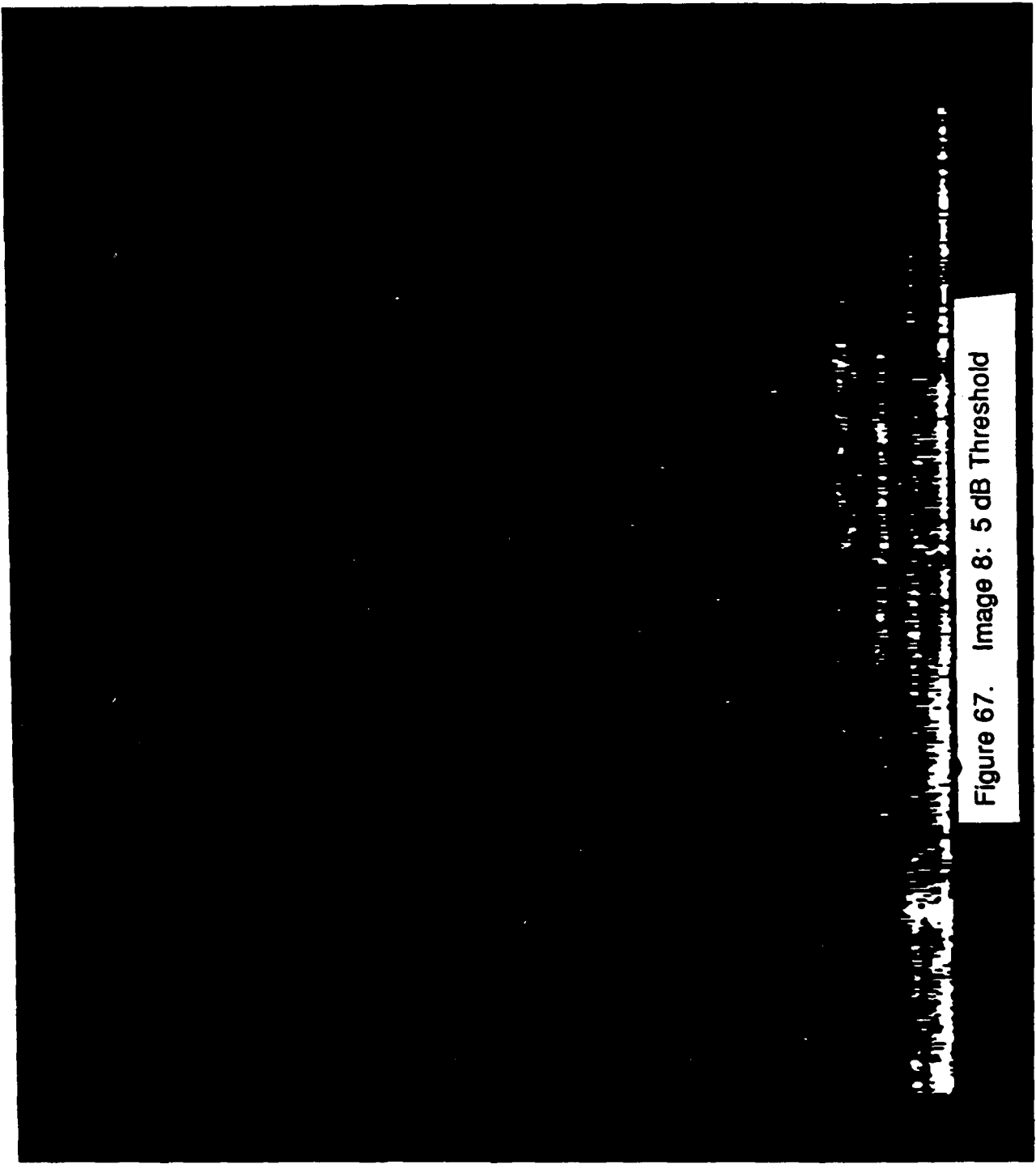
Figure 67. Image 8: 5 dB Threshold

88-11280-25A

89-11917
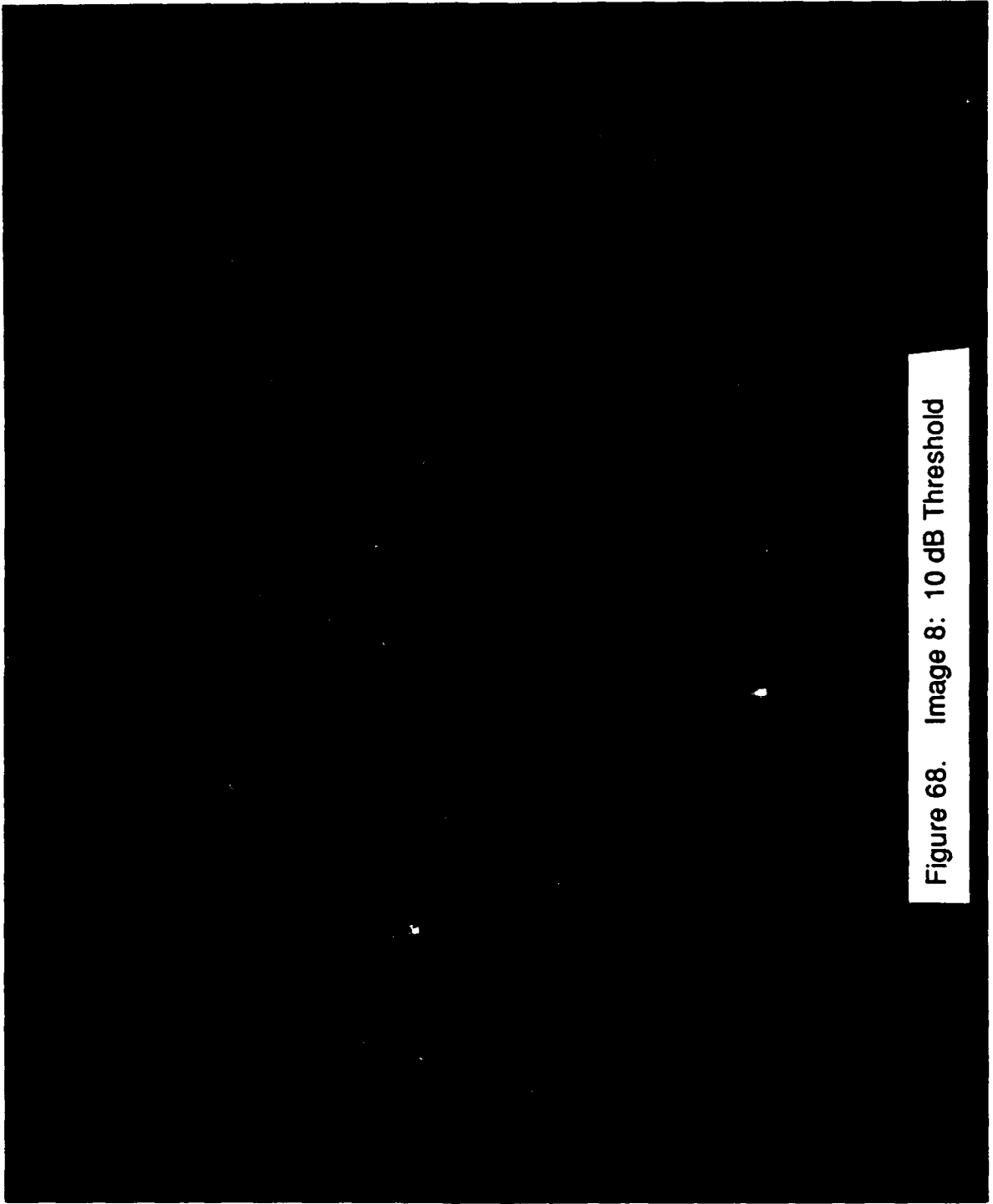
Figure 68.   Image 8: 10 dB Threshold

88 11280 28A

201
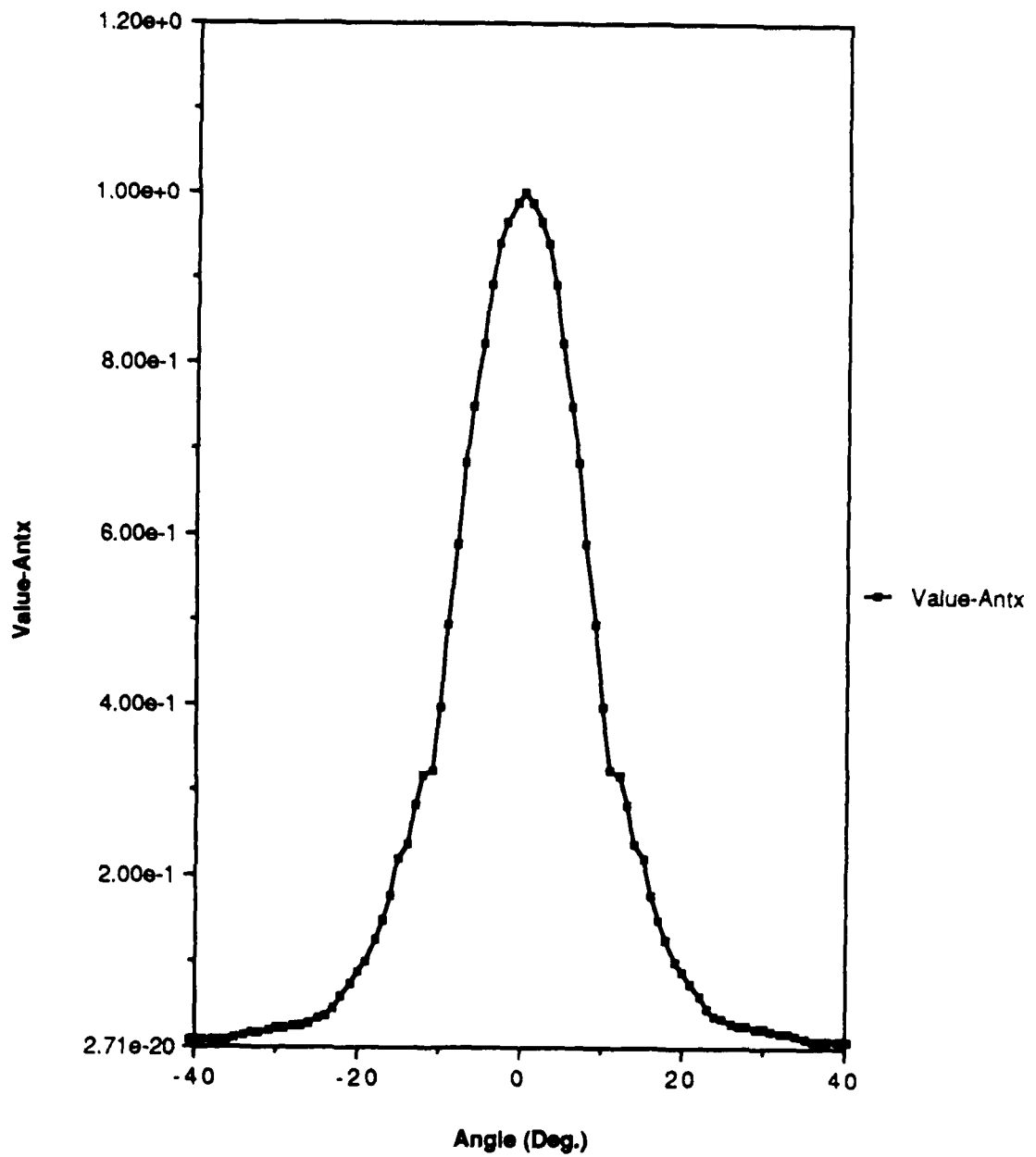
Figure 69. The SAR Antenna Pattern is Shown in the Figure.
The Gain Values Beyond 15 Degress were Estimated Based
on the Expected Antenna Pattern Shape Function

203

# Probability Density Function
of Forest Clutter Areas
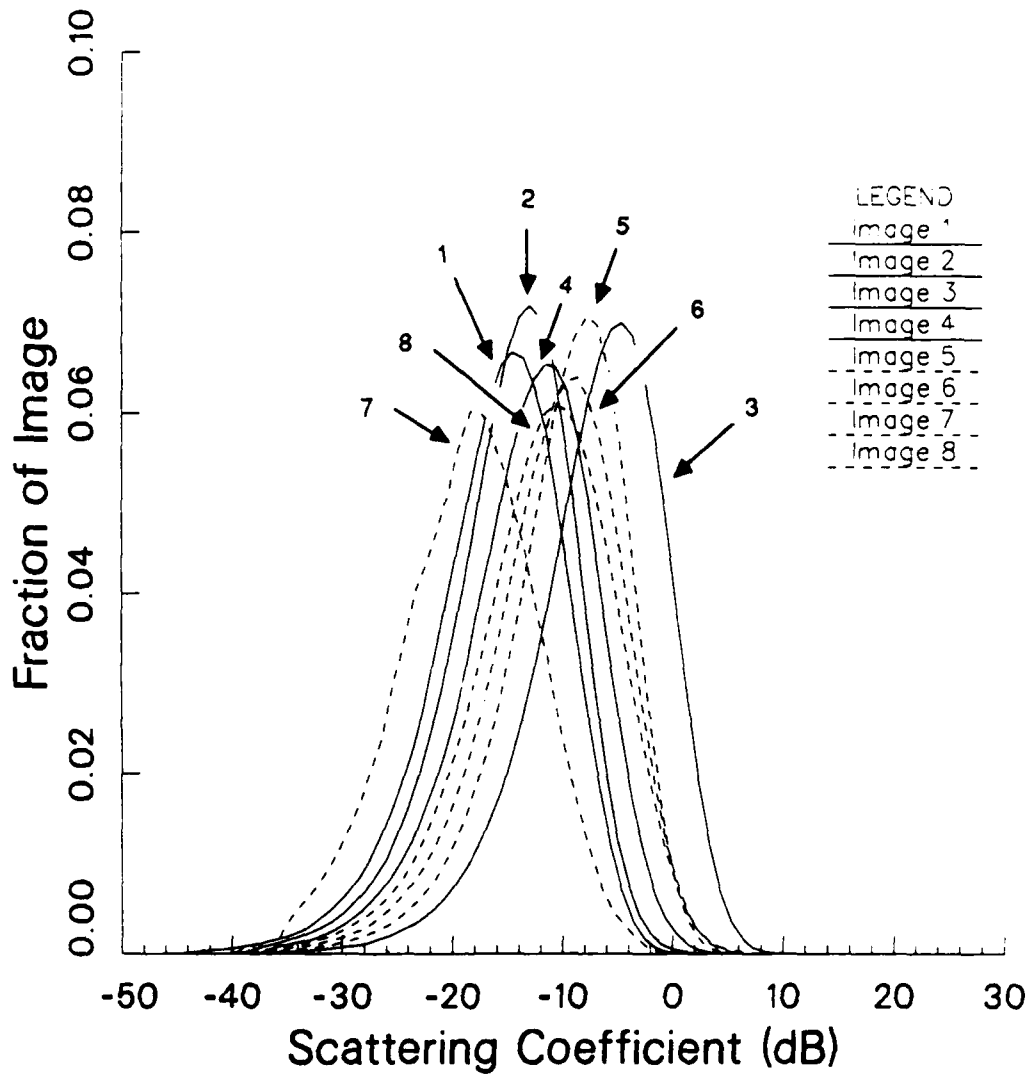
Figure 70.

Probability Density Function
# of Field Clutter Areas
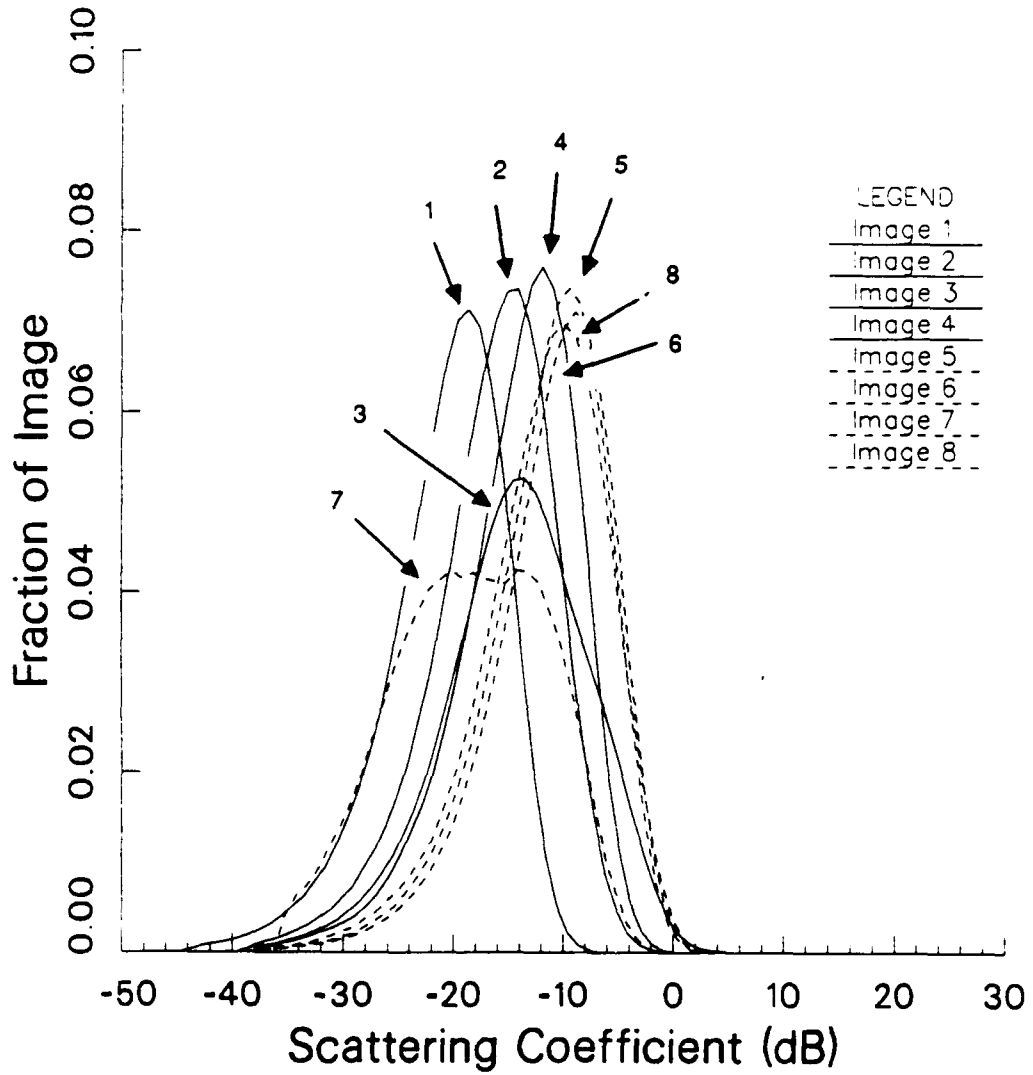
Figure 71.

Probability Density Function
of Farmland Clutter Areas
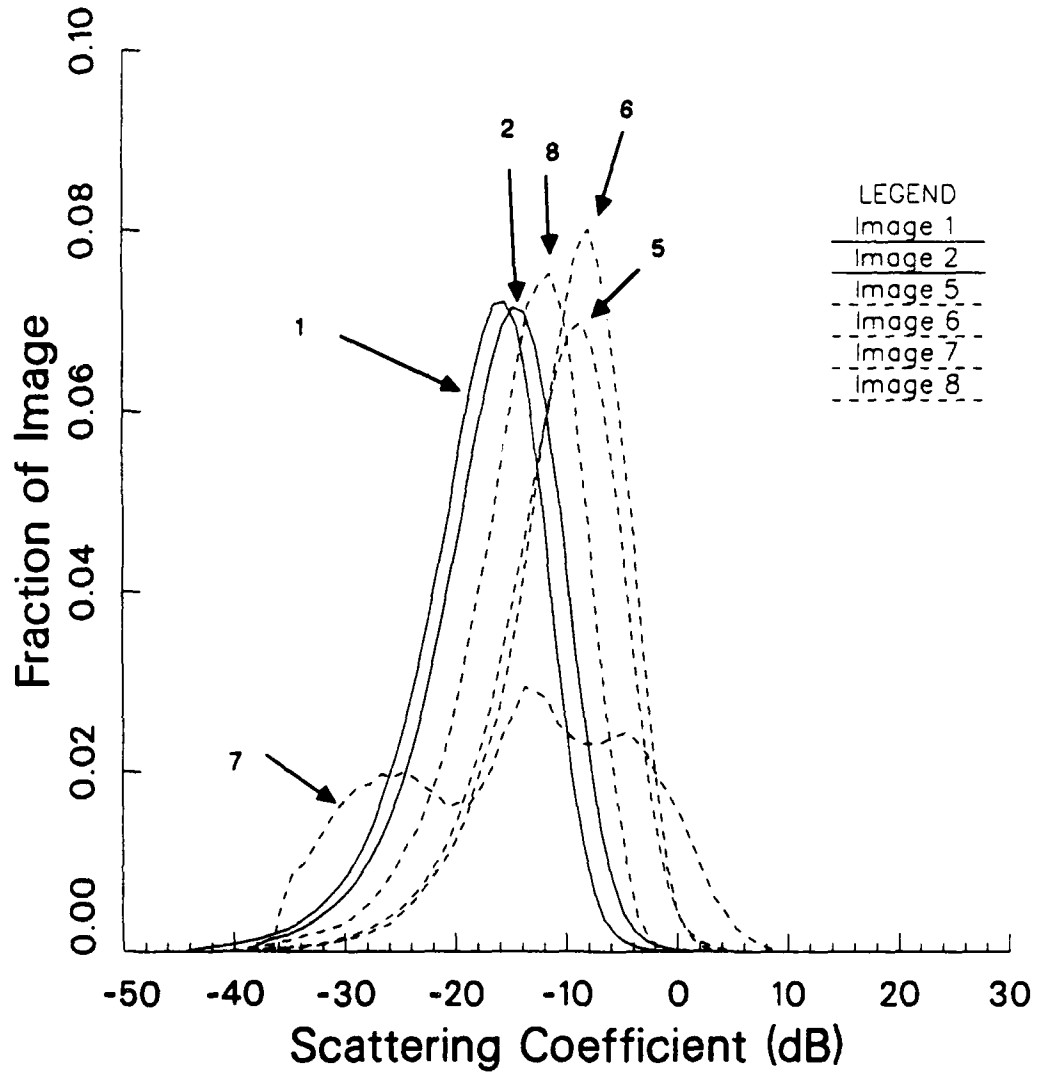
Figure 72.

Probability Density Function
of Water Clutter Areas
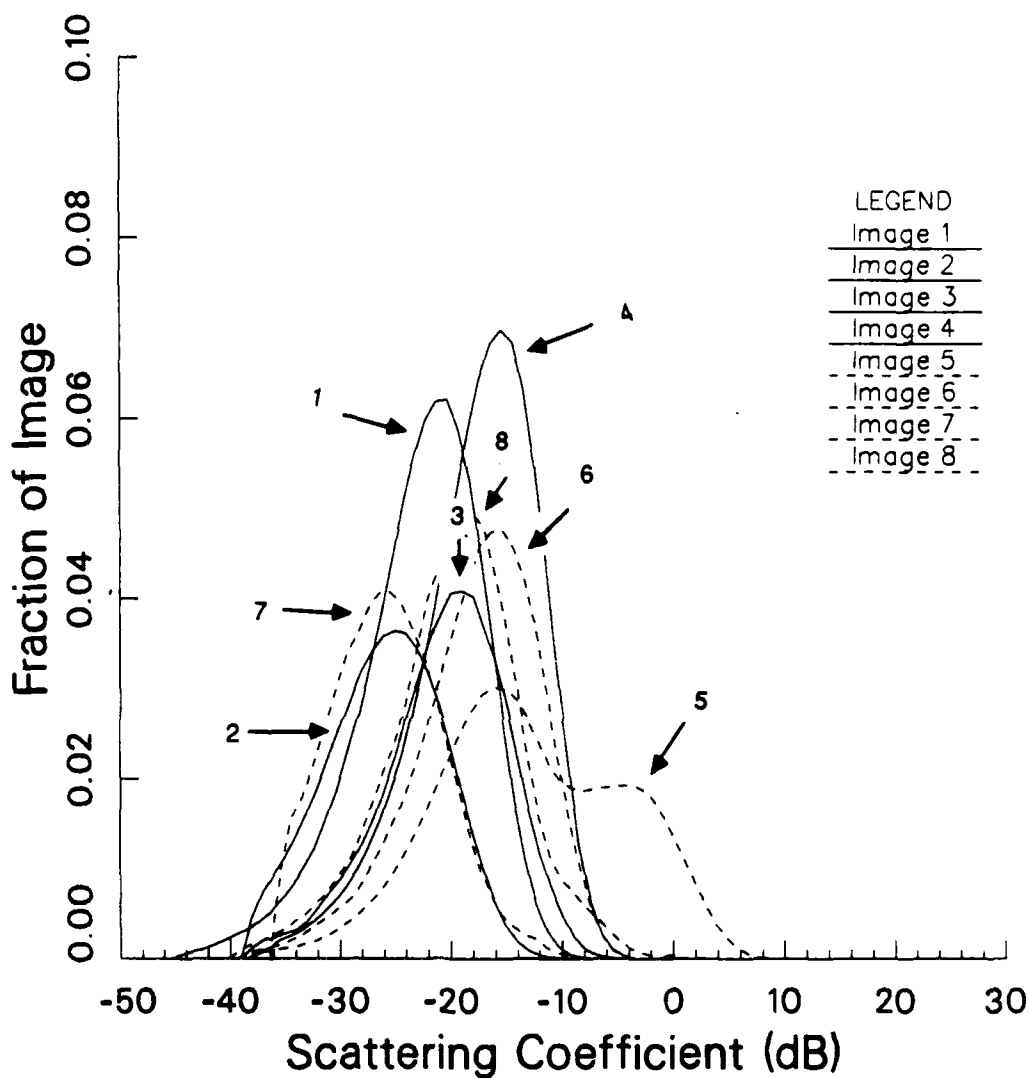
Figure 73.

Probability Density Function
of Runway Clutter Areas
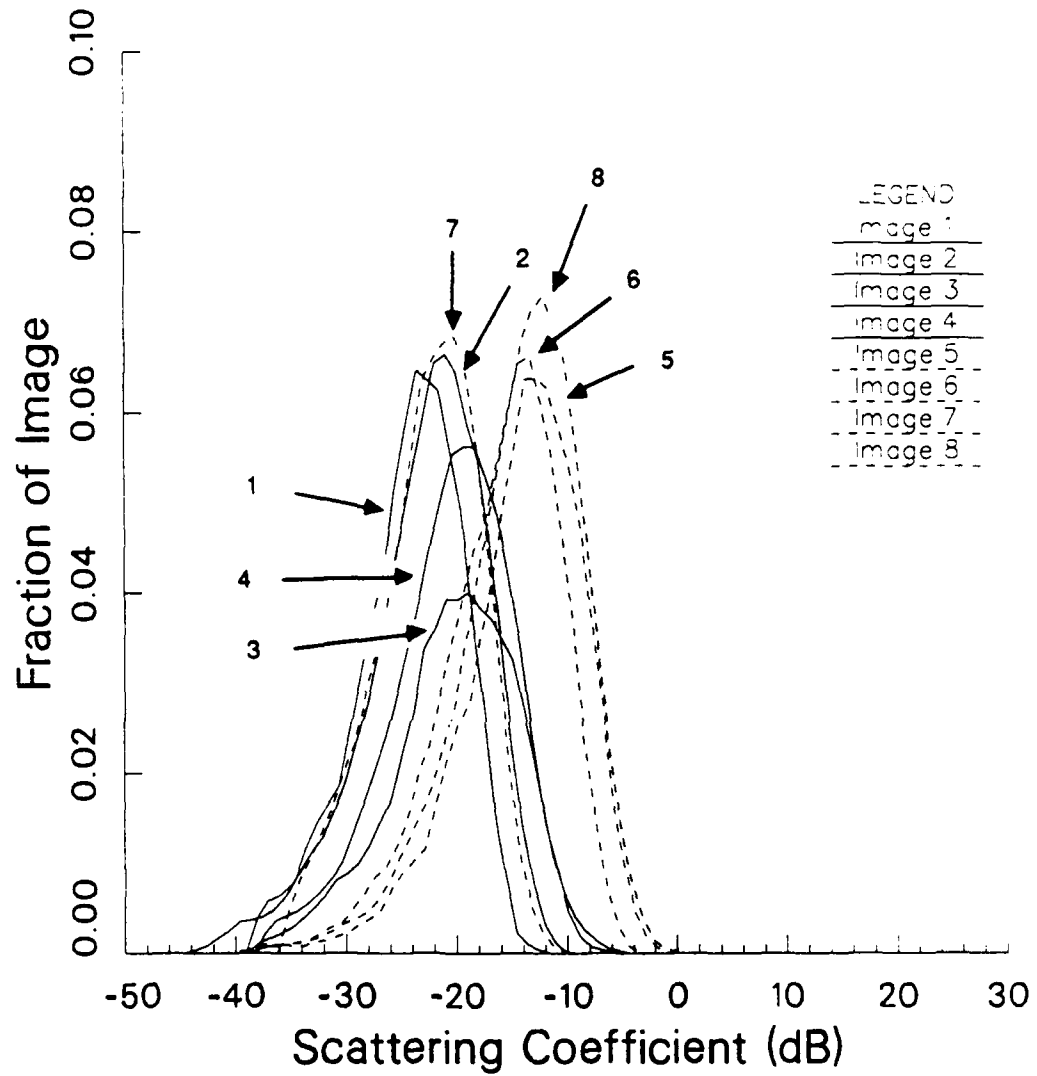
Figure 74.

Probability Density Function
of Highway Clutter Areas

Figure 75.

215
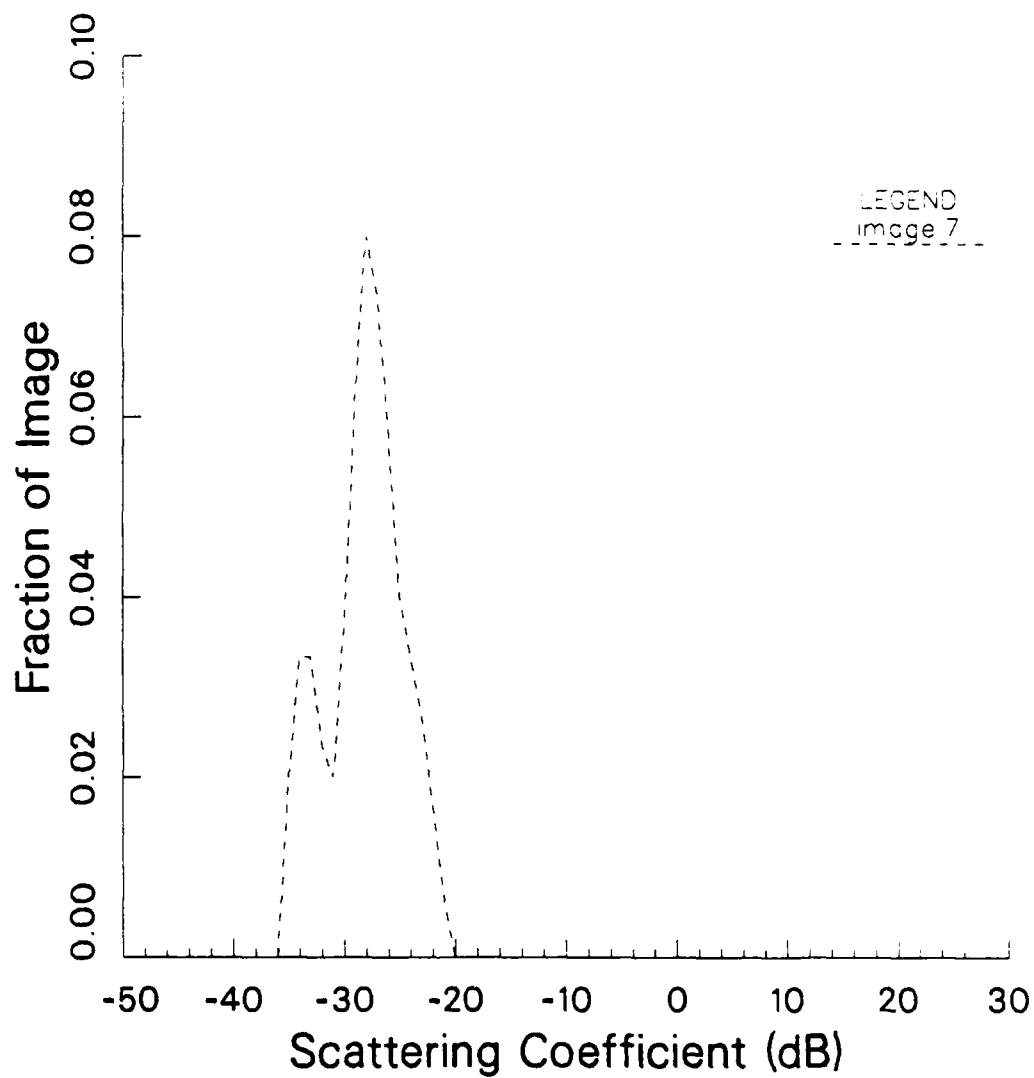
Probability Density Function
## of Urban Clutter Areas
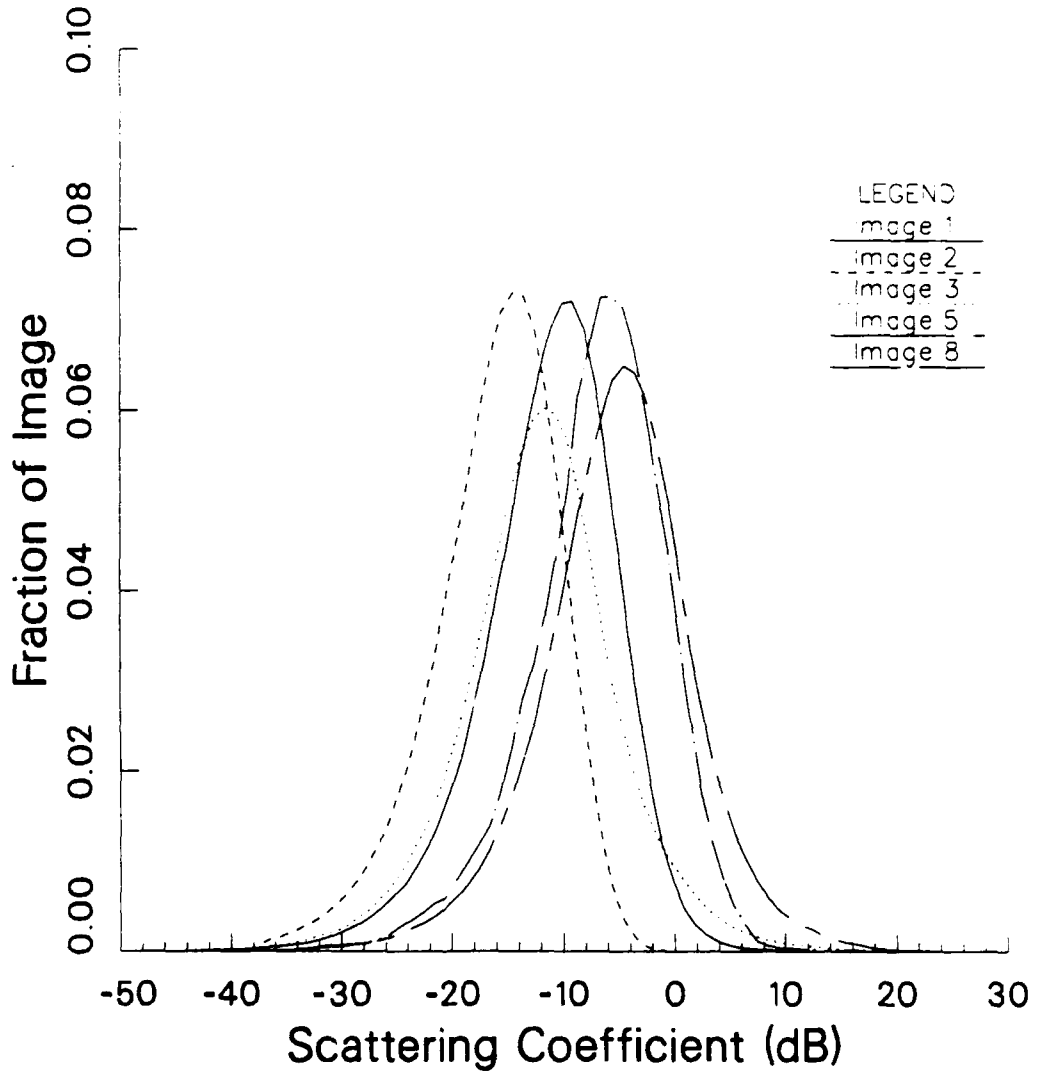
Figure 76.

Probability Density Function
of Plant Clutter Areas
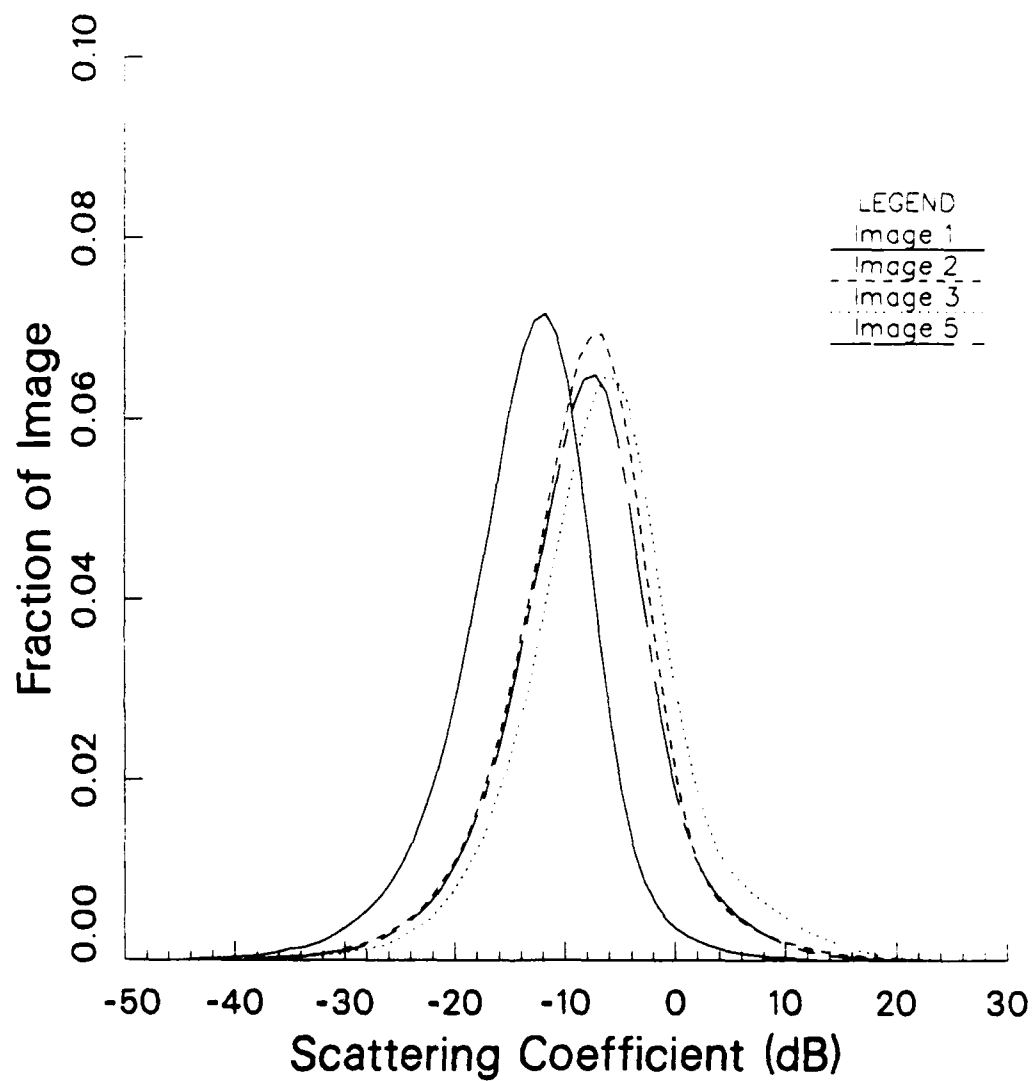
Figure 77.

Probability Density Function
of Building Clutter Areas
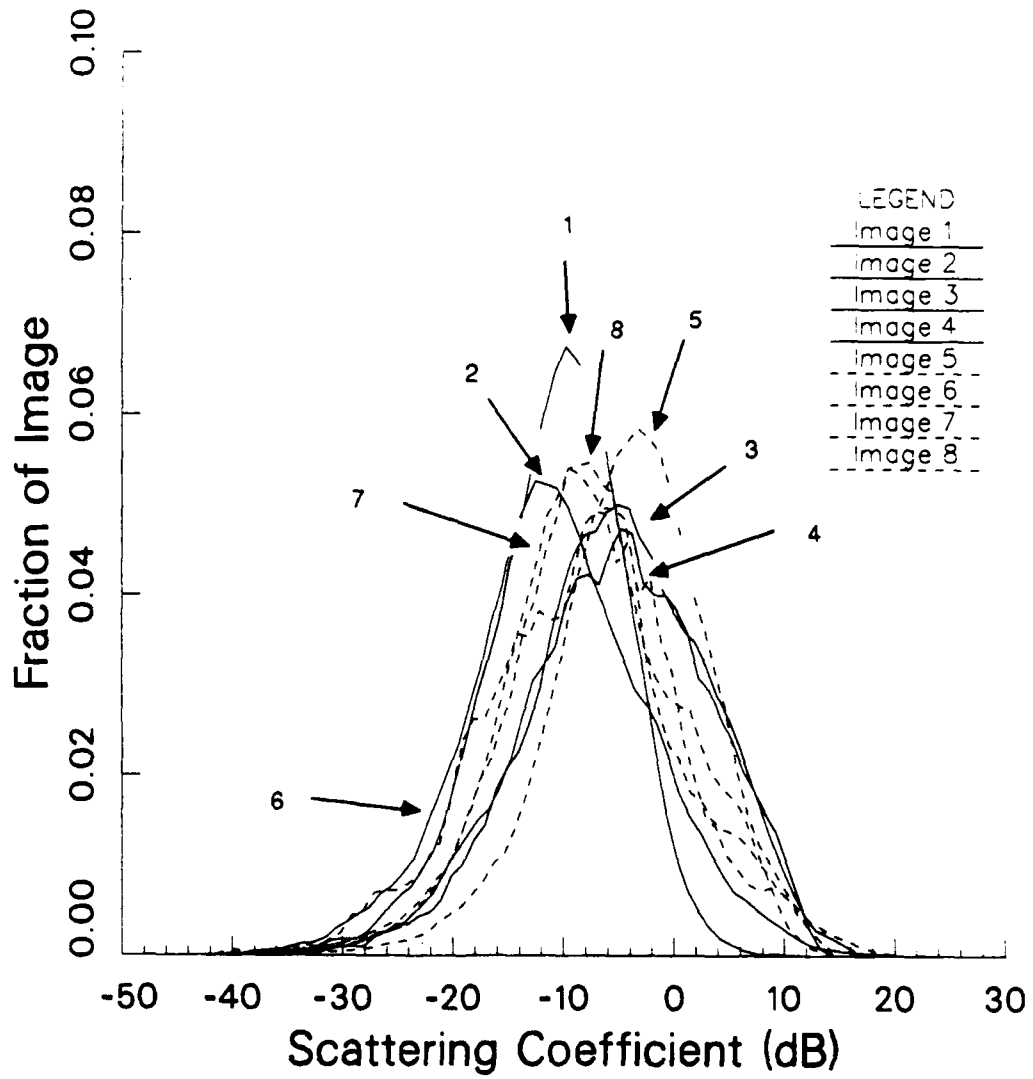
Figure 78.

Probability Density Function
of Forest and Urban Clutter Areas
Image 1
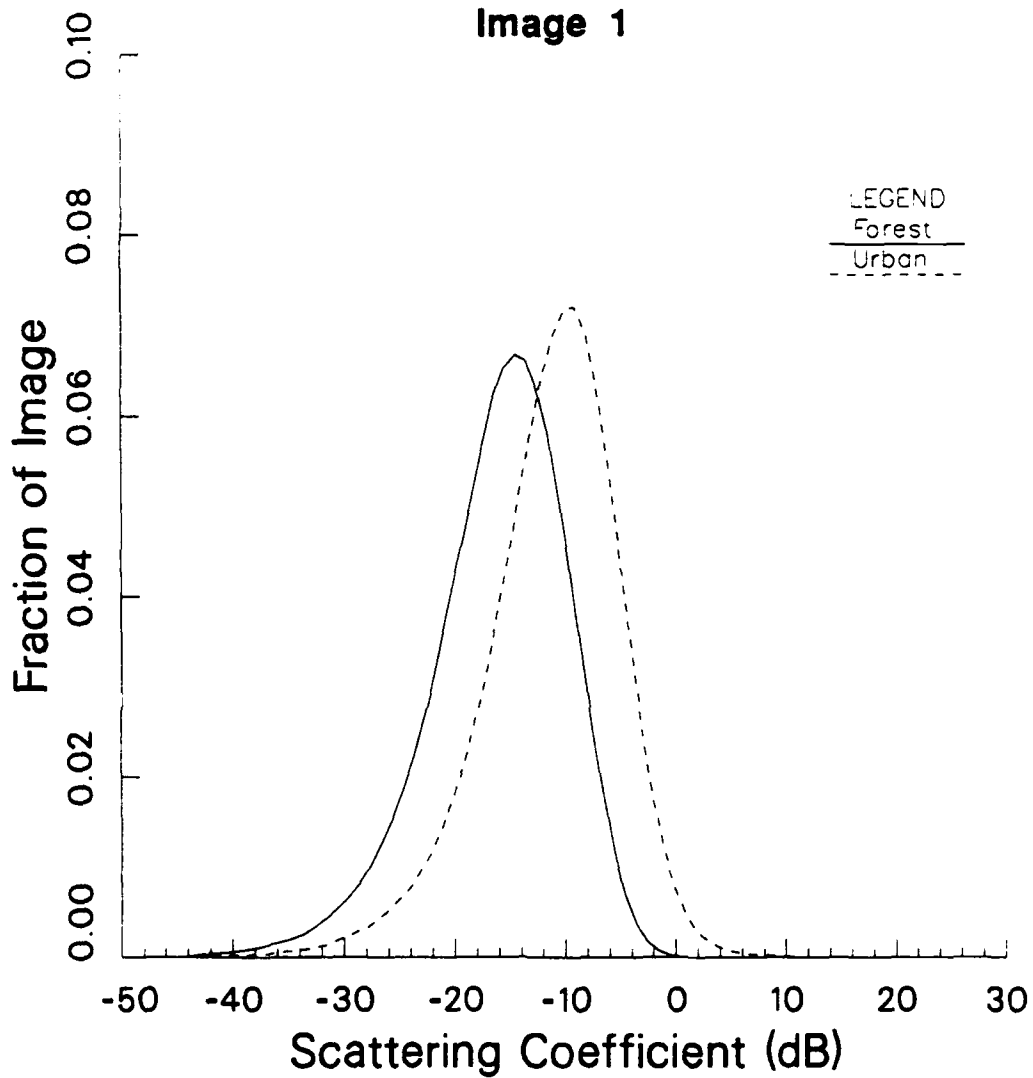
Figure 79.

Probability Density Function
of Forest and Urban Clutter Areas

Image 2
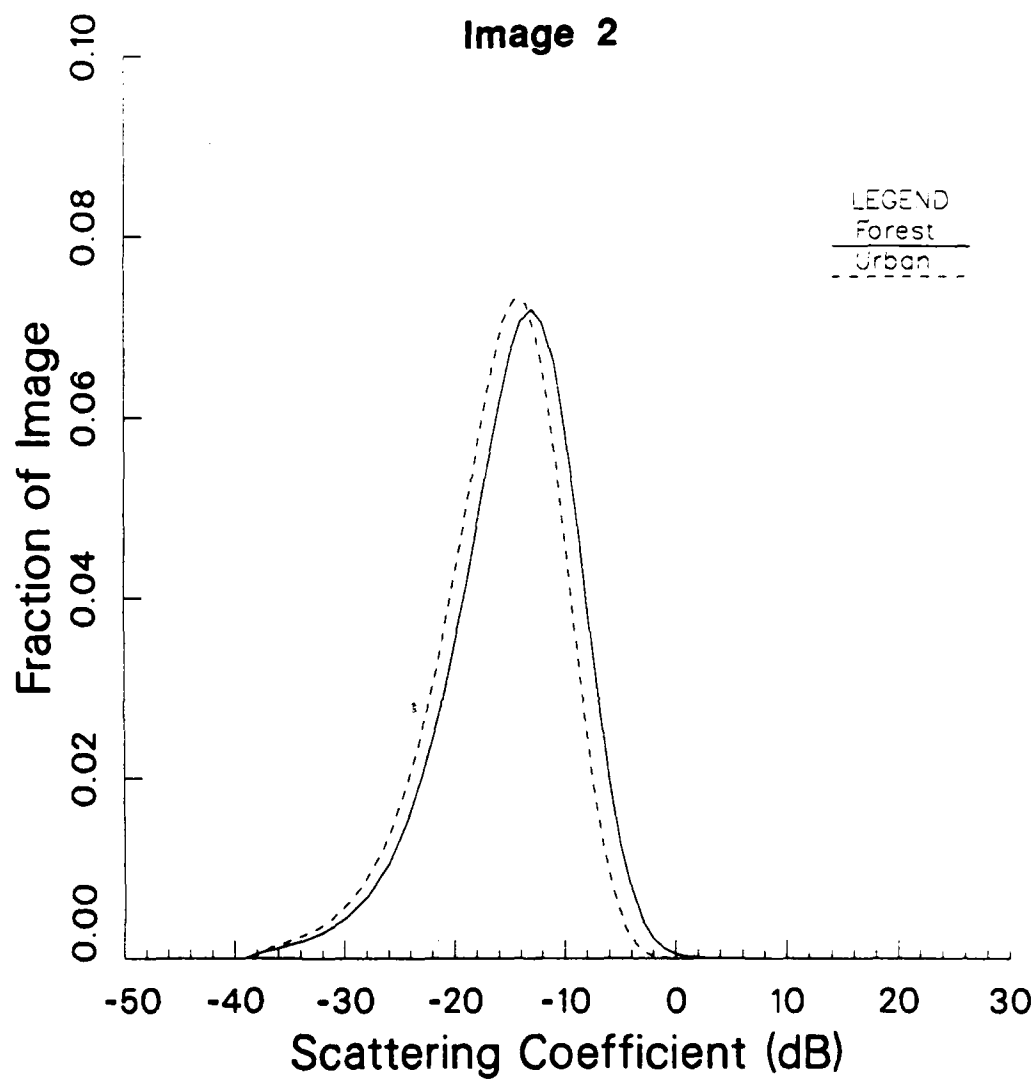
Figure 80.

Probability Density Function
of Forest and Urban Clutter Areas

Image 5
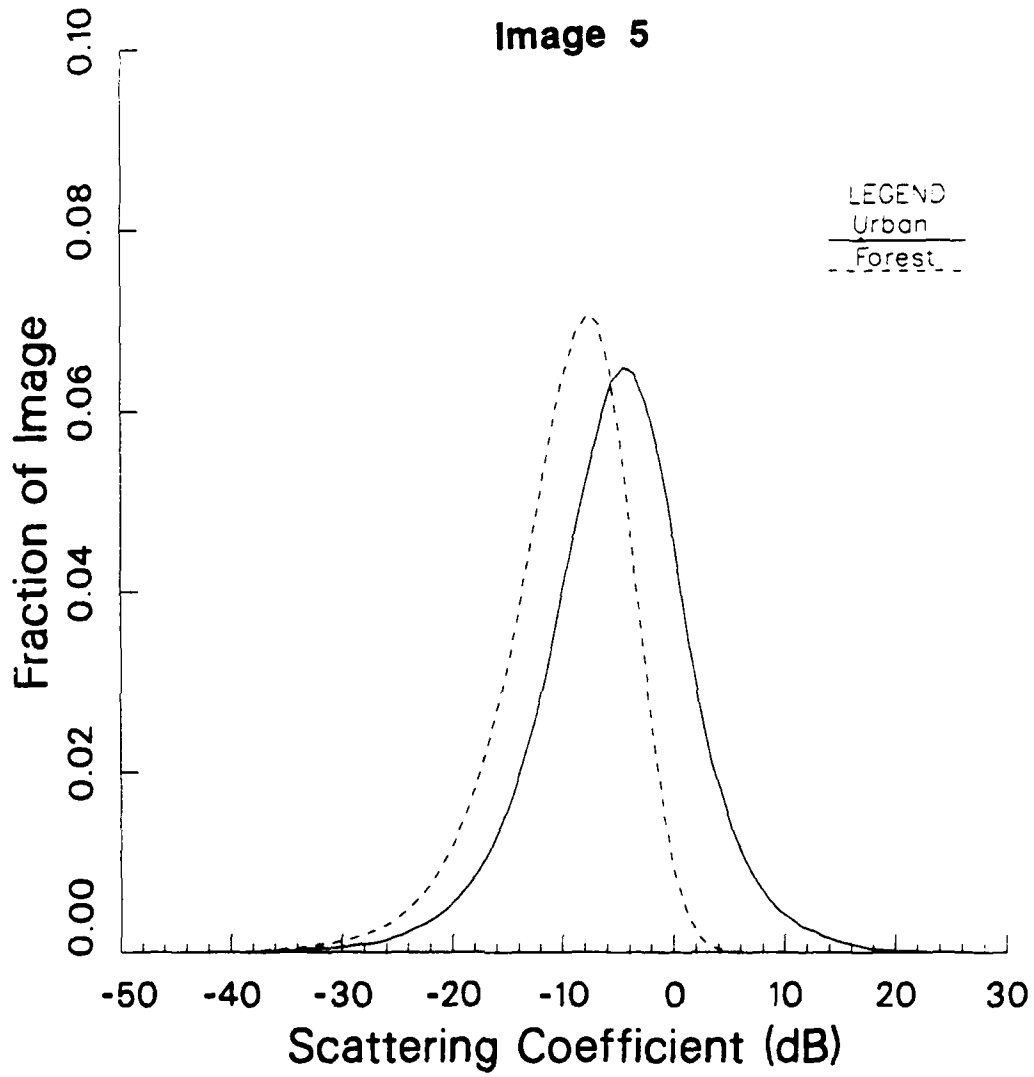
Figure 81.

Probability Density Function
of Pt. Target Clutter Areas
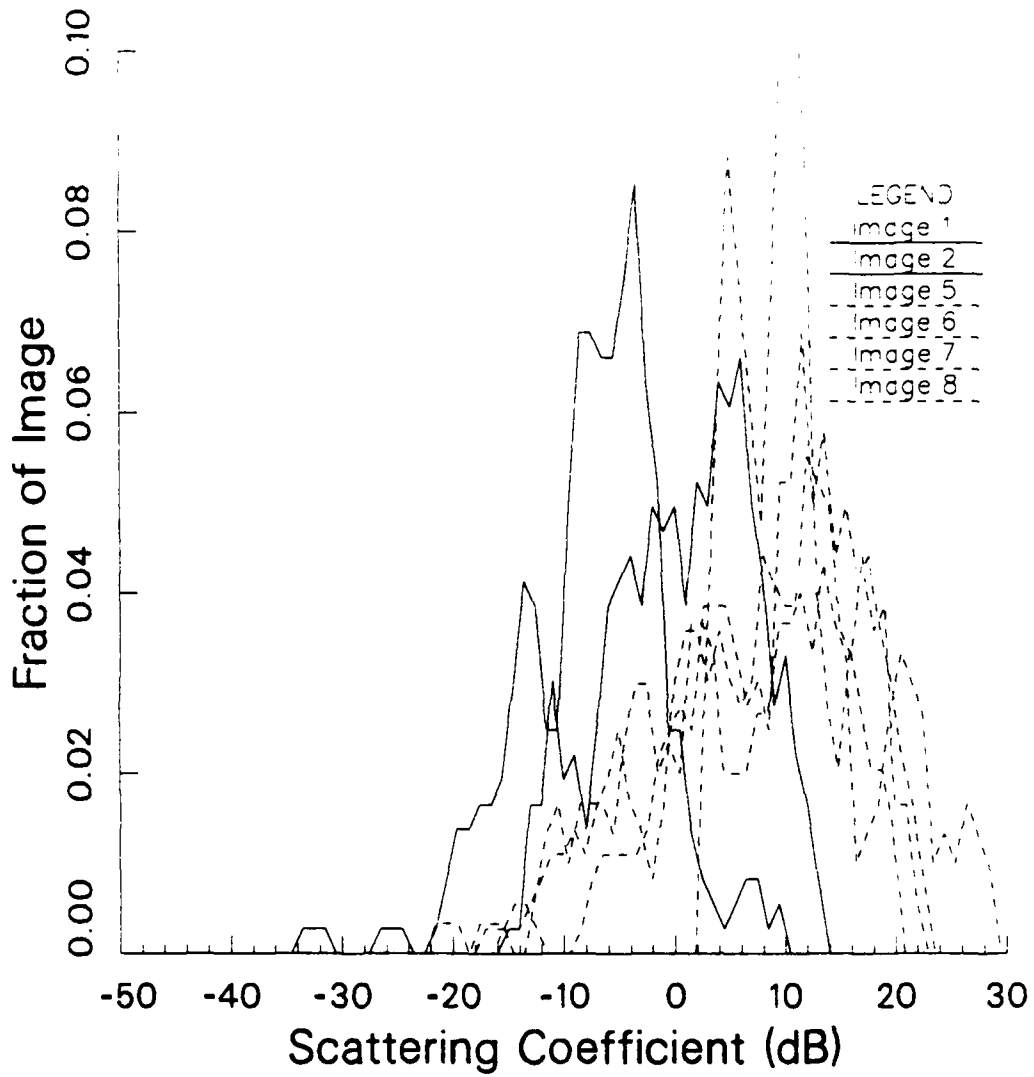
Figure 82.

Probability Density Function
of Automobile Clutter Areas
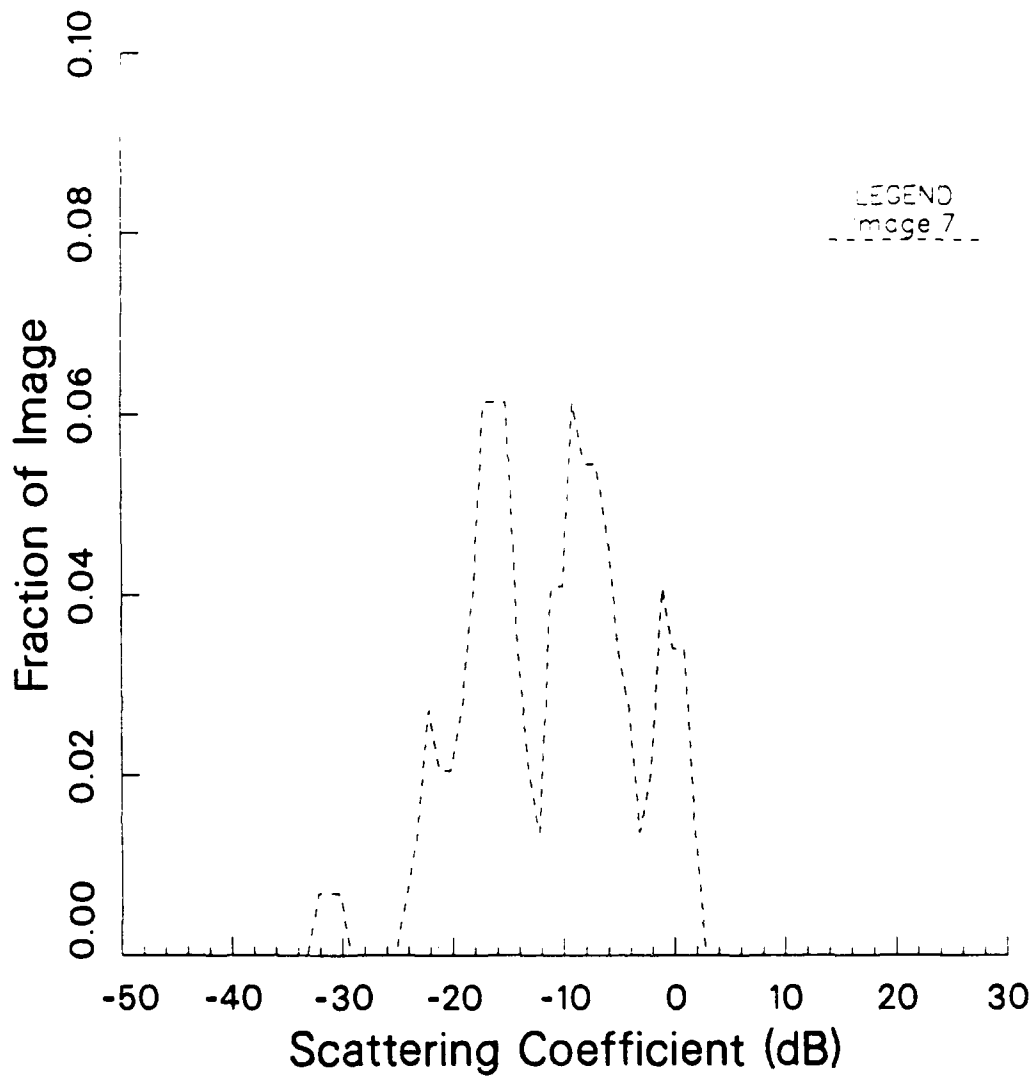
Figure 83.

Probability Density Function
of Airplane Clutter Areas
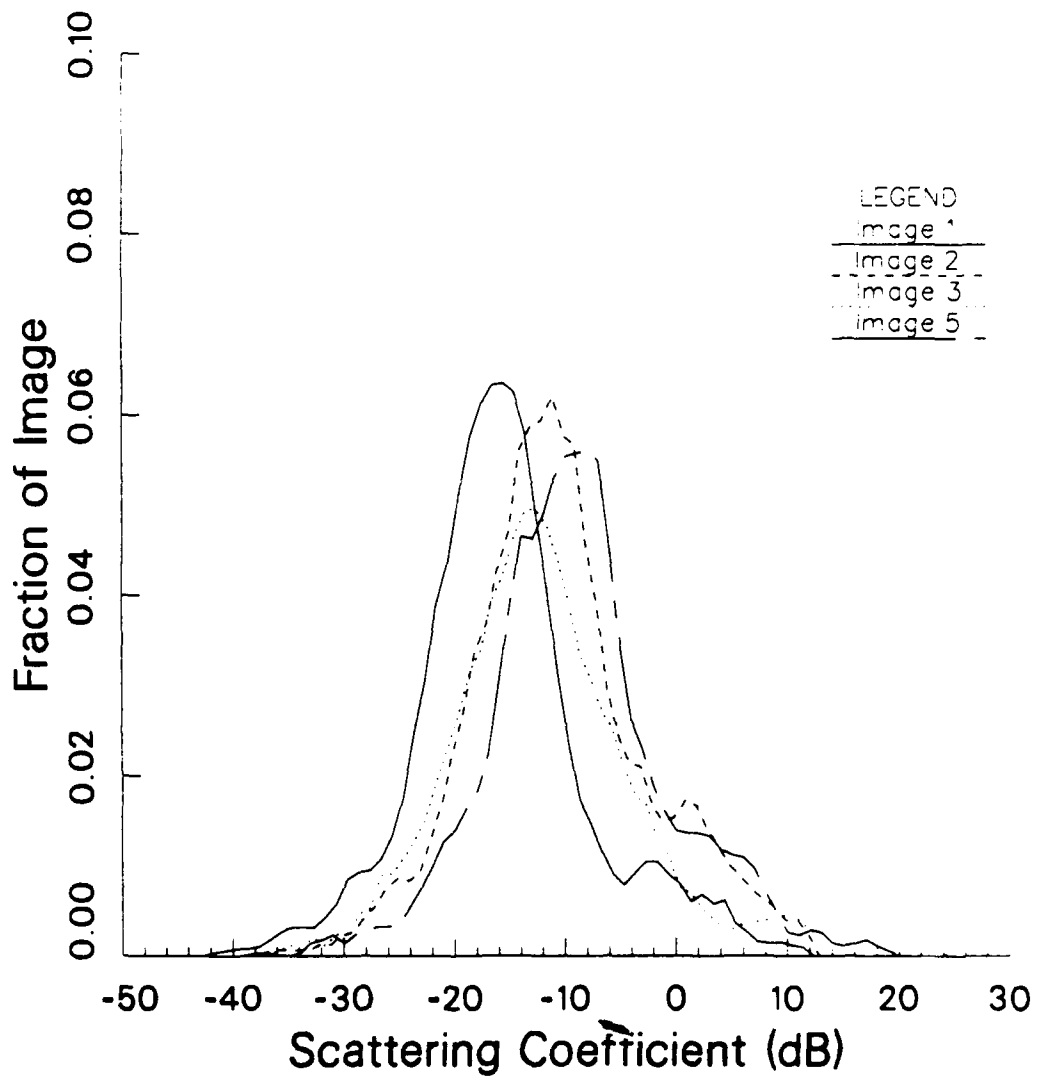
Figure 84.

Probability Density Function
of Pier Clutter Areas
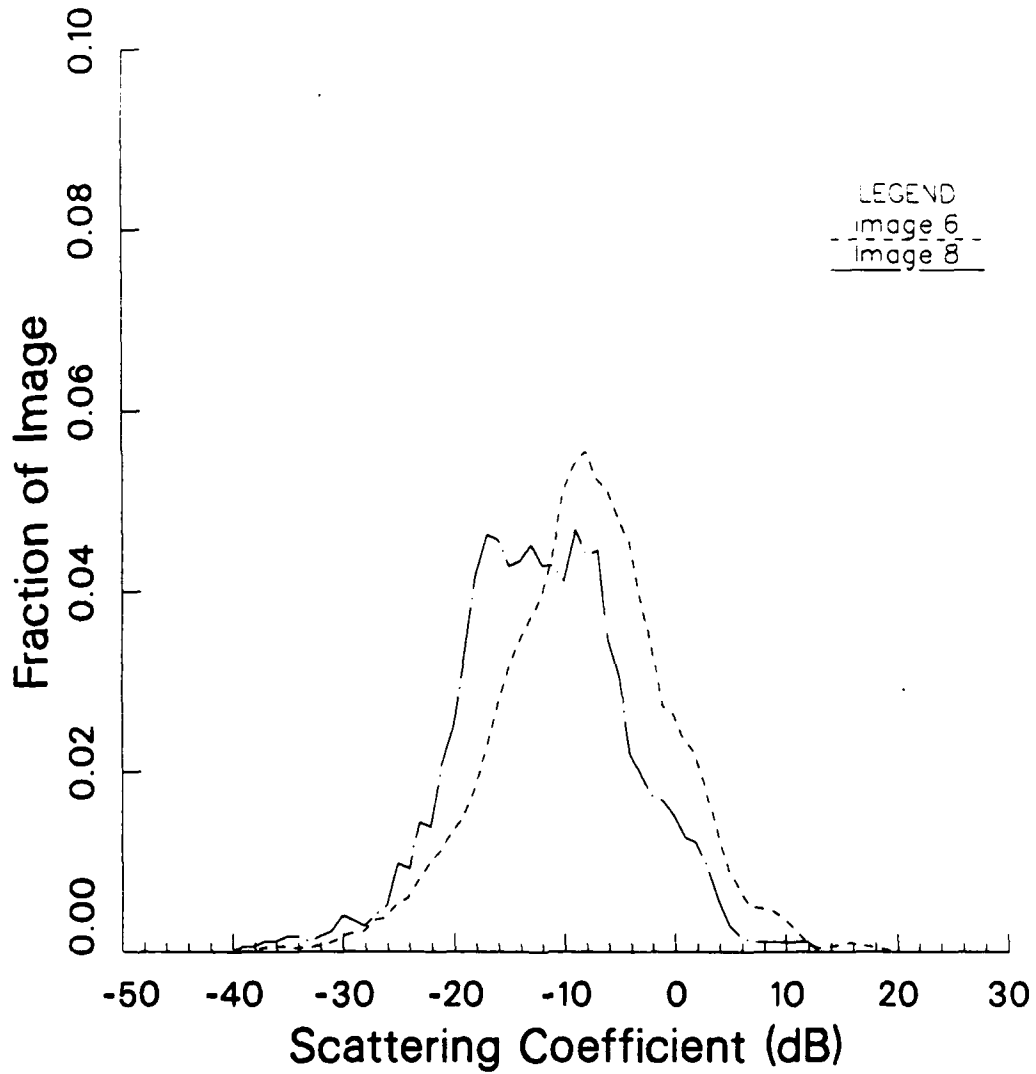
Figure 85.

Probability Density Function
of Boat Clutter Areas
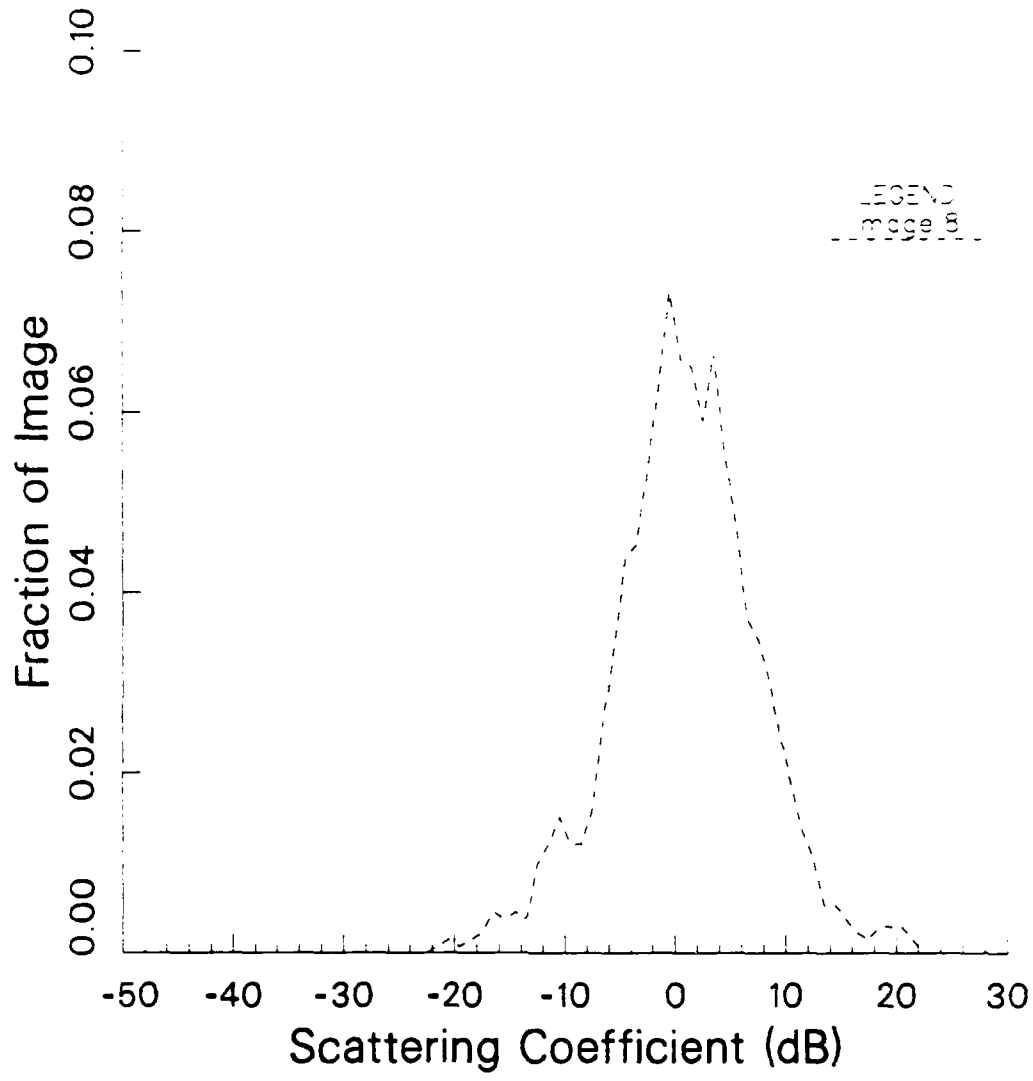
Figure 86.

Probability Density Function
of Bridge Clutter Areas

Figure 87.

239
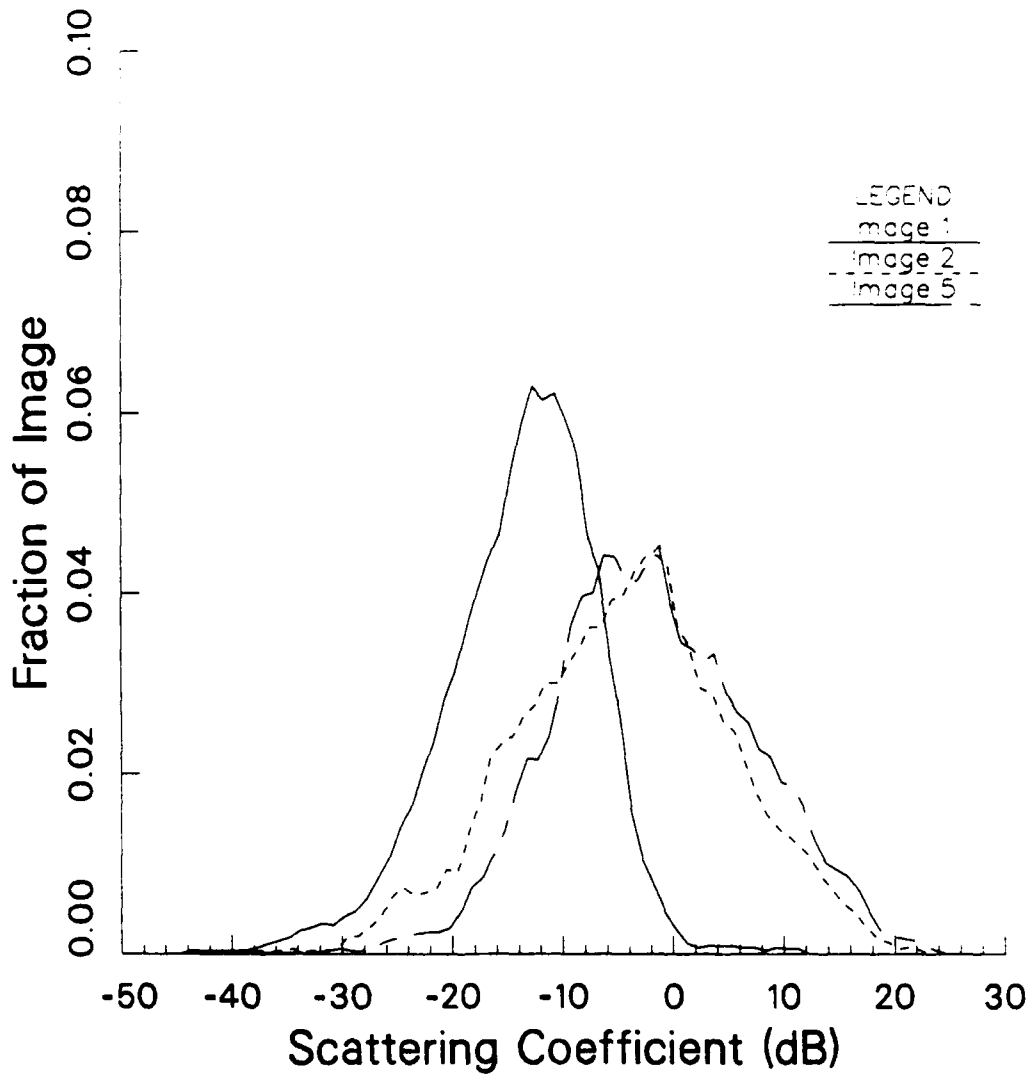
Probability Density Function
## of Dock Clutter Areas
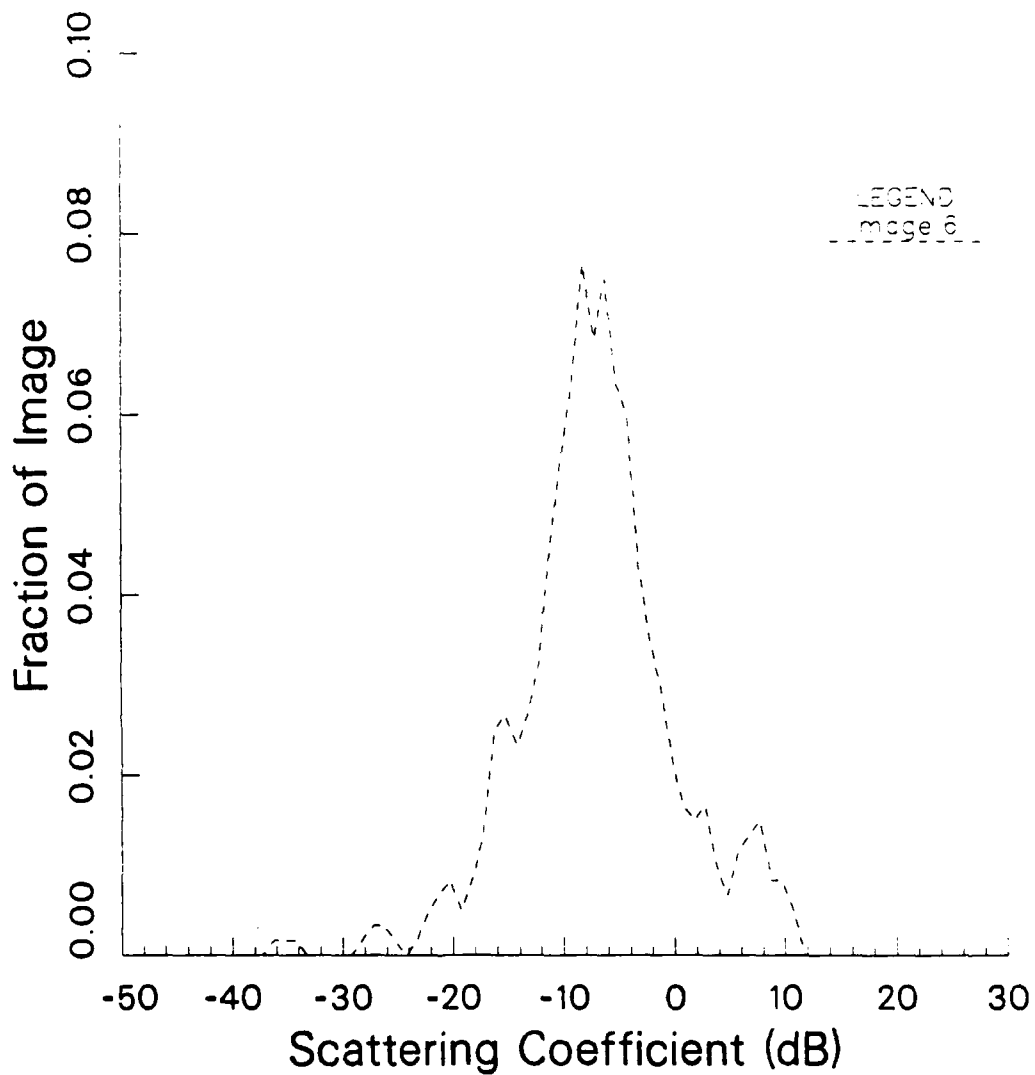
Figure 88.

89-11935
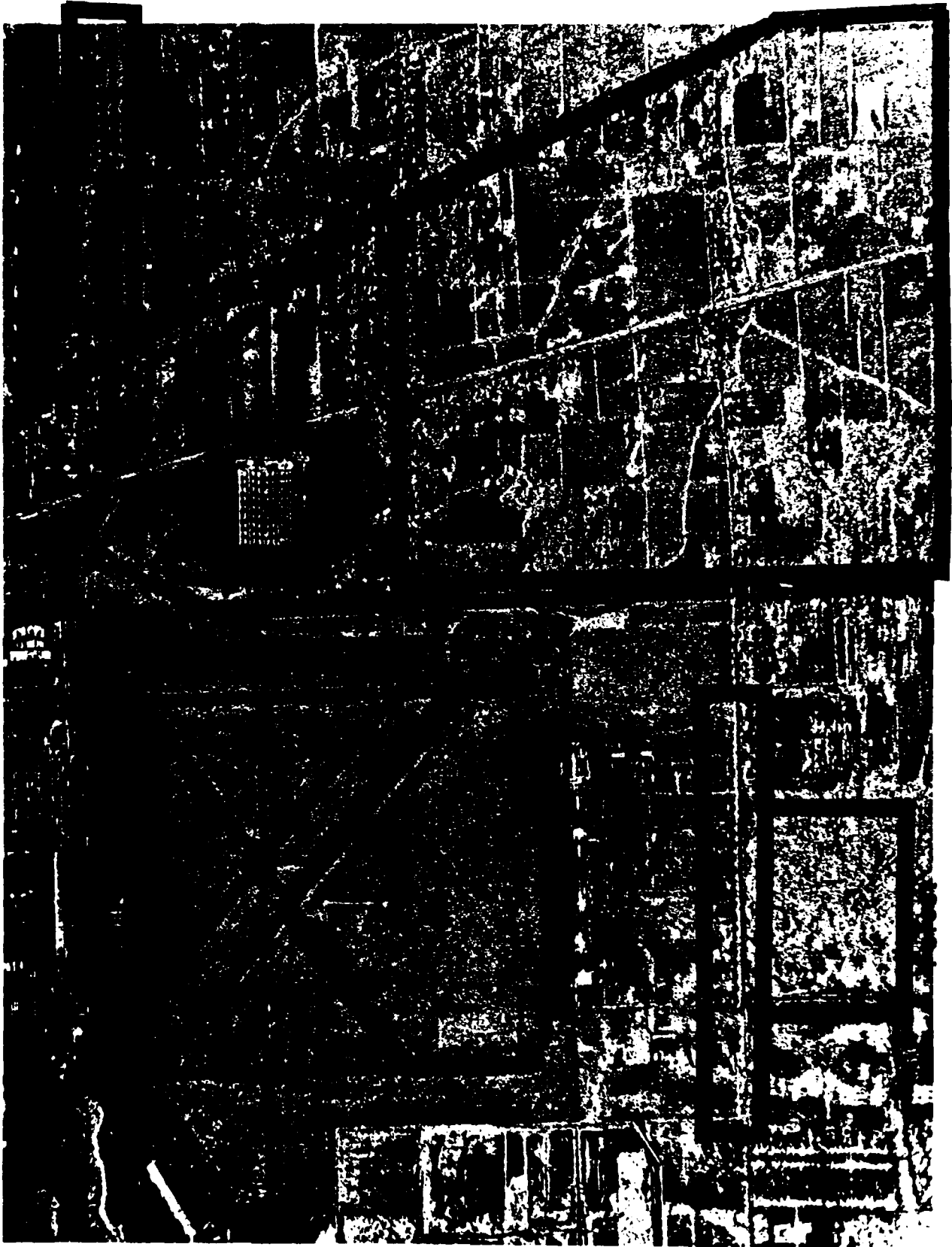
Figure 89. Willow Run X - VV Acquired on April 7, 1984

243

Figure 90. Willow Run X - HH Acquired on April 7, 1984

89-11936

245
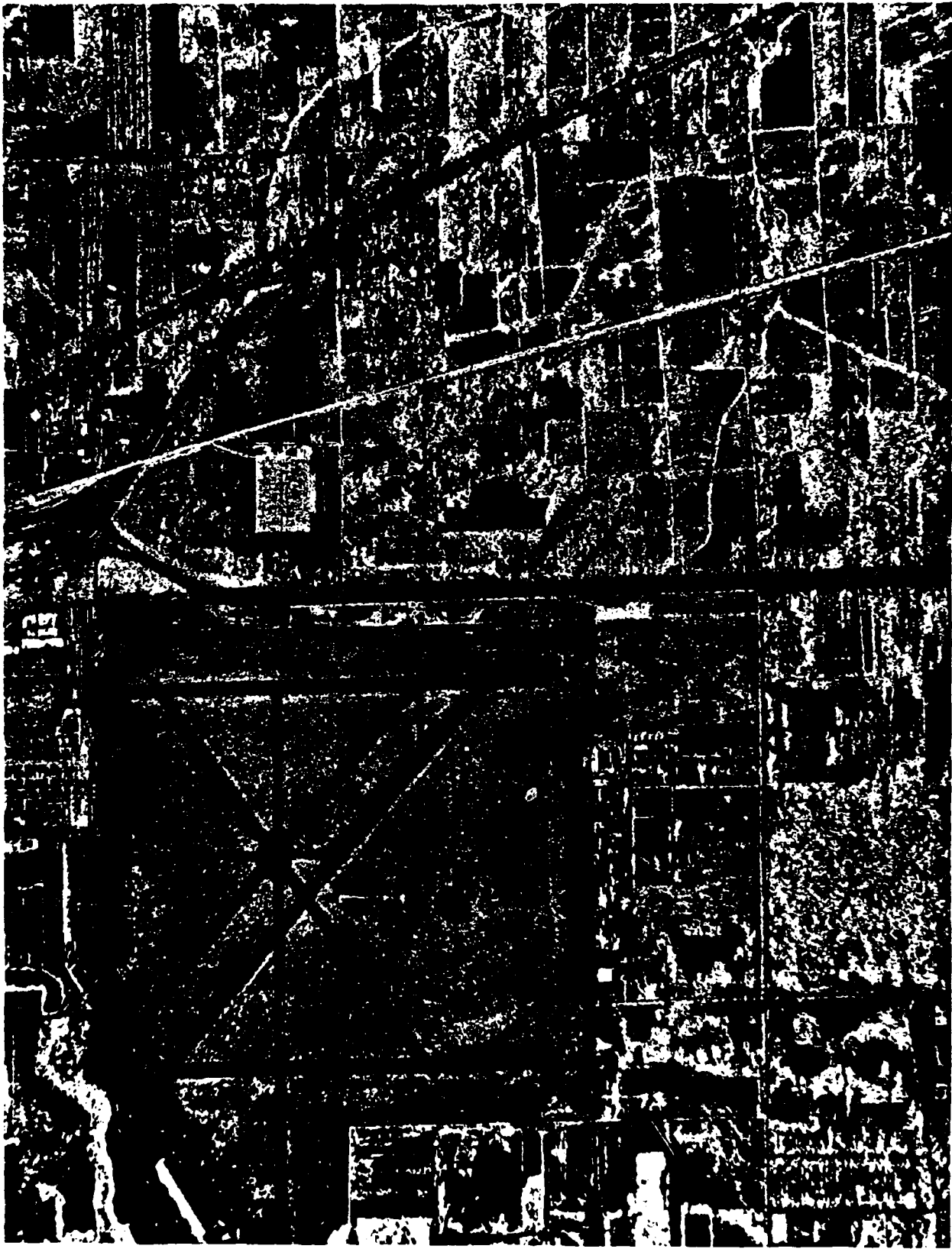
Figure 91. Willow Run X - HV Acquired on April 7, 1984

REFERENCES

Ament, W.S., MacDonald F.C., and Shewbridge R.D., Radar Terrain Reflections for Several Polarizations and Frequencies, NOTS TP 2339, Trans. 1959 Symposium on Radar Return, Part 2, University of New Mexico, Albuquerque, 11-12 May 1969.

Bracalente, E.M., Britt C.L., and Jones W.R., Airborne Doppler Radar Detection of Low Altitude Windshear, paper presented at The AIAA Conference on Sensor and Measurement Techniques for Aeronautical Application, Sept 7-9, 1988/Atlanta, GA. AIAA-88-4657.

Bush, T.F., Ulaby, F.T., and Metzler, T., (1975). Radar Backscatter Properties of Milo and Soybeans, University of Kansas, RSL Technical Report, 177-59.

Cosgriff, R.L., Peake, W.H. and Taylor, R.C., (1960). Terrain Scattering Properties for Sensor System Design Engineering Experiment Station Bulletin, Ohio State University, Vol. XXIX, No. 3.

Daley, J.C. (1973). Wind Dependence of Radar Sea Return, JGR Vol. 78, No. 33, pgs. 7823-7833.

Guinard, N.W., and Daley, J.C., (1970). An Experimental Study of a Sea Clutter Model, Proc. IEEE, vol. 58, pgs. 543-550.

Lyzenga, D.R., Maffett, A.L., and Shuchman, R.A., (1983). The Contribution of Wedge Scattering to the Radar Cross Section of the Ocean Surface, IEEE Transactions on Geoscience and Remote Sensing, Vol. GE-21, No. 4, pgs. 502-505.

Masuko, H., Okamoto, K., Shinmada, M., and Niwa, S., (1986). Measurements of Microwave Backscattering Signatures of the Ocean Surface Using X Band and Ka Band Airborne Scatterometers, JGR Vol. 91, No. C11, pgs. 13065-13083.

Ruck, G.T., Barrick, D.E., Stuart, W.D., and Krichbaun, C.K., (1970). Radar Cross Section Handbook Plenum Press.

Sloknik, M.I., (1970). Radar Handbook, McGraw Hill Book Co.

Stiles, W.H., Ulaby, F.T., and Wilson, E., (1979). Backscatter of Roads and Roadside Surfaces, RSL Technical Report 377-1, University of Kansas.

Ulaby, F.T., Moore, R.K., Fung, A.K., (1986). Microwave Remote Sensing, Vol. III, From Theory to Applications, Artzch House.

Valenzuela, G.R., Laing, M.B., and Daley, C., (1971). Ocean Spectra for the High-Frequency Waves from Airborne Radar Measurements, J. Marine Res. 29, pgs. 69-84.

APPENDIX A

CLUTTER SCENE LOCATIONS
AND CLUTTER STATISTICS FOR
IMAGES 1 THROUGH 8

APPENDIX A - LIST OF FIGURES

APPENDIX A - LIST OF TABLES

89-11292

Figure A-1. Clutter Location Map of Image 1

IMAGE 1
STATISTICAL SUMMARY
FILE: X1395

Category	Site#	#Pts	Sig Min (dB)	Sig Max (dB)	Sig Mean (dB)	STD (Mag)	PDF	Angle
Urban	001	76245	-45.00	19.07	-8.26	72.454	Gamma	61.1
Interchange	002	68753	-45.00	5.90	-11.30	34.598	Gamma	63.0
Plant	003	87465	-45.00	24.40	-5.44	147.44	Gamma	57.6
Plant	004	92865	-45.00	20.30	-5.25	114.54	Gamma	60.2
Auto	005	396	-15.33	8.56	-4.65	129.55	Gamma	60.7
Hangar	006	11205	-15.37	18.11	-5.86	125.41	Gamma	62.1
Tarmac	007	5529	-15.33	16.12	-8.58	120.62	Gamma	63.2
Field	008	39005	-45.00	-0.63	-13.31	30.48	Gamma	63.9
Runway	009	3477	-45.00	-5.96	-17.92	17.123	Gamma	65.8
Water	010	88917	-45.00	-6.40	-18.57	15.993	Gamma	69.3
Shoreline	011	2121	-45.00	18.17	-3.87	206.51	Gamma	70.4
Farmland	012	45325	-45.00	-0.26	-11.16	35.799	Gamma	68.2
Forest	013	14661	-45.00	3.74	-8.76	50.628	Gamma	68.0
Farmland	014	42653	-45.00	-0.39	-12.26	32.136	Gamma	68.0
Farmland	015	46221	-45.00	-3.18	-15.14	22.797	Gamma	69.1
Field	016	218161	-45.00	-2.54	-14.51	24.185	Gamma	68.7

* These measurements are taken from a clutter analysis of Image 1 performed in December.

89-11848

Figure A-2.   Clutter Location Map of Image 2

TABLE A-2

IMAGE 2
STATISTICAL SUMMARY
FILE: X944

| Category	Site#	#Pts	Min. (dB)	Max. (dB)	Mean (dB)	STD (Mag)	PDF	Angle
Pt. Target	001	25	-14.06	13.00	5.72	4.59E+0	Gamma	51.33
Pt. Target	002	25	-25.02	11.37	4.18	3.54E+0	Gamma	51.99
Pt. Target	003	25	-12.88	9.15	1.16	1.86E+0	Gamma	52.69
Pt. Target	004	25	-12.79	11.27	5.76	3.56E+0	Gamma	53.36
Pt. Target	005	25	-12.64	6.42	0.12	1.16E+0	Gamma	54.02
Plant	006	175000	-40.70	31.62	-2.24	7.88E+0	Gamma	43.41
Water	007	30000	-40.02	-5.87	-22.25	8.87E-3	Gamma	51.28
Water	008	30000	-39.88	-13.16	-24.91	4.55E-3	Gamma	53.29
Water	009	75000	-39.80	-13.84	-27.76	2.92E-3	Gamma	55.01
Water	010	40000	-39.69	-12.89	-28.77	3.50E-3	Gamma	57.00
Water	011	40000	-39.55	-17.53	-31.70	1.33E-3	Gamma	59.80
Bridge	012	1320	-40.52	22.37	4.01	9.12E+0	Gamma	43.50
Bridge	013	480	-40.14	19.81	4.33	8.48E+0	Gamma	48.64
Shoreline	014	1200	-40.02	4.71	-5.34	3.88E-1	Gamma	50.62
Shoreline	015	600	-40.09	-2.27	-11.41	7.82E-2	Gamma	53.13
Forest	016	36000	-39.93	6.57	-9.33	1.53E-1	Gamma	52.94
Farmland	017	250000	-39.78	11.42	-13.62	8.56E-2	Gamma	56.08
Farmland	018	21000	-39.77	-1.54	-14.19	4.52E-2	Gamma	54.98
Farmland	019	40000	-39.74	4.39	-13.50	5.31E-2	Gamma	55.62
Farmland	020	80000	-39.65	-1.60	-16.30	2.76E-2	Gamma	57.63
Field	021	14000	-39.60	-5.03	-17.29	2.03E-3	Gamma	58.49
Field	022	60000	-39.81	-4.62	-15.96	2.73E-2	Gamma	55.01
Field	023	30000	-40.15	-1.23	-11.79	6.87E-2	Gamma	49.41
Field	024	30000	-39.92	-3.65	-14.30	3.84E-2	Gamma	52.65
Runway	025	1500	-39.84	-15.02	-24.23	4.76E-3	Gamma	53.90
Runway	026	1500	-39.96	-11.76	-21.07	8.97E-3	Gamma	51.79
Runway	027	1500	-40.04	-12.25	-20.52	9.82E-3	Gamma	50.51
Forest	028	70000	-39.55	-1.52	-13.55	5.10E-2	Gamma	50.02
Building	029	6250	-40.19	15.66	-9.82	8.08E-1	Gamma	47.97
Prkd Plns	030	1000	-40.13	12.01	-3.07	1.54E+0	Gamma	48.93
Plant	031	87500	-40.47	23.05	-2.10	3.06E+0	Gamma	45.89
Building	032	400	-40.03	-15.34	-24.35	4.38E-3	Gamma	50.35
Building	033	400	-40.06	9.12	-3.94	8.62E-1	Gamma	49.93
Building	034	6750	-40.47	24.01	0.18	5.06E+0	Gamma	44.33
Building	035	2400	-40.56	10.39	-2.83	8.36E-1	Gamma	43.11
Forest	036	15300	-39.85	-0.06	-10.67	8.42E-2	Gamma	53.84
Forest	037	80000	-39.99	0.99	-11.87	7.31E-2	Gamma	52.38
Urban	038	57500	-40.92	24.40	-3.64	2.59E+0	Gamma	39.91
Forest	039	140000	-39.54	-0.74	-14.00	4.84E-2	Gamma	55.33
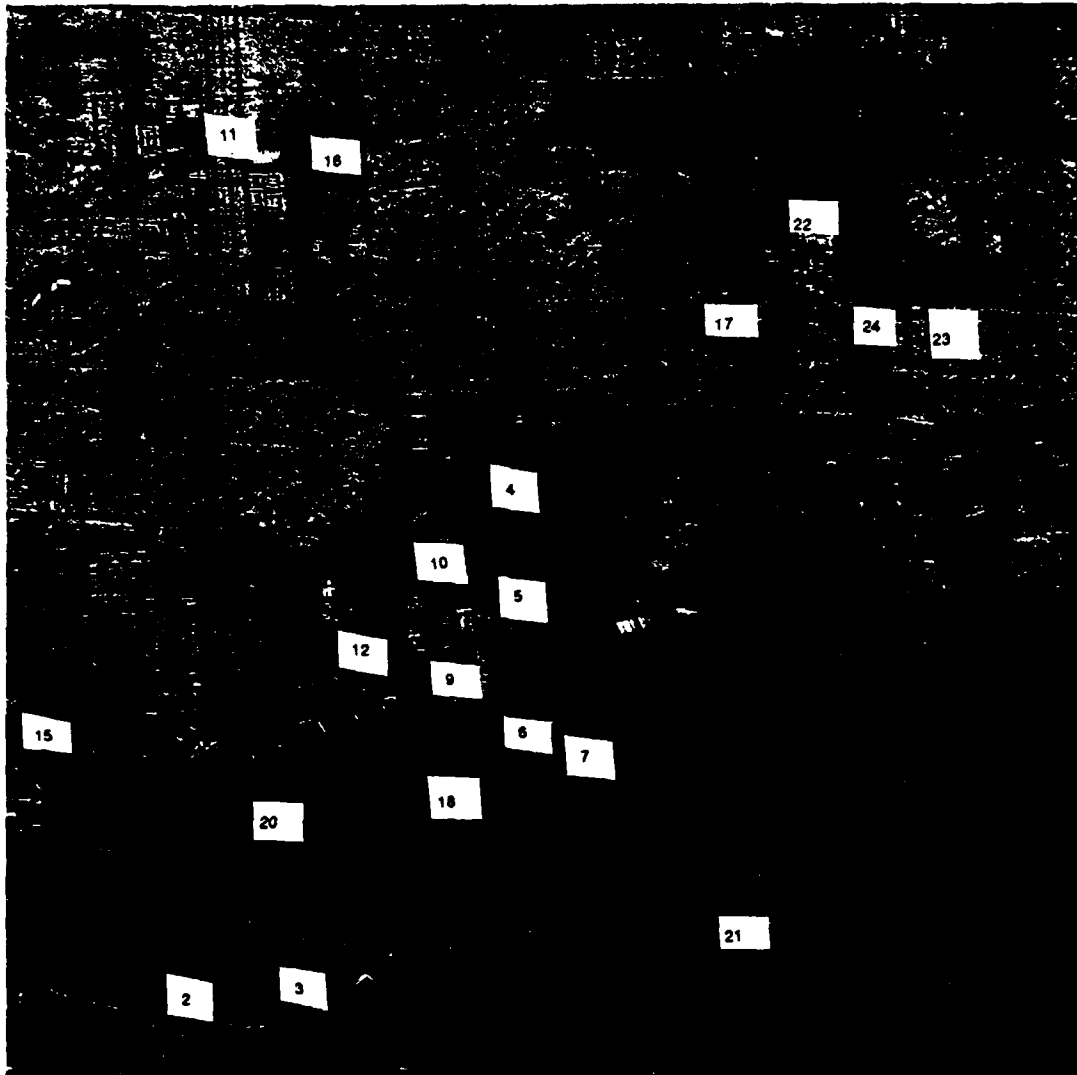
88-11448

Figure A-3.   Clutter Location Map of Image 3

TABLE A-3

IMAGE 3
STATISTICAL SUMMARY
FILE: X1084

| Category	Site#	#Pts	Min. (dB)	Max. (dB)	Mean (dB)	STD (Mag)	PDF	Angle
Water	001	6400	-39.61	-10.02	-20.91	1.26E-2	Gamma	61.30
Water	002	19600	-39.55	-10.66	-23.87	7.46E-3	Gamma	62.91
Water	003	6400	-39.54	-8.68	-22.26	1.02E-2	Gamma	62.98
Runway	004	1500	-39.93	-7.80	-17.86	2.16E-2	Gamma	54.69
Runway	005	1500	-39.86	-8.61	-18.33	1.88E-2	Gamma	56.03
Runway	006	1500	-39.76	-11.72	-22.79	8.92E-3	Gamma	58.01
Runway	007	2500	-39.66	-11.80	-25.58	5.51E-3	Gamma	60.16
Building	008	2025	-39.78	13.00	2.37	2.62E+0	Gamma	57.43
Building	009	2000	-39.77	7.84	-4.96	5.87E-1	Gamma	57.74
Urban	010	50000	-39.80	20.23	-5.79	1.73E+0	Gamma	57.44
Urban	011	6000	-40.65	25.74	-0.14	7.37E+0	Gamma	46.42
Urban	012	50000	-39.77	23.82	-6.85	2.39E+0	Gamma	58.19
Forest	013	125000	-40.65	9.26	-3.49	5.32E-1	Gamma	44.90
Field	014	72000	-40.14	11.04	-7.28	2.49E-1	Gamma	51.60
Field	015	26400	-39.71	-2.21	-16.72	2.92E-2	Gamma	59.05
Field	016	46800	-40.52	6.35	-7.64	1.92E-1	Gamma	46.05
Forest	017	122500	-40.19	11.40	-4.37	4.83E-1	Gamma	51.24
Field	018	86400	-39.66	6.11	-17.23	3.36E-2	Gamma	60.52
Forest	019	30000	-39.95	8.13	-5.78	3.84E-1	Gamma	54.74
'rkd Plns	020	1380	-39.62	23.00	3.46	1.30E+1	Gamma	60.88
Field	021	250000	-39.59	9.55	-16.38	5.99E-2	Gamma	62.45
Plant	022	30000	-40.30	23.76	-0.13	4.97E+0	Gamma	49.18
Forest	023	108900	-40.14	8.46	-5.05	4.05E-1	Gamma	51.92
Plant	024	7800	-40.14	22.18	0.14	5.26E+0	Gamma	51.32
Water	025	7150	-39.95	-5.84	-16.66	2.70E-2	Gamma	54.40
Field	026	120000	-39.86	12.76	-9.68	1.59E-1	Gamma	56.53
Shoreline	027	600	-39.60	8.01	-6.26	5.60E-1	Gamma	61.50
Shoreline	028	900	-39.59	2.31	-9.29	1.91E-1	Gamma	61.64
Shoreline	029	900	-39.53	2.69	-7.18	2.56E-1	Gamma	53.27

89-11921
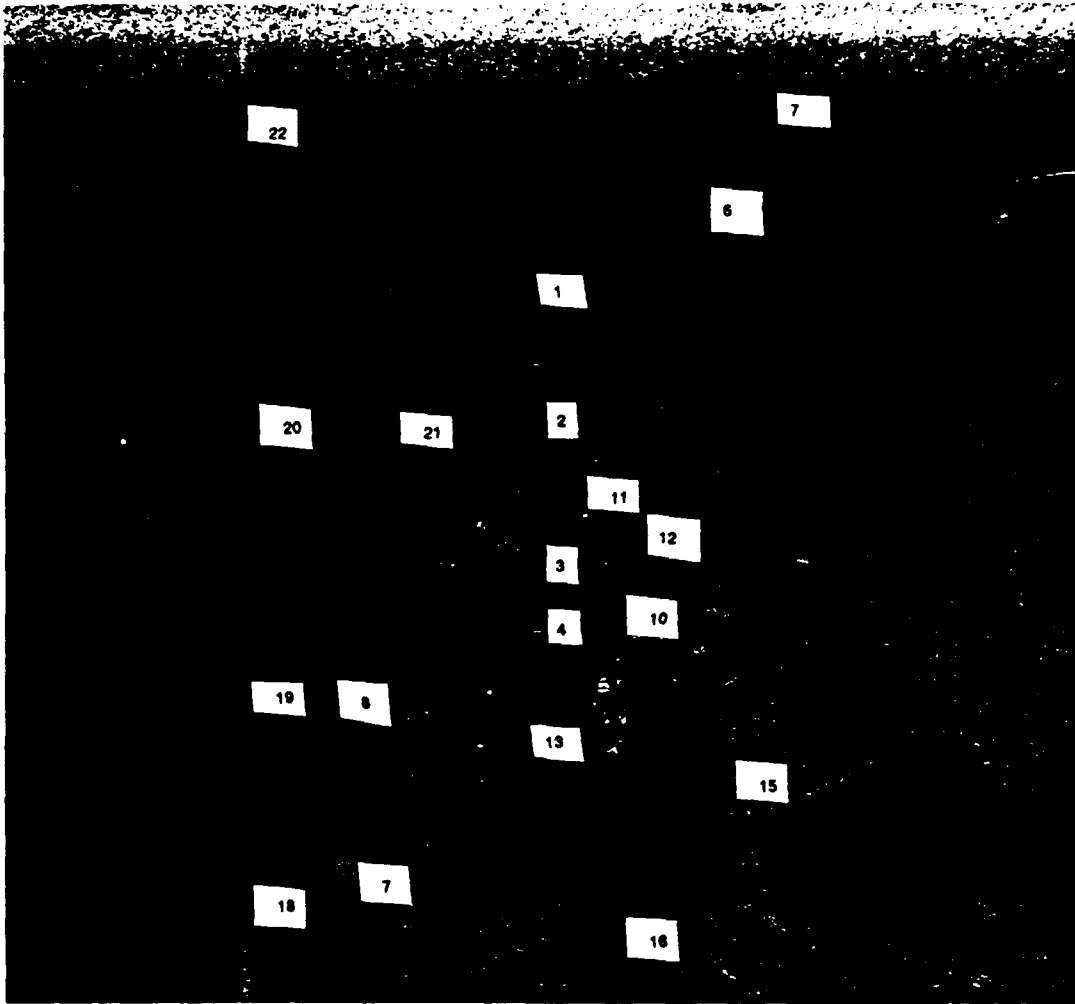
88-11449

Figure A-4. Clutter Location Map of Image 4

TABLE A-4

IMAGE 4
STATISTICAL SUMMARY
FILE: X952

Category	Site#	#Pts	Min. (dB)	Max. (dB)	Mean (dB)	STD (Mag)	PDF	Angle
Runway	001	4000	-39.34	-1.34	-18.19	3.20E-02	Gamma	44.08
Runway	002	4000	-39.21	-11.60	-21.84	9.02E-03	Gamma	45.61
Runway	003	4000	-38.87	-8.57	-20.19	1.32E-02	Gamma	50.38
Runway	004	4125	-38.70	-6.44	-18.54	1.88E-02	Gamma	52.71
Shoreline	005	2250	-40.01	-4.21	-16.42	3.27E-02	Gamma	36.07
Shoreline	006	1500	-39.82	0.61	-9.81	1.25E-01	Gamma	37.93
Water	007	80000	-40.18	-3.78	-15.22	3.40E-02	Gamma	35.82
Shoreline	008	1500	-38.74	2.48	-6.98	2.34E-01	Gamma	52.30
Shoreline	009	1500	-38.50	-0.96	-10.26	9.97E-02	Gamma	56.59
Building	010	2400	-38.71	15.41	1.90	3.32E+00	Gamma	52.58
Building	011	460	-38.96	7.70	-0.33	1.24E+00	Gamma	48.48
Field	012	18000	-38.91	-2.11	-12.48	6.16E-02	Gamma	49.61
Field	013	62500	-38.66	1.11	-12.41	6.58E-02	Gamma	54.05
Forest	014	90000	-38.47	1.01	-12.44	7.44E-02	Gamma	57.53
Forest	015	122500	-38.62	7.39	-9.32	1.61E-01	Gamma	54.85
Forest	016	40000	-38.49	1.89	-12.54	7.40E-02	Gamma	56.83
Building	017	1650	-39.10	13.98	-1.67	1.57E+00	Gamma	46.69
Water	018	120000	-38.50	-6.35	-18.23	1.90E-02	Gamma	57.22
Water	019	150000	-38.78	-4.07	-15.98	2.93E-02	Gamma	52.81
Water	020	150000	-39.37	-3.85	-15.20	3.41E-02	Gamma	45.20
Water	021	10000	-39.23	-8.90	-21.82	1.07E-02	Gamma	45.08
Water	022	250000	-40.40	-2.97	-15.52	3.21E-02	Gamma	36.19
Water	023	100000	-43.45	-4.61	-17.74	1.92E-02	Gamma	19.19
Runway	001	2000	-39.08	-12.09	-21.85	8.93E-03	Gamma	46.92
Field	002	5000	-38.99	-1.57	-13.89	4.76E-02	Gamma	48.42
Building	003	800	-38.70	15.42	3.08	3.40E+00	Gamma	52.58
Forest	004	2500	-38.56	-2.16	-11.00	8.34E-02	Gamma	55.27
Field	005	2500	-38.49	-2.04	-13.25	5.53E-02	Gamma	56.55
Forest	006	10000	-38.69	2.65	-8.75	1.67E-01	Gamma	53.08
Runway	007	1225	-38.82	-10.56	-19.94	1.30E-02	Gamma	50.67
Shoreline	008	175	-24.06	13.34	6.12	3.85E+00	Gamma	36.01
Shoreline	009	175	-26.03	7.82	1.21	1.32E+00	Gamma	36.15
Water	001	250000	-43.86	-1.65	-16.91	2.58E-02	Gamma	22.76
Water	002	250000	-40.49	-2.97	-15.65	3.11E-02	Gamma	35.61
Water	003	200000	-39.34	-3.24	-15.09	3.49E-02	Gamma	45.54
Water	004	175000	-38.83	-4.07	-15.69	3.13E-02	Gamma	51.93
Water	005	175000	-38.53	-4.80	-17.98	2.00E-02	Gamma	56.90
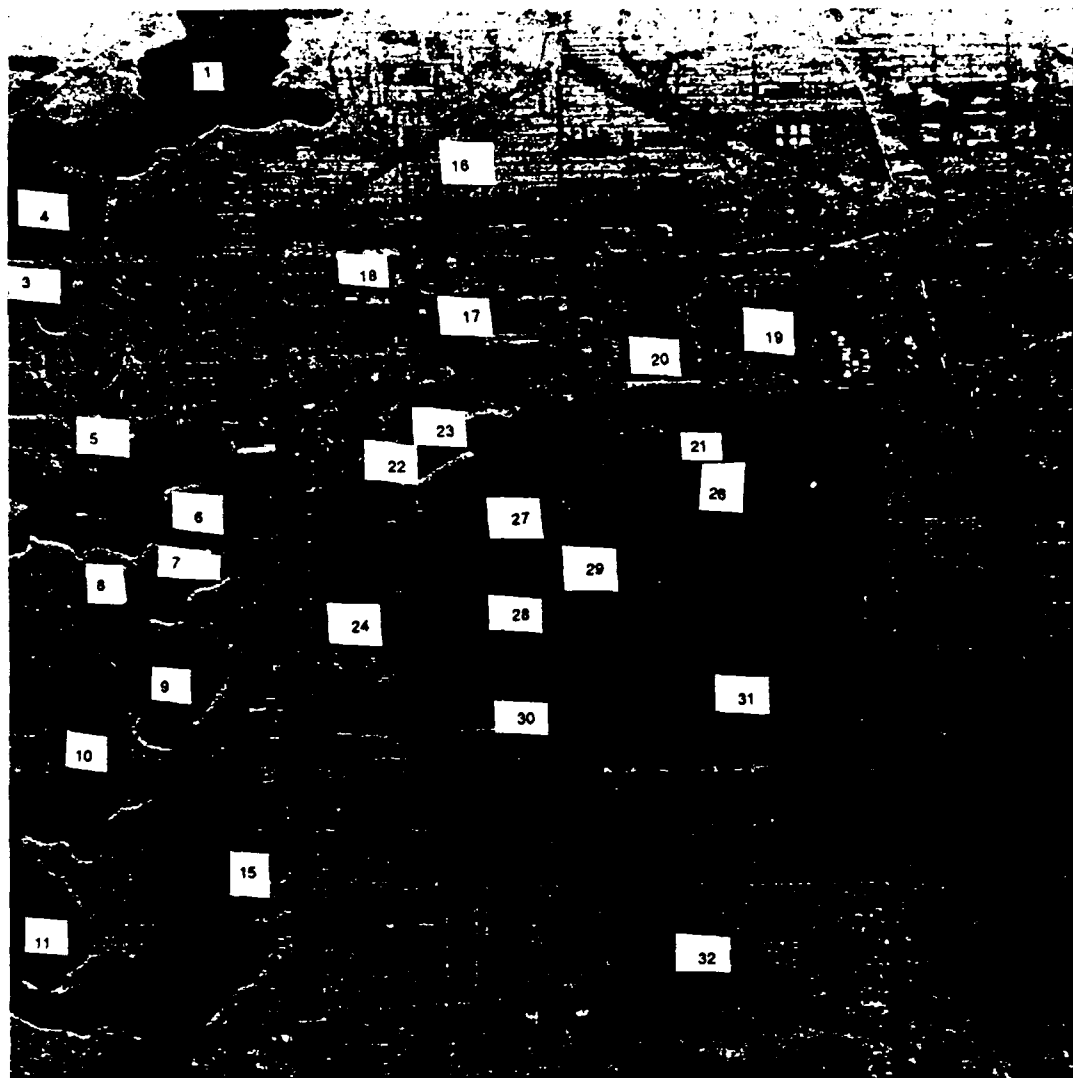
88-11227

Figure A-5.   Clutter Location Map of Image 5

TABLE A-5

IMAGE 5
STATISTICAL SUMMARY
FILE: X1404

| Category	Site#	#Pts	Min. (dB)	Max. (dB)	Mean (dB)	STD (Mag)	PDF	Angle
Water	001	75000	-41.18	9.69	-3.37	5.58E-1	Gamma	18.92
Plant	002	68000	-40.26	27.15	-2.48	4.67E+0	Gamma	36.92
Bridge	003	1320	-40.25	23.69	6.55	1.44E+1	Gamma	36.11
Water	004	180000	-40.49	1.84	-11.49	8.41E-2	Gamma	31.62
Bridge	005	480	-39.97	18.29	3.45	6.86E+0	Gamma	42.75
Shoreline	006	1200	-39.88	6.39	-2.91	6.44E-1	Gamma	45.18
Shoreline	007	600	-39.76	12.62	-0.88	1.72E+0	Gamma	48.16
Water	008	30000	-39.77	-6.39	-19.80	1.89E-2	Gamma	48.34
Water	009	75000	-39.71	-4.45	-20.45	1.76E-2	Gamma	50.40
Water	010	40000	-39.61	-4.26	-20.10	1.99E-2	Gamma	52.92
Water	011	54000	-39.53	-4.34	-20.01	1.87E-2	Gamma	55.60
Farmland	012	50000	-39.67	4.23	-9.80	1.27E-1	Gamma	51.04
Farmland	013	67500	-39.60	6.96	-9.61	1.37E-1	Gamma	53.25
Farmland	014	250000	-39.67	6.96	-9.01	1.76E-1	Gamma	52.30
Field	015	14000	-39.56	-1.65	-13.33	6.29E-2	Gamma	54.33
Urban	016	67500	-40.56	27.22	-0.04	5.24E+0	Gamma	30.54
Building	017	3500	-40.22	17.46	-0.77	1.77E+0	Gamma	37.21
Building	018	2500	-40.28	19.44	2.20	3.90E+0	Gamma	35.57
Plant	019	112500	-40.22	26.60	-3.82	2.87E+0	Gamma	39.38
Building	020	6250	-40.02	18.54	1.78	4.54E+0	Gamma	41.52
Prkd Plns	021	1125	-39.96	18.71	-0.62	4.28E+0	Gamma	43.13
Building	022	400	-39.89	3.47	-5.14	3.31E-1	Gamma	44.87
Building	023	400	-39.91	11.37	-3.32	1.16E+0	Gamma	44.38
Forest	024	72000	-39.84	2.68	-9.41	1.31E-1	Gamma	47.65
Forest	025	20000	-39.77	2.81	-8.80	1.64E-1	Gamma	48.52
Field	026	36000	-39.94	3.05	-7.89	1.77E-1	Gamma	44.36
Runway	027	1200	-39.84	-2.01	-12.48	7.46E-2	Gamma	46.44
Runway	028	1200	-39.76	-4.41	-13.51	5.56E-2	Gamma	48.58
Field	029	34000	-39.80	1.54	-9.21	1.38E-1	Gamma	47.63
Runway	030	1200	-39.68	-4.38	-13.64	5.41E-2	Gamma	50.68
Field	031	175000	-39.71	3.32	-9.86	1.12E-1	Gamma	50.60
Forest	032	250000	-39.53	9.01	-7.69	2.18E-1	Gamma	56.10
Pt. Target	033	9	5.98	11.23	9.10	3.24E+0	Uniform	46.83
Pt. Target	034	9	10.46	19.58	16.64	2.63E-1	Mult.	47.67
Pt. Target	035	9	8.71	12.04	10.81	2.66E+0	Mult.	48.43
Pt. Target	036	9	2.52	10.32	7.90	2.96E+0	Uniform	48.73
Pt. Target	037	9	2.84	10.61	8.54	3.52E+0	Uniform	49.43
Pt. Target	038	9	0.81	5.13	3.85	6.08E-1	Uniform	49.82
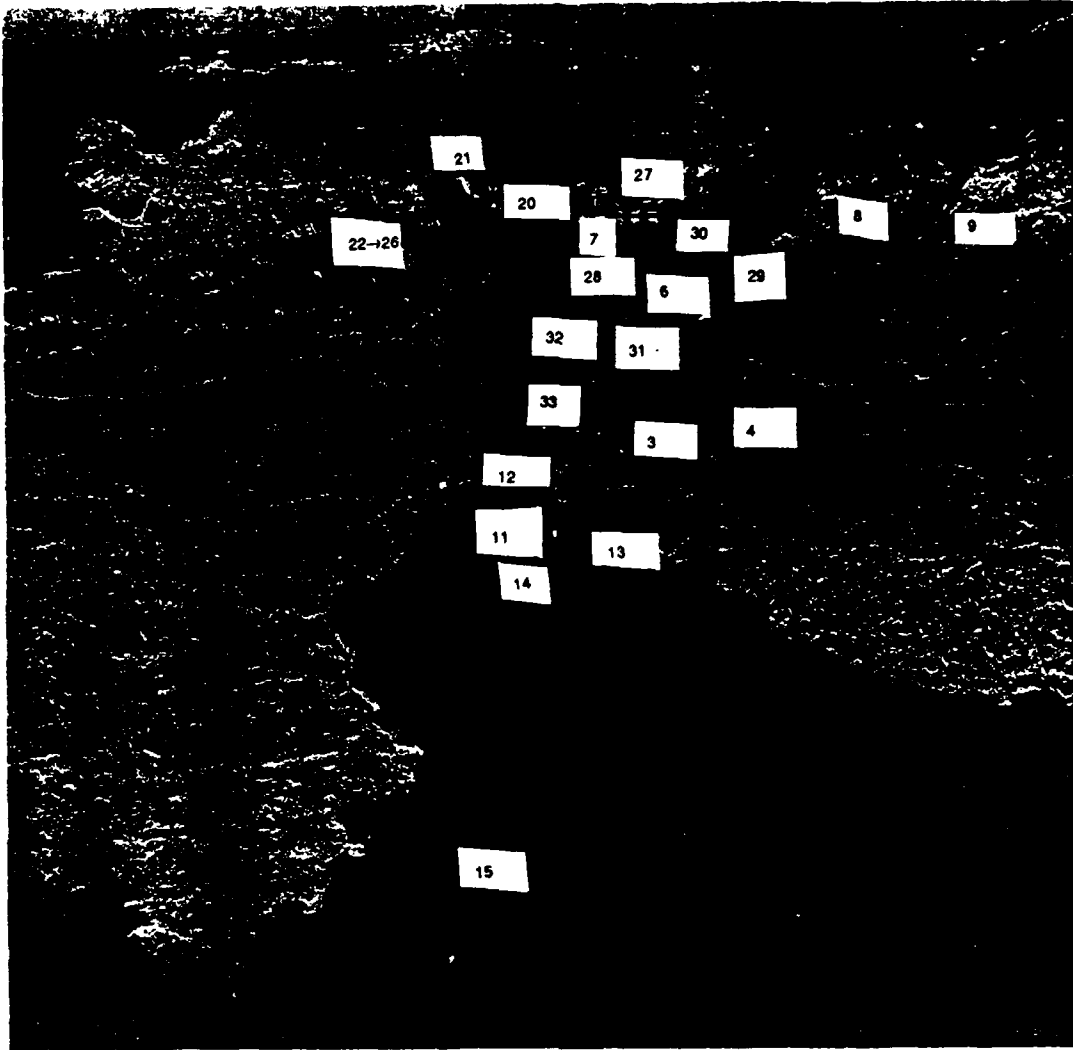
88-11231

Figure A-6.   Clutter Location Map of Image 6

TABLE A-6

IMAGE 6
STATISTICAL SUMMARY
FILE: X931

Category	Site#	#Pts	Min. (dB)	Max. (dB)	Mean (dB)	STD (Mag)	PDF	Angle
Farmland	001	10000	-39.81	3.56	-8.09	1.72E-01	Gamma	49.82
Forest	002	10000	-39.73	5.40	-7.24	2.62E-01	Gamma	51.11
Field	003	10000	-39.92	0.56	-9.34	1.27E-01	Gamma	48.17
Farmland	004	10000	-40.01	-0.13	-8.98	1.28E-01	Gamma	46.94
Field	005	5000	-40.00	-0.29	-11.02	9.48E-02	Gamma	47.10
Field	006	22500	-40.34	1.58	-9.45	1.34E-01	Gamma	43.03
Field	007	10000	-40.42	-1.47	-11.64	7.79E-02	Gamma	41.84
Forest	008	22500	-40.54	4.42	-7.64	2.17E-01	Gamma	40.84
Forest	009	90000	-40.64	7.09	-7.25	2.67E-01	Gamma	40.61
Forest	010	160000	-40.17	5.30	-9.70	1.53E-01	Gamma	46.15
Pier/Wharf	011	1500	-39.80	19.20	-1.13	3.93E+00	Gamma	50.05
Building	012	625	-39.86	9.42	-5.21	7.41E-01	Gamma	18.81
Water	013	10000	-39.73	-10.66	-23.37	8.76E-03	Gamma	50.96
Water	014	2500	-39.72	-8.12	-17.32	2.23E-02	Gamma	51.09
Water	015	10000	-39.50	-6.51	-17.80	2.42E-02	Gamma	54.91
Shoreline	016	250	-39.58	12.75	3.84	2.97E+00	Gamma	53.31
Shoreline	017	250	-28.34	10.36	2.09	1.71E+00	Gamma	53.14
Shoreline	018	250	-39.49	1.45	-4.50	2.97E-01	Gamma	54.86
Shoreline	019	250	-39.41	7.44	-2.51	7.54E-01	Gamma	56.44
Building	020	100	-10.91	8.47	4.40	1.64E+00	Uniform	40.01
Building	021	150	-17.37	11.16	2.96	1.97E+00	Multiple	39.15
Pt. Target	022	25	-2.60	19.39	11.97	2.06E+01	Gamma	40.71
Pt. Target	023	25	-7.49	20.09	12.82	2.49E+01	Gamma	40.59
Pt. Target	024	25	-15.20	18.59	12.09	1.92E+01	Gamma	40.70
Pt. Target	025	25	-40.47	19.76	13.19	2.67E+01	Gamma	40.76
Pt. Target	026	25	-5.42	22.28	15.75	4.63E+01	Gamma	40.69
Building	027	3675	-40.51	13.90	-1.56	2.04E+00	Gamma	40.49
Runway	028	1750	-40.27	-6.84	-15.31	3.50E-02	Gamma	43.25
Runway	029	1000	-40.32	-5.42	-14.57	4.04E-02	Gamma	43.03
Runway	030	1250	-40.44	-5.20	-14.12	4.55E-02	Gamma	41.23
Building	031	200	-40.18	5.90	-5.07	5.89E-01	Gamma	44.34
Runway	032	1500	-40.20	-6.58	-16.18	3.24E-02	Gamma	44.10
Runway	033	400	-40.02	-5.80	-14.86	4.52E-02	Gamma	46.54
Forest	001	2025	-40.55	2.97	-6.68	2.64E-01	Gamma	40.15
Building	002	50	-24.08	14.54	5.61	5.55E+00	Gamma	42.70
Forest	003	11400	-39.56	7.40	-7.02	2.84E-01	Gamma	53.81
Field	004	2500	-39.44	-2.03	-10.79	9.16E-02	Gamma	55.91
Shoreline	005	75	-40.03	4.88	-1.77	6.66E-01	Gamma	46.22
Shoreline	006	100	-40.28	6.14	0.78	8.44E-01	Gamma	43.03
Water	007	2500	-40.36	-6.99	-16.83	2.75E-02	Gamma	42.28
Docks	008	200	-40.27	11.13	-1.67	1.69E+00	Gamma	43.15
Pier/Wharf	009	780	-40.22	10.77	-3.95	9.20E-01	Gamma	43.99
Field	010	10000	-39.95	0.23	-9.02	1.31E-01	Gamma	47.77
Water	011	10000	-39.44	-4.21	-14.98	3.97E-02	Gamma	56.14
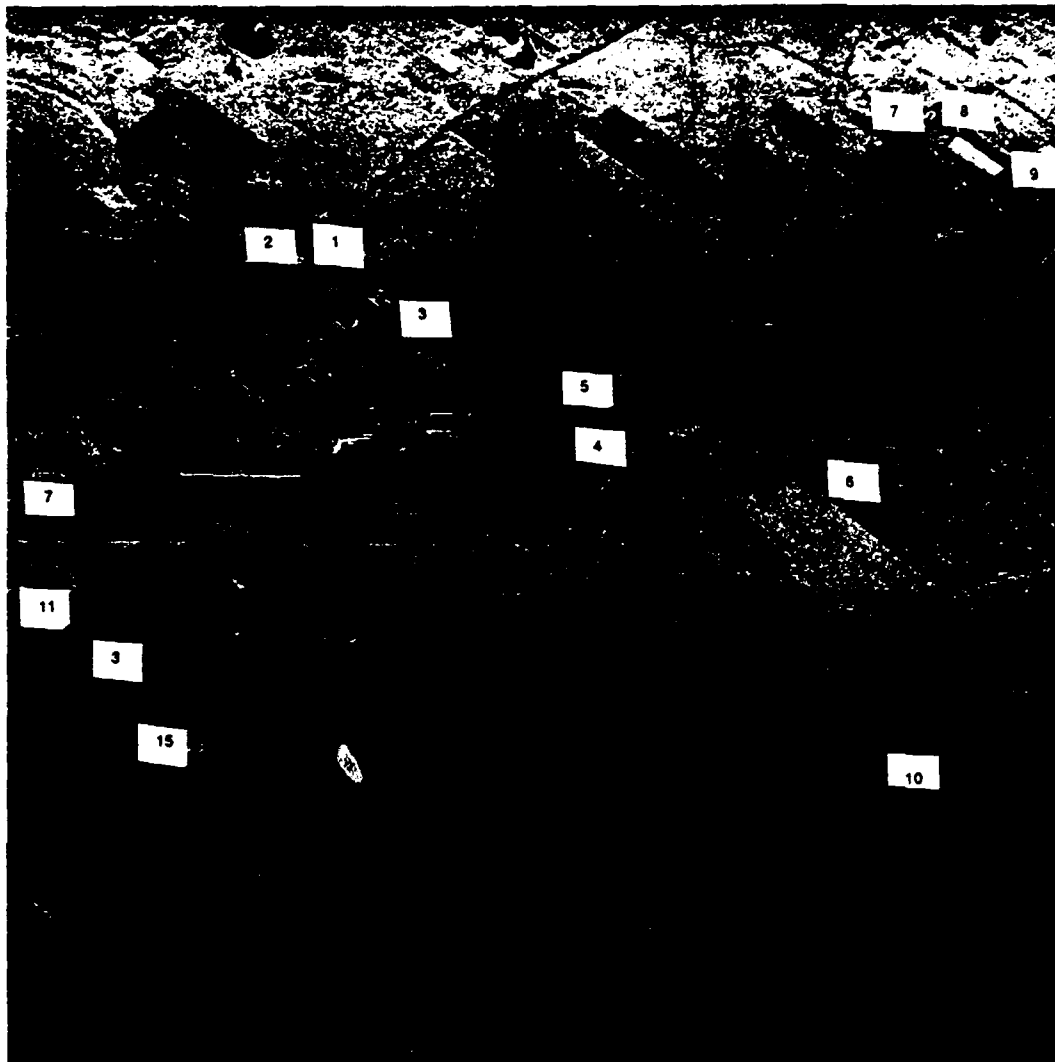
88-11228

Figure A-7.   Clutter Location Map of Image 7

TABLE A-7

IMAGE 7
STATISTICAL SUMMARY
FILE: X1137

Category	Site#	#Pts	Min. (dB)	Max. (dB)	Mean (dB)	STD (Mag)	PDF	Angle
Forest	001	1600	-37.07	-2.16	-15.60	4.40E-02	Gamma	65.87
Water	002	3000	-37.07	-15.91	-26.20	3.16E-03	Gamma	66.07
Field	003	10000	-37.05	-13.02	-23.86	4.99E-03	Gamma	66.65
Forest	004	10000	-37.07	-5.80	-16.72	2.57E-02	Gamma	65.95
Runway	005	2000	-37.15	-13.16	-21.87	7.27E-03	Gamma	63.68
Field	006	4500	-37.16	-3.89	-15.79	2.97E-02	Gamma	63.36
Building	007	540	-37.17	17.86	-0.52	3.84E+00	Gamma	63.03
Water	008	5000	-37.37	-11.94	-23.77	5.39E-03	Gamma	58.64
Shoreline	009	30	-15.14	1.72	-2.50	3.63E-01	Gamma	60.19
Shoreline	010	100	-37.01	-4.06	-11.01	8.68E-02	Gamma	67.59
Water	011	1500	-37.02	-17.86	-27.33	2.44E-03	Gamma	67.43
Field	012	2500	-36.98	-10.95	-20.70	9.93E-03	Gamma	68.61
Building	013	100	-36.91	4.47	-7.69	3.94E-01	Gamma	71.08
Farmland	014	2500	-36.92	-19.71	-30.25	1.42E-03	Gamma	70.88
Field	015	2500	-36.99	-17.85	-27.64	2.34E-03	Gamma	68.18
Forest	016	900	-36.98	-10.59	-22.11	8.29E-03	Gamma	68.78
Water	017	10000	-36.90	-18.86	-31.46	1.09E-03	Gamma	71.56
Shoreline	018	50	-36.90	-4.08	-12.75	7.35E-02	Gamma	71.47
Building	019	225	-35.12	5.74	-4.31	4.60E-01	Gamma	58.20
Road Sign	020	16	-19.25	3.49	-1.64	5.67E-01	Gamma	65.70
Water	021	900	-37.01	-18.70	-28.38	2.00E-03	Gamma	57.70
Highway	022	50	-37.00	-22.50	-29.34	1.42E-03	Gamma	57.78
Highway	023	50	-37.04	-23.72	-29.95	1.01E-03	Gamma	66.56
Forest	024	900	-36.96	-10.72	-21.95	8.68E-03	Gamma	69.25
Building	001	100	-25.67	14.19	3.82	4.61E+00	Gamma	57.83
Water	002	900	-37.38	-9.41	-17.29	1.92E-02	Gamma	58.23
Forest	003	2500	-37.35	-2.08	-10.87	8.88E-02	Gamma	58.84
Runway	004	1875	-37.20	-11.24	-21.77	7.88E-03	Gamma	62.27
Field	005	4000	-37.24	-3.60	-13.95	4.28E-02	Gamma	61.50
Field	006	10000	-37.14	-2.10	-11.69	6.92E-02	Gamma	64.12
Farmland	007	2500	-37.60	-5.22	-14.88	3.47E-02	Gamma	54.09
Farmland	008	1600	-37.67	8.80	-1.26	8.03E-01	Gamma	52.57
Farmland	009	1600	-37.59	1.82	-7.04	2.06E-02	Gamma	54.14
Farmland	010	1600	-36.97	-18.0	-29.44	1.72E-03	Gamma	69.02
Forest	011	2500	-36.94	-11.43	-22.27	8.52E-03	Gamma	69.87
Pt. Target	012	25	-11.06	28.37	19.88	1.74E+02	Gamma	52.04
Pt. Target	013	25	-26.56	20.91	13.29	3.52E+01	Gamma	51.87
Pt. Target	014	25	-16.80	26.48	18.10	1.09E+02	Gamma	53.98
Pt. Target	015	25	-21.19	20.12	11.92	2.55E+01	Gamma	53.82
Rnwy Light	016	9	-12.93	4.29	-0.28	8.42E-01	Gamma	57.93
Rnwy Light	017	9	-6.32	6.43	2.32	1.33E+00	Gamma	57.89
Prkd Auto	018	25	-24.07	1.74	-6.08	3.86E-01	Gamma	51.70
Prkd Auto	019	25	-37.21	-0.81	-7.64	2.55E-01	Gamma	52.04
Building	020	100	-26.51	7.89	-0.09	1.13E+00	Gamma	50.53
Boat	046	25	-13.25	0.47	-3.38	3.54E-01	Gamma	50.95
Boat	047	25	-21.90	5.35	-2.15	8.00E-01	Gamma	50.93
Boat	048	25	-8.65	1.82	-1.74	4.28E-01	Gamma	51.02
Boat	049	25	-7.92	4.60	0.83	7.68E-01	Uniform	50.83
Boat	050	50	-16.92	11.90	3.93	3.23E+00	Gamma	55.92
Wake (#50)	051	600	-40.51	-1.81	-9.89	1.15E-01	Gamma	55.94
Water	052	2500	-40.42	-2.21	-11.34	8.18E-02	Gamma	57.83
Boat	053	25	-11.95	7.21	1.88	1.67E+00	Gamma	47.15
Pier/Wharf	054	100	-41.10	3.67	-4.31	4.57E-01	Gamma	46.28
Building	055	250	-41.27	7.52	-2.53	7.82E-01	Gamma	44.02
Boat	056	25	-6.61	8.27	4.06	1.86E+00	Uniform	49.14
Boat	057	100	-12.02	21.25	10.05	2.09E+01	Gamma	56.83
Forest	058	2500	-40.93	-3.23	-13.28	5.98E-02	Gamma	48.89
Urban	001	2500	-42.62	9.28	-3.64	6.06E-01	Gamma	31.08
Urban	002	2500	-42.62	16.09	-3.13	1.71E+00	Gamma	31.08
Urban	003	2500	-42.37	7.53	-4.98	4.71E-01	Gamma	33.01

89-11925
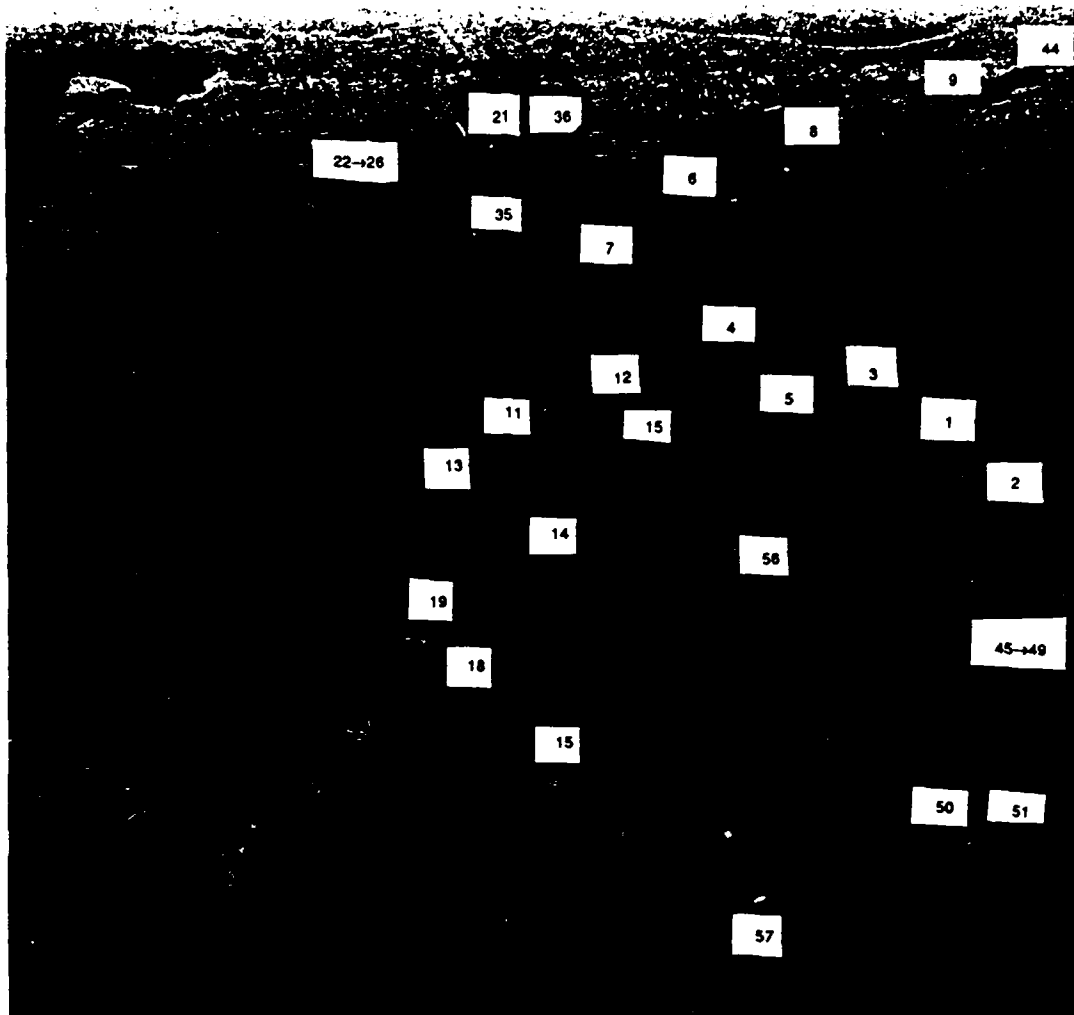
88-11229

Figure A-8   Clutter Location Map of Image 8

TABLE A-8

IMAGE 8
STATISTICAL SUMMARY
FILE: X946

Category	Site#	#Pts	Min. (dB)	Max. (dB)	Mean (dB)	STD (Mag)	PDF	Angle
Farmland	001	10000	-41.16	-3.03	-13.24	5.24E-02	Gamma	45 95
Forest	002	10000	-41.05	-1.06	-13.11	6.57E-02	Gamma	47 30
Field	003	10000	-41.28	-2.72	-13.20*	5.24E-02	Gamma	44 37
Farmland	004	10000	-41.43	-0.71	-11.67	7.50E-02	Gamma	42 57
Field	005	2500	-41.37	-2.10	-13.83	4.92E-02	Gamma	43.06
Field	006	22500	-41.87	3.32	-8.43	1.62E-01	Gamma	38 24
Field	007	10000	-41.96	0.50	-9.68	1.23E-01	Gamma	37.00
Forest	008	15625	-42.12	4.86	-7.35	2.17E-01	Gamma	35.71
Forest	009	90000	-42.65	12.53	-6.12	3.61E-01	Gamma	32.00
Forest	010	160000	-41.65	4.16	-11.43	1.04E-01	Gamma	41 69
Pier/Wharf	011	500	-41.10	12.01	-6.51	1.01E+00	Gamma	46.49
Building	012	100	-41.21	7.64	-2.07	1.07E+00	Gamma	44.78
Water	013	10000	-41.08	-8.82	-21.17	1.11E-02	Gamma	46 95
Water	014	2500	-41.06	-10.05	-22.63	9.93E-03	Gamma	47.02
Water	015	10000	-40.83	-9.38	-20.25	1.34E-02	Gamma	50.64
Shoreline	016	250	-40.85	5.94	-3.08	5.71E-01	Gamma	49.90
Shoreline	017	250	-40.87	2.78	-5.11	3.34E-01	Gamma	49.70
Shoreline	018	250	-40.63	3.35	-3.16	4.76E-01	Gamma	53.72
Shoreline	019	250	-40.64	0.97	-6.85	2.37E-01	Gamma	53.58
Building	020	100	-16.45	7.54	2.45	1.50E+00	Gamma	34 95
Building	021	150	-42.19	11.13	3.93	2.28E+00	Gamma	34 26
Pt. Target	022	25	-4.59	18.96	11.21	1.96E+01	Gamma	35.76
Pt. Target	023	25	-10.68	18.64	11.44	1.87E+01	Gamma	35 60
Pt. Target	024	25	-11.63	17.57	11.23	1.70E+01	Gamma	35.72
Pt. Target	025	25	-12.99	19.94	12.78	2.44E+01	Gamma	35 78
Pt. Target	026	25	-42.03	21.84	14.72	4.01E+01	Gamma	35.71
Building	027	3675	-42.08	13.33	-3.60	1.16E+00	Gamma	35 49
Runway	028	1750	-41.68	-4.64	-14.03	4.7?E-02	Gamma	39.47
Runway	029	1000	-41.83	-4.30	-13.30	5.38E-02	Gamma	38 25
Runway	030	1250	-41.99	-1.61	-11.73	7.95E-02	Gamma	36 23
Building	031	200	-41.65	11.98	0.39	1.93E+00	Gamma	39 64
Runway	032	1500	-41.77	-2.78	-11.64	7.49E-02	Gamma	38 47
Runway	033	2000	-41.44	-2.91	-15.57	3.48E-02	Gamma	42 18
Runway	034	2000	-41.60	-0.25	-12.56	6.94E-02	Gamma	40 34
Runway	035	2000	-41.82	-1.78	-11.80	7.29E-02	Gamma	38 09
Runway	036	2000	-42.22	-0.65	-10.89	8.66E-02	Gamma	34 30
Boat	037	25	-23.52	6.02	0.76	1.28E+00	Gamma	48 50
Boat	038	25	-13.89	8.38	2.83	1.99E+00	Gamma	48.71
Boat	039	25	-7.83	4.03	0.70	7.58E-01	Uniform	51 57
Boat	040	25	-9.60	6.19	2.11	1.07E+00	Uniform	51 79
Wake (#40)	041	50	-40.74	1.19	-4.01	2.77E-01	Uniform	51 79
Shoreline	042	50	-20.19	8.34	2.89	1.60E+00	Gamma	50 47
Boat	043	25	-13.89	11.41	6.57	4.50E+00	Gamma	57 70
Building	044	200	-42.60	12.36	4.27	2.92E+00	Gamma	30 89
Boat	045	25	-19.64	2.62	-2.60	5.34E-01	Gamma	50 88
Boat	046	25	-13 25	0.47	-3 38	3.54E 01	Gamma	50 95
Boat	047	25	-21.90	5 35	-2 15	8.00E-01	Gamma	50 93
Boat	048	25	-8 65	1.82	-1 74	4 28E 01	Gamma	51 02
Boat	049	25	-7.92	4.60	0 83	7.68E-01	Uniform	50 83
Boat	050	50	-16.92	11.90	3 93	3 23E+00	Gamma	55 02
Wake (#50)	051	600	-40 51	-1.81	9 39	1.15E-01	Gamma	55 94
Water	052	2500	-40.42	-2.21	-11 34	8.18E-02	Gamma	57 83
Boat	053	25	-11 95	7.21	1.88	1.67E+00	Gamma	47 16
Pier/Wharf	054	100	-41.10	3.67	-4.31	4.57E-01	Gamma	46 28
Building	055	250	-41.27	7.52	-2.53	7.82E 01	Gamma	44 02
Boat	056	25	-6.61	8.27	4.06	1.86E+00	Uniform	19 11
Boat	057	100	-12 02	21.25	10.05	2.09E+01	Gamma	56 83
Forest	058	2500	-40.93	-3.23	-13.28	5.98E-02	Gamma	48 89
Urban	001	2500	-42.62	9.28	-3.64	6.06E-01	Gamma	31 08
Urban	002	2500	-42.62	16.09	-3.13	1.71E+00	Gamma	31 08
Urban	003	2500	-42 37	7.53	-4 98	4.71E 01	Gamma	33 01

A-37

APPENDIX B

BACKSCATTER RESPONSE OF POINT TARGETS

APPENDIX B - LIST OF FIGURES

APPENDIX B

BACKSCATTER RESPONSE OF POINT TARGETS

Presented in Figures B-1 through B-4 are empirical backscattering responses for point targets which were used in the validation of the calibration of the images. These data have been collected from a variety of sources.
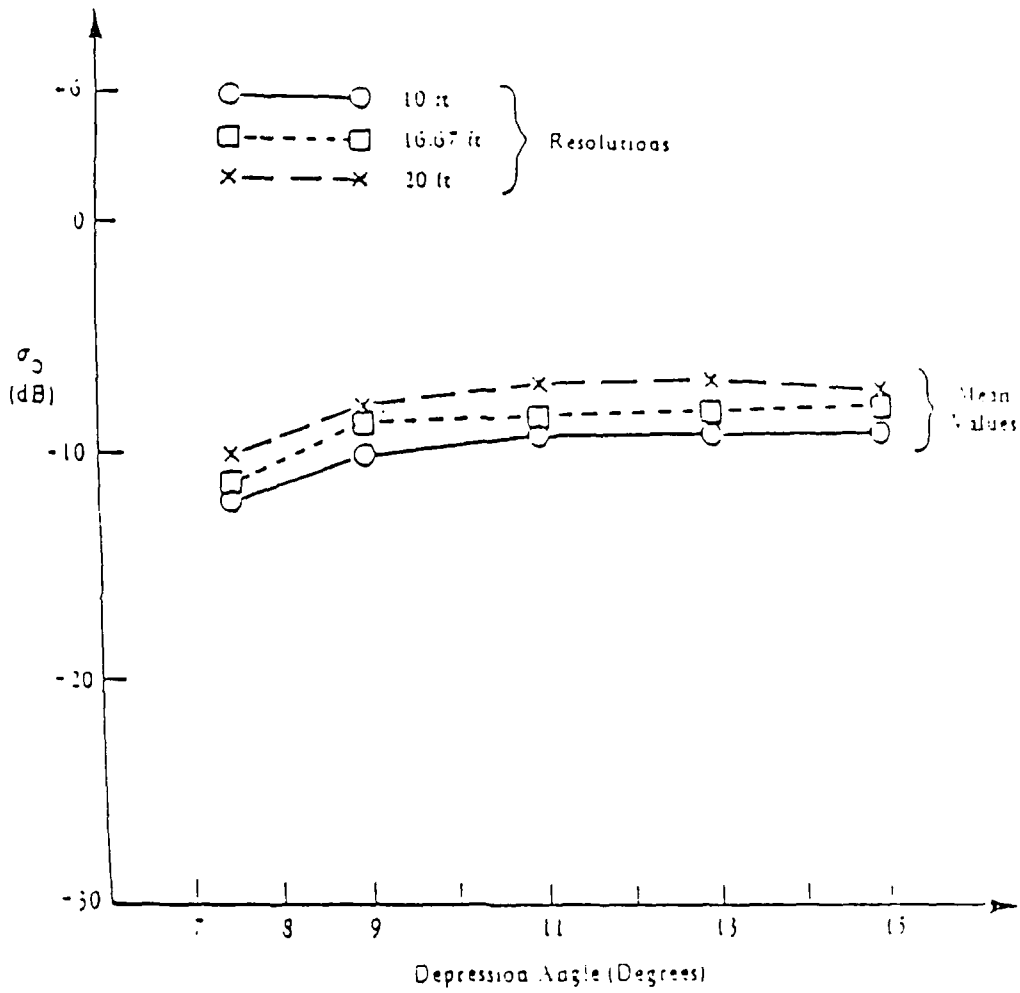
Figure B-1. Measurements of the Backscattering Cross-Section of a Densely Populated Urban Area.
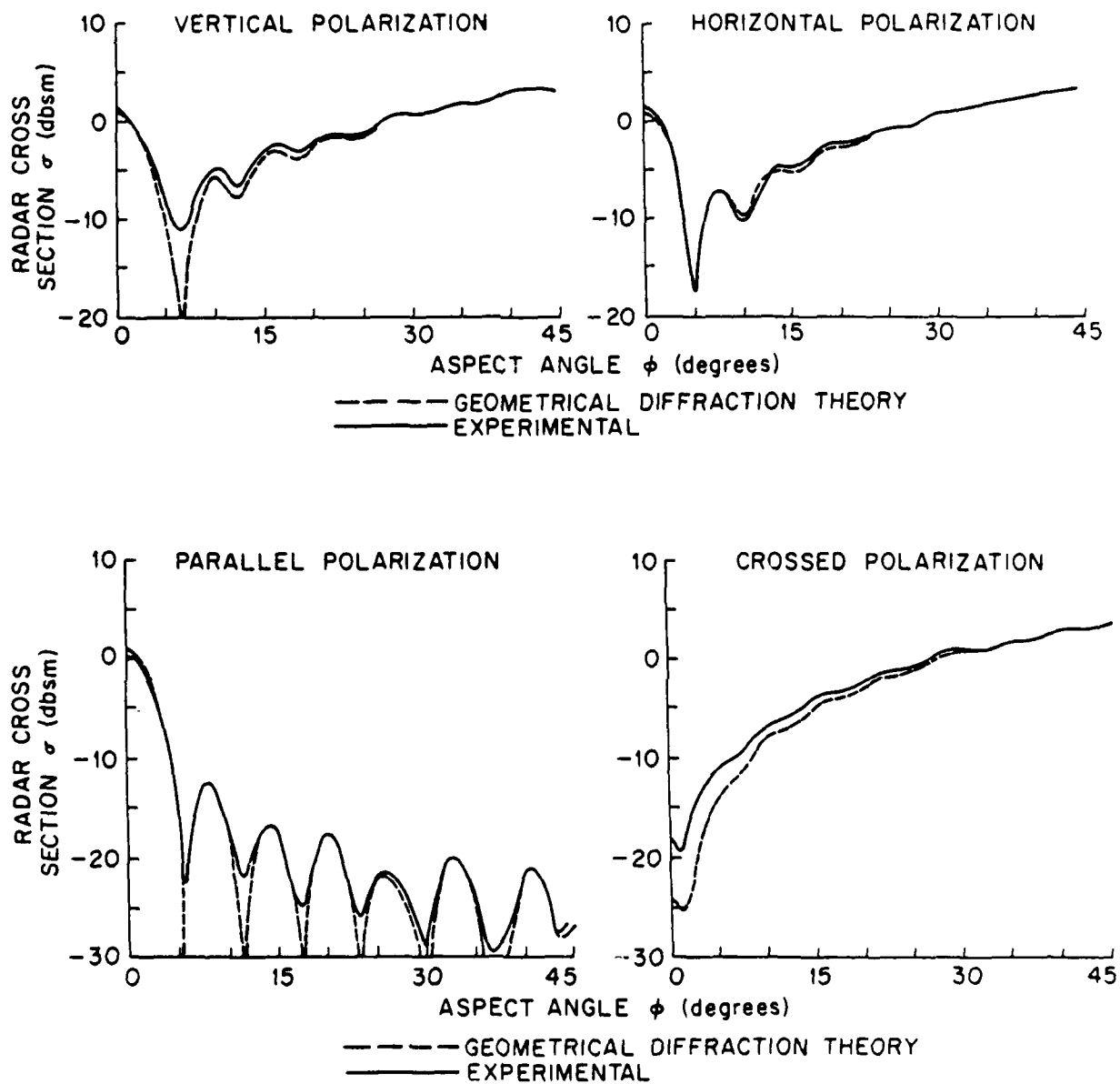
Figure B-2. Measurements of the Backscattering Cross-Section for a Dihedral Corner Reflector, (Skolnik, 1970). The Aspect Angle in Skolnik, 1970, is Equal to the Depression Angle.
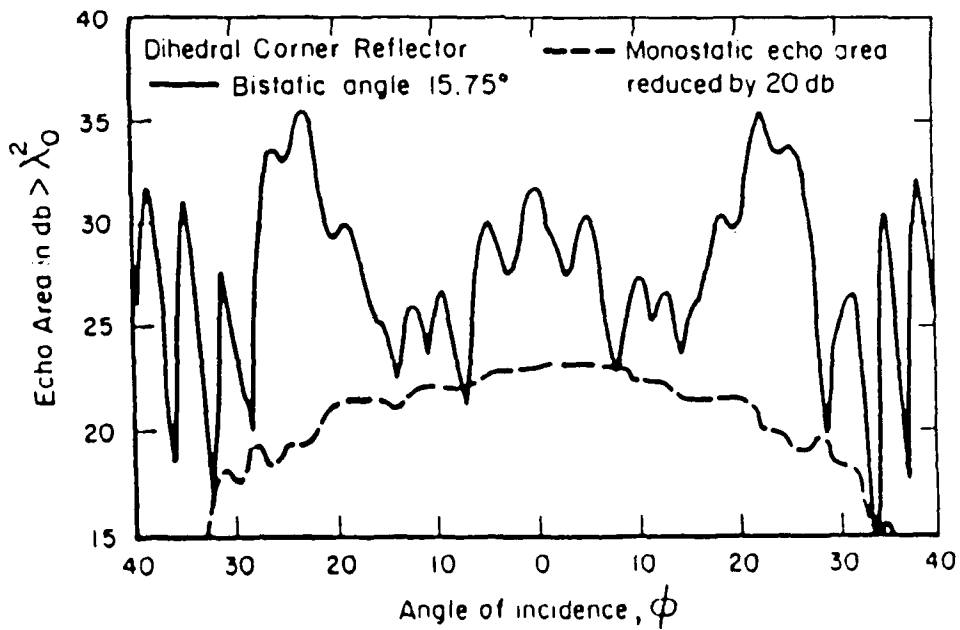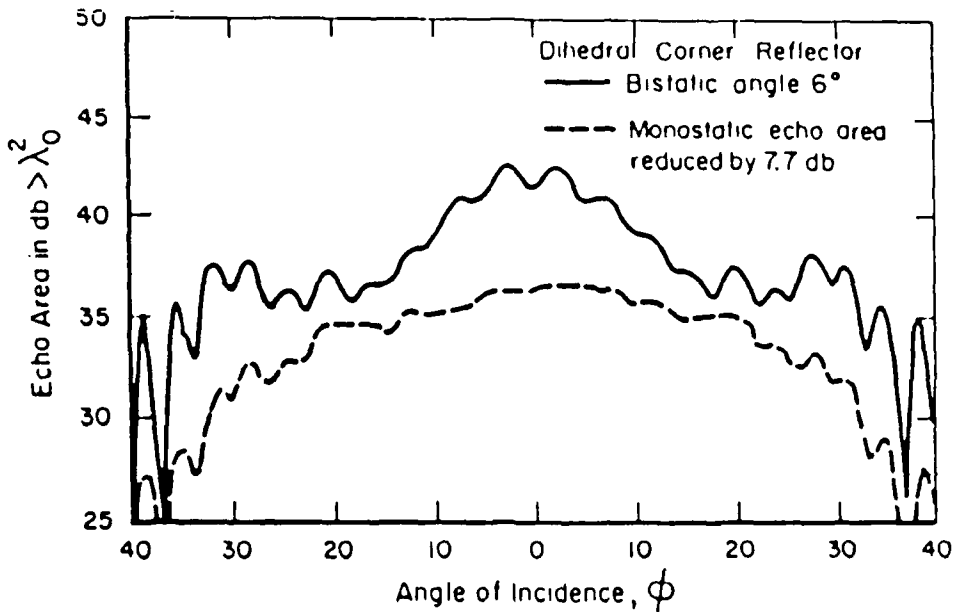
Figure B-3. Monostatic and Bistatic Cross-Section Measurements for
a Dihedral Corner Reflector. ø is Incidence Angle
(Ruck et al, 1970) λ_0 is the Radar Wavelength
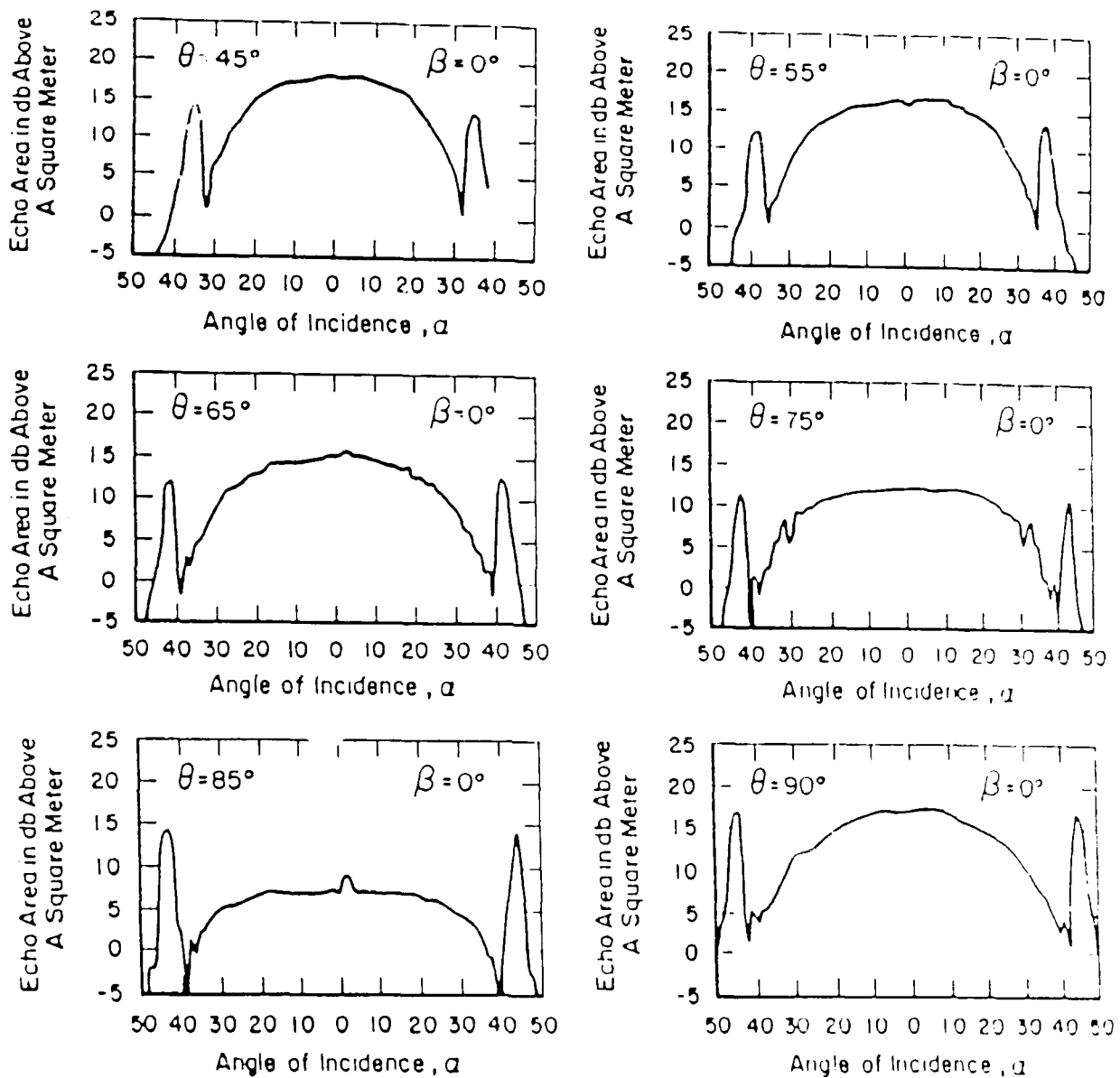
Figure B-4. Radar Backscattering Cross-Section of a Triangular Trihedral Reflector. θ is Depression Angle to the Target (Ruck, et al., 1970). β = 0° Implies a Monstatic System. α = (φ - 45°) sin θ. φ is the Offside Angle.

APPENDIX C

SIMULATION OF AN IMAGE REFLECTIVITY MAP
AT AN ARBITRARY INCIDENCE ANGLE

APPENDIX C - LIST OF FIGURES

APPENDIX C

SIMULATION OF AN IMAGE REFLECTIVITY MAP
AT AN ARBITRARY INCIDENCE ANGLE

In the course of this activity it became of interest to remap the airport clutter scene to an 87 degree incidence angle, the angle which corresponds to the angle of an aircraft on approach. The strategy used here to create these images was to separate the scene into basically two categories: distributed targets which tend to produce backscatter levels less than 5 dB and the man-made targets of greatest concern which produce backscatter levels greater than 0 dB. The first task was to determine if the backscatter coefficient angular response of distributed clutter such as water, concrete, asphalt, grass, and forest could be modeled with a polynomial function. Published data as shown in this appendix were fit with fourth order polynomials. Three of the four backscatter coefficients were then selected such that the error which arose due to the shape of the polynomial function (i.e., the angular response characteristics) was minimized. Therefore, what was required for each clutter type was that they have similar angular response characteristics while having dissimilar absolute backscatter levels. The polynomial used is

eq(C-1)

$$\sigma^\circ(dB)(\theta) = -6.180E\text{-}6\theta^4 + 9.416E\text{-}4\theta^3 - 4.339E\text{-}2\theta^2 + 0.331\theta + e$$

where θ is in degrees and e sets the absolute NRCS level. A more useful version of this equation is

eq(C-2)

$$\sigma^\circ(dB)(\theta^2) = A(\theta_2^4 - \theta_1^4) + B(\theta_2^3 - \theta_1^3) + C(\theta_2^2 - \theta_1^2) + D(\theta_2 - \theta_1) + \sigma^\circ(dB)(\theta_1)$$

C-5

Asphalt
Stiles, Ulaby, and Wilson
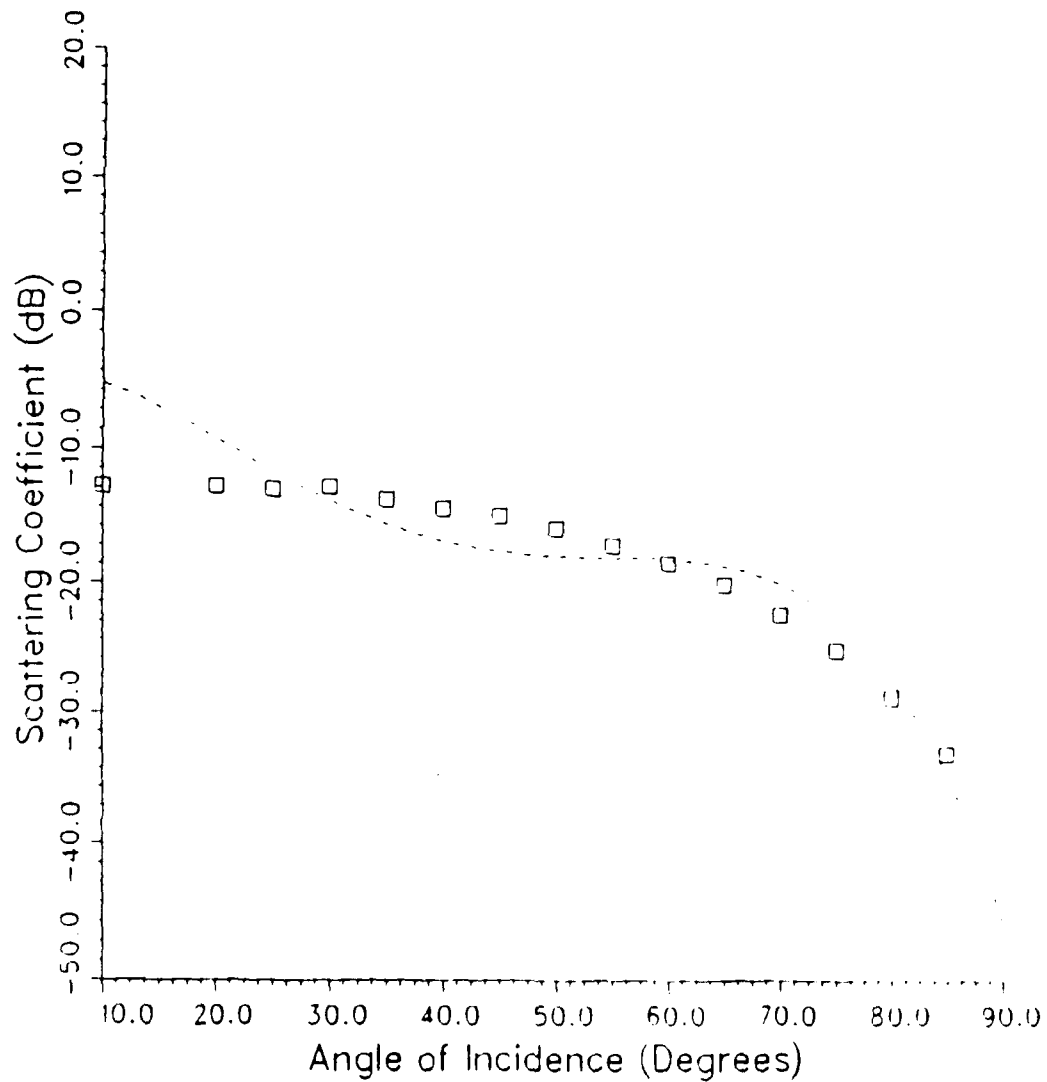
Figure C-1.   Comparison of Polynomial Fit to Asphatt Data

Concrete

Stiles, Ulaby, and Wilson
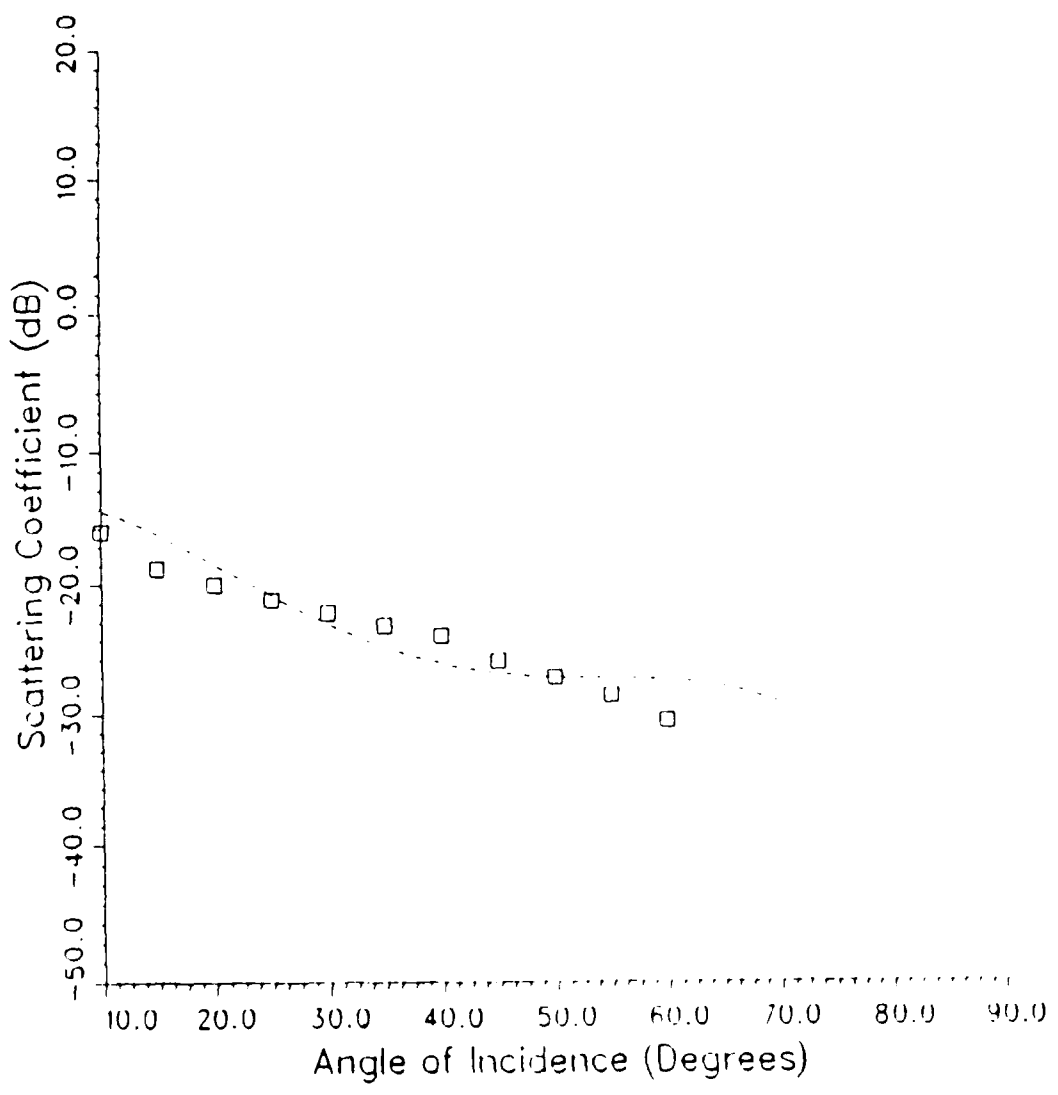
Figure C-2.   Comparison of Polynomial Fit to Concrete Data

Grass
Stiles, Ulaby, and Wilson
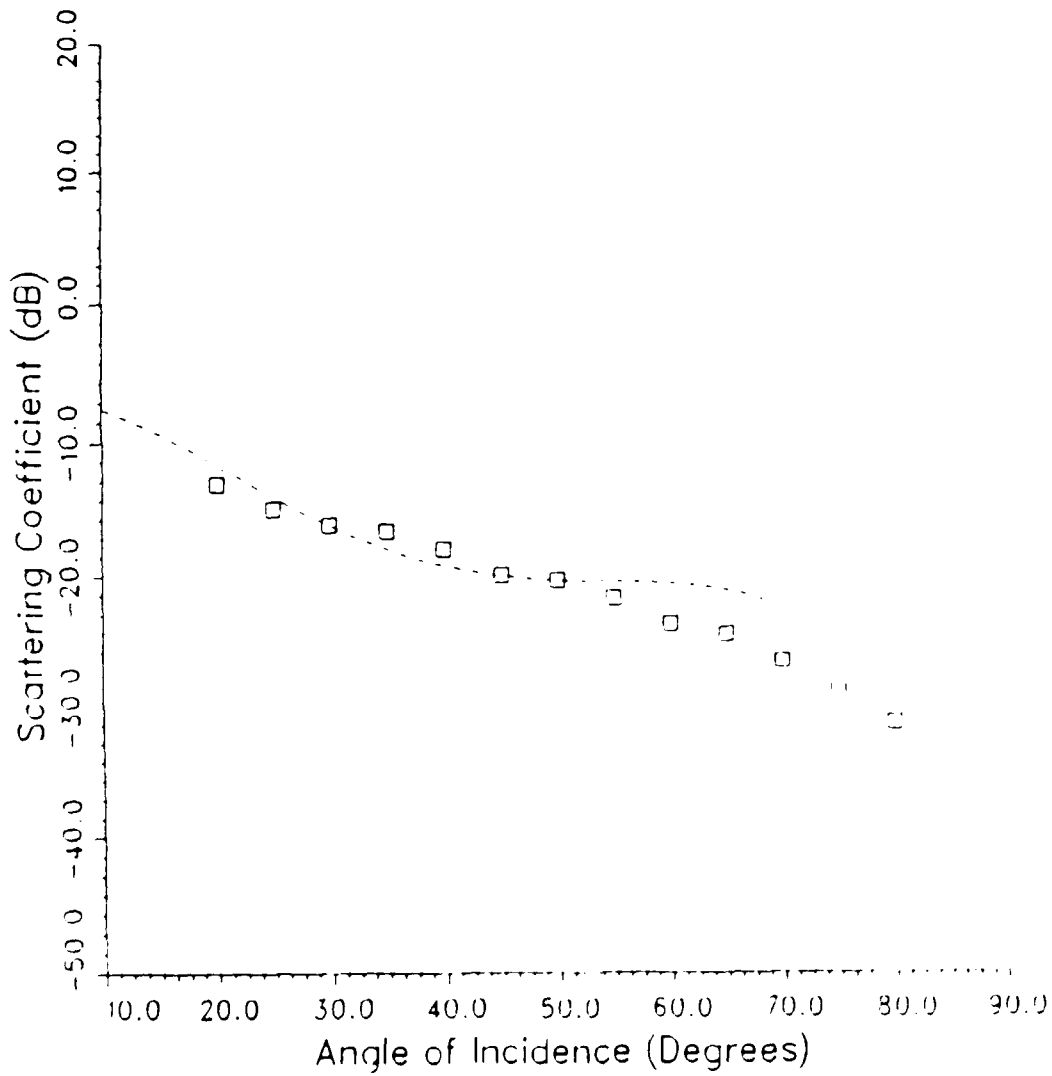
Figure C-3.   Comparison of Polynomial Fit to Grass Data

Water
IEEE Vol. GE-21 #4 10/83
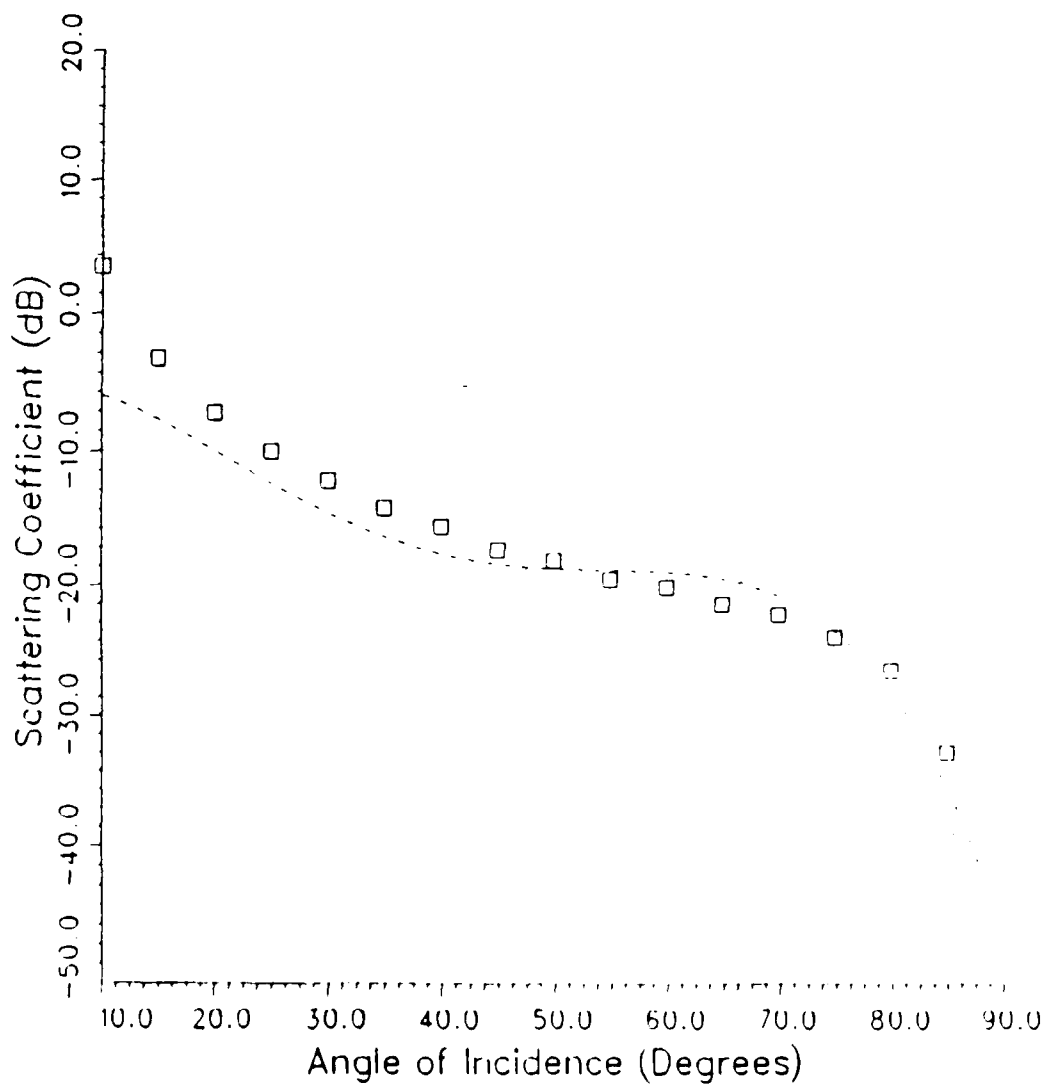
Figure C-4.   Comparison of Polynomial Fit to Water Data

Forest

Ament, MacDonald, and Shewbridge
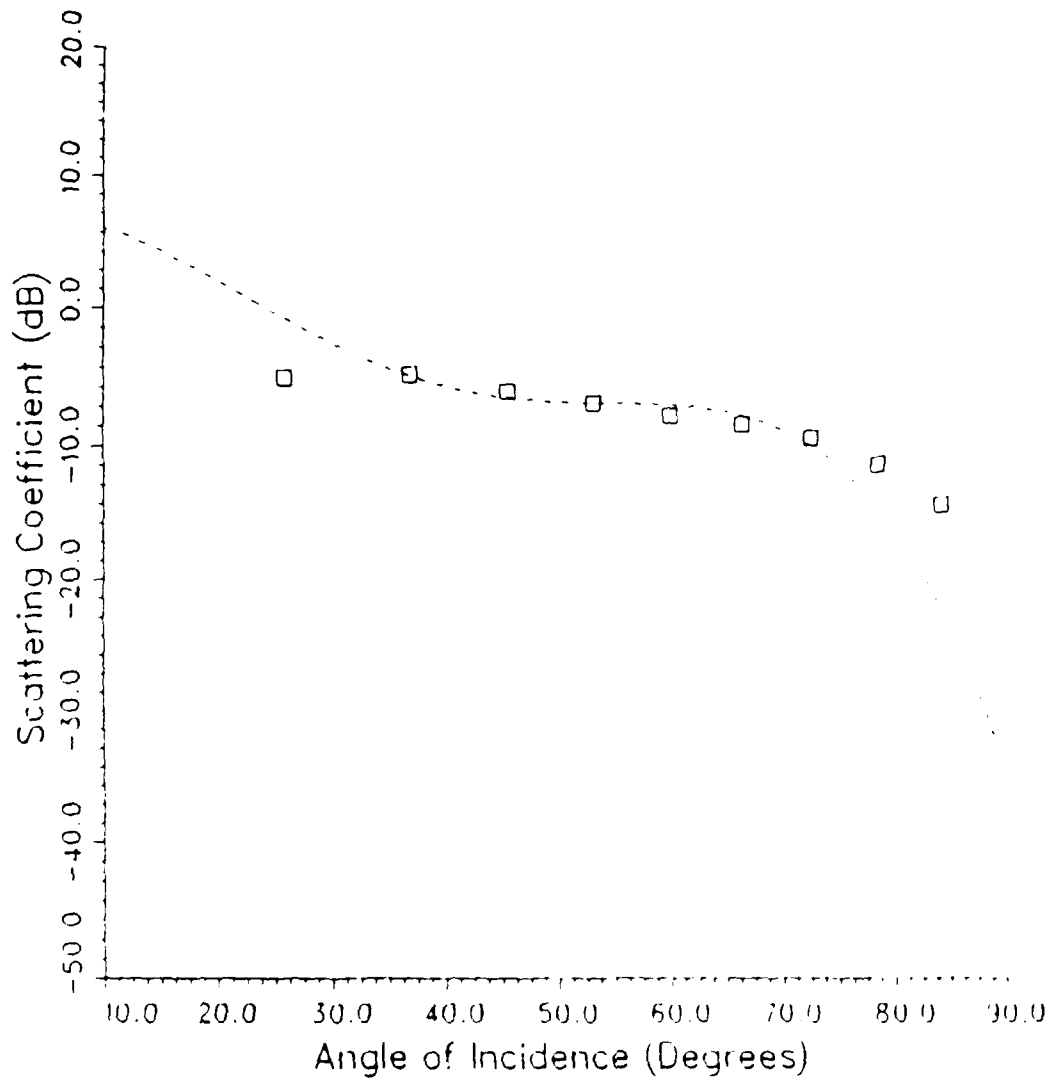
Figure C-5.   Comparison of Polynomial Fit to Forest Data

Figure C-6.   Image 1 Simulated at 87° Incidence Angle

88-11253.B

Figure C-7. Image 2 Simulated at 87° Incidence Angle

Figure C-8.   Image 3 Simulated at 87° Incidence Angle

89-11929
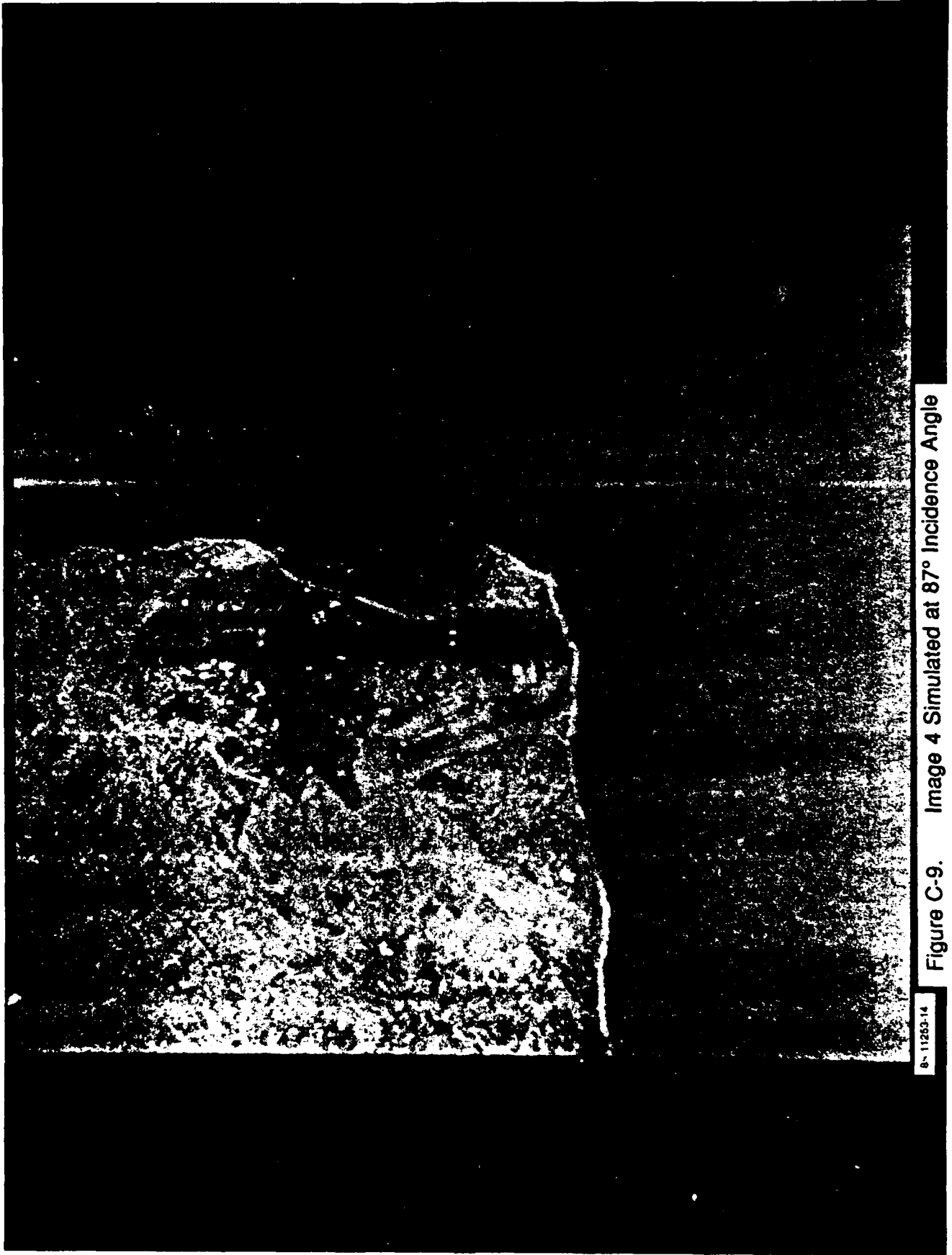
Figure C-9.   Image 4 Simulated at 87° Incidence Angle

8-11263-14

C-23
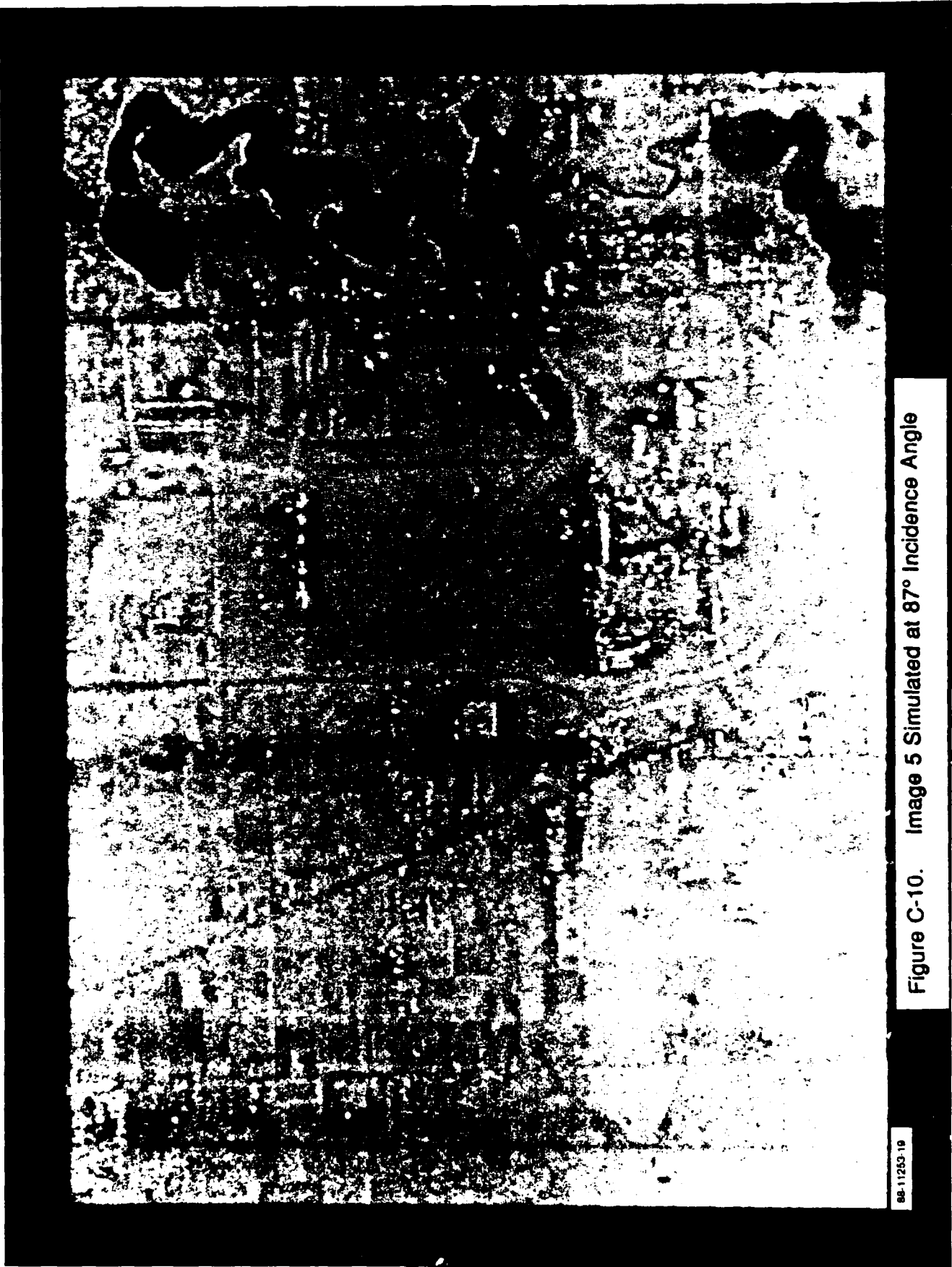
Figure C-10. Image 5 Simulated at 87° Incidence Angle

89-11931

Figure C-11.   Image 6 Simulated at 87° Incidence Angle

86-11253-21
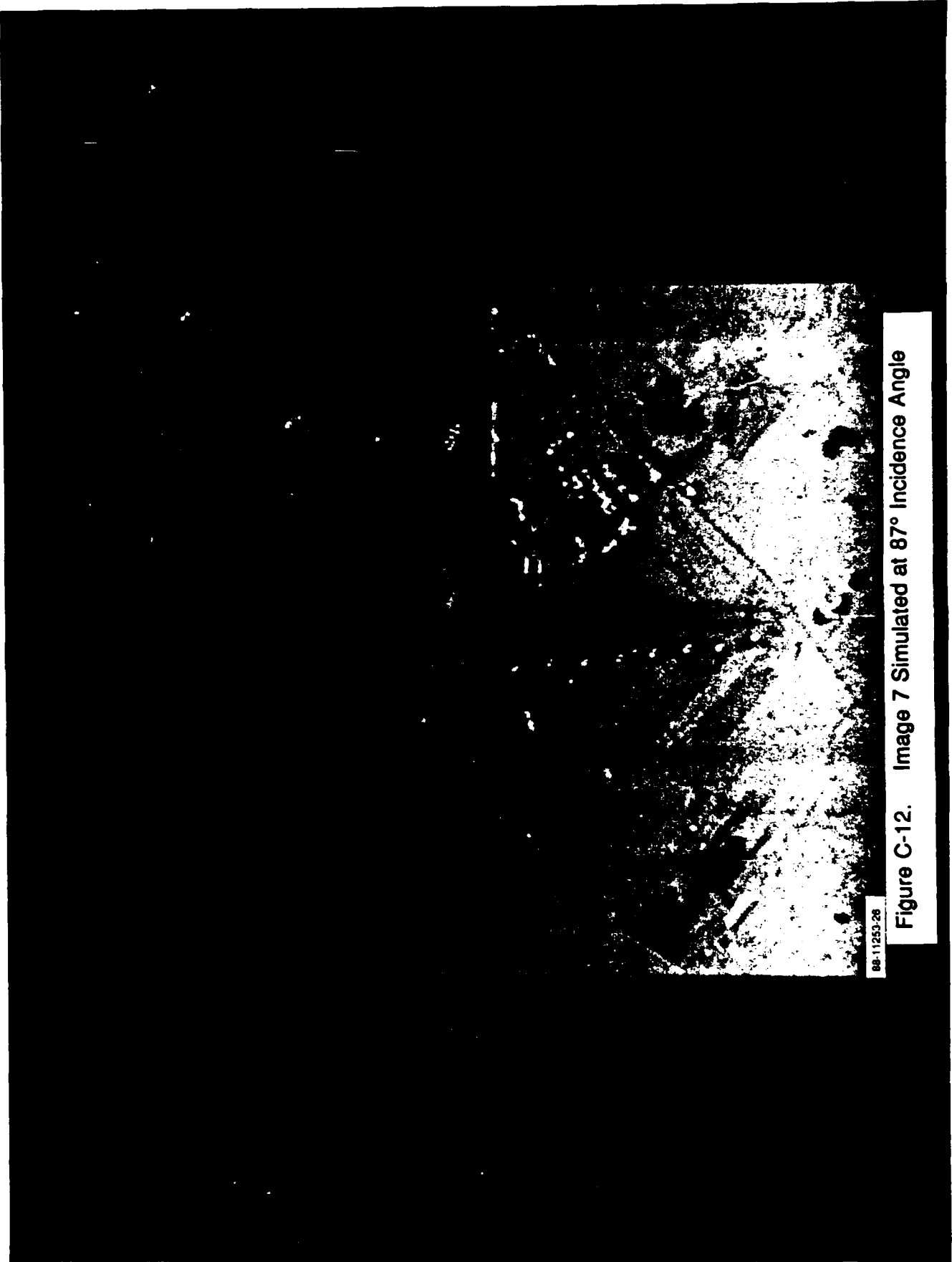
Figure C-12. Image 7 Simulated at 87° Incidence Angle

Figure C-13. Image 8 Simulated at 87° Incidence Angle

APPENDIX D

EXPERIMENTALLY DERIVED RADAR BACKSCATTER RESPONSE
OF DISTRIBUTED TARGETS

APPENDIX D - LIST OF FIGURES

APPENDIX D

EXPERIMENTALLY DERIVED RADAR BACKSCATTER RESPONSE
OF DISTRIBUTED TARGETS

Presented in Figures D-1 through D-15 of this section are experimentally derived backscattering values for distributed targets. These values were used in the validation of the calibration of the images. These data have been collected from a variety of sources.
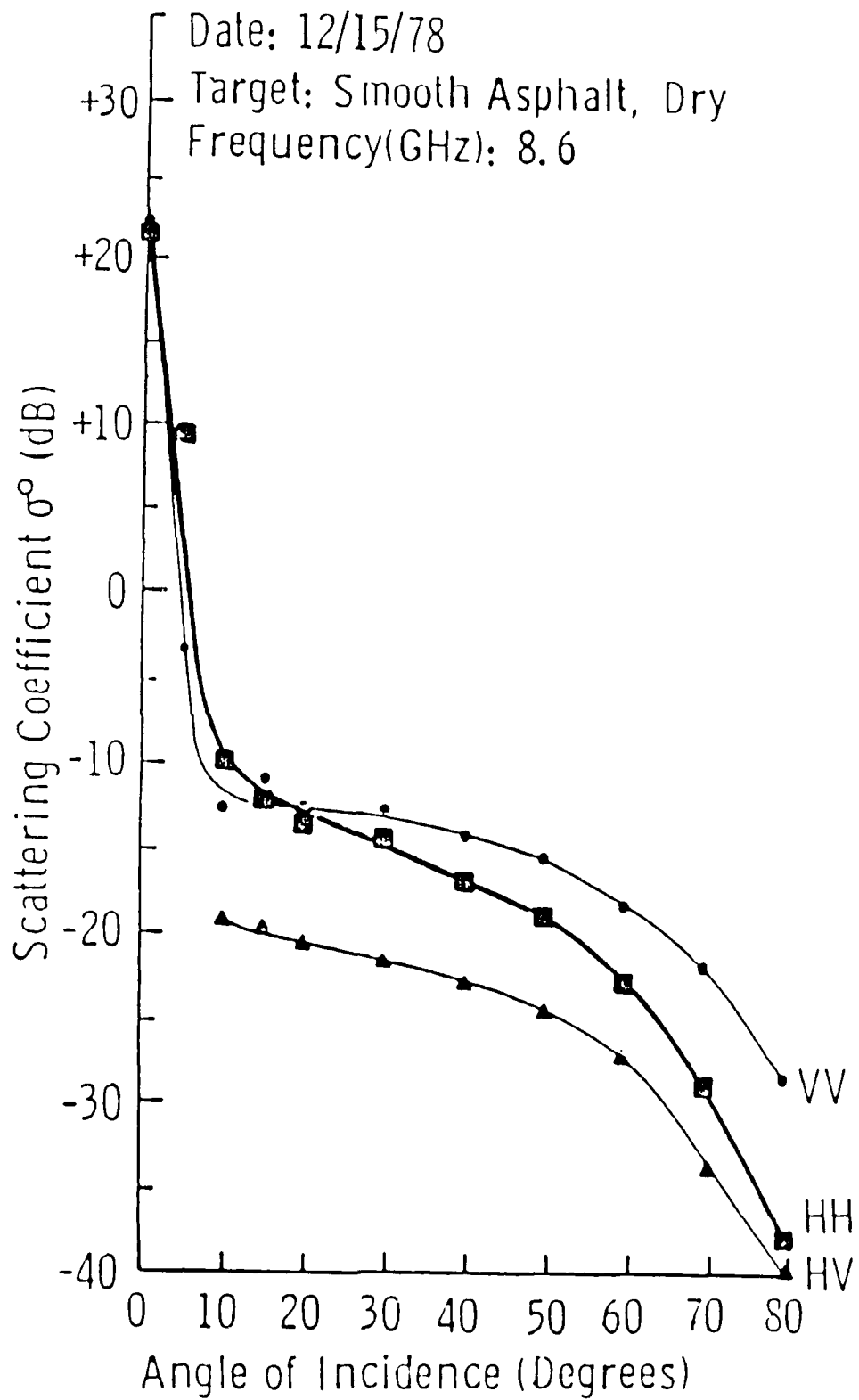
Figure D-1.   Measurements of the Backscatter Coefficient of Smooth Dry Asphalt
(Stiles et al, 1979)
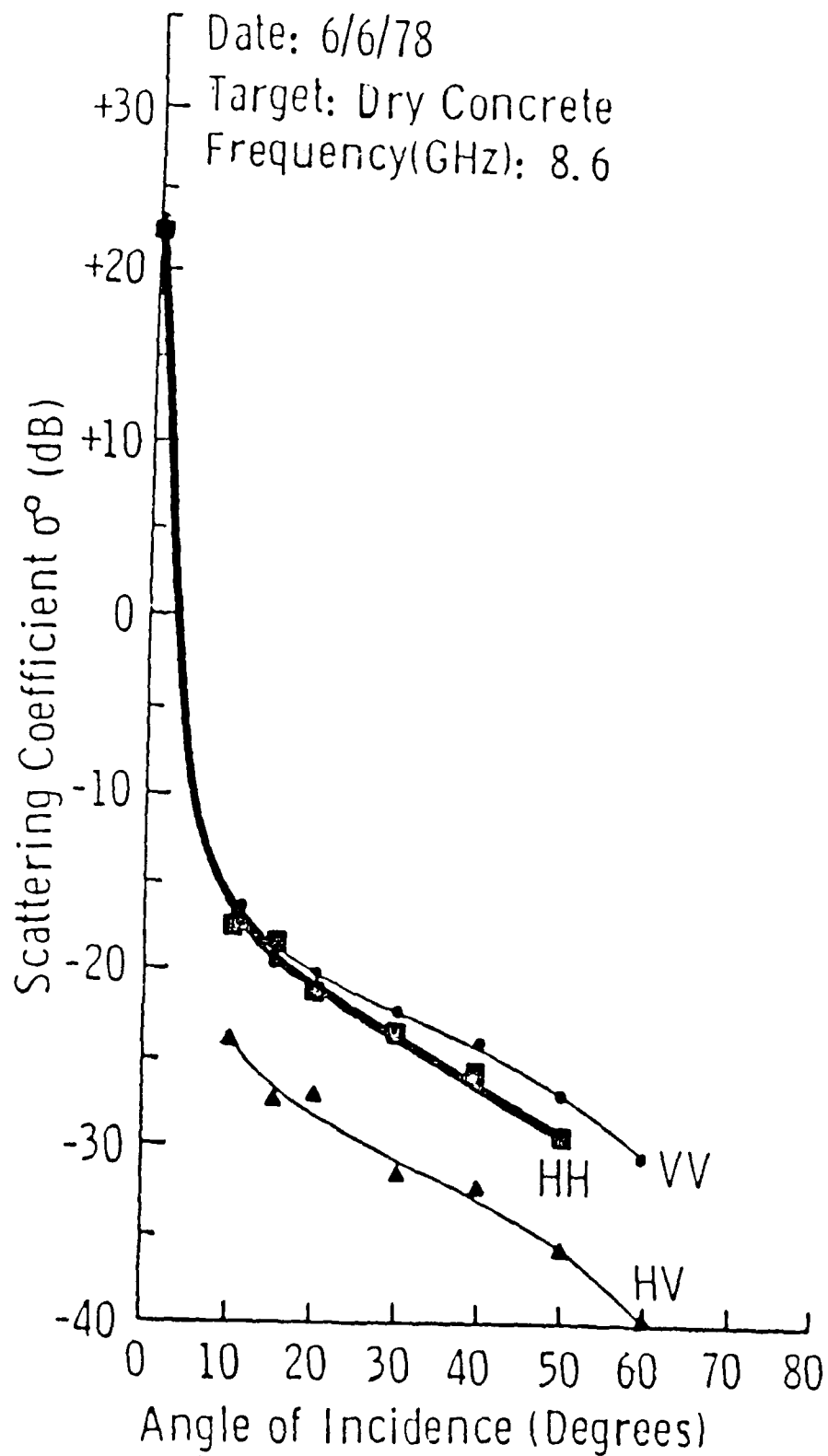
Figure D-2.   Measurements of the Backscatter Coefficient of Dry Concrete
(Stiles et al, 1979)
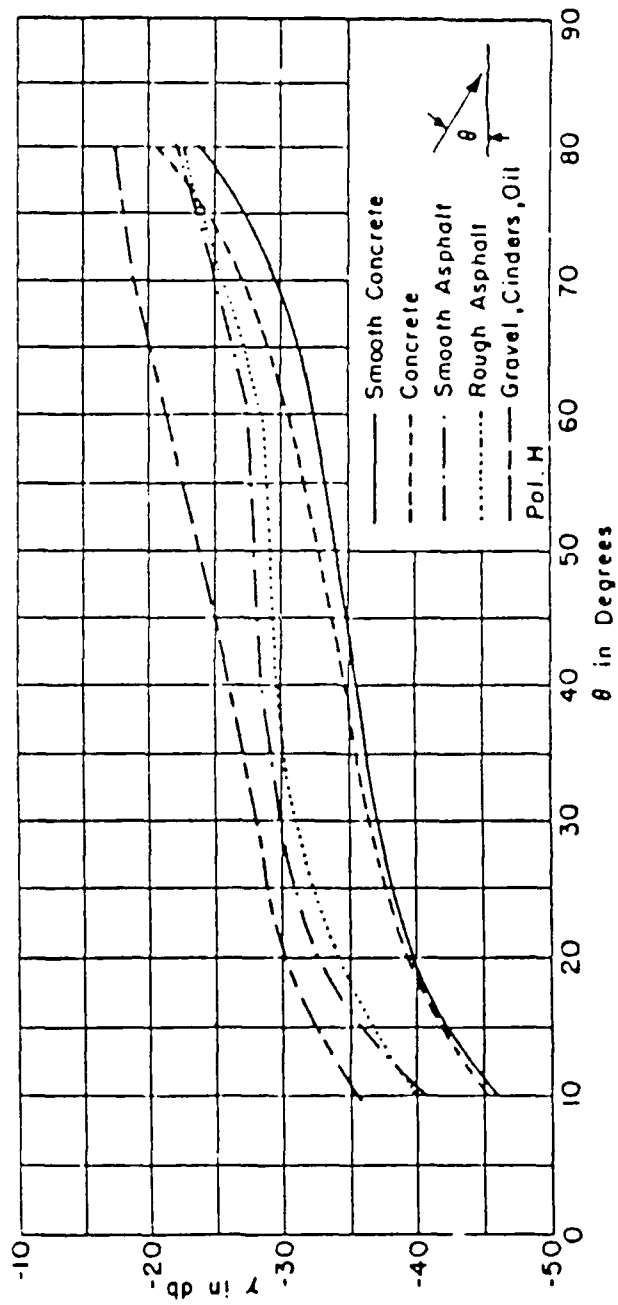
Figure D-3. Measurements of γ for Several Man-Made Surfaces (Cosgriff et al, 1960)
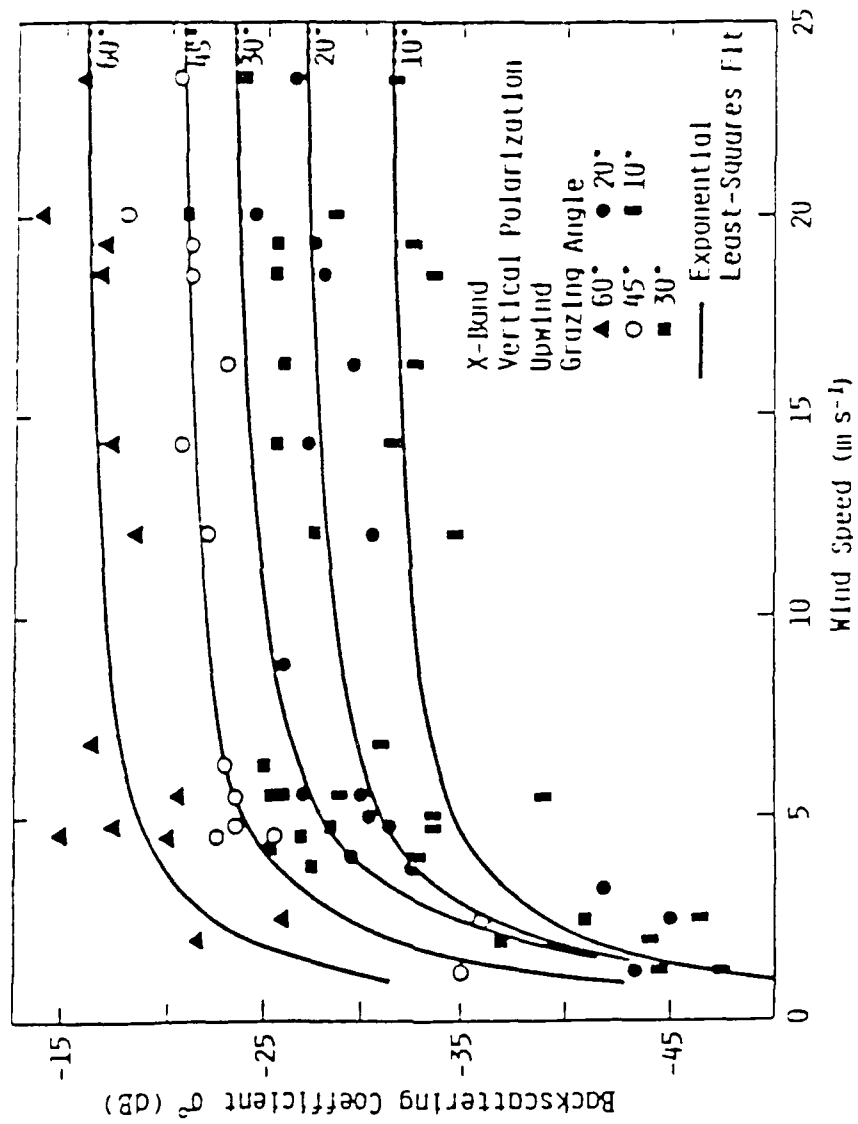
Figure D-4.   Measurement of the NRCS for Oceans at Various Wind
Speeds (Ulaby et al, 1986, Valenzuela et al, 1971)
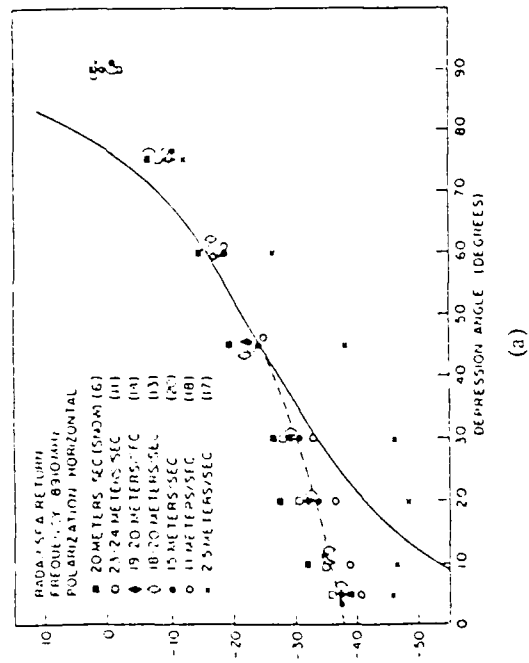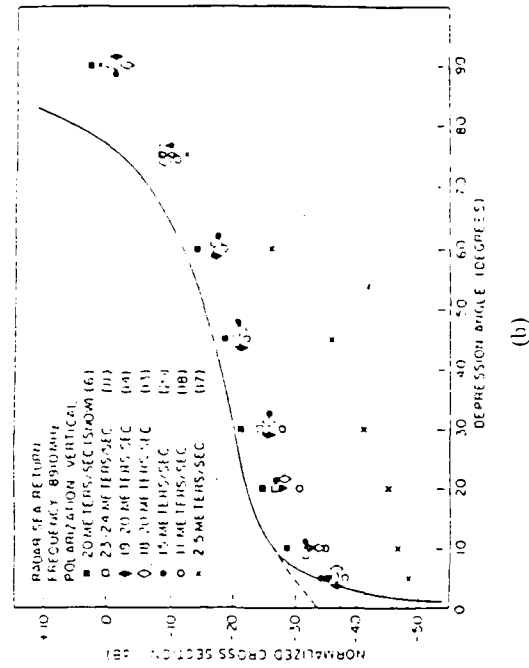
Figure D-5.   Measurements of the Backscattering Coefficient of the Ocean
Surface at X-Band from Guinard and Daley, (Lyzenga et al, 1983)
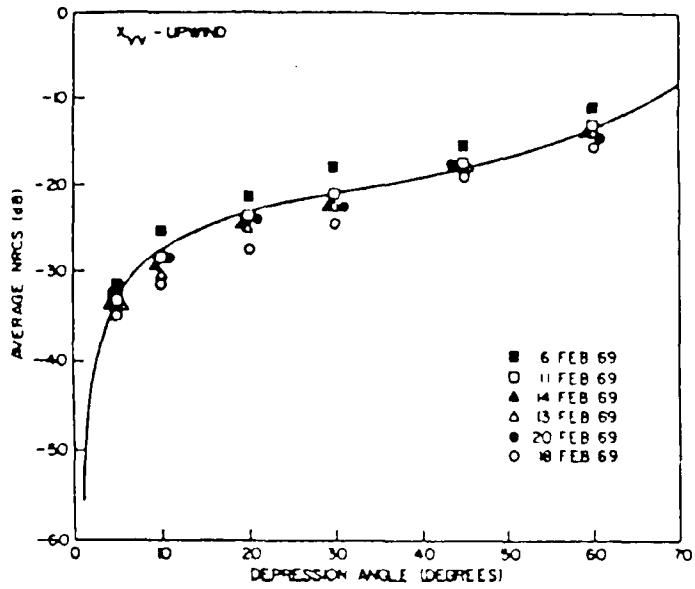
Figure D-6.   Backscatter Coefficient vs. Depression Angle (Daley 1973)

(a)

(b)
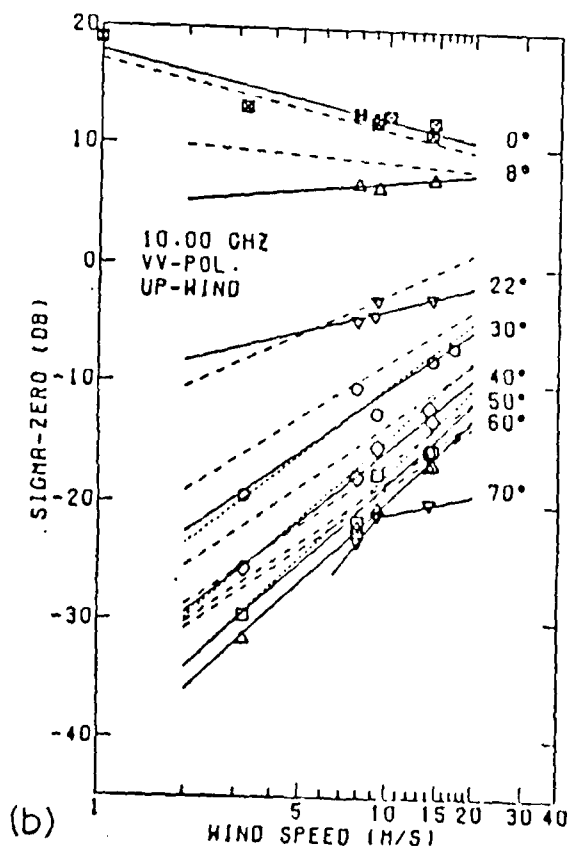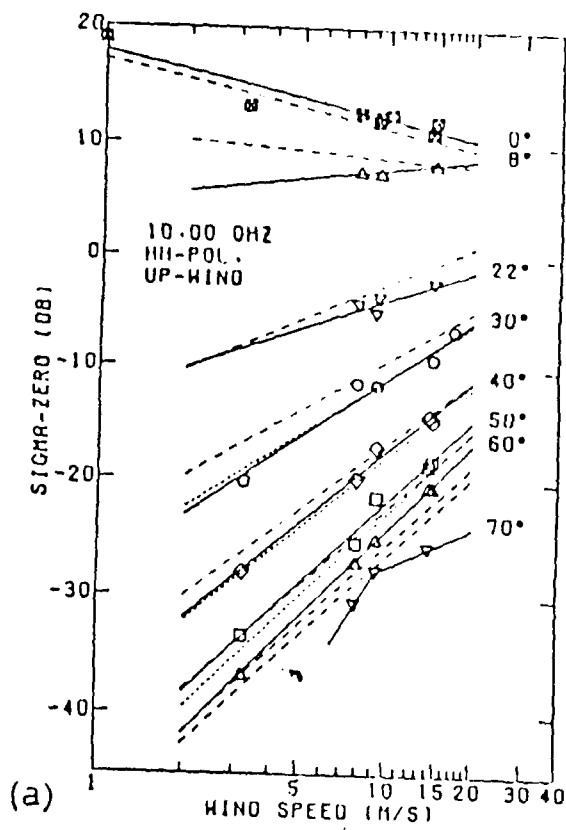
Figure D-7. Measurements of NRCS as a Function of Wind Speed and Incidence Angle (Masuko et al,1986)
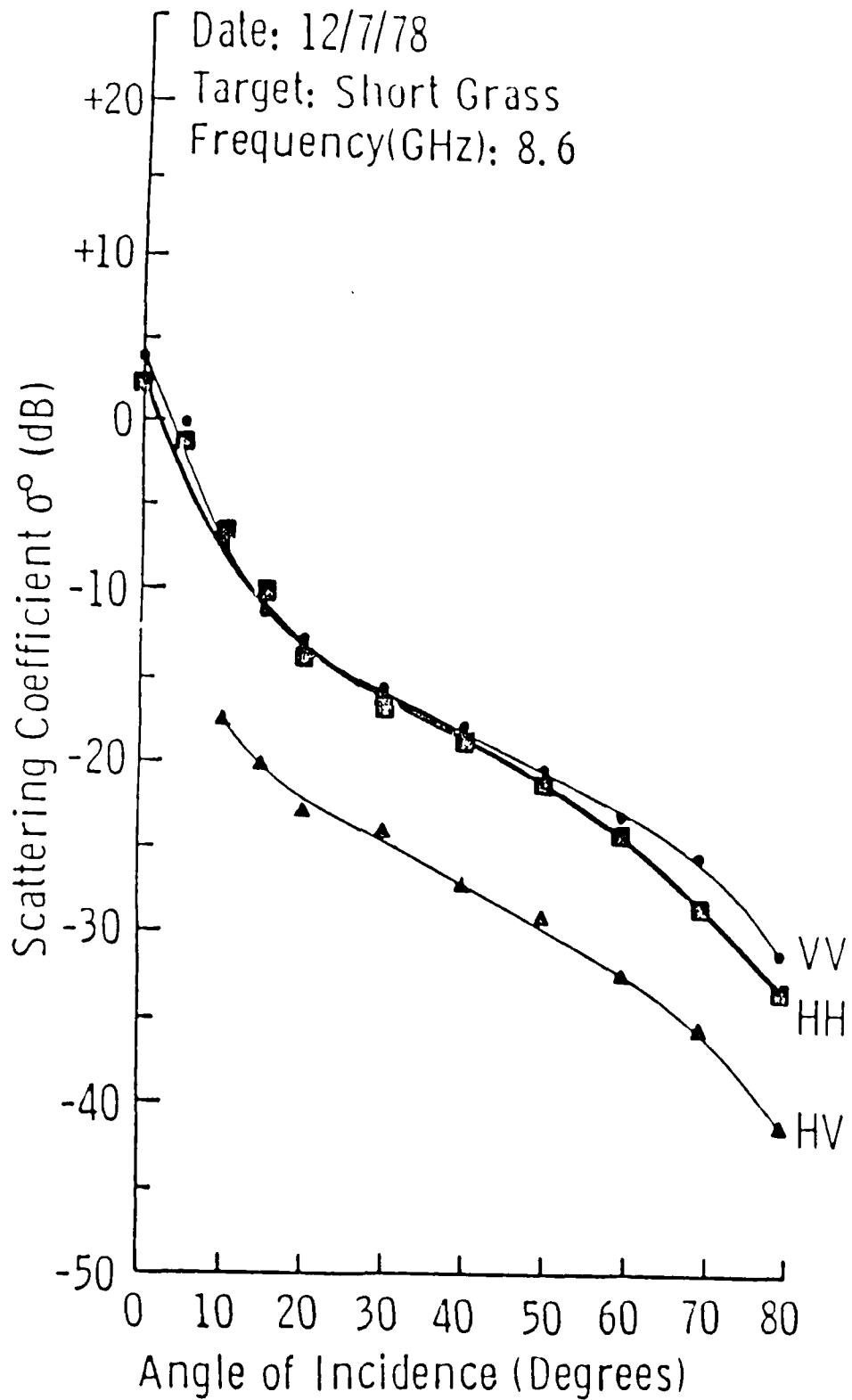
Figure D-8.   Measurements of the Backscatter Coefficient of Short Grass
(Stiles et al, 1979)

D-21
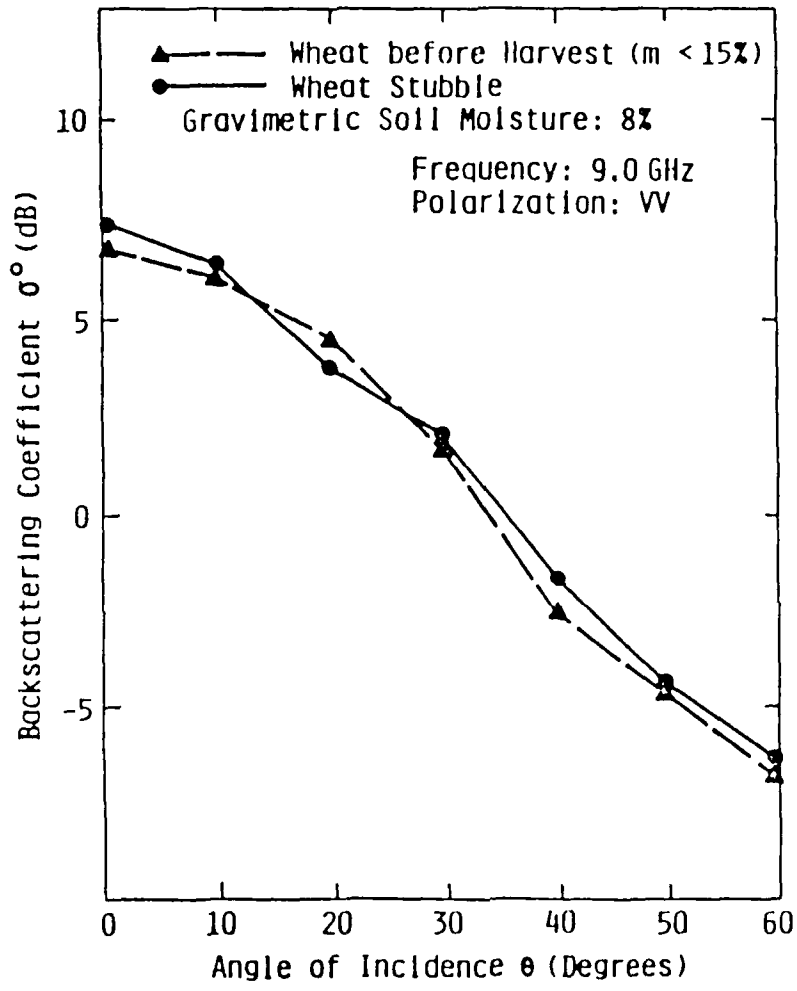
Figure D-9.   Measurements of NRCS for Wheat (Ulaby et al, 1986)
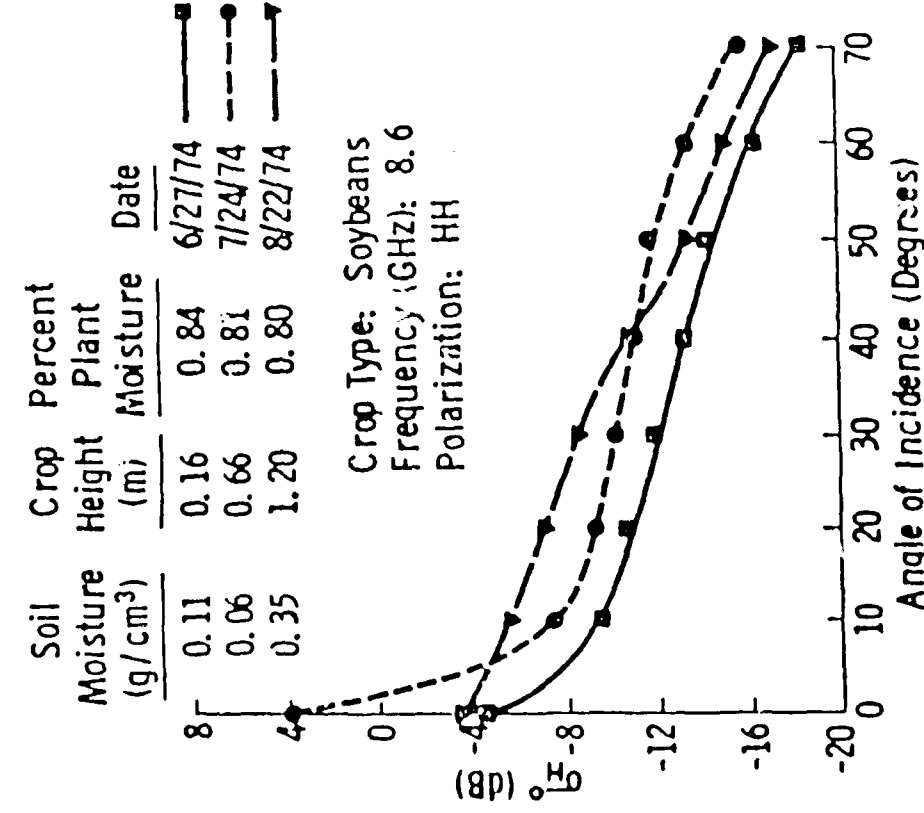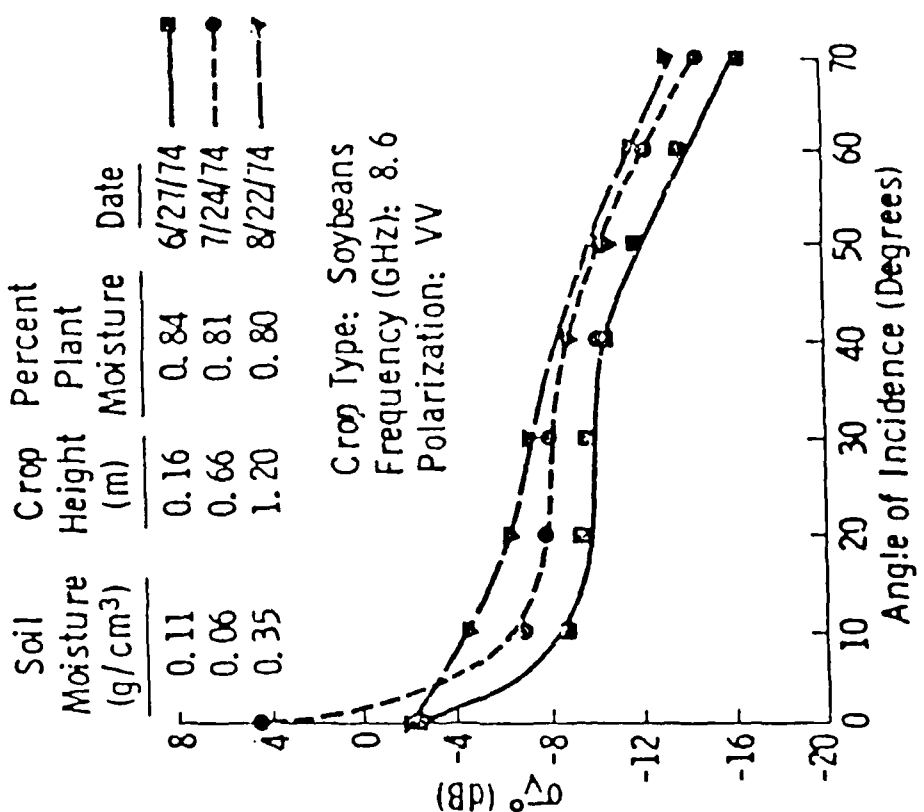
Figure D-10.   Backscatter Coefficient of Soybeans Various Soil Moisture
(Bush et al, 1975)
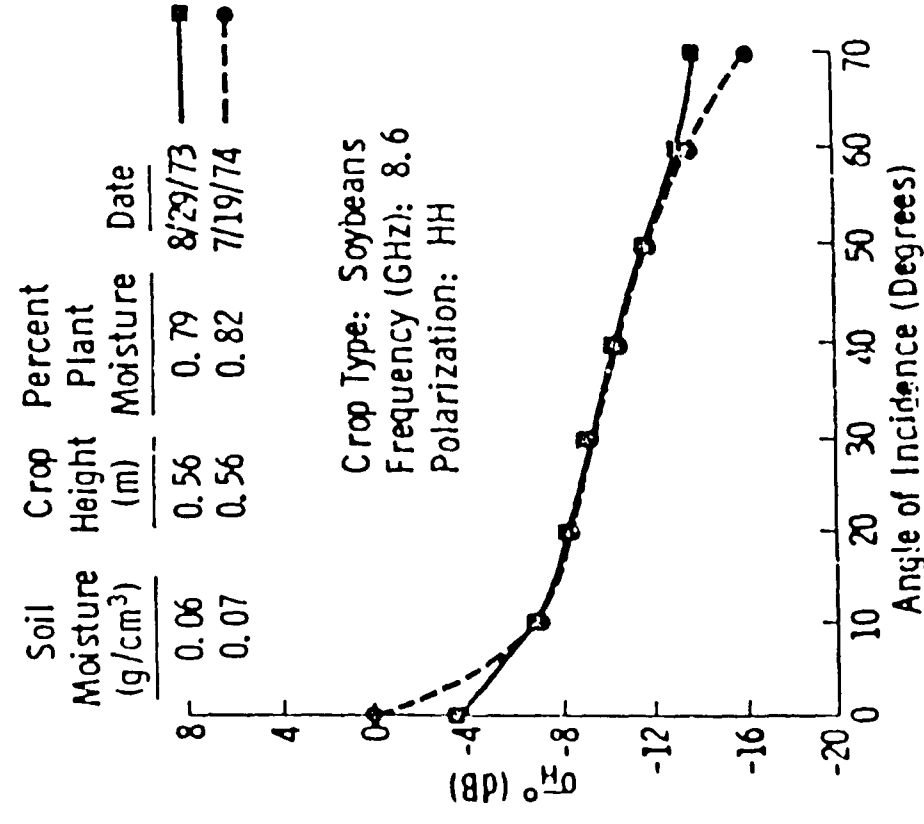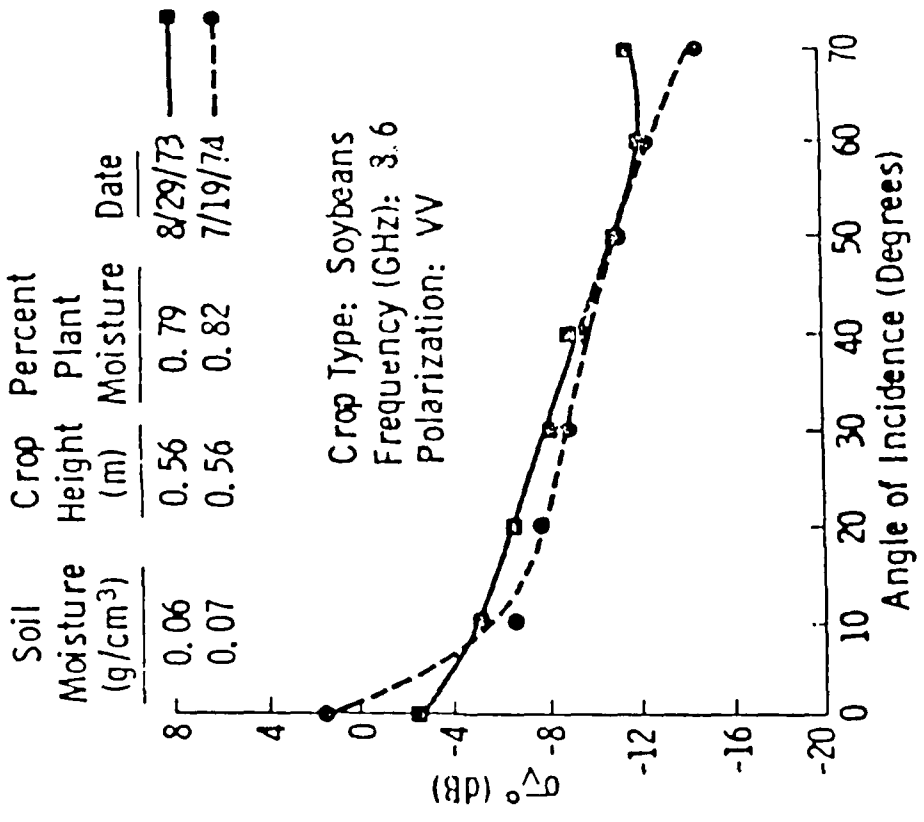
Figure D-11.   Backscatter Coefficient of Soybeans Various Soil Moistures
(Continued) (Busth et al, 1975)
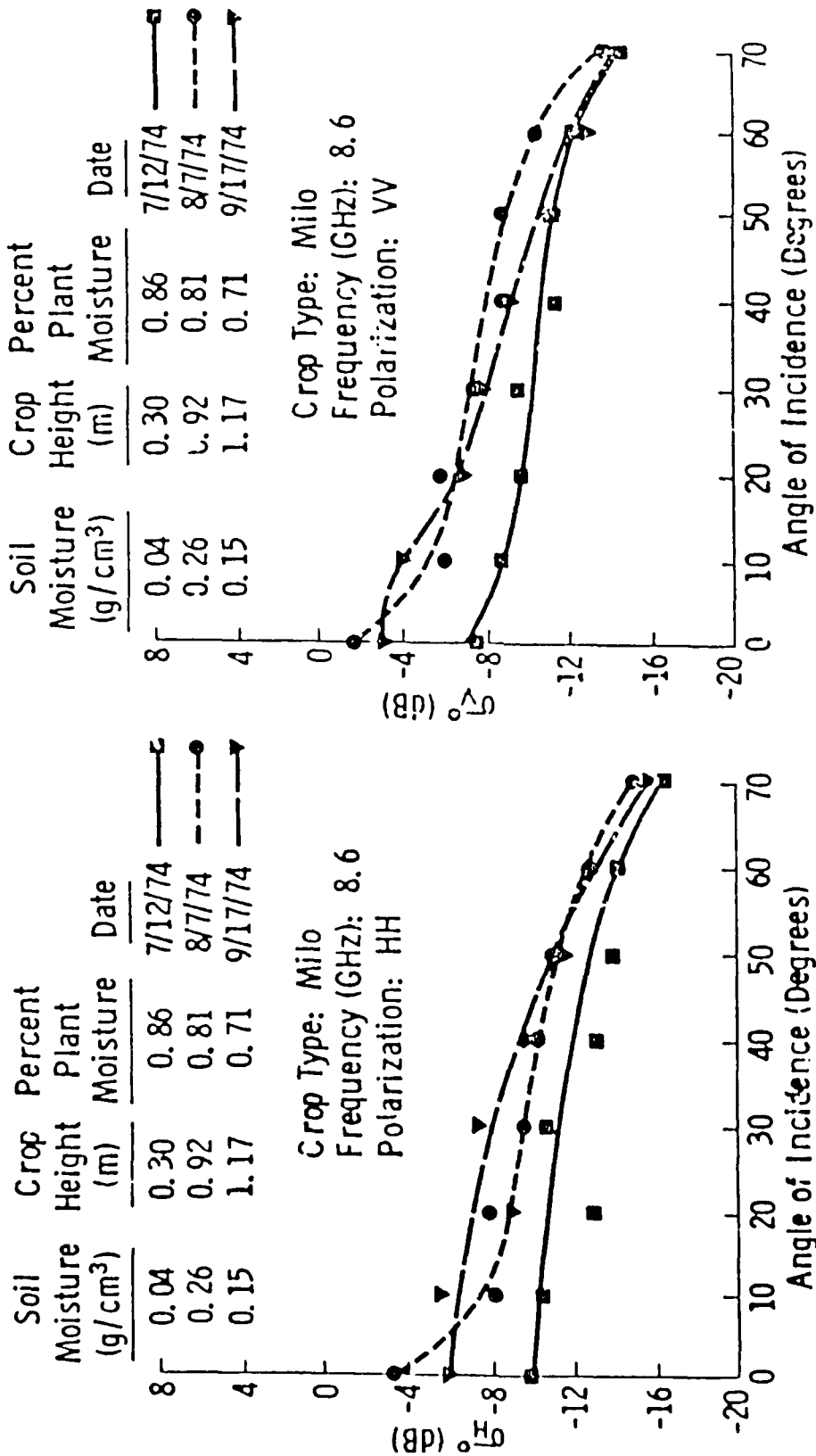
Figure D-12.   Backscatter Coefficient of Milo Various Soil Moistures
   (Continued) (Bush et al, 1975)
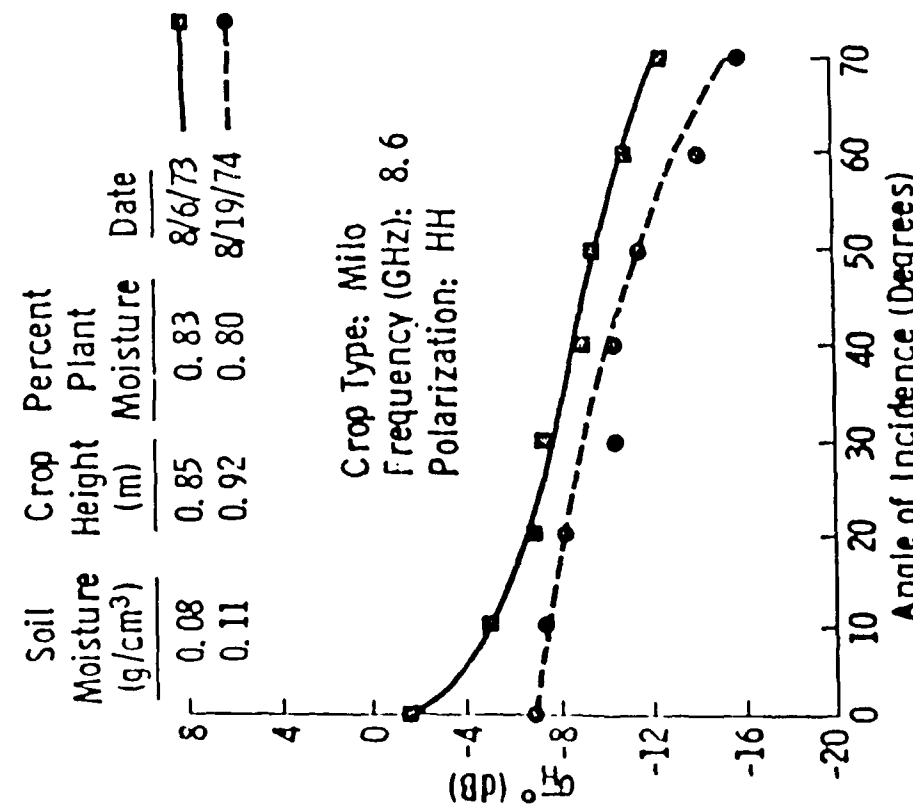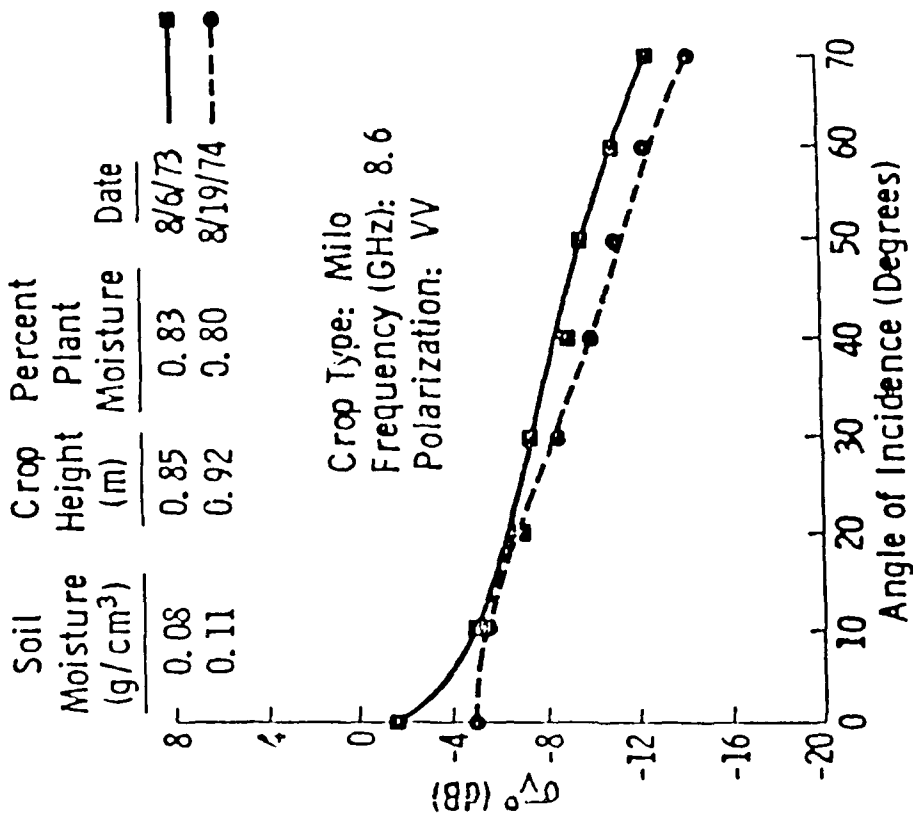
Figure D-13. Backscatter Coefficient of Milo Various Soil Moistures (Continued) (Bush et al, 1975)
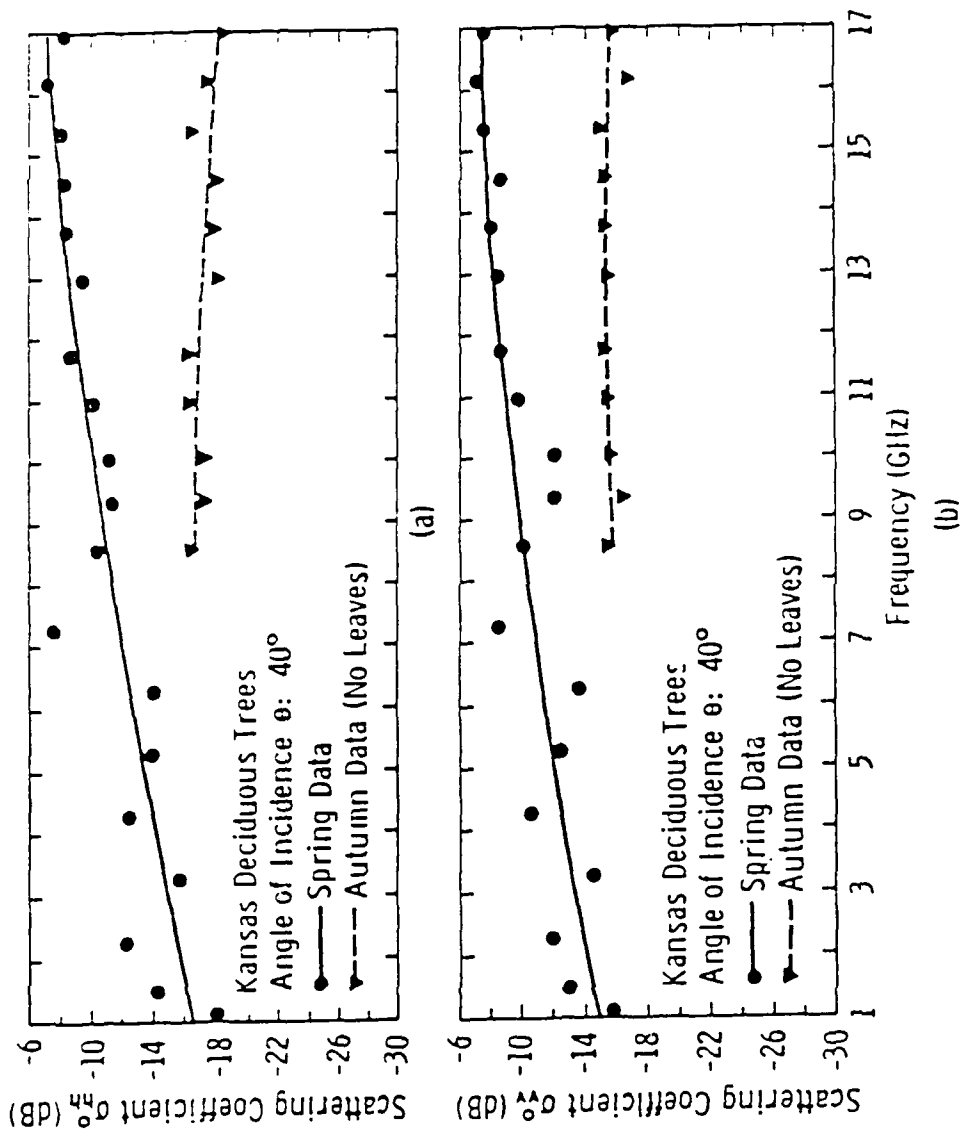
Figure D-14.   Measurements of the Backscatter Coefficient of Deciduous Trees (Ulaby et al, 1986)
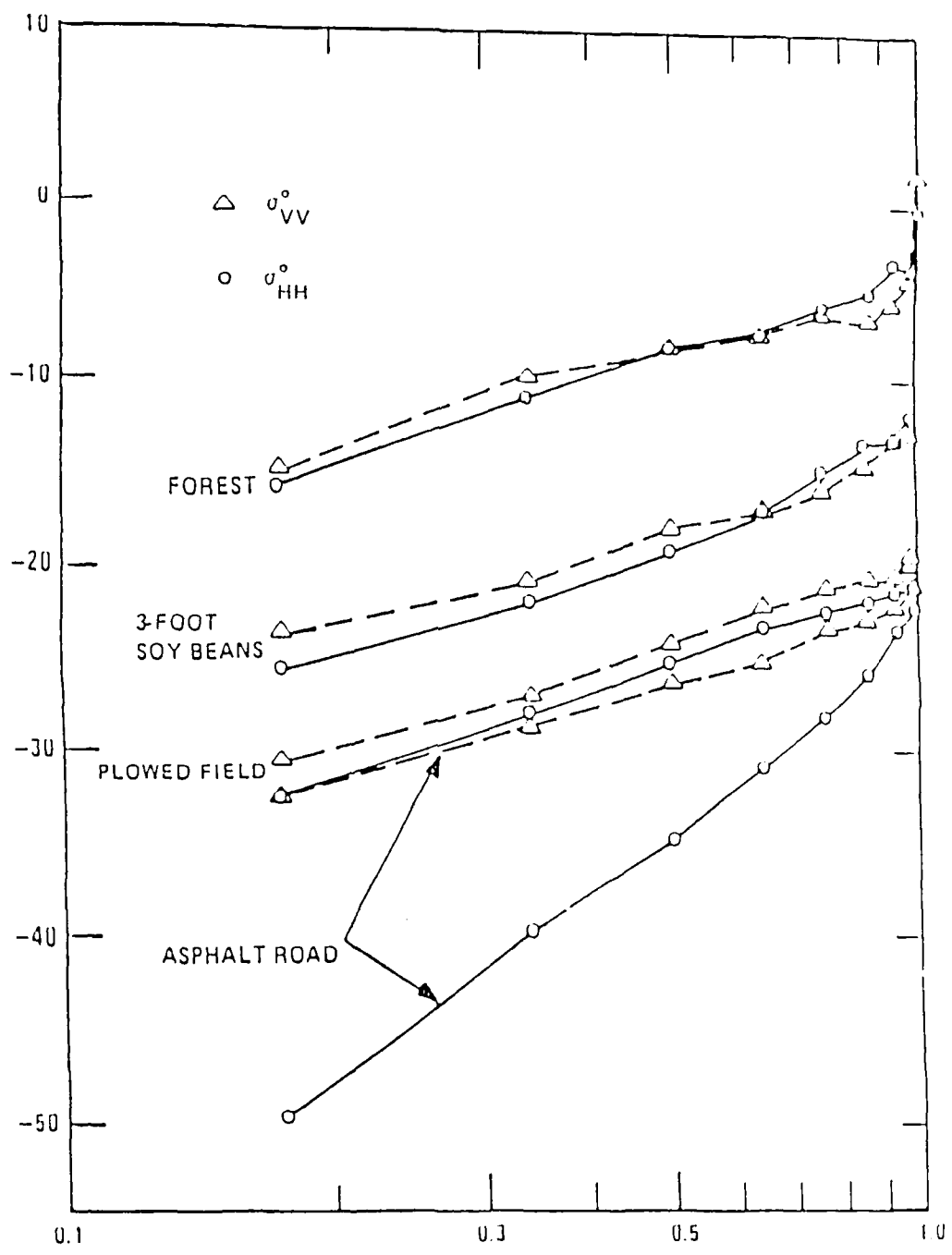
Figure D-15.   Measurements of Backscatter Coefficient of Assorted
Distributed Targets (Ament et al, 1959) (Cosgriff et al, 1960)

Report Documentation Page

NASA
National Aeronautics and
Space Administration

1. Report No.	2. Government Accession No.	3. Recipient's Catalog No

4. Title and Subtitle	5. Report Date
Synthetic Aperture Radar Imagery of Airports and Surrounding Areas, Archived SAR Data	November, 1989
	6. Performing Organization Code

7. Author(s)	8. Performing Organization Report No.
Dr. Robert G. Onstott Denise J. Gineris	
	10. Work Unit No.

9. Performing Organization Name and Address	11. Contract or Grant No.
Environmental Research Institute of Michigan (ERIM) 1975 Green Rd. Ann Arbor, MI 48105	NAS1 - 18465
	13. Type of Report and Period Covered

12. Sponsoring Agency Name and Address	31 Aug. 87 - 30 Nov. 89
NASA Langley Research Center	14. Sponsoring Agency Code

15. Supplementary Notes

16. Abstract

This report is the first in a series of three which address the statistical description of ground clutter at an airport and in the surrounding area. These data are being utilized in a program to detect microbursts. Synthetic aperture radar (SAR) data were acquired from the ERIM SAR data archive and were examined for utility to this program. Eight digital scattering coefficient images were created. Data used were of four airports observed with a set of parameters which more closely matched those which are anticipated to be encountered by an aircraft on its approach to an airport. This report describes these data and the results of the clutter study. These scenes which are greater than 6 km x 6 km scene were imaged at 9.38 GHz and HH- and VV-polarizations, and contained airport grounds and facilities, industrial, residential, fields, forest, and water. Incidence angles ranged from 12° to 72°. Even at the largest depression angles the distributed targets such as forest, fields, water, and residential rarely had mean scattering coefficients greater than -10 dB. Eighty-seven percent of the image had scattering coefficients less than -17.5 dB. About 1 % of the scattering coefficients exceeded 0 dB, with about 0.1 % above 10 dB. Sources which produced the largest cross-sections were largely confined to the airport grounds and areas highly industrialized. The largest cross-sections were produced by observing broadside large buildings surrounded by smooth surfaces. Example combinations include terminals/tarmac, docks/water, industrial-facility/parking-lot, and refinery-tanks/ground.

17. Key Words (Suggested by Author(s))	18. Distribution Statement
Clutter, Backscatter, SAR, Microburst	

19. Security Classif. (of this report)	20. Security Classif. (of this page)	21. No. of pages	22. Price
Unclassified	NA		

NASA FORM 1626 OCT 86